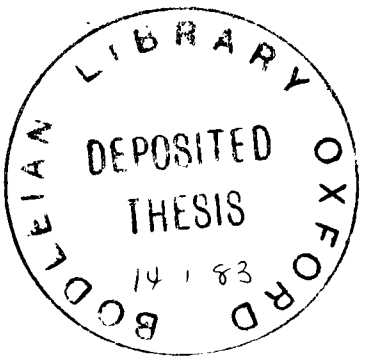
Thesis presented to the

University of Oxford

for the Degree of

Doctor of Philosophy



COARSE-GRAINED ROCKS OF

ASCENSION ISLAND

CHRISTOPHER HARRIS

VOLUME TWO

TABLES, FIGURES AND PLATES

Department of Geology and Mineralogy

and

The Queen's College, Oxford

Michaelmas 1982

CONTENTS VOLUME TWO

CHAPTER ONE

Tables 197

Figures 200

Plates 202

CHAPTER TWO

Figures 207

CHAPTER THREE

Tables 215

Figures 218

Plates 232

CHAPTER FOUR

Tables 241

Figures 264

Plates 319

CHAPTER FIVE

Tables 352

Figures 368

CHAPTER SIX

Tables 398

Figures 402

CHAPTER SEVEN

Tables 408

Figures 419

CHAPTER EIGHT

Tables 426

Figures 431

CHAPTER NINE

Figures 437

Specimen localities 1979/80 439

Map one inside back cover

Map two "

Representative analyses on microfiche "

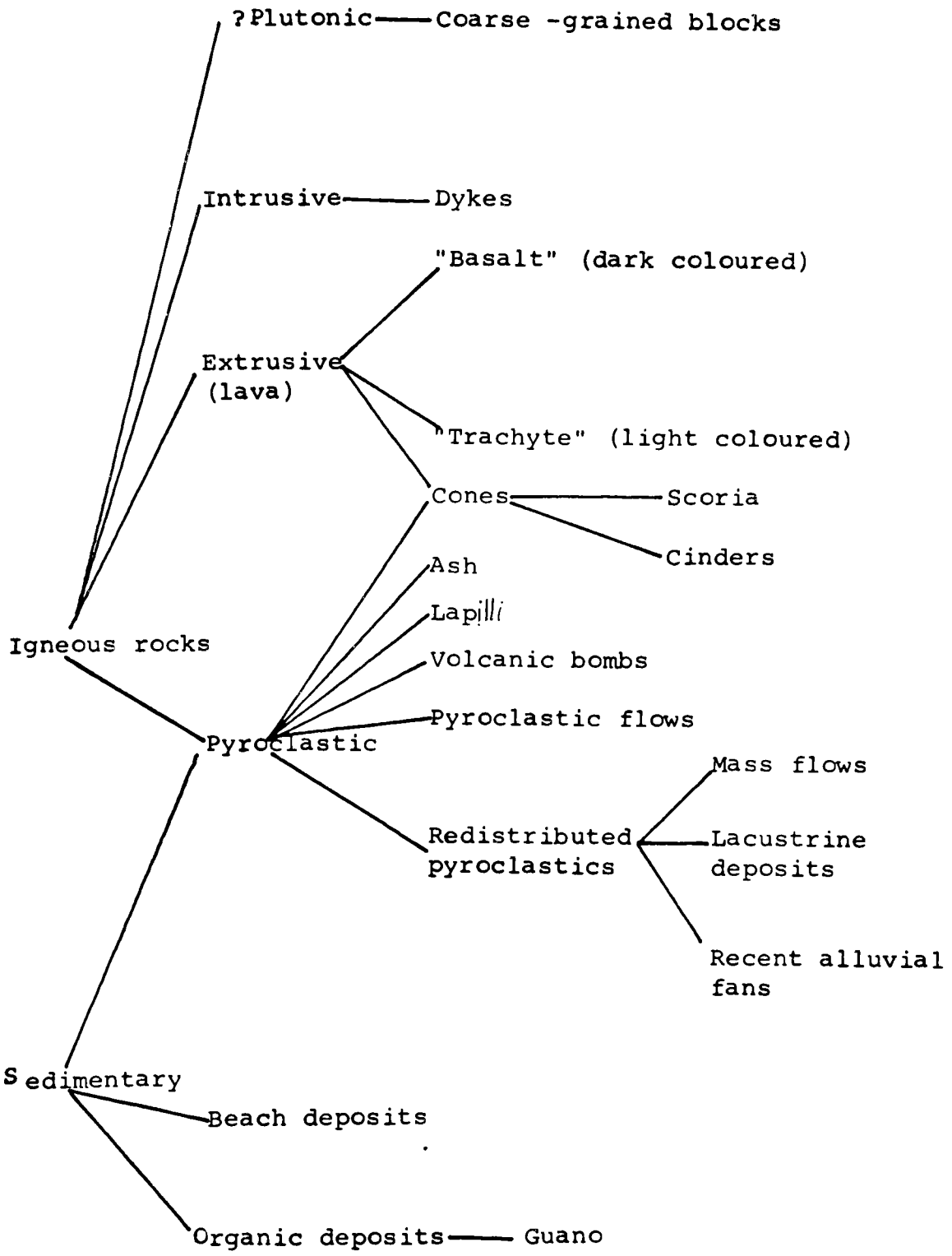
CHAPTER ONE

TABLES, FIGURES AND PLATES

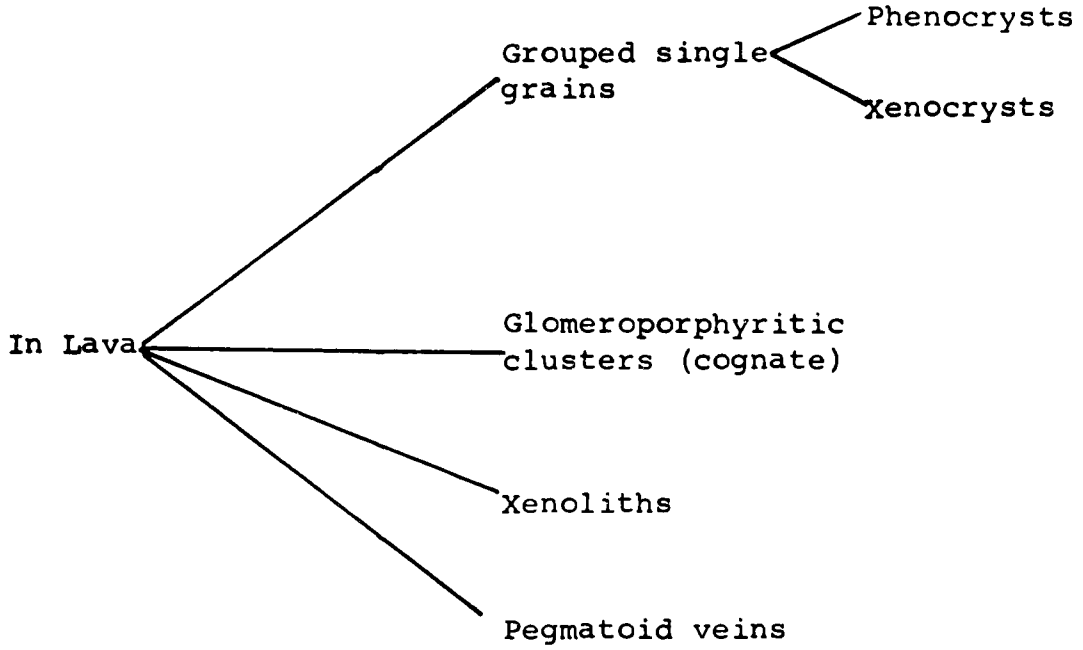
Table 1.1 Previous research on Ascension Island rocks

Atkins et al (1964)	Brief account of general geology
Cann (1967)	Second occurrence of vlasovite
Darwin (1844)	General geology and petrology
Daly (1926)	Geology , petrography and petrology
Gast et al	Sr and Pb isotopes
O'Nions and Pankhurst (1974)	Interisland comparison of isotope and other trace elements
O'Nions et al (1978)	Sm Nd isotopes
Renard (1889)	Petrography
Roedder and coombs (1967)	Fluid inclusions in the granite blocks
van Tassel (1952)	First occurrence of dalyite in granite blocks
van Andel and Heath (1970)	Tectonics of the ocean floor around Ascension island
van Andel et al (1973)	Tectonics of Ascension Fracture Zone etc

Table 1.2 'In the field' classification of Ascension Island rocks.



Classification Scheme for Coarse-grained material



In Pyroclastics (and other sediment) ——— Coarse-grained blocks

Throughout this thesis the term coarse-grained block is used to describe all descrete coarse-grained lumps whether they occur in lava as xenoliths or in pyroclastics.

Fig 1.1 Regional setting of Ascension Island (after van Andel et al, 1973)

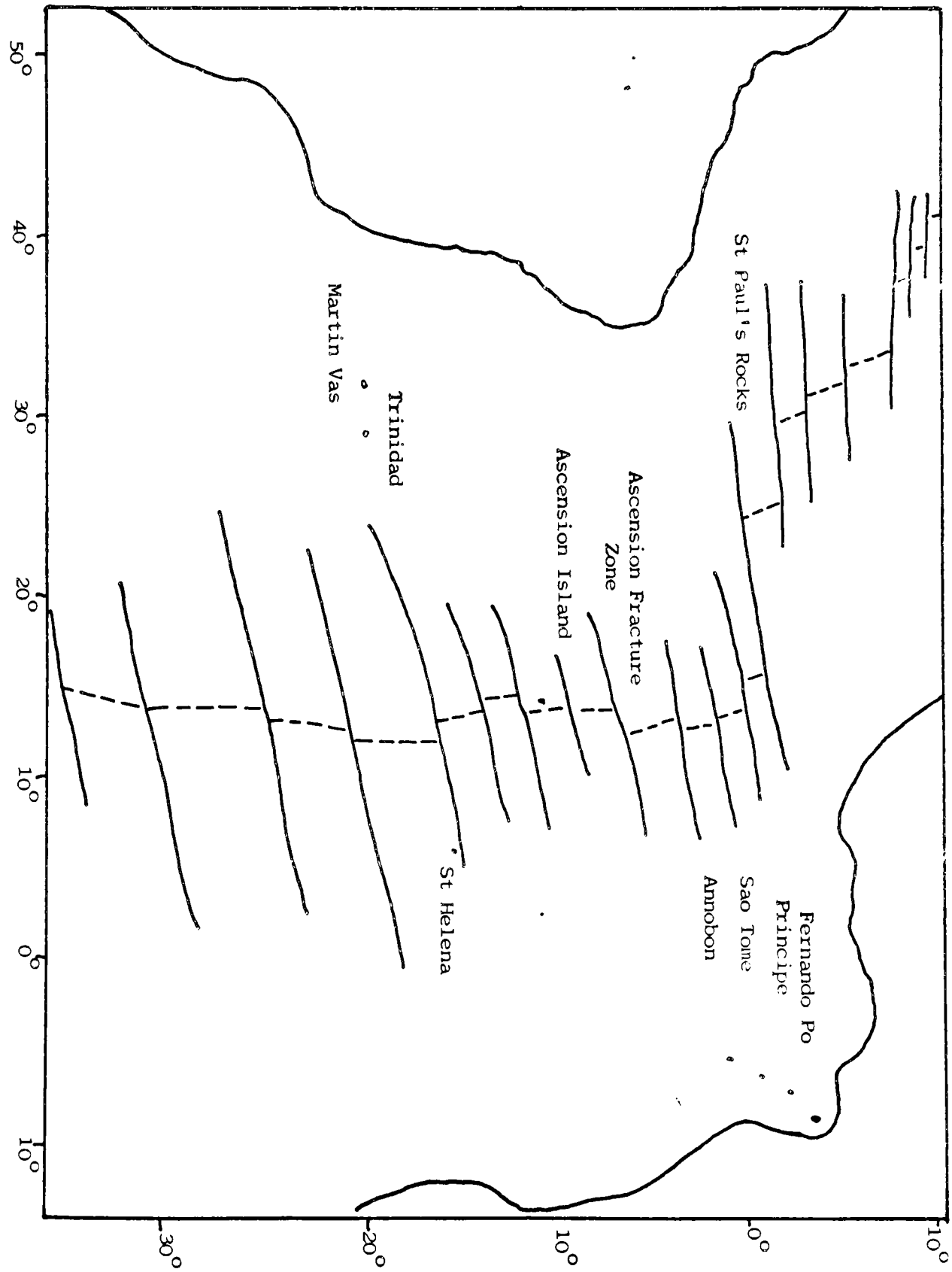


Fig 1.2 Ascension Island showing relative sizes of total cone and the exposed part

(a) cross section

cone height = 3600m

exposed portion = 850m



(b) plan view

diameter of cone base= 50km

volume of cone = 2350 km^2

volume of exposed portion = 26km^2

Ascension Island is therefore 1.1%

of the total cone

(data from van Andel et al, 1973)

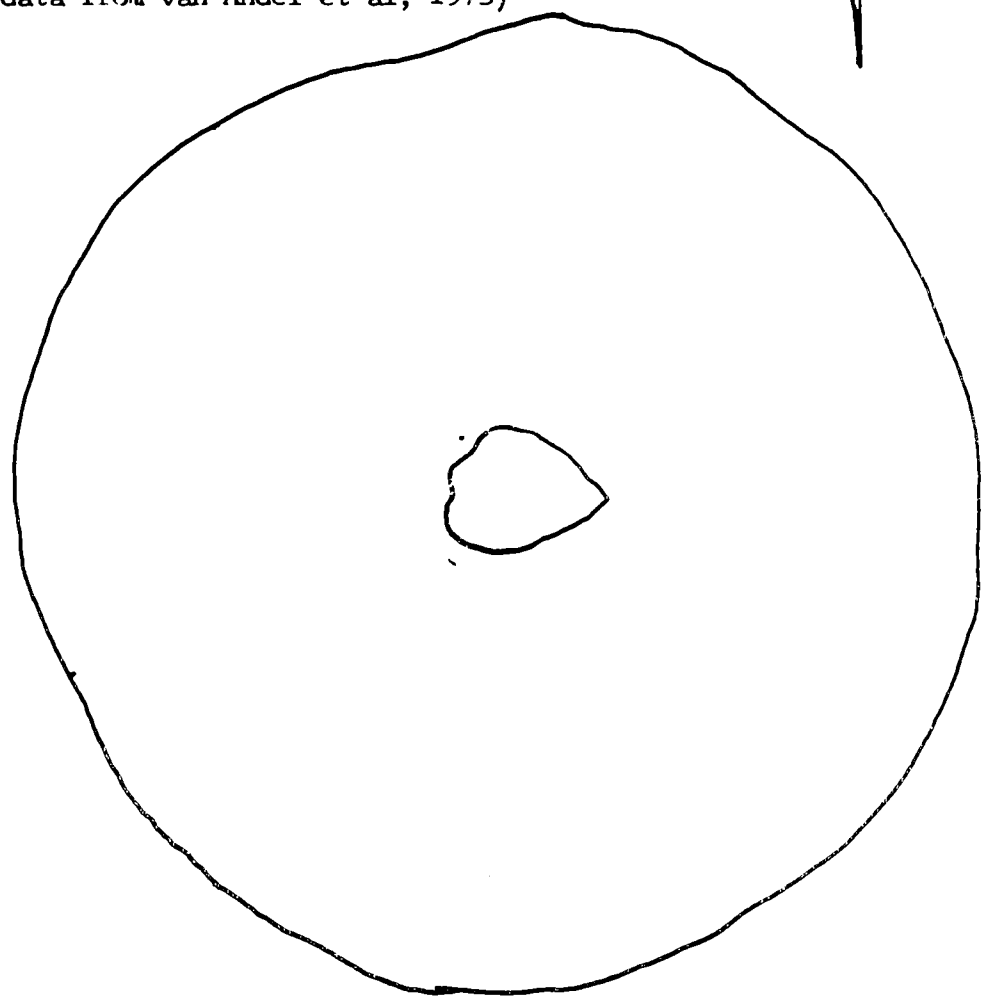


Plate 1.1 Mountain Red Hill. This composite cone is partly dissected, revealing sheets of basic lava alternated with cinders and scoria.



Plate 1.1 Possible pyroclastic flow topped by pumice and cut by a small normal fault. Green Mountain road.



Plate 1.3 Cricket Valley. The pegmatoid is found in the basalt wall towards the right of the photograph. Taken from Weatherpost looking west.



Plate 1.4 Spoon Crater (left) and South Gannet Hill and the airstrip (right) from Middleton's Ridge. The white rocks in the foreground (over which the road runs) belong to the Middletons Facies. Note the dip of the strata caused by later updoming of trachyte beneath.



Plate 1.5 Coarse-grained block in situ in the East Crater flow. Note its flat tablet shape.



Plate 1.6 The Devil's Riding School. Concentric rings of interbedded cinders and redistributed pyroclastics dip towards the centre. N.B. sheep in the foreground for scale.



Plate 1.7 The Devil's Riding School (centre) and Dark Slope Crater (left) from Mountain Red Hill.



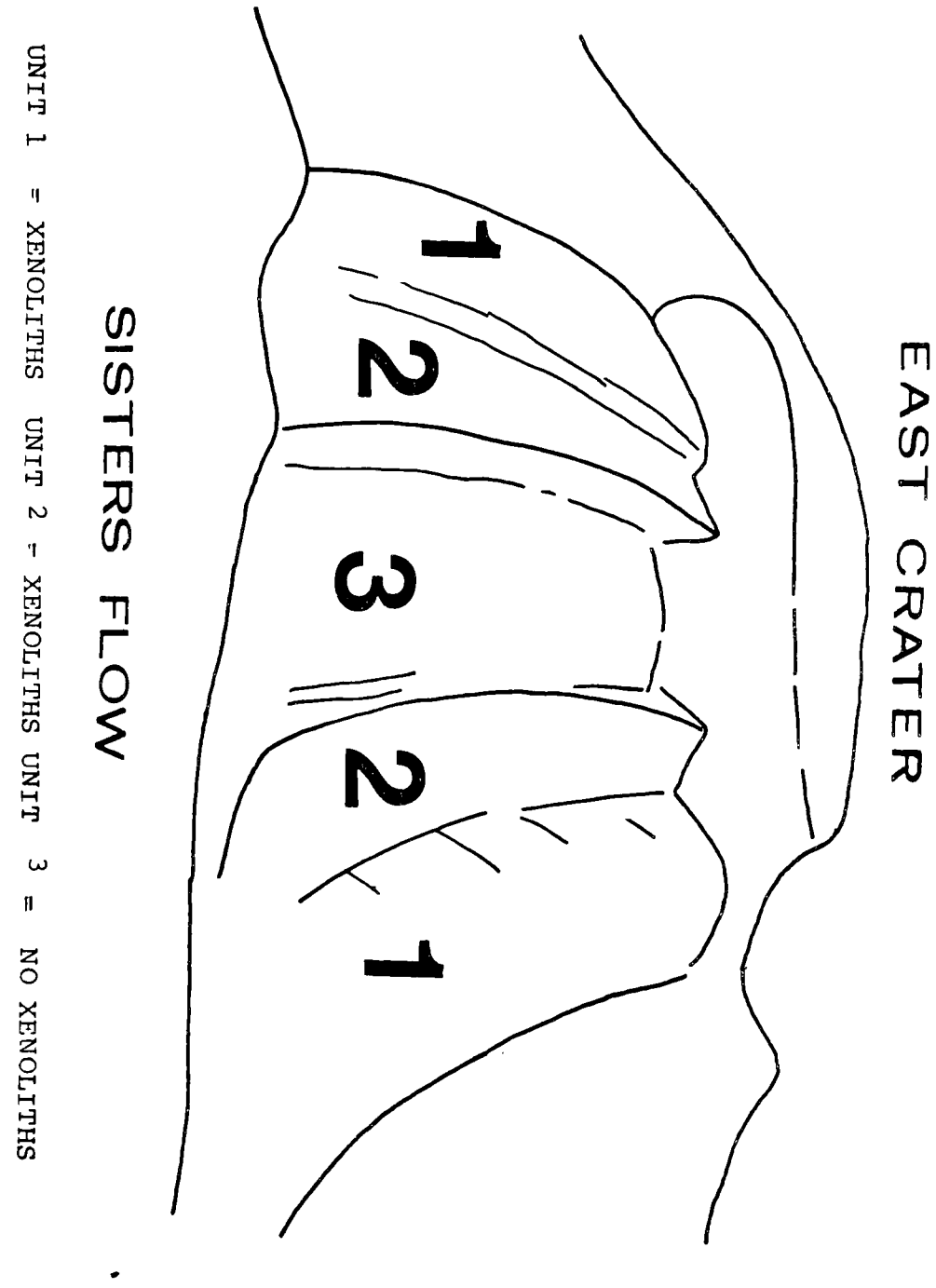
Plate 1.8 Little White Hill and South East Head from White Hill. Note the basaltic scoria rim to Little White Hill and the South East Head fissure (top left) with the black Devil's Ink Stain trachyandesite flow.



CHAPTER TWO

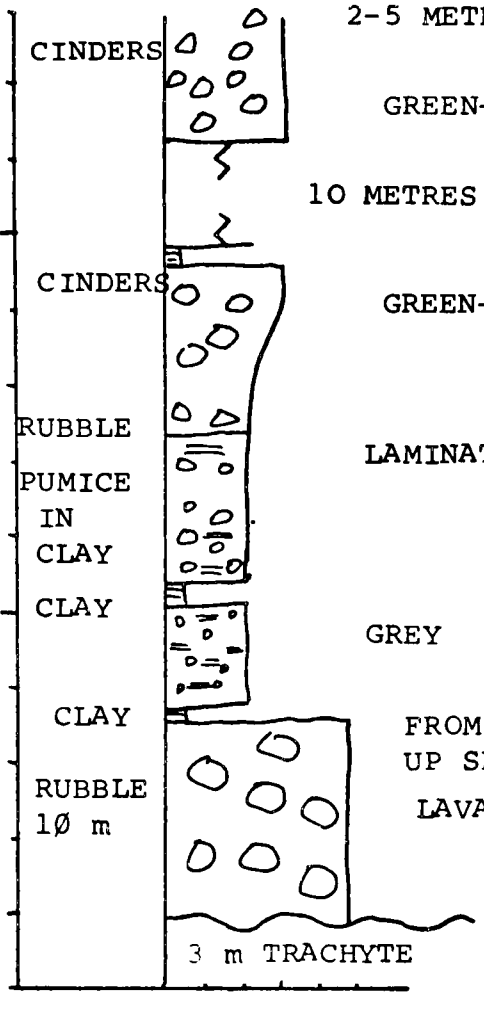
FIGURES

Fig 2.1 East Crater from Sisters Flow showing the three units to the East Crater Flow



GENERALISED VERTICAL SECTIONS

Fig 2.2a



2-5 METRES TO THE TOP

GREEN-BLACK BASALTIC

10 METRES SIMILAR UNIT

GREEN-BLACK

LAMINATED YELLOW BANDS

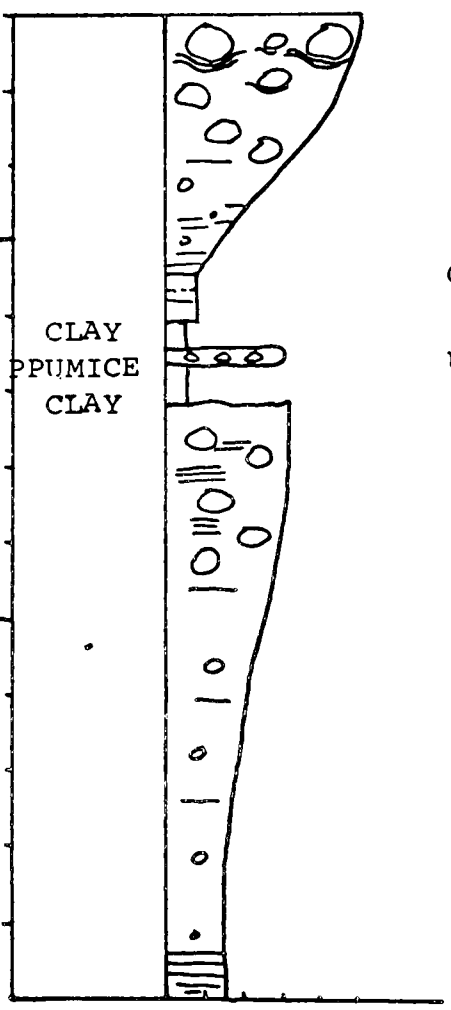
GREY

FROM HERE FEW LARGE CLASTS UP SECTION

LAVA AND COARSE-GRAINED BLOCKS

(A) DEVILS RIDING SCHOOL

Fig 2.2b



IRREGULAR CLAY BANDS

FEWER COARSE-GRAINED BLOCKS

COARSE-GRAINED BLOCKS

UNDULATING IN SEQUENCE

RARE COARSE-GRAINED BLOKKS

(B) WEST SIDE CRICKET VALLEY

Fig 2.3aN.A.S.A ROAD-ASHPIT SECTIONS (N.A.S.A ROAD FACIES)

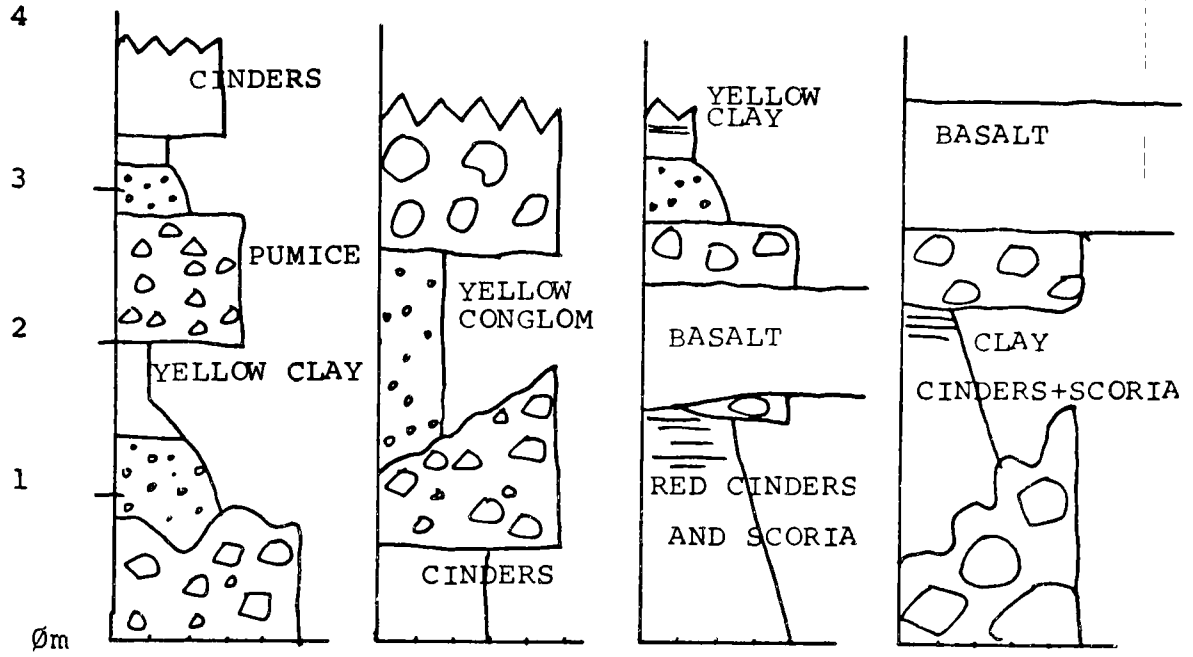


Fig 2.3b N.A.S.A SPOON CRATER SECTION (MIDDLETON'S FACIES)

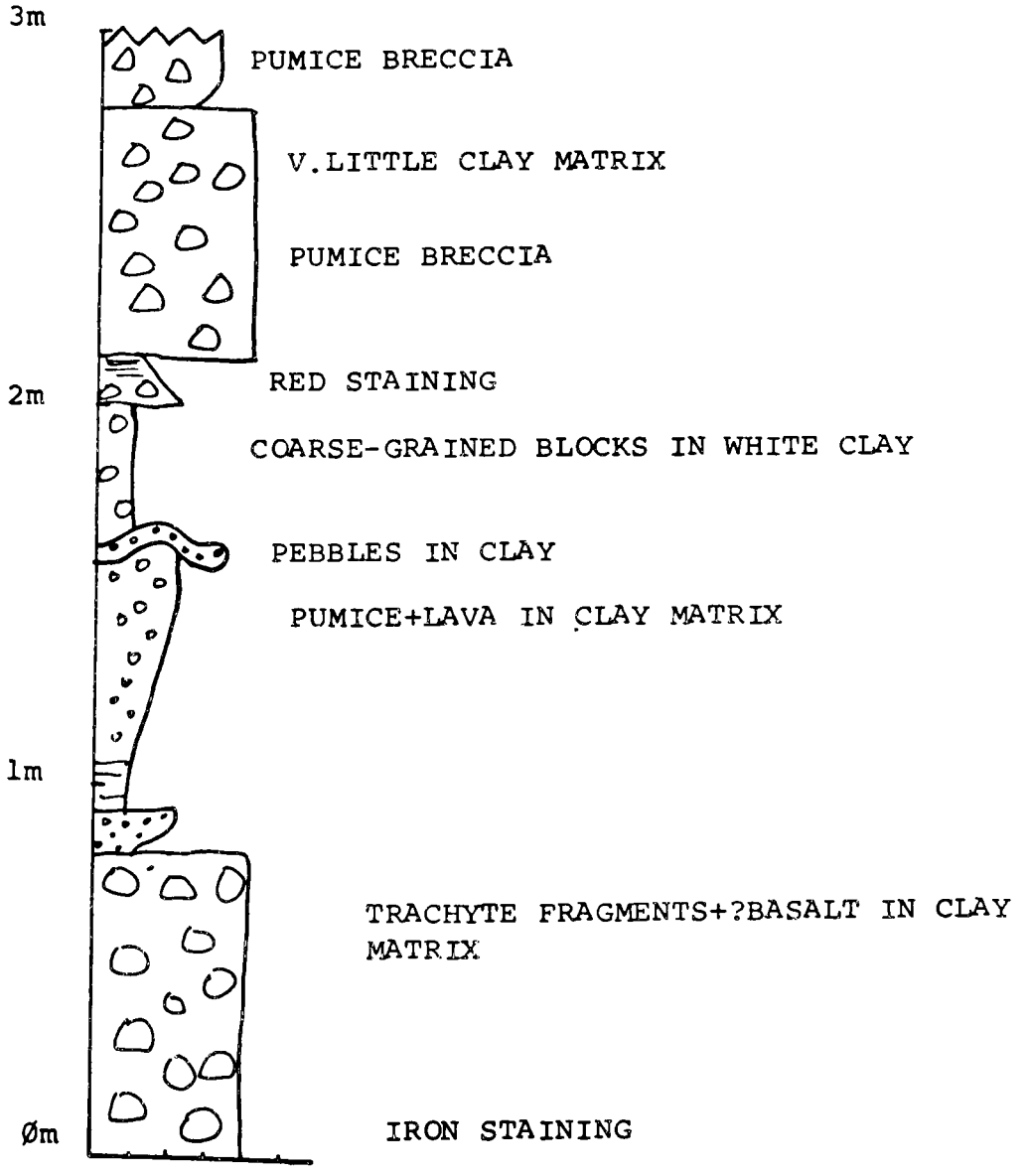


Fig 2.4 Representative section of Middleton's Ridge pyroclastics

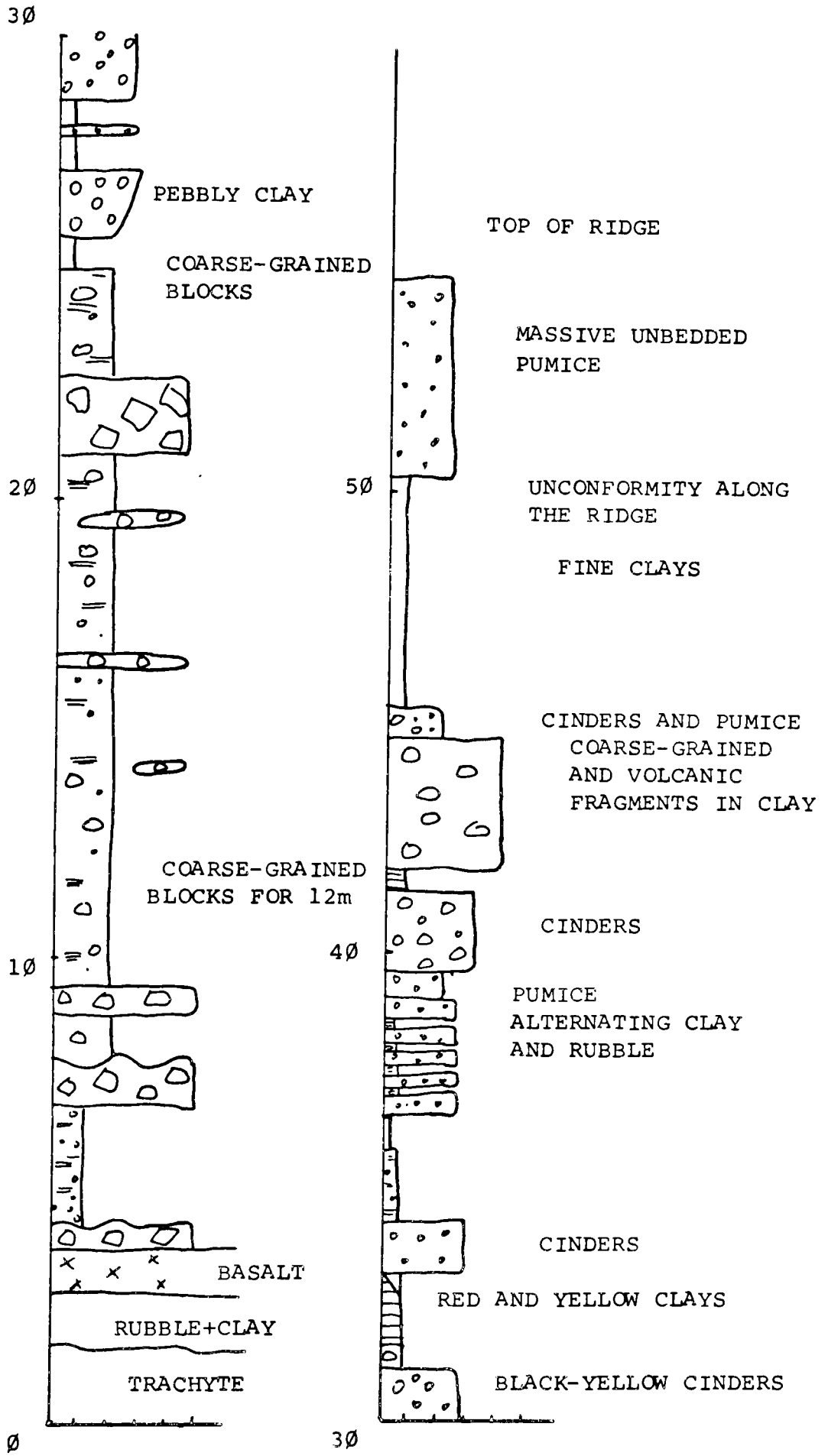


Fig 2.5 Two sections from the valley above Bear's Back

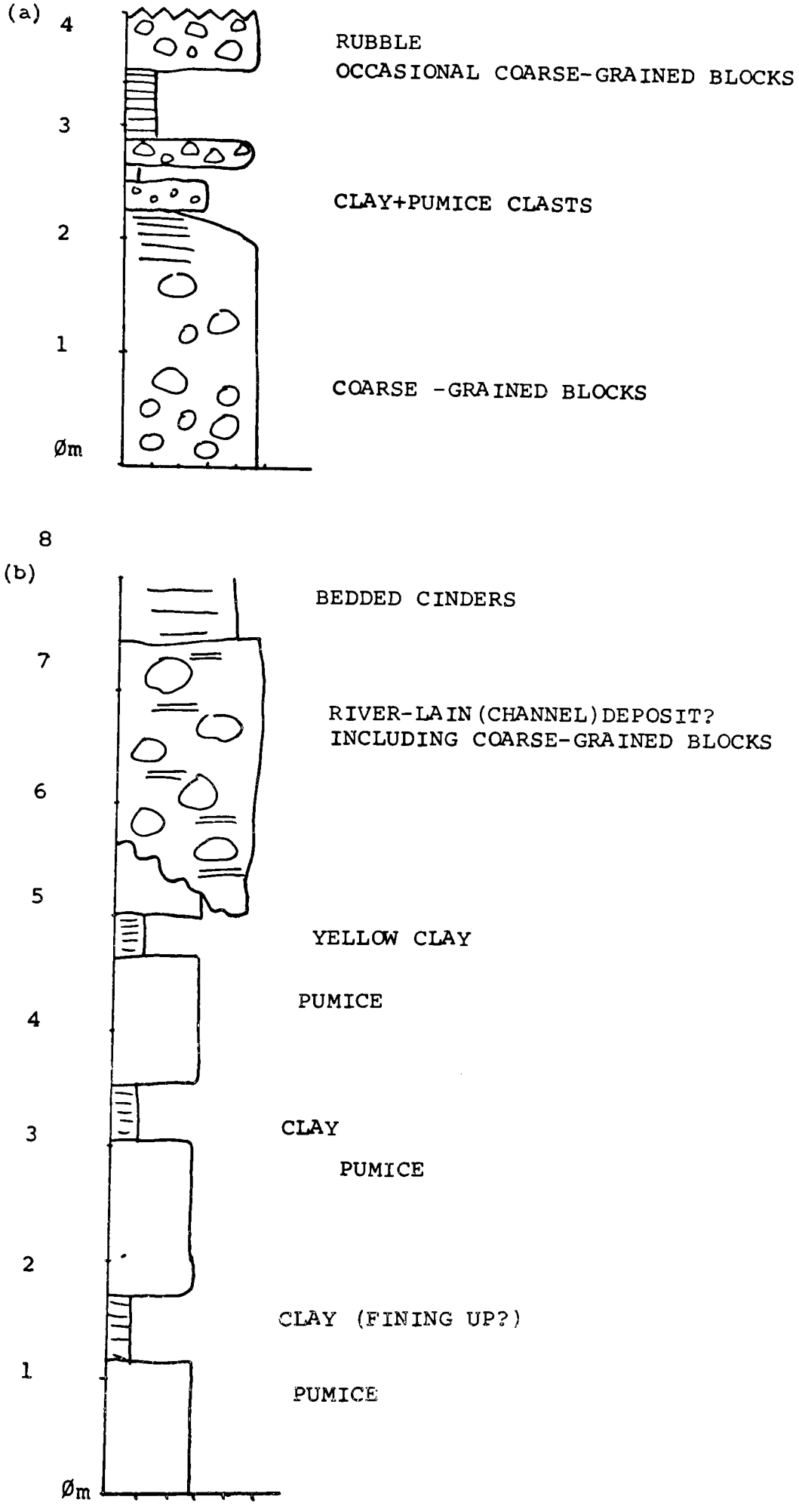


Fig 2.6 The occurrence of coarse-grained blocks at their original eruptive centres

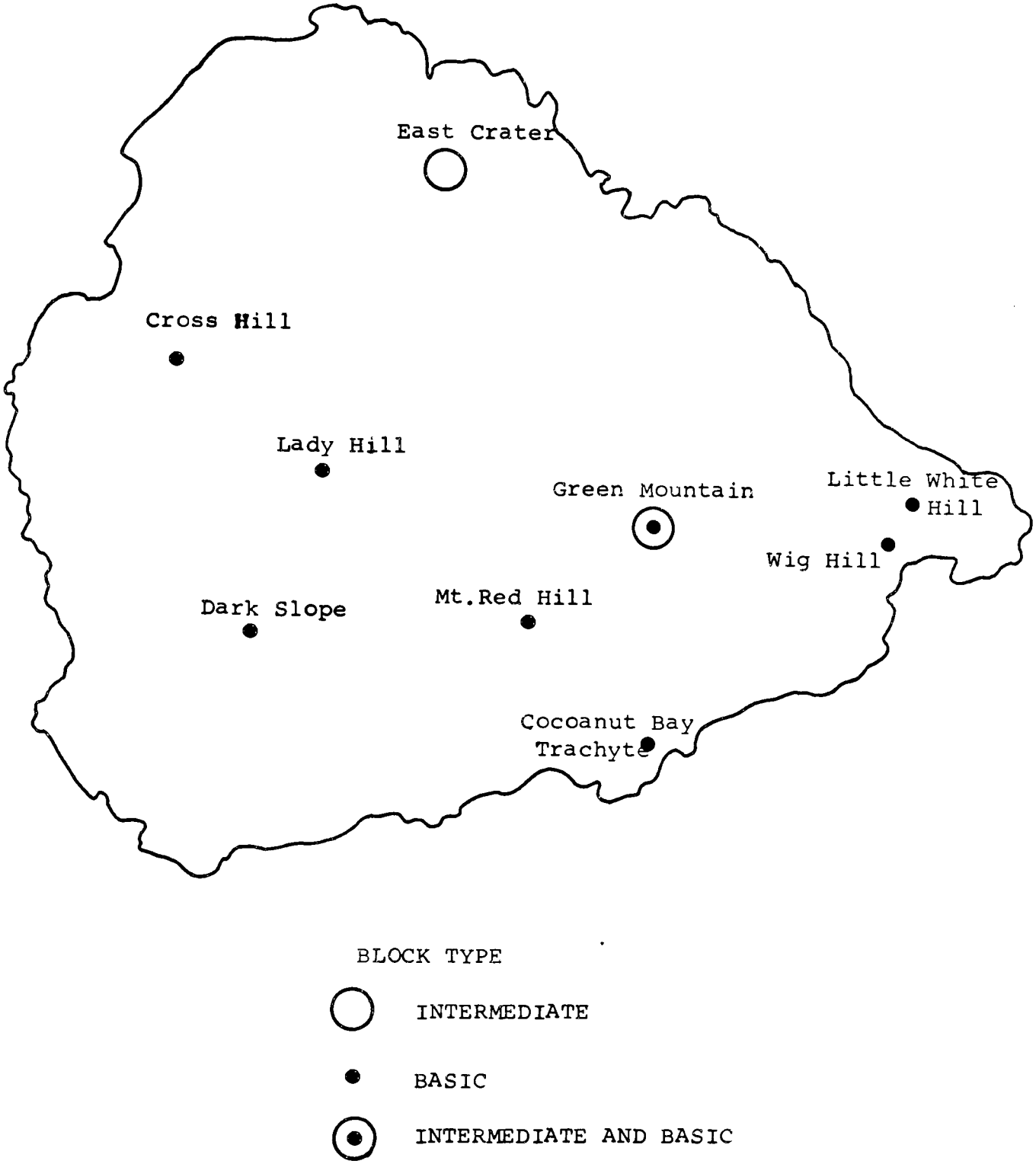
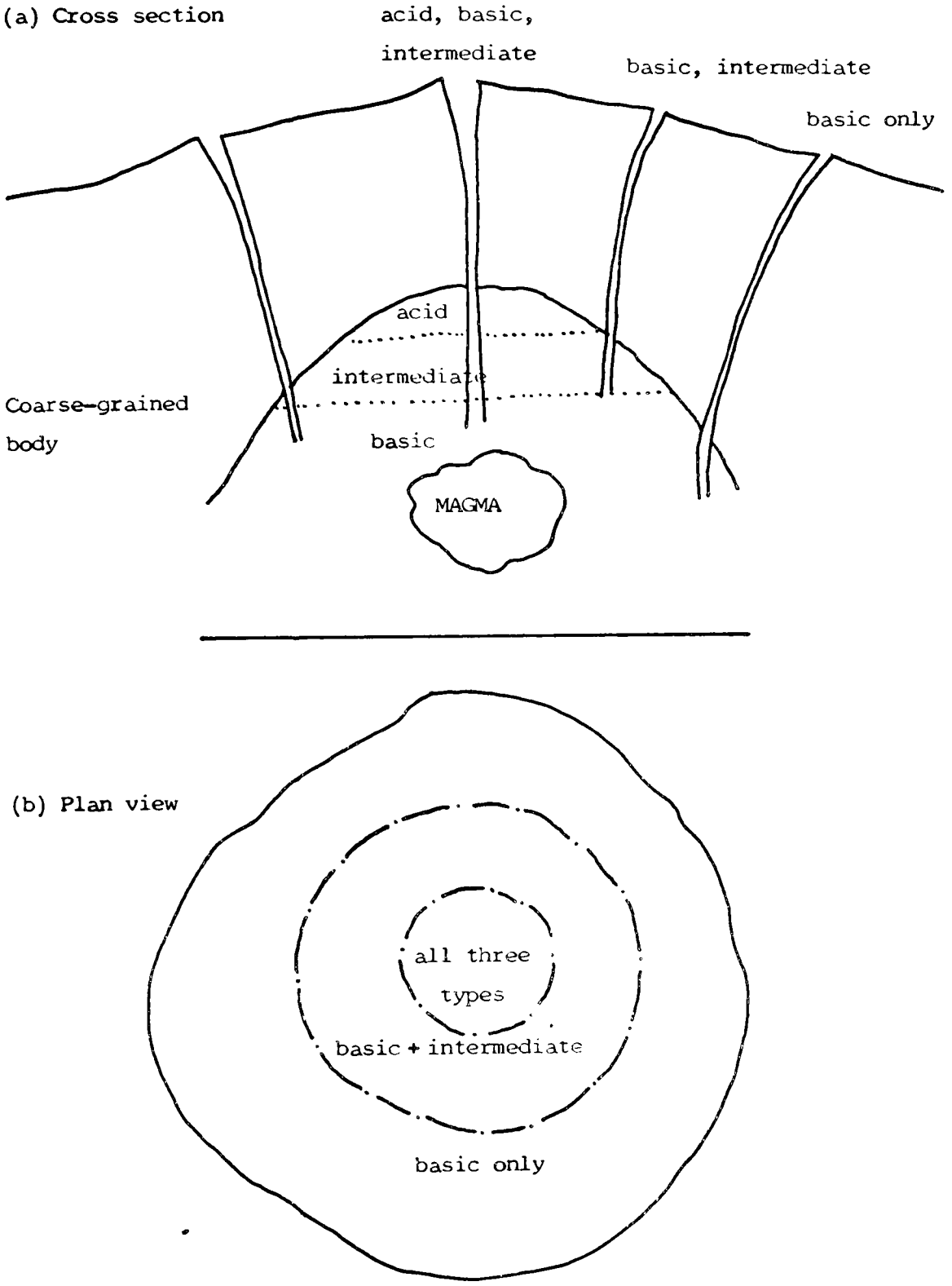


Fig 2.7 Schematic dependence of xenolith distribution on magma chamber morphology.



CHAPTER THREE

TABLES, FIGURES AND PLATES

NOMENCLACTURE OF ASCENSION ISLAND LAVAS

	Basalt	Hawaiite	Trachybasalt	Tr.andesite	Trachyte	Comendite
Feldspar phenocrysts	>AN 50	>AN 50	AN 40-60	AN 30-50	Anorthoclase	Sanidine
Other phenocrysts	+cpx+ol+op		+cpx+op+(ol)		+fayalitic ol +ferro-hedenbergite	
Groundmass Fsp composition	>AN 50	AN 40-50	AN 10-40	Sanidine	Sanidine glass increasing →	
Texture	Unorientated groundmass		Semi-trachytic	Trachytic	Trachytic	Flow banded
Wt% SiO_2	47-52		52-56	57-63	64-69	70-74

Table 3.1

Table 3.2 LAVAS WHOSE PHENOCRYSTS WERE ANALYSED BY MICROPROBE
Locality and flow morphology

Sample No.	Locality	Flow Morphology
15006	Cocoanut Bay	
DS19L	Dark Slope Crater	Lava/scoria cone
H81L	W.side Cricket Valley	Thick basic ?flow
H49	Crystal Bay	Loose block
H49(12)	Crystal Bay	
17407	E.S.E.slopes Green Mt.	Lava in composite cone
H39L	East Crater Flow	Large basic flow
A63(1)	Devils Ink Stain	Thin basic flow
15146	Little White Hill	Acid dome
H90L	1 km S.Hummock Point	Basic flow exposed in stream bed
17446	As H90L	
H6L	Cross Hill	Loose block
14954	N.of crater by airstrip	Old basic flow
17470	W.side Devil's Ashpit	Basic flow (?Cricket Valley type)
17409	E.side Green Mt.	Part of cone
17406	Castle Hill	Basic flow
17349	2 km S.Hummock Point	Small acid flow
14944	Thistle Hill	Acid complex
17345	Little Ascension Flow	Acid flow
17453	Hummock Point	?Acid flow
17434	S.E.side Cricket Valley	Thick basic ?flow
15226(13)	S.slopes Middletons	?loose block
15217	Breakneck Valley	Acid flow
15004	Cocoanut Bay	Acid dome
14922	Devils Riding School	Acid ?dome
15174	Daly"s Crags	Acid dome
17478	N. of explosion craters	Acid dome
Obsidian	Middleton's Ridge	Base of acid flow
15255	Five Mile Post	Loose block assoc.with granite blocks

Table 3.3

PHENOCRYST TYPES IN ANALYSED LAVAS

Rock No.	SiO_2	cpx	ol	fsp		clusters	
15006	62.67	X	X	X	Kfsp,Plag	X	+mgt
DS19L	49.69	X	X	X	Plag	X	+mgt
H81L	51.42	X	X	X	Plag	X	+ilm
H49		X		X	Plag	X	+mgt
H49(12)		X		X	Plag	X	+mgt
17407		X	X	X	Plag		+ilm
H39L	59.61	X	X	X	Plag	X	
A63(1)	59.42	X	X	X	Plag	X	+ilm,mgt,amph
15146	70.61		X	X	Kfsp		+ilm
H90L	52.06	X	X	X	Plag		
17446		X	X	X	Plag		
H6L		X	X	X	Plag		
14954			X	X	Plag	X	
17470		X	X	X	Plag	X	+ilm
17409		X	X	X	Plag		+ilm,mgt,amph
17406		X	X	X	Plag	X	+mgt
17349		X	X	X	Plag	X	
14944		X		X	Plag	X	+mgt
17345		X	X	X	Plag	X	+mgt
17453	63.46	X	X	X	Plag	X	+mgt
17434		X	X	X	?Kfsp Plag	X	+mgt
15226(13)		X		X	Kfsp		+mgt
15217	65.74			X	Kfsp		
15004			X	X	kfsp		+mgt,ilm
14922			X	X	Kfsp		
15174				X	Kfsp		
17478				X	kfsp		
Obsid.	72.22			X	Kfsp		
15255	73.06			X	Kfsp		

This table excludes analyses from xenocrysts and clusters

Fig 3.1 Phenocryst proportions in analysed volcanics

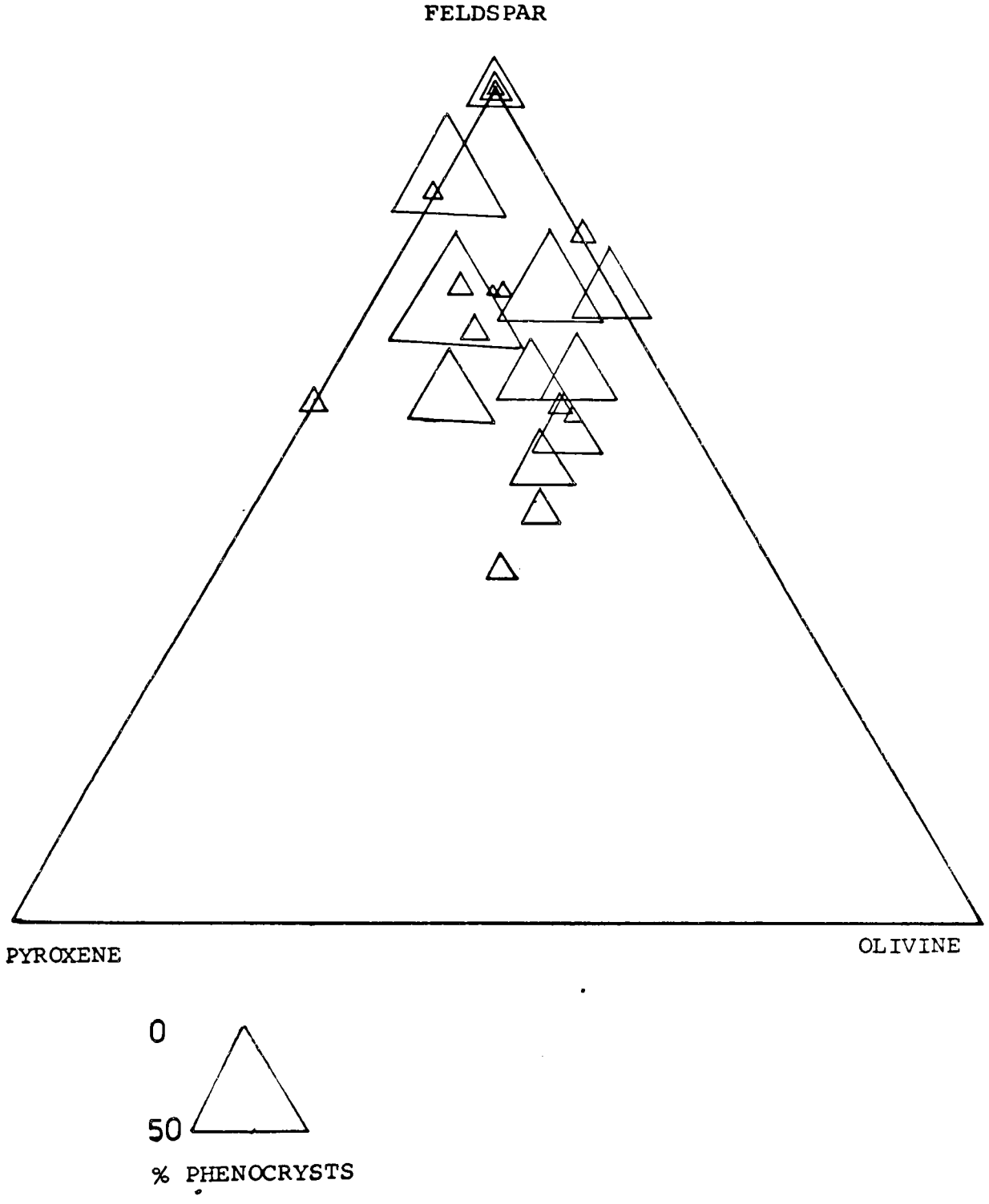


Fig 3.2 Mineralogy of glomeroporphritic clusters

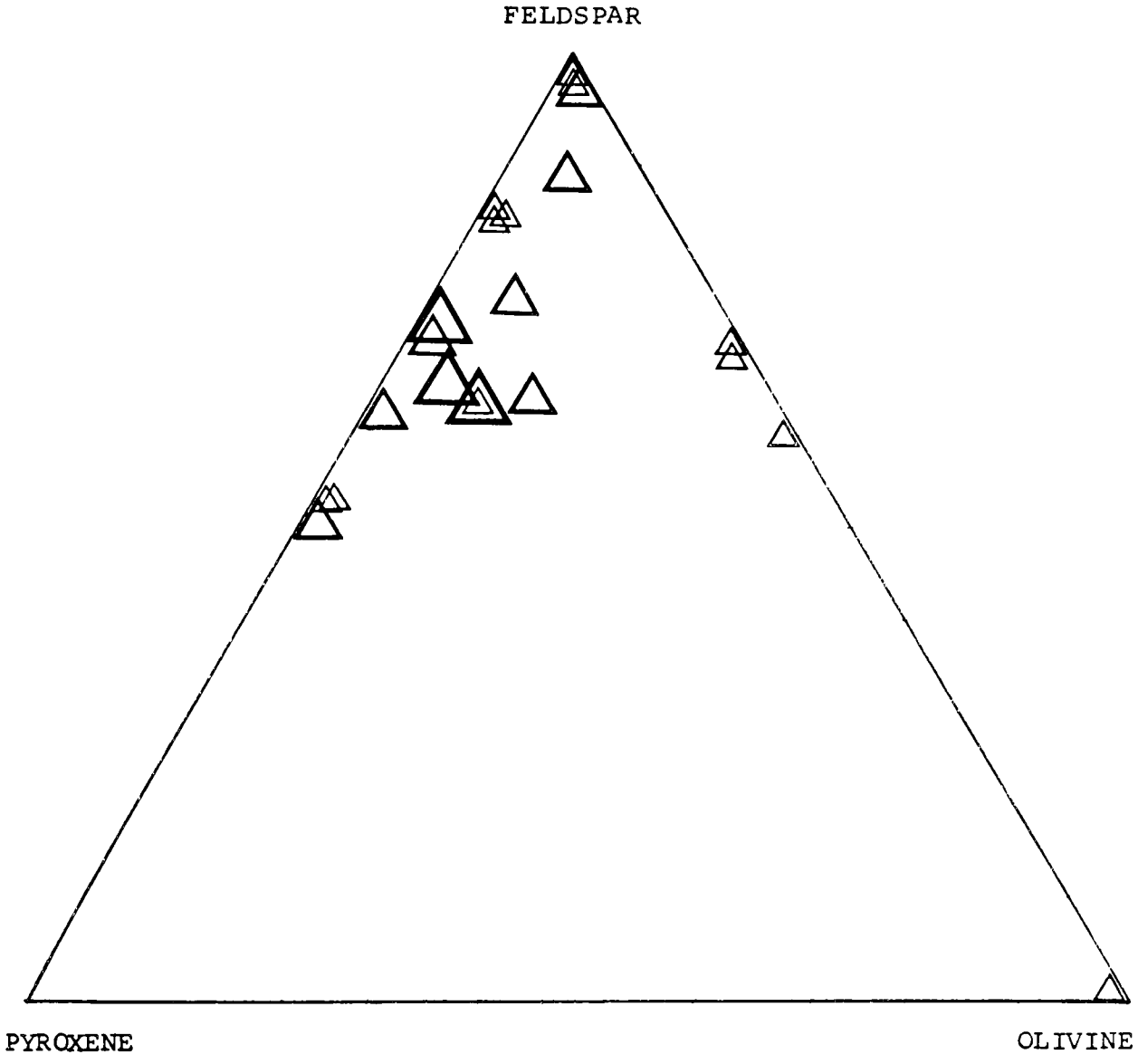


Fig 3.3 Composition of feldspar phenocrysts in all analysed lavas

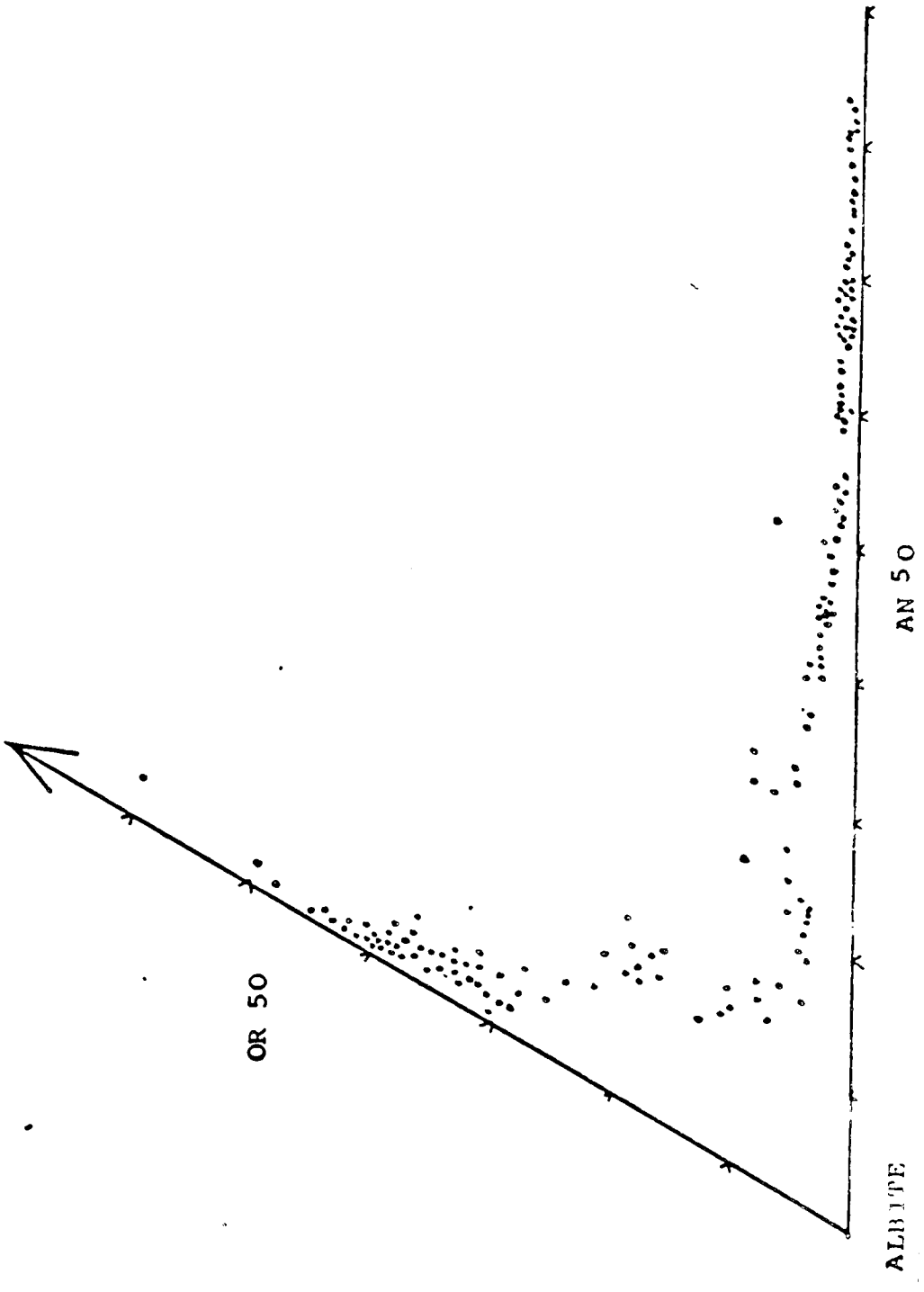


Fig 3.4 Variation in chemistry of groundmass feldspars

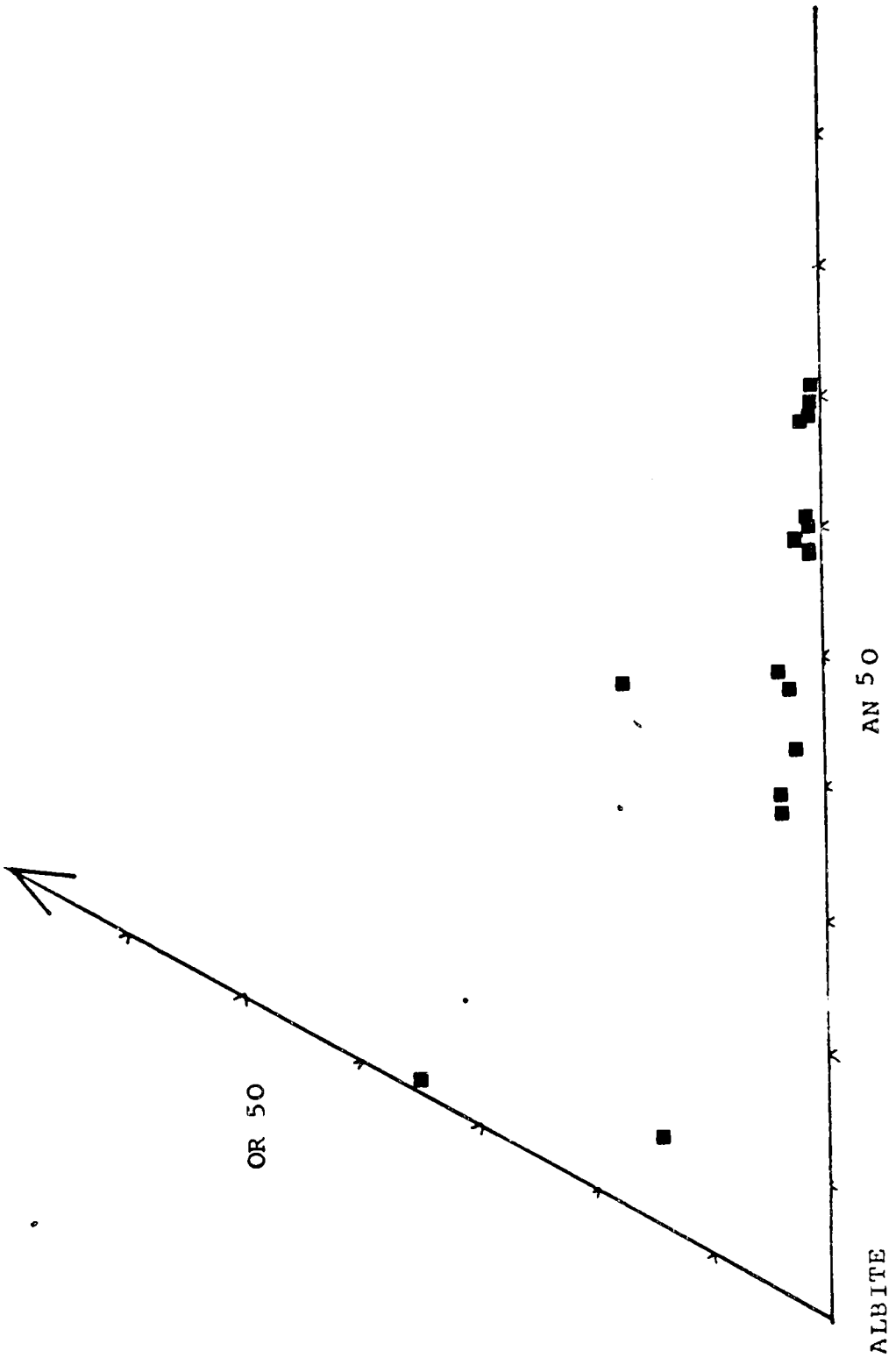


Fig 3.5 Intrasample variation of feldspar macrocrysts

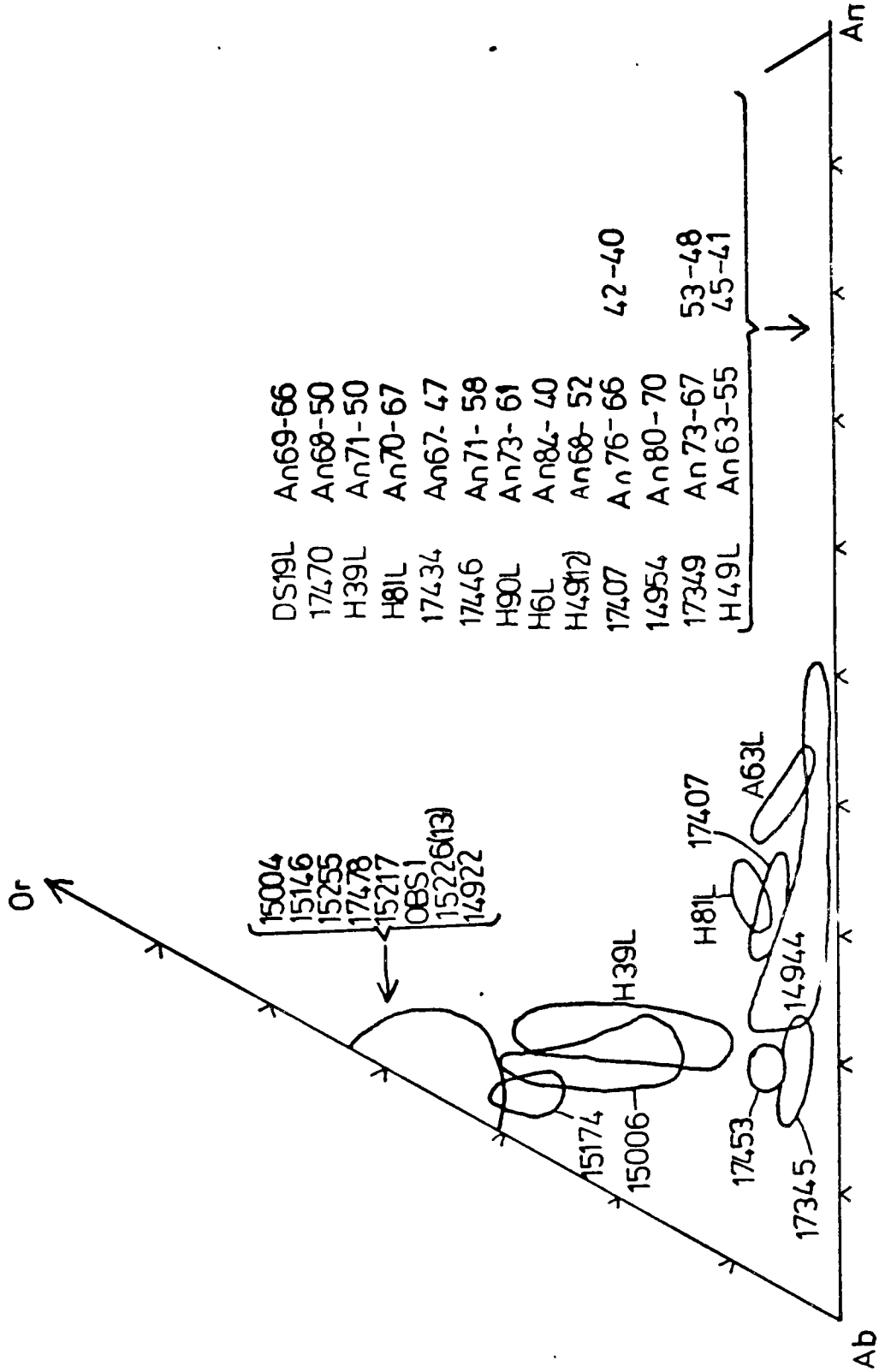
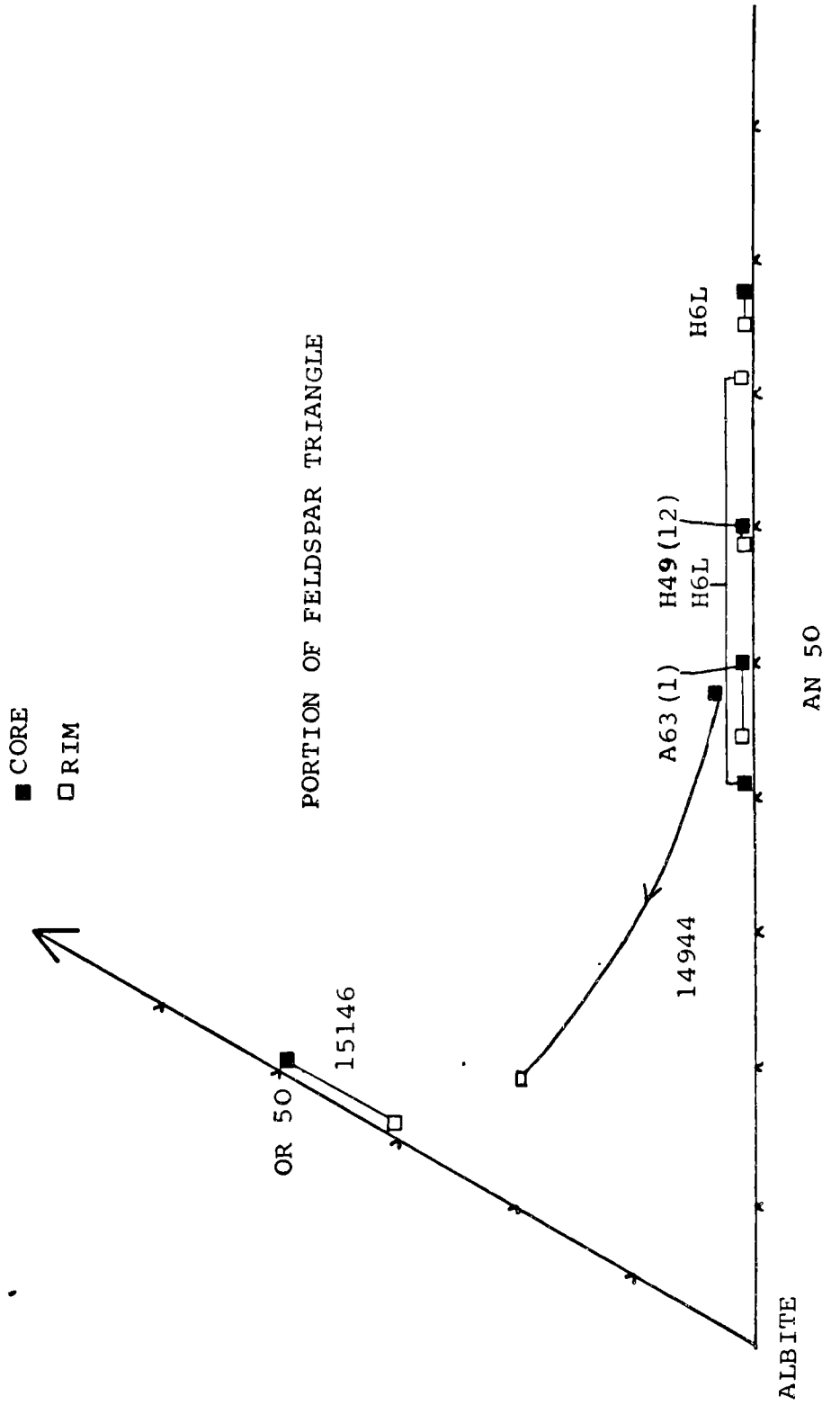
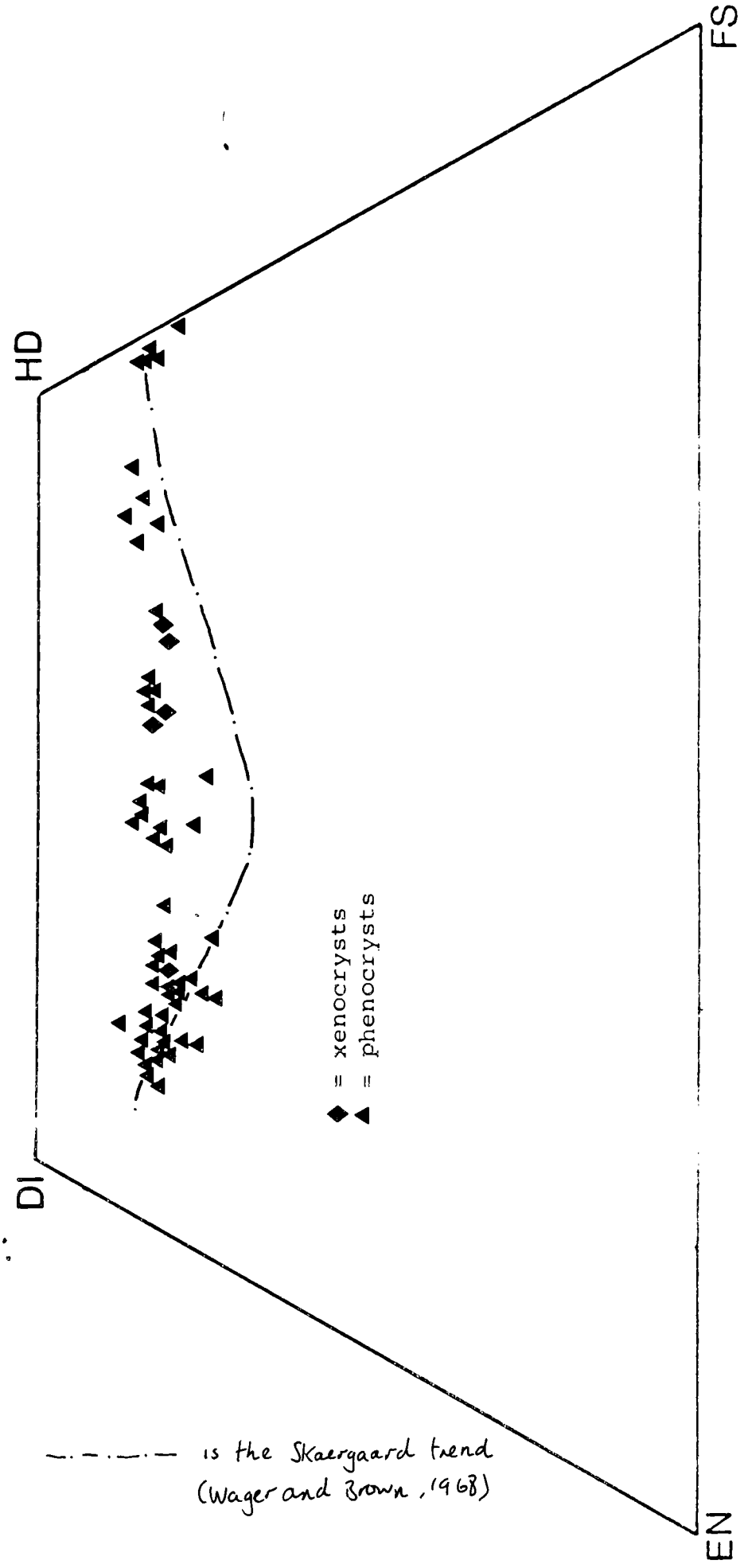


Fig 3.6 ZONING IN FELDSPAR PHENOCRYSTS AND XENOCRYSTS FROM LAVAS



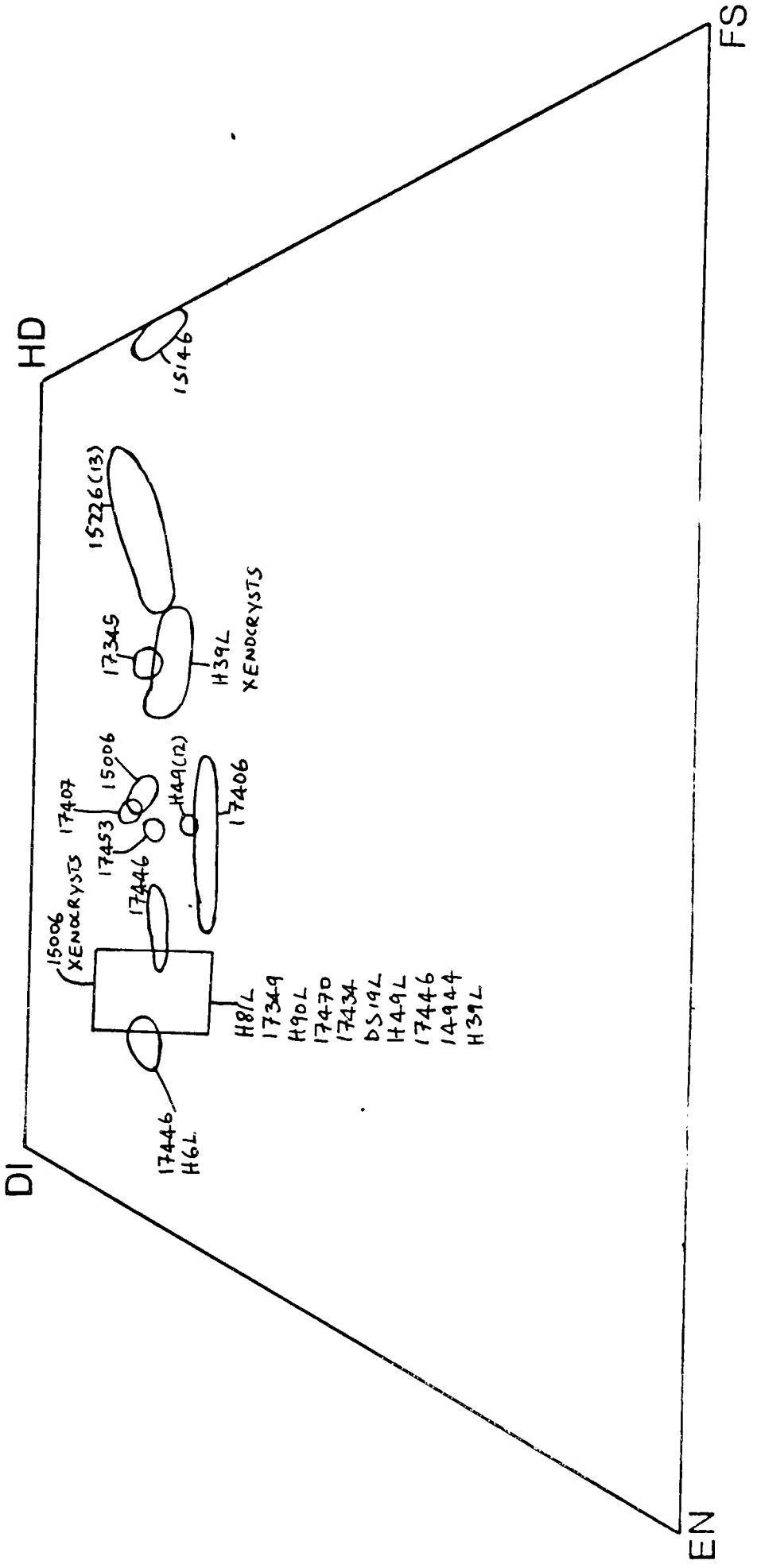
VARIATION IN PYROXENES FROM ASCENSION LAVAS
(phenocrysts and some xenocrysts)

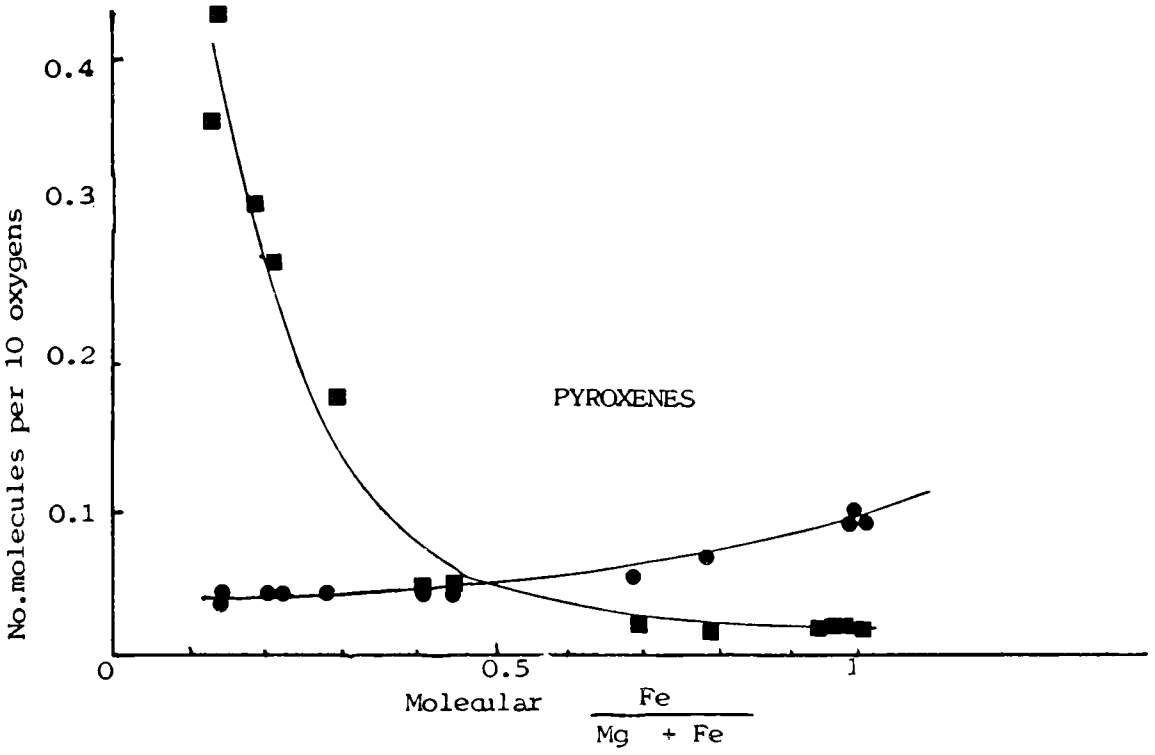
Fig 3.7



INTRA-SAMPLE VARIATION OF PYROXENE ANALYSES FROM LAVAS

Fig 3.8

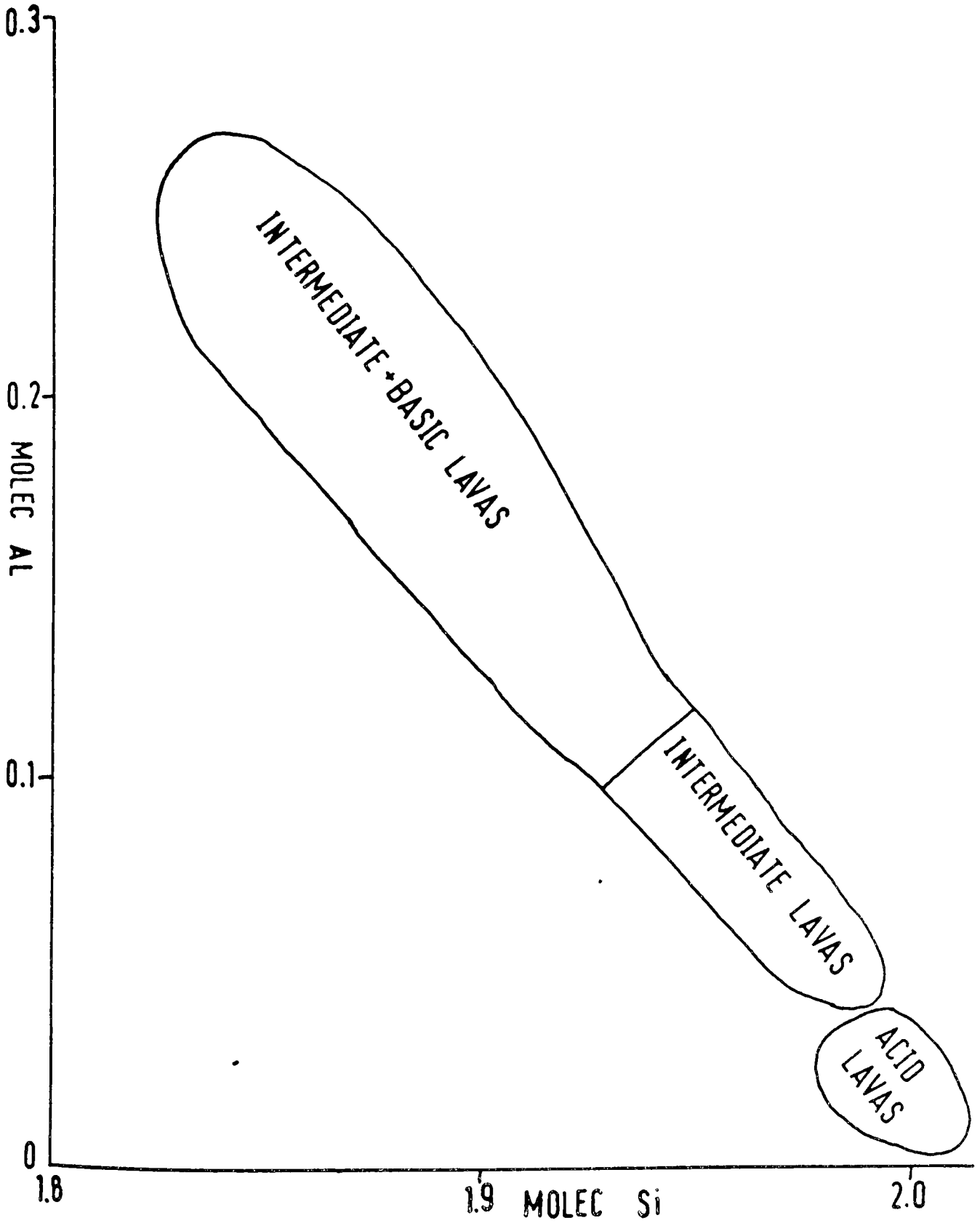




Graph to show variation of Na and Al with $\frac{Fe}{Mg+Fe}$ in lavas

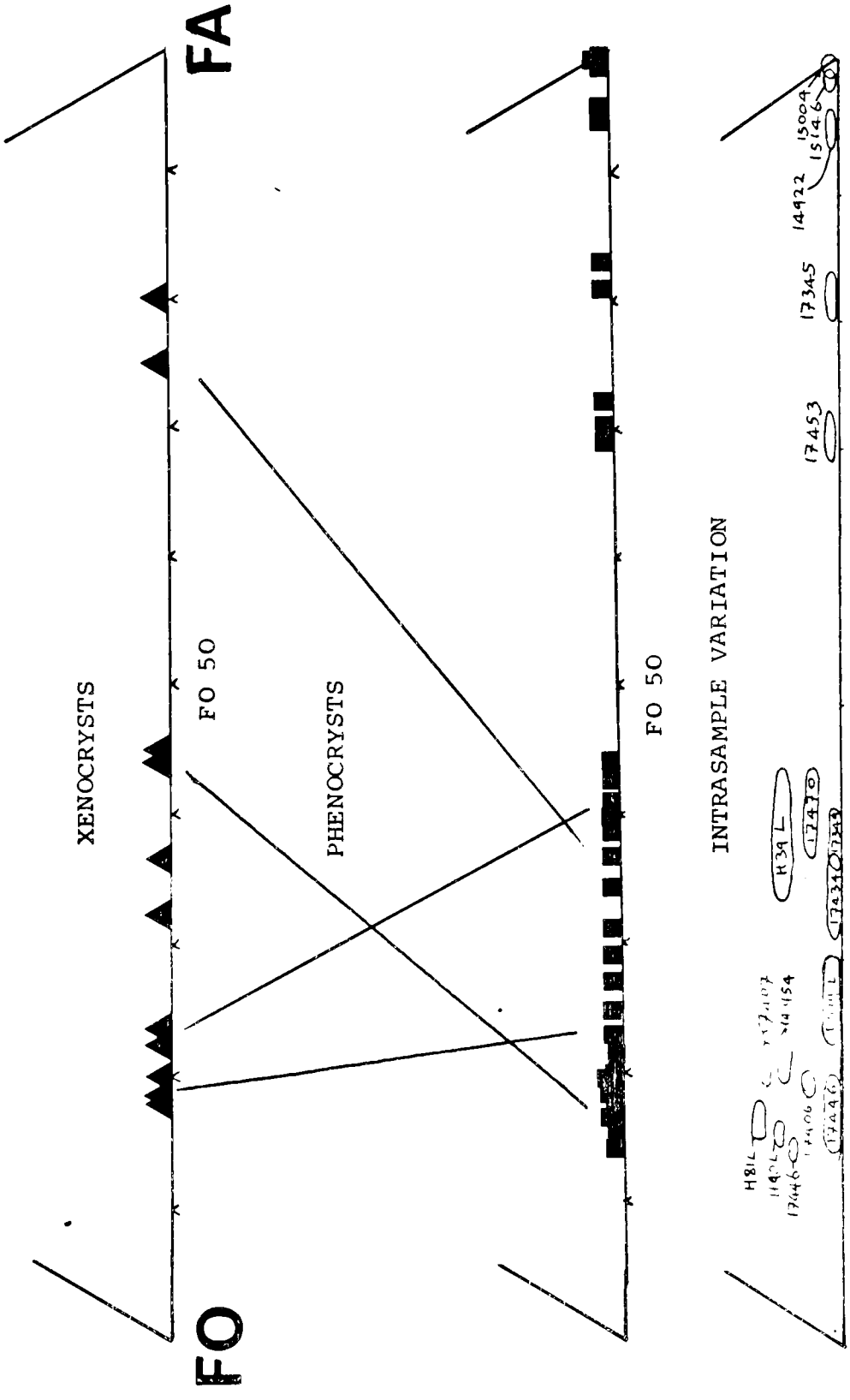
● Sodium
■ Aluminium

Fig 3.10 Molecular Al vs Si in pyroxenes from lavas (assuming 6 oxygens)



VARIATION IN OLIVINE COMPOSITION IN OLIVINE PHENOCRYSTS

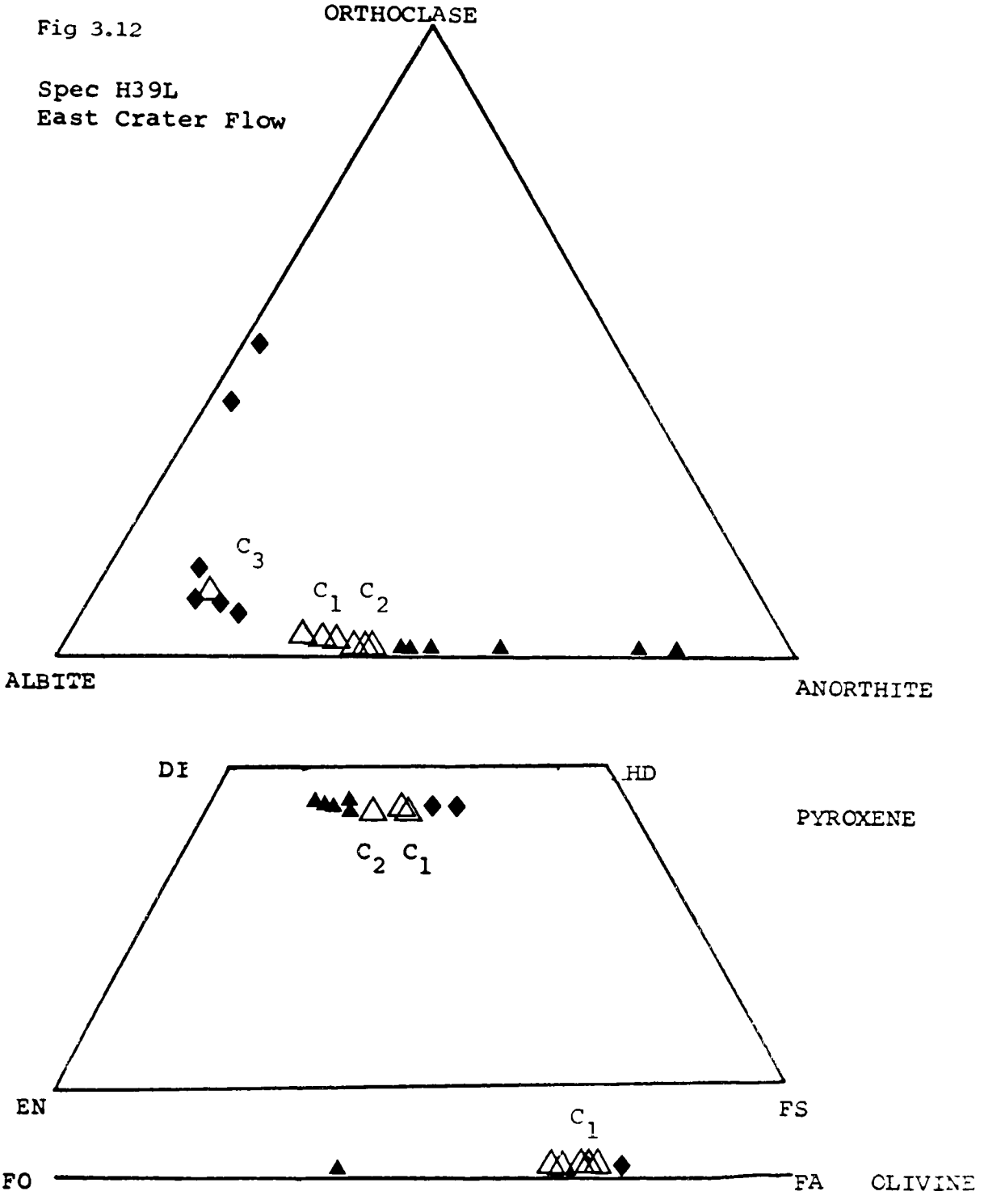
3.11 Tie lines are between phenocrysts and xenocrysts from the same lavas.



COMPOSITION OF PHENOCRYSTS, XENOCRYSTS AND CLUSTERS

Fig 3.12

Spec H39L
East Crater Flow



▲ phenocryst

◆ xenocryst

△ cluster

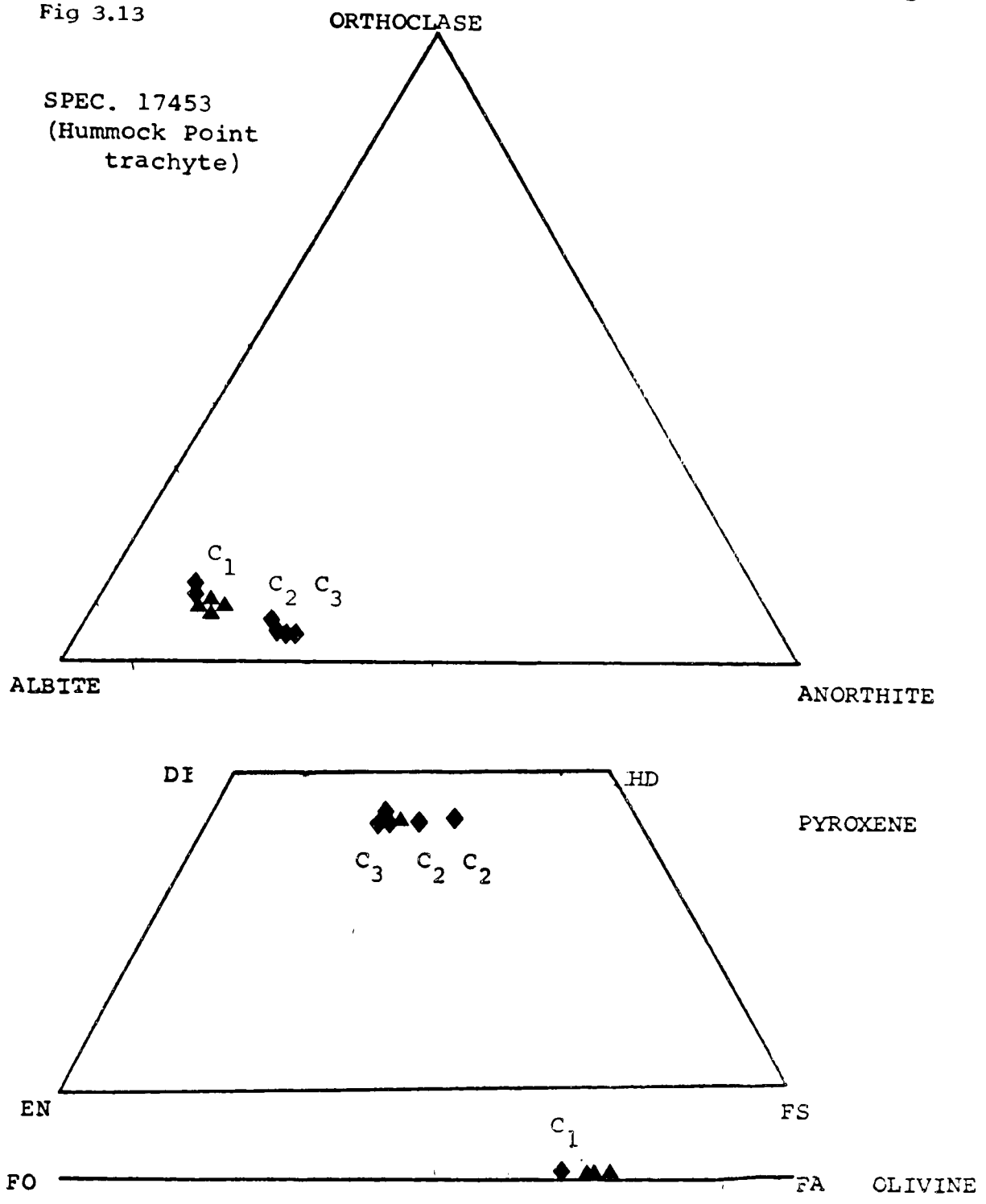
C_1 small (5 grain) cluster

C_2 small (10 grain) cluster

C_3 portion of coarse grained block

COMPOSITION OF PHENOCRYSTS AND GLOMEROPORPHYRITIC CLUSTERS

Fig 3.13



▲ phenocrysts

◆ clusters

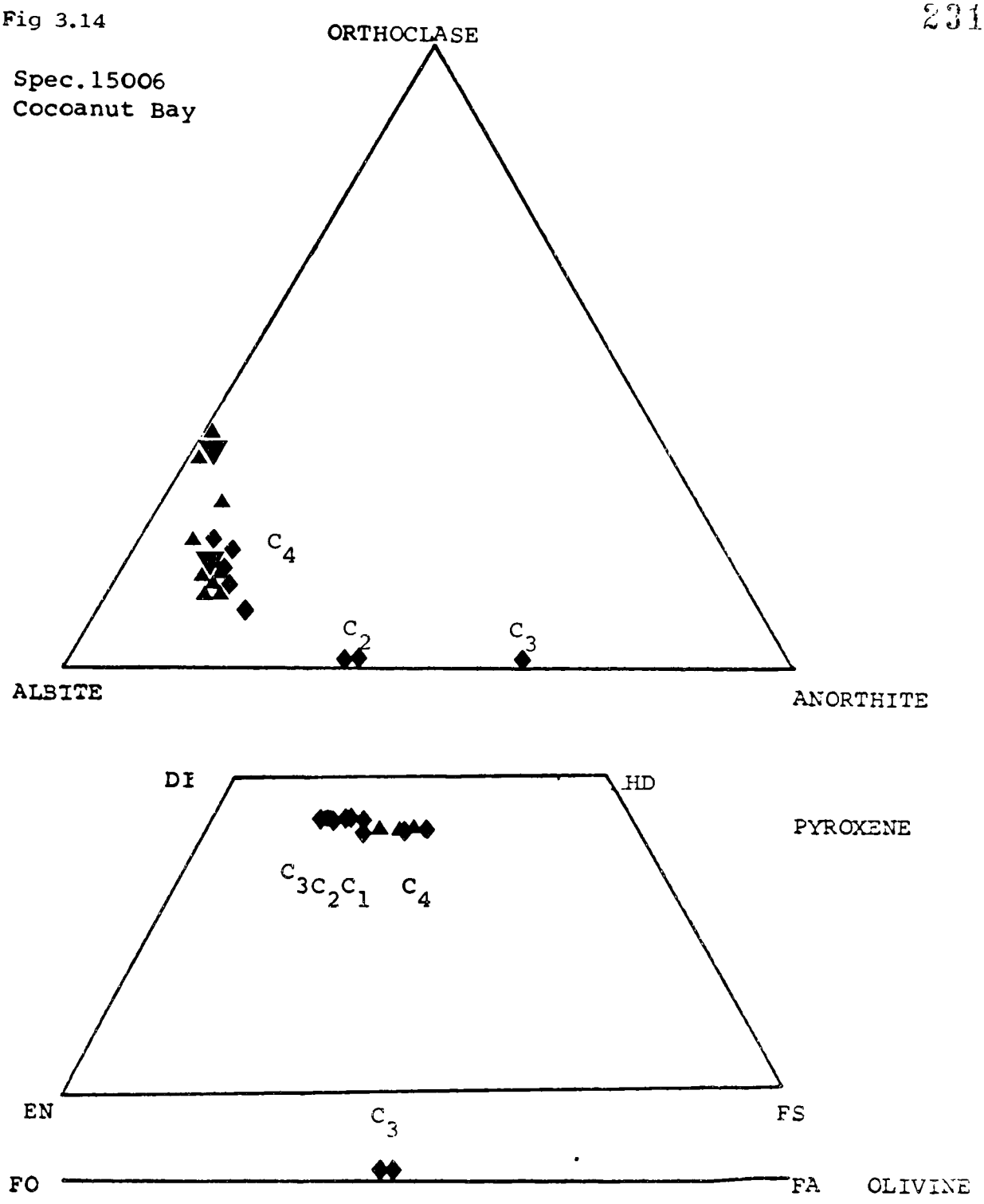
C_1 small cluster

C_2 large cluster

C_3 large cluster

COMPOSITION OF PHENOCRYSTS XENOCRYSTS AND CLUSTERS

Fig 3.14



▼ groundmass

▲ phenocrysts

○ xenocryst

◆ cluster

C_1 small cpx+opaque cluster

C_2 small cluster

C_3 medium cluster (15 grains)

C_4 large (>20 grains) cluster

Plate 3.1 Typical basalt groundmass of plagioclase clinopyroxene olivine and Fe-Ti oxides (14997) . PPL

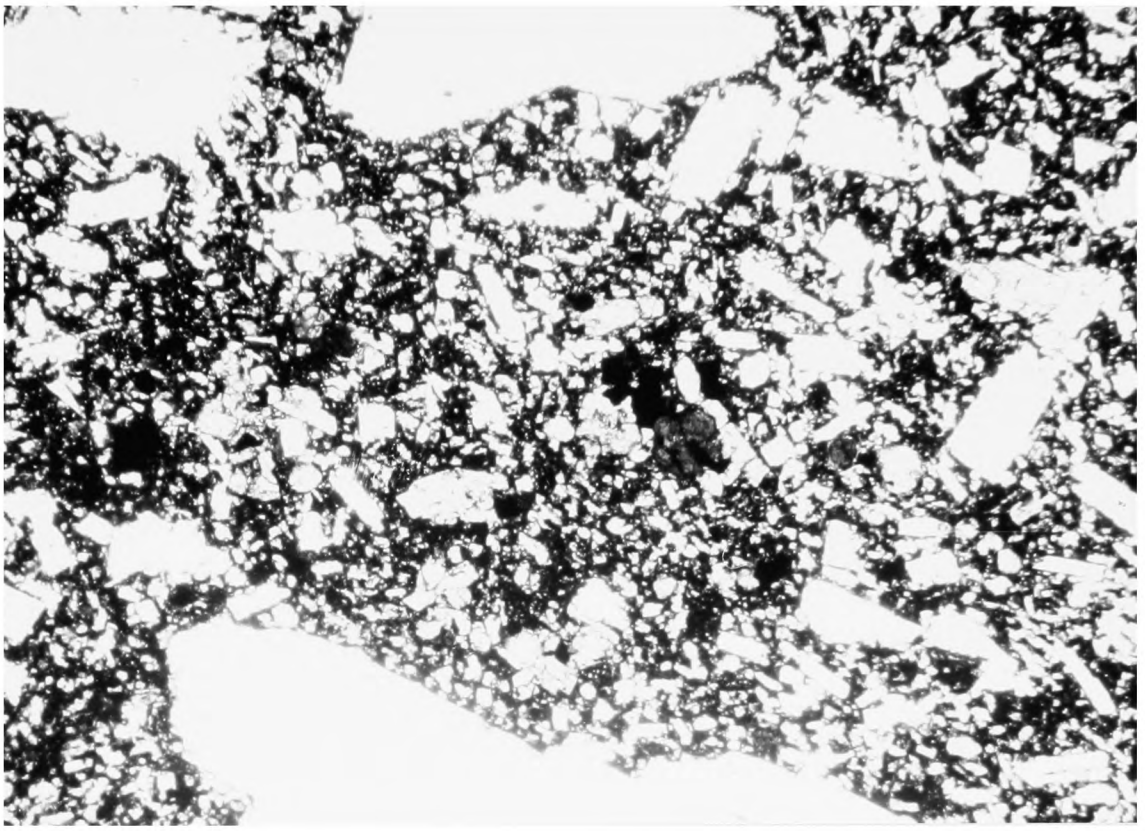
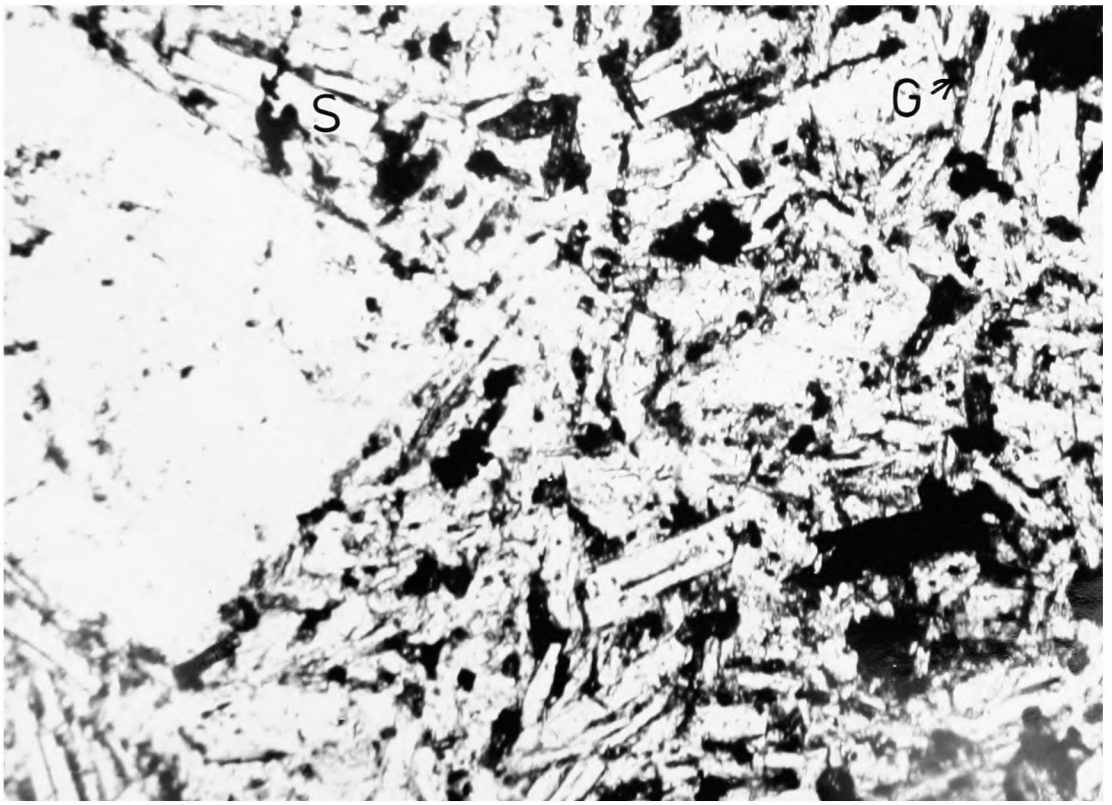
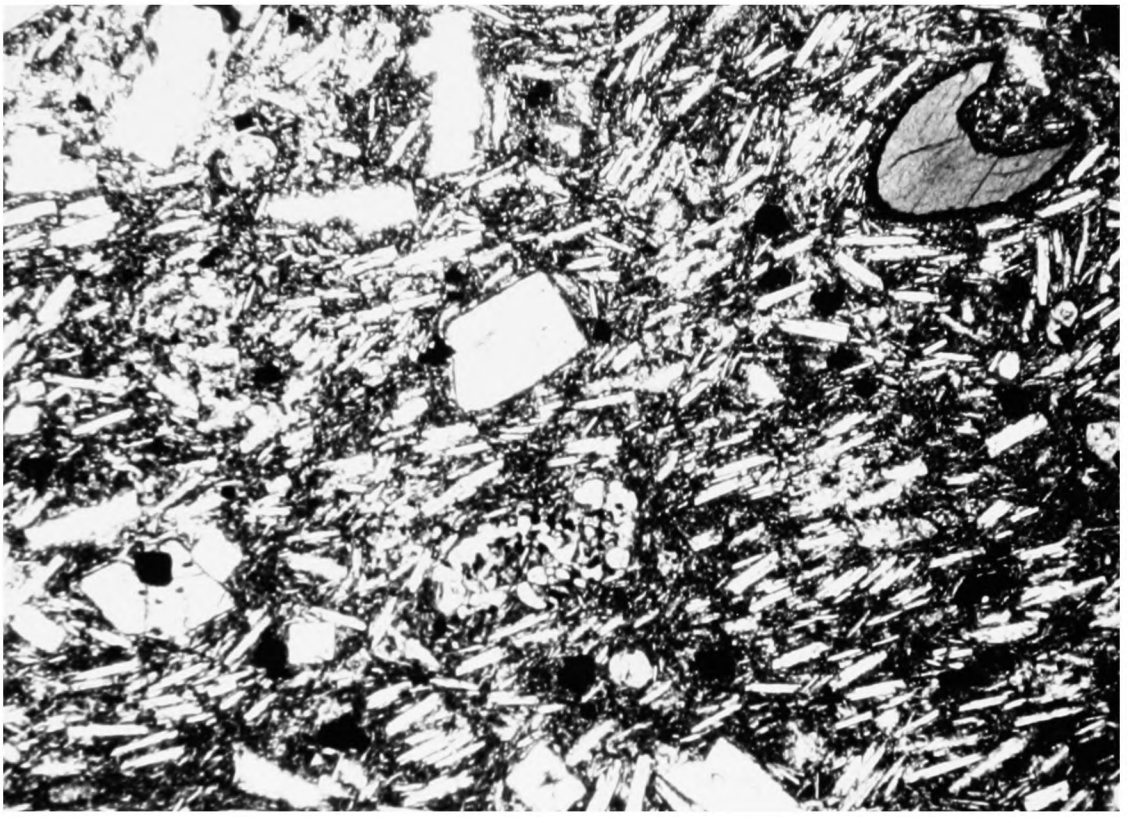
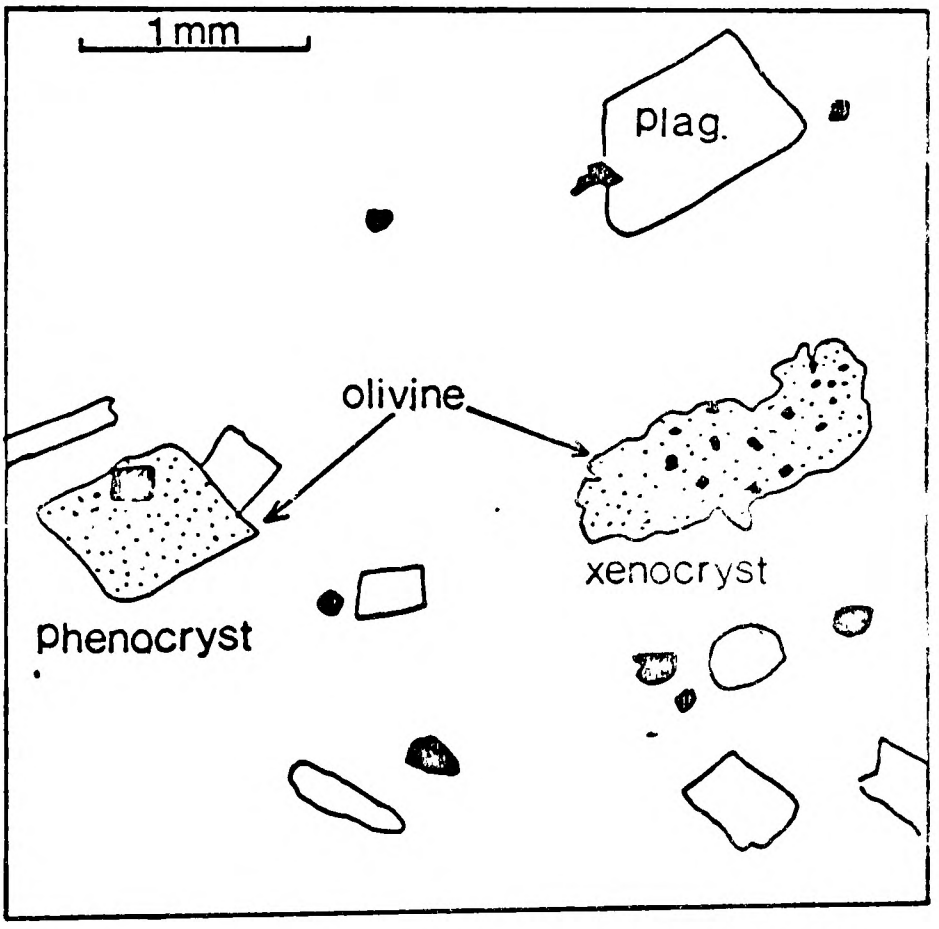


Plate 3.2 Trachyte groundmass with sanidine laths (S) set in glass (G) (17469). PPL







Olivine phenocryst and xenocryst in lava from Devils Ink Stain. (spec.15094)

Plate 3.4 Comendite with sanidine phenocryst (S), ferrohedenbergite phenocryst (F) and flow alignment in the glassy groundmass (15146). PPL

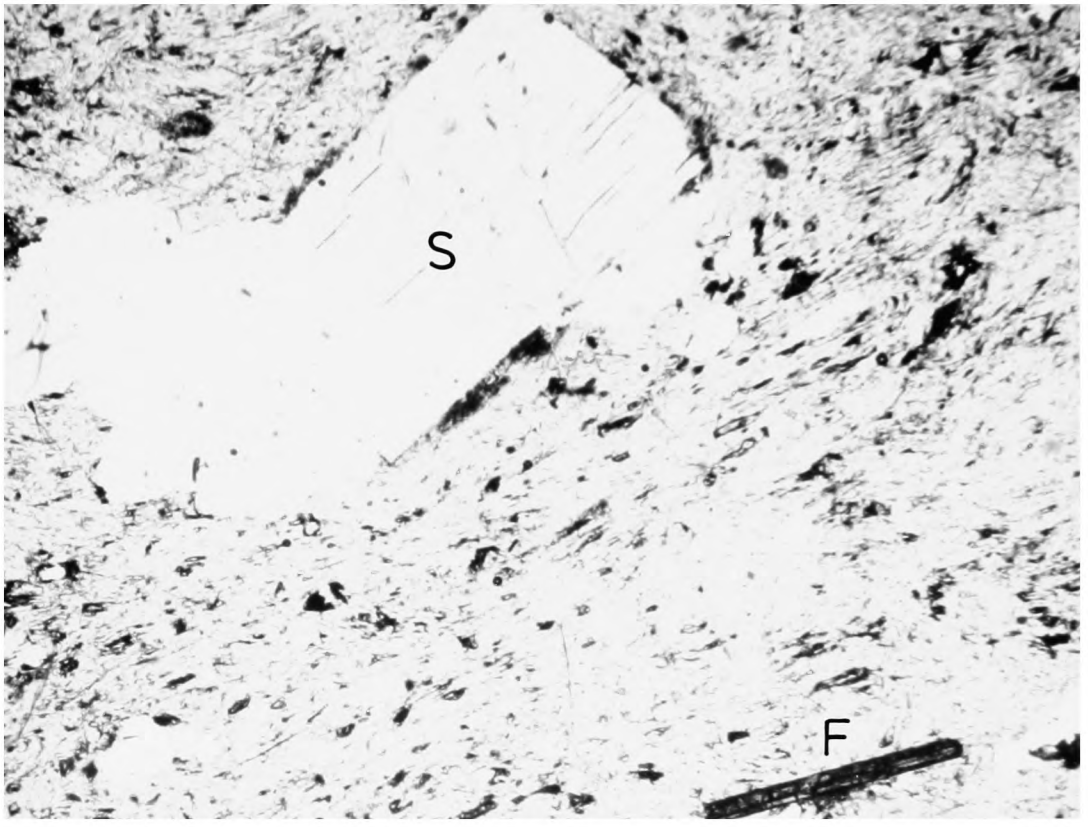


Plate 3.5 Dolerite block from NASA facies (14949). X polars

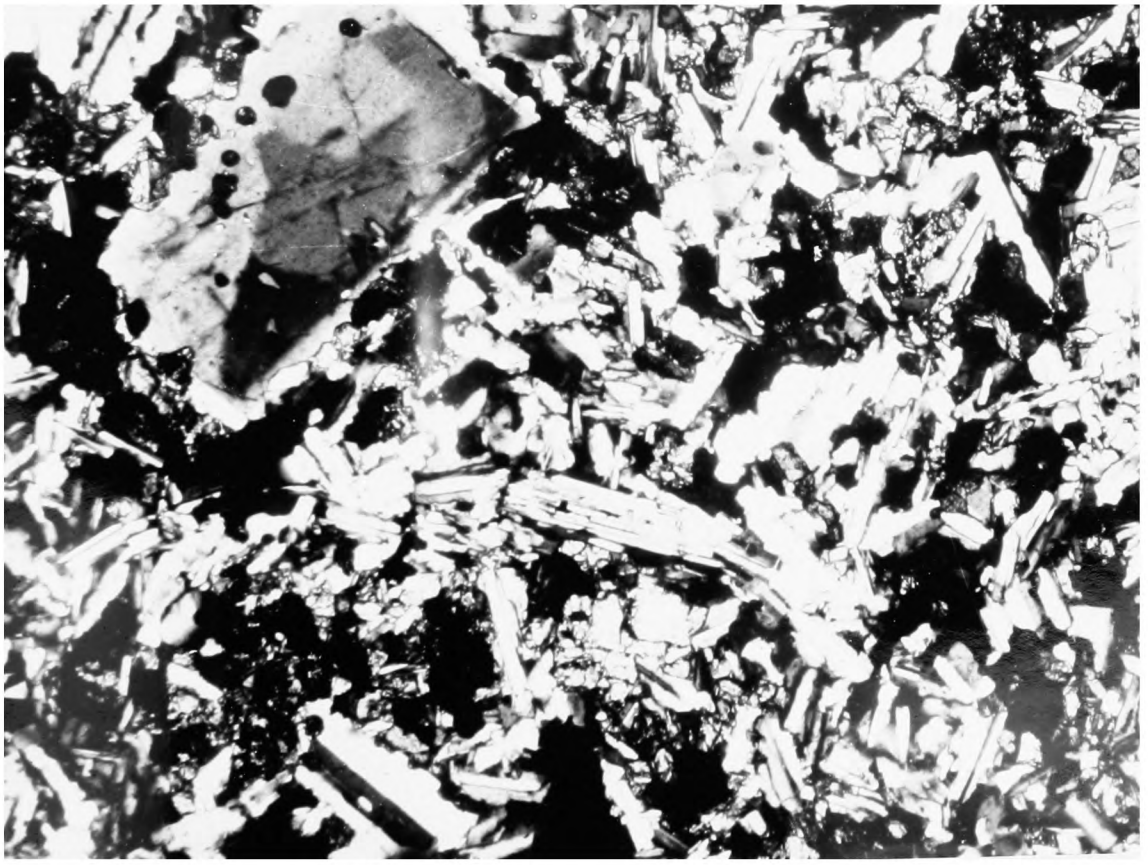


Plate 3.6 Groundmass quartz (Q) surrounding sanidine phenocryst(S) in comendite (17478). X polars

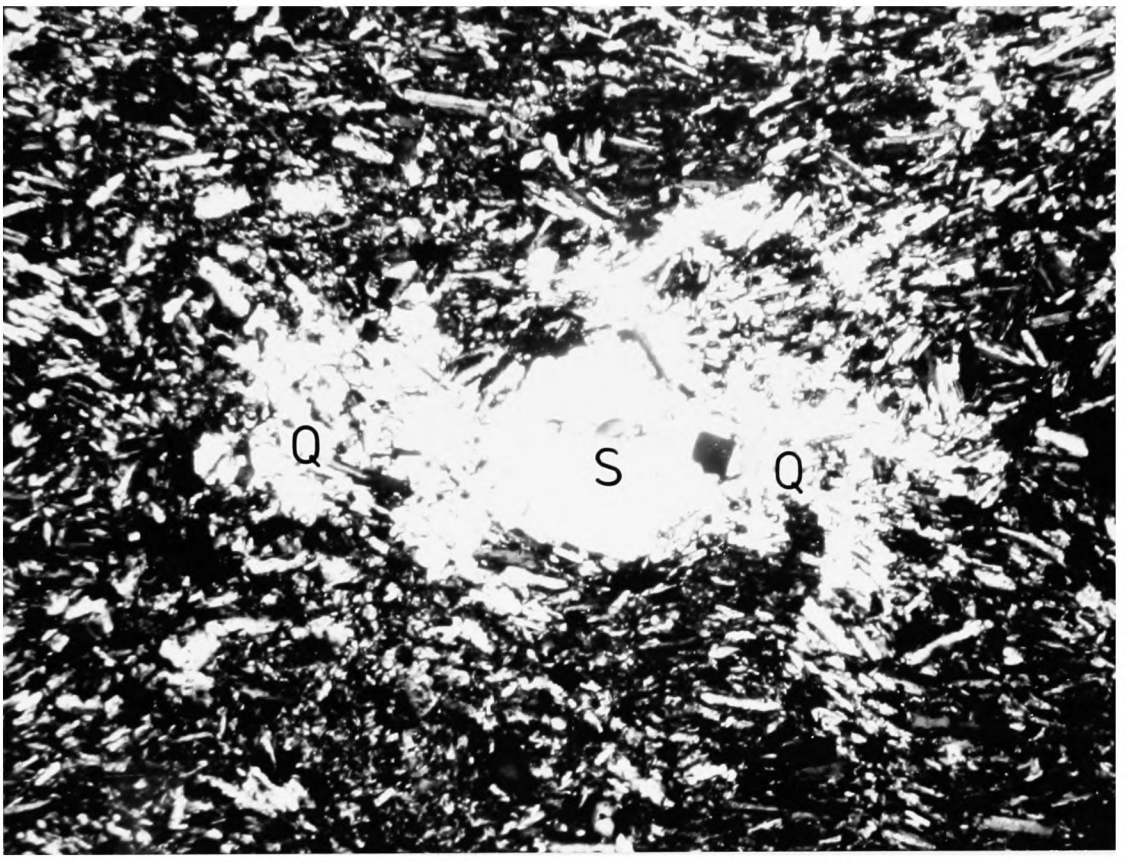
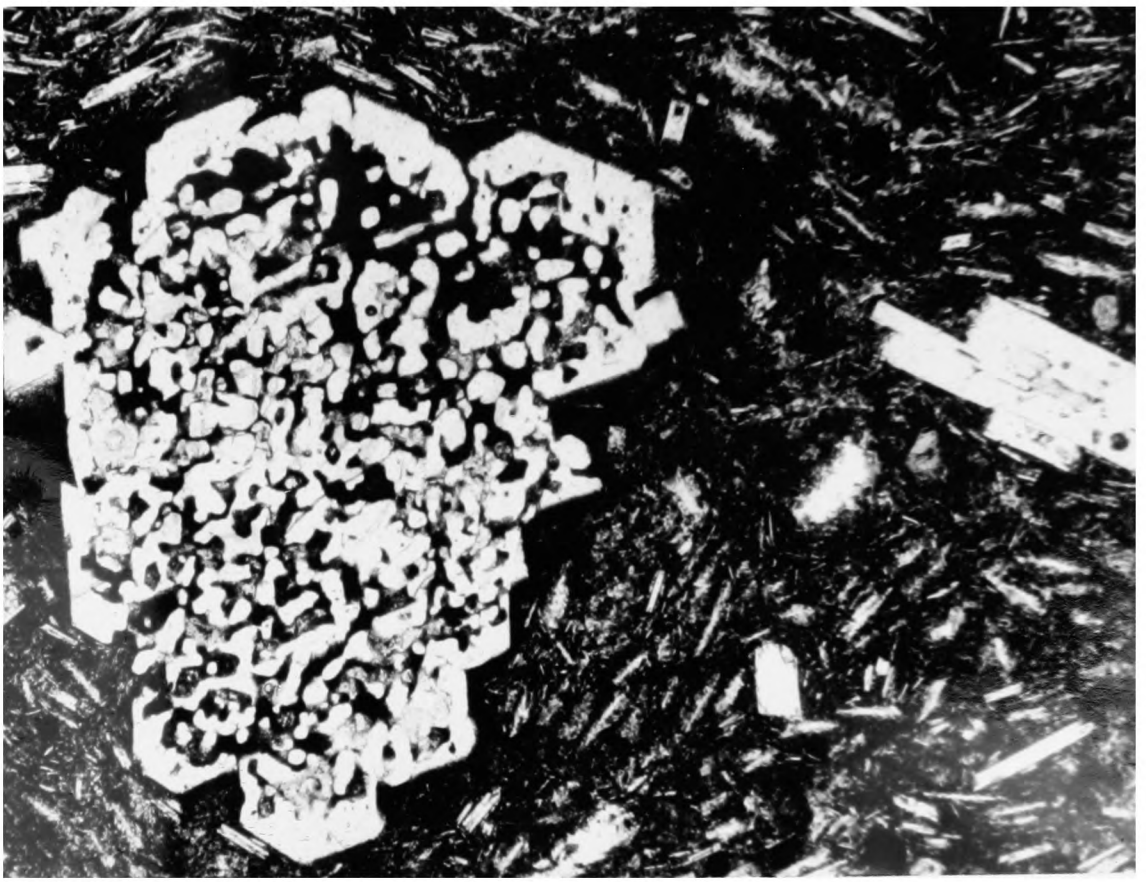
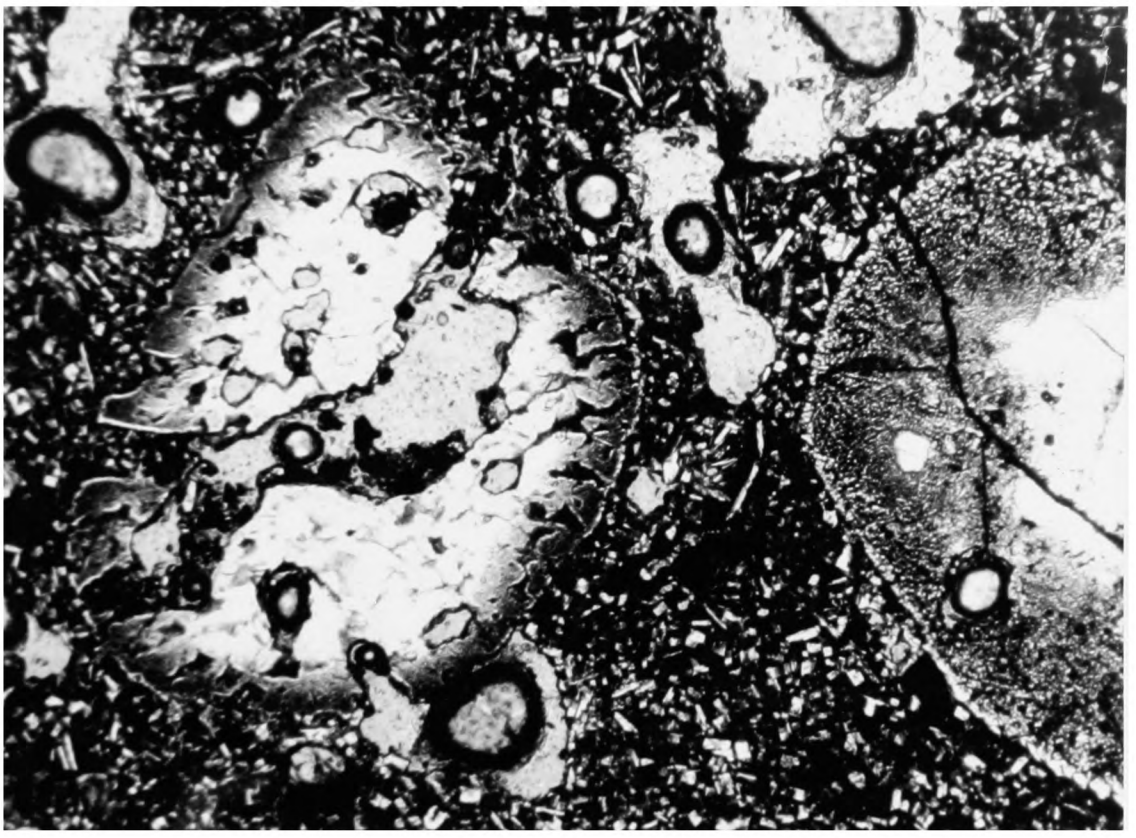
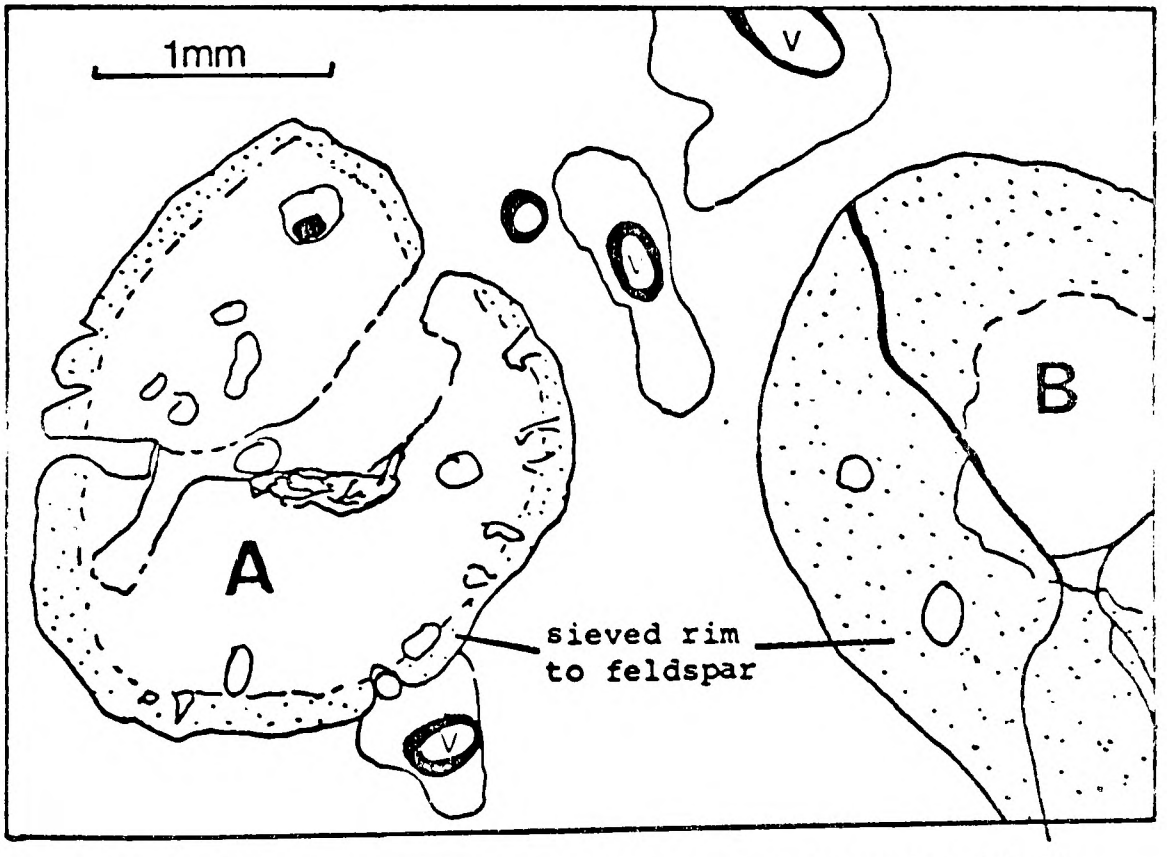


Plate 3.7 Euhederal but embayed macrocryst from trachyandesite lava (A63L). PPL

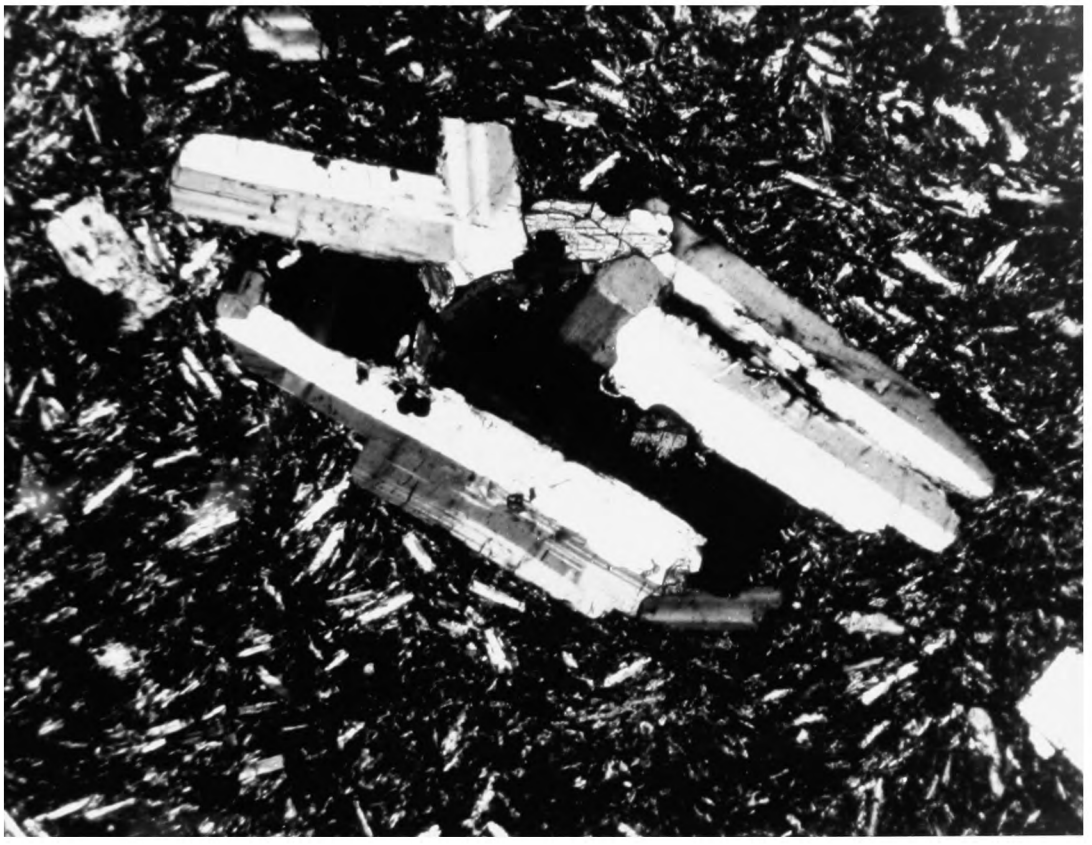




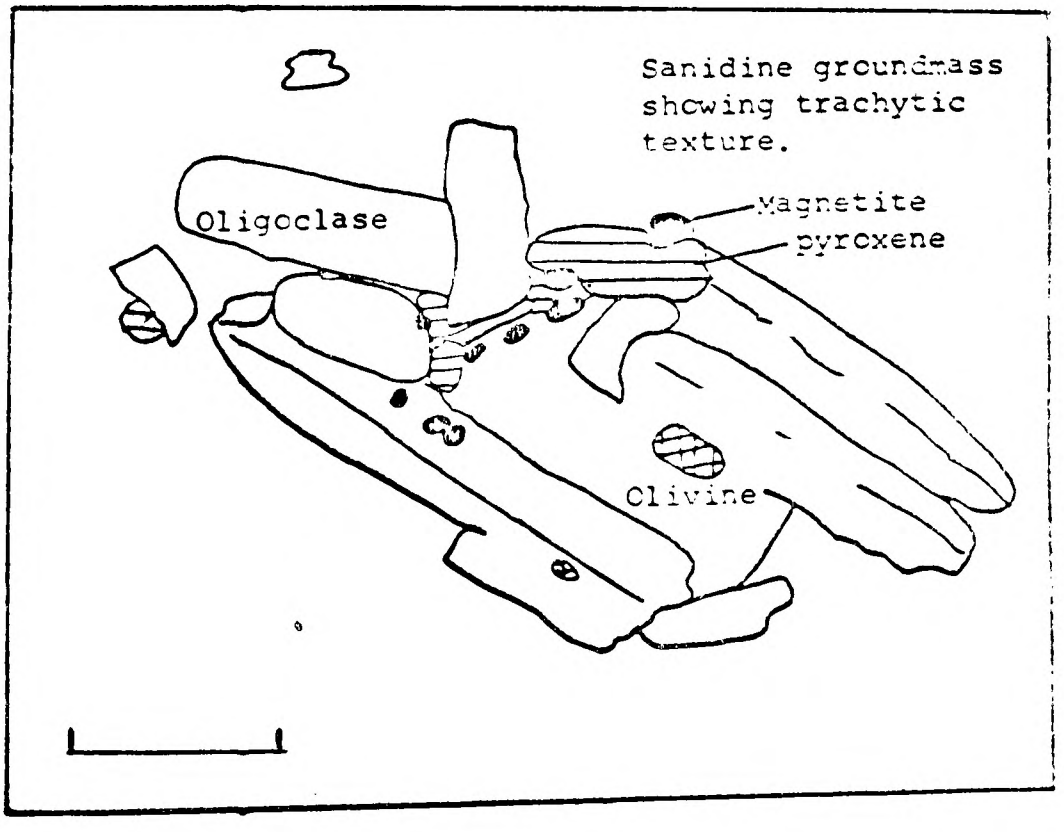


A=anorthoclase xenocryst detached from feldspathic block, of which B is the edge.

(spec. H39L)



Typical cluster in trachyte. Phenocrysts and minerals in the cluster have the same chemical composition. Spec.17345,Little Ascension Flow.





Basalt lava (H49) from Crystal Bay flows with small cumulate xenolith of cumulus plag.and intercumulus augite (bottom part of photo)

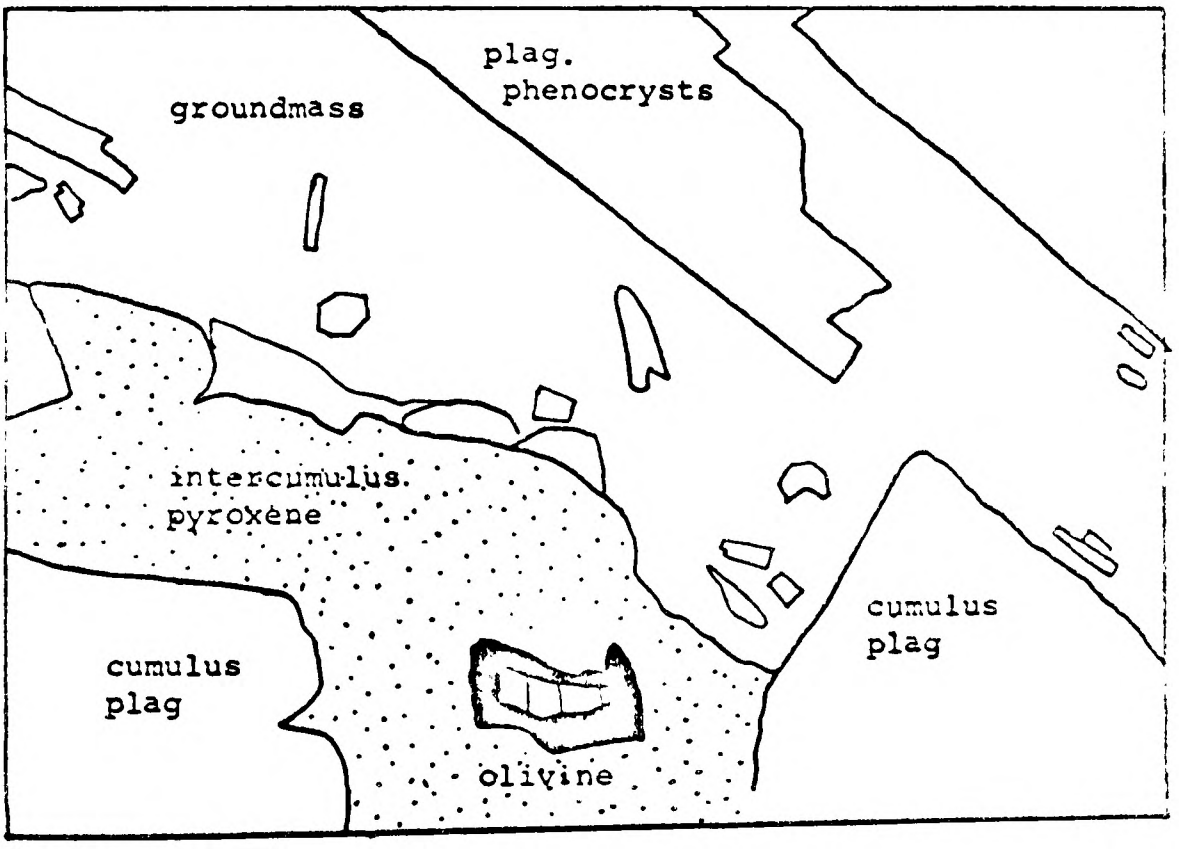
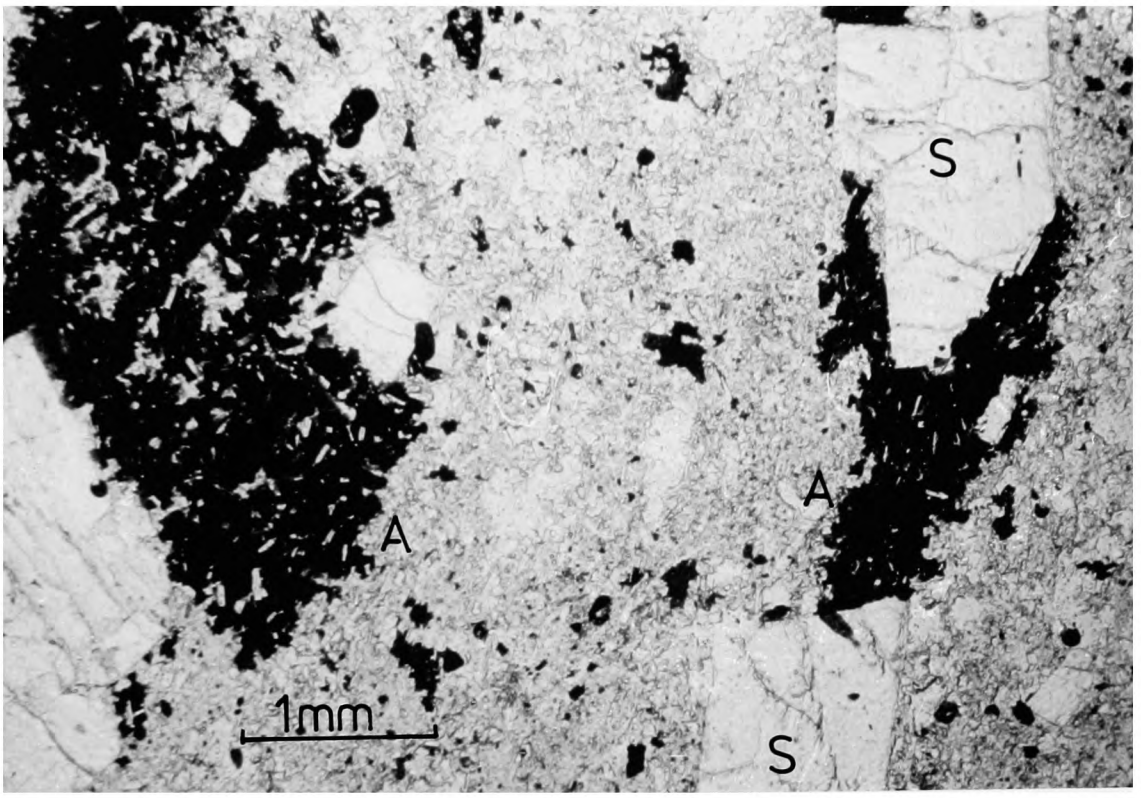


Plate 3.11 Groundmass amphibole (A) in comendite lava. The amphibole is arfvedsonite and clusters around the sanidine phenocrysts (S) (H15231F). PPL



CHAPTER FOUR

TABLES, FIGURES AND PLATES

Table 4.1 Mineralogy of Dark Slope Crater Blocks

	Plag	Cpx	Ol	Opx	Ilm	Mgt	CrSp
DS37	X	X	X				X
DS7	X	X	X				X
DSA3	X	X			X	X	
DS12	X	X	X				
DS1	X	X	X		X	X	
DS5	X	X			X	X	
DS23	X	X	X				
DS22	X	X	X				
15227	X	X	X	X			
DS24	X	X			X	X	
15227(13)	X	X	X	X			
HDSA(5)	X	X			X	X	
15227(4)	X	X	X	X			
15227(VI)	X	X	X	X			
15227(13ii)	X	X	X	X			
HDSA3	X	X	X				
15227(5)	X	X	X	X			
DS56	X	X	X				
DS30	X	X				X	
17317P	X	X	X				
17317N	X		X				

Table 4.2 Opaque oxides in Dark Slope Crater blocks.

	DSA3	DS24	DS 30	HDSA 5	DS 1	DS 5
No. types distinguishable	3	3	1	2	1	1
Quantity	10-15%	30%	1	50-60%	1	1
Texture	Large intercumulus masses	Large cumulus grains	Small rounded grains	Large cumulus grains	Small rounded grains	Small intercumulus shaped grains
Properties in reflected light	(1)White isotropic (2) " anisotropic (3)Red in trans. light	(1)White isotropic (2)Pink +exsoln. &twinning Anisotropic twins	Slightly pink isotropic	(1)White isotropic (2) " anisotropic	White isotropic	Grey/pink isotropic
Exsolution	No	In some grains	No	No	No	No
Minerals	(1)Magnetite$_{ss}$ (2)Ilmenite$_{ss}$	(1)Ilmenite$_{ss}$ (2)Magnetite exolving ilmenite	Magnetite$_{ss}$ (2)Ilmenite$_{ss}$	(1) Magnetite$_{ss}$ (2)Ilmenite$_{ss}$	Ilmenite$_{ss}$ +Magnetite$_{ss}$ identical in ref.light	

Table 4.3 Mineralogy of Blocks from Cones

	Estimated Modes				
	PL	PX	OL	OP	Notes
H83(6)	65	25		10	Partial melting, altered.
H83(10)	60	10	-	35	Opaques = altered olivine
H83(12)	85	altered			Zoned Fsp, some partial melting
H83(14)	85	10	2	3	Comparatively fresh
H95(5)	80	15	-	5	Fresh but broken up
H95(7)	50	35	<1	15	Possible fine-scale layering
H95(16)	65	10	20	5	Fresh; intercumulus olivine
H3	65	15	20	-	Fresh but very broken up

Table 4.4 Petrography of Blocks from Green Mountain

	Main Minerals	Textures
15243(B)	Plag/Cpx/Ol/Mgt	)
15254-1	Plag/Cpx/Ol/Mgt/Ap	) Probed. Identical to Middleton's gabbros.
A44B	K Fsp/Qz	Highly altered.
A44(2)	K Fsp/Qz	Very highly altered.
A44(1)	Plag/bi/op	Highly altered.
A42(1)	Plag/Cpx/Ol/Op/zirc	Mafics altered to biotite.
15243A	Plag/Cpx/amph/bi/op	Slight amount of melting.
15243C	Plag/Cpx/amph/bi/ap	Mafics altered to amphibole and biotite
15243D	Plag/Cpx/amph/bi	No melting
15368a	Plag/ol	Partial melting (see Plate 4.23).
15368b	Plag/Cpx/op	Some partial melting.

Table 4.5 Petrography of Middleton's Syenites and Monzonites

	Qz	Plag	KFsp	Amph	Bi	Cpx	Zirc	Ap	Op	Ol	Notes
H15226(1)	X	X	X	X	X		X	X	X		
15226(17)	X	X	X	X	X	X	X	X	X		
15226(15)	X		XP		X	X			X	X	
15226(4)	X	X	XP	X	X	X	X		X	X	Z
15226(14)	X		XP	X			X		X		
15226(2)	X		XP	X	X		X		X		
15226(9)	X	X	XP	X	X	X	X		X		
15226(12)	X		XP	X	X	X	X		X		G
15226(8)	X		XP	X	X	X			X		G
15226(6)	X		XP	X		X			X	X	
15226(7)	X		XP			X			X		A
15226(5)	X		X		X	X	X		X		A+G
79949	X	X	X	X	X		X		X		Z
15226(12a)	X	X	XP	X	X		X		X		
71725	X		X	X				X	X		

Notes

P = Perthite

G = Granophyric veins

A = Aegirine rim to pyroxene

Z = Zoned feldspar with clear cores and inclusion filled rims.

Table 4.6 Aegirine-Augite Analyses from Five Mile Post Granites

	1	2	3	4
SiO_2	54.00	53.41	52.05	52.12
TiO_2	5.32	1.13	1.93	5.79
Al_2O_3	0.29	0.34	0.68	0.24
Fe_2O_3	22.13	30.77	28.51	22.20
FeO	5.15	0.88	1.88	5.05
MnO	0.42	0.88	0.46	0.81
MgO	0.02	0.08	0.05	0.02
CaO	0.68	0.18	0.29	0.80
Na_2O	13.30	13.45	13.71	13.14
K_2O	0.01	-	0.02	-
Total	101.20	101.12	99.58	100.17
		(+0.92 ZrO_2)		
			Six oxygens	
Si	2.13	2.17	2.14	2.09
Al	-	-	-	-
Al	0.01	0.02	0.03	0.01
Ti	0.17	0.03	0.06	0.17
Fe_{3+}	0.65	0.94	0.88	0.67
Fe_{2+}	0.17	0.03	0.06	0.17
Mn	0.01	0.03	0.02	0.02
Mg	-	-	-	-
Na	1.01	1.06	1.09	1.02
Ca	0.03	0.01	0.01	0.03
K	-	-	-	-

1 - Ti-rich (H17318P), 2 - H17318F, 3 - H15231(5), 4 - Ti-rich (H17318)

Table 4.7 Aenigmatite Analyses - Five Mile Post Granites

	H30(3)	H30(3)	*Picture Gorge	H17318F
SiO_2	41.83	41.02	40.70	42.56
TiO_2	8.29	8.28	8.70	8.55
Al_2O_3	0.15	0.55	0.29	0.55
FeO^T	38.47	39.48	41.50	38.58
MnO	2.76	2.39	0.44	2.43
MgO	0.05	0.05	0.55	0.03
CaO	0.11	0.35	0.31	0.12
Na_2O	7.36	7.10	6.8	7.42
K_2O	0.01	0.02	-	0.01
ZrO_2	0.03	-	-	-
	99.06	99.24	99.30	100.25
		Twenty [O]		
Si	6.05	5.96	5.96	6.05
Al	-	0.04	0.04	-
	(6.05)	[6.00]	(6.00)	(6.05)
Al	0.02	0.05	0.01	0.01
Fe^{2+}	4.65	4.78	4.90	4.58
Ti	0.90	0.90	0.96	0.91
Mg	0.01	0.01	0.12	-
Mn	0.34	0.29	0.06	0.29
Ca	0.02	0.05	-	0.02
	(5.94)	(6.08)	(6.05)	(5.81)
Ca	-	-	0.05	-
Na	2.06	2.00	1.93	2.04
K	-	-	-	-
	(2.06)	(2.00)	(1.18)	(2.04)

* From Picture Gorge Pegmatoids (Lindsley et al., 1972)

Table 4.8 Localities with Single Specimens

Locality	Spec. No.	Block Type
Wighill	H33(1)	Plag-cpx-gabbro, very like S. Coast blocks
Powers Peak	H53L	Small fragment (½ cm) in basalt-syenite-gabbro
Hammock Pt.	H79	Very small, (1 cm) microgabbro
Bear's Back		Small fragment identical to Middleton's gabbro in palagonite tuff.
Devil's Cauldron	H91	Altered ?syenite
Dampiers	H41	V. Altered ?syenite
Little White Hill	A36	V. small, gabbroic block

Table 4.9

Estimated modal proportions of sections of pegmatoid analysed by microprobe

	17428 B	H59 B	H59 (1,2)
Clinopyroxene	15	15	10
Fe-Ti oxide	15	25	15
Plagioclase	40	40	40
K-feldspar (+ intergrowth with silica)	27	15	31
Olivine	< 1	-	-
Apatite	3	5	3
Silica in vugs	-	-	<1

N.B. Slides H59 (1) and H59 (2) are from the same piece of pegmatoid

Table 4.10 Representative analyses of feldspar from the pegmatoid.

	1	2	3	4	5	6
SiO_2	60.29	64.35	63.79	64.49	68.14	66.34
TiO_2	0.13	0.06	0.09	0.07	0.09	0.04
Al_2O_3	25.05	21.66	22.09	21.54	18.78	18.24
FeO	0.43	0.33	0.39	0.35	0.35	0.32
MnO	0.01	0.00	0.00	0.03	0.00	0.01
MgO	0.08	0.02	0.02	0.02	0.00	0.00
CaO	7.42	3.47	5.05	3.10	0.24	0.03
Na_2O	6.50	8.50	2.54	8.16	6.13	5.65
K_2O		2.02	2.02	3.07	7.75	9.77
TOTAL	100.68	100.42	100.99	100.83	101.48	100.29
			8 oxygens			
K	0.04	0.11	0.11	0.18	0.44	0.52
Na	0.56	0.73	0.65	0.70	0.52	0.49
Cu	0.35	0.16	0.24	0.14	0.01	0.02
Si	2.67	2.85	2.82	2.86	3.01	3.01
Al	1.31	1.13	1.13	1.12	0.98	0.97

Key to analyses

1 Cone of framework feldspar (group A)
2 Rim of framework feldspar (group A)
3 Feldspar from pyroxene/feldspar intergrowth (group B)
4 Feldspar from pyroxene/feldspar intergrowth (group B)
5 Core of small euhedral feldspar (group C)
6 Rim of small euhedral feldspar (group C)

Table 4.11 Representative pyroxene analyses from the pegmatoid.

	1	2	3	4	5	6
SiO_2	52.20	51.52	50.91	50.45	50.77	51.17
TiO_2	0.94	1.15	0.40	0.81	0.75	0.03
Al_2O_3	1.33	1.54	1.16	0.98	0.93	0.72
FeO	13.93	13.73	15.83	16.43	18.41	18.97
MnO	0.46	0.39	0.49	0.59	0.62	0.79
MgO	13.81	12.83	10.05	10.03	8.45	0.81
CaO	17.45	18.46	19.86	19.69	19.14	18.87
Na_2O	0.31	0.30	0.30	0.34	0.48	0.40
K_2O	0.00	0.02	0.00	0.18	0.05	0.59
	6 oxygens					
Si	1.97	1.95	1.97	1.95	1.97	1.99
Al	0.06	0.07	0.05	0.05	0.04	0.03
Ti	0.02	0.03	0.02	0.02	0.02	0.02
Fe	0.44	0.43	0.51	0.53	0.60	0.61
Mg	0.74	0.73	0.52	0.58	0.52	0.51
Ca	0.73	0.75	0.82	0.82	0.78	0.79
Na	0.02	0.02	0.02	0.02	0.02	0.03

Key to analyses

1 Framework pyroxene (group A)
2 Framework pyroxene (group A)
3 Rim to framework pyroxene (group B)
4 Rim to framework pyroxene (group B)
5 Small pyroxene next to silica filled vug (group C)
6 Small pyroxene next to silica filled vug (group C)

Table 4. 12

Aegirine-augite Analyses from the Pegmatoid Section 17428 B

SiO_2	53.06	52.87	52.49	53.55	51.64
TiO_2	0.72	0.70	0.35	0.88	0.85
Al_2O_3	0.26	0.28	0.35	0.31	1.09
Fe_2O_3	13.62	5.89	4.20	13.73	0.70
FeO	9.82	12.62	13.78	8.97	16.08
MnO	0.63	0.53	0.63	0.64	0.50
MgO	5.24	8.58	7.58	5.87	9.88
CaO	13.19	17.93	17.56	13.00	19.42
Na_2O	5.28	2.25	1.90	5.28	0.32
K_2O	0.01	0.00	0.00	0.00	0.01
TOTAL	101.71	101.13	101.26	102.22	100.52
			6 oxygens		
Si }	2.07	2.03	2.03	2.07	1.98
Al }					0.02
Al)	0.01	0.01	0.02	0.01	0.03
Ti	0.02	0.02	0.01	0.02	0.02
Fe^{3+}	0.40	0.17	0.14	0.40	0.02
Fe^{2+}	0.32	0.39	0.51	0.29	0.51
Mn	0.02	0.02	0.02	0.02	0.02
Mg)	0.31	0.49	0.44	0.34	0.56
Na)	0.40	0.17	0.14	0.40	0.02
Ca	0.55	0.74	0.73	0.54	0.80
K)	-	-	-	-	-

Analyses by microprobe

Fe_2O_3 calculated assuming charge balance, i.e. Molec. $Fe^{3+} = Na^+$

Table 4.13 Five Mile Post Probe Sections

No.	Zircon				No. of grains vlasovite or dalyite*	Petrography Notes
H30(3)	✓	✓			C	aeg/arfv perthite
H30(1)			✓	✓	C	aeg/arfv perthite
17318P	✓		✓	✓?	R	aeg/arfv perthite
H17318F			✓		R	aeg/arfv perthite
17318B			✓		R	aeg/arfv perthite + granophyre
15231D		✓			R	aeg/arfv perthite + granophyre
15231A	✓				-	non-perthitic, fine grained in places
15231(5a)		✓			M	aeg/arfv perthite + granophyre
15231(6)	✓**	✓			C	aeg/arv perthite
15231b	✓	✓			R	aeg/arfv perthite
K17318	✓		✓		M	aeg/arfv perthite
15231(5b)		✓			R	aeg/arfv perthite + granophyre
L17318(1)		✓			R	aeg/arfv perthite
L17318(11)		✓			R	aeg/arfv perthite + Ol
H15231(6)	✓**	✓			M	aeg/arfv perthite
H15231(5)	✓	✓			M	aeg/arfv perthite + granophyre
15231-5		✓			M	aeg/arfv perthite + granophyre
H2809	✓**	✓			M	aeg/arfv perthite
15231(a)					-	aeg/arfv-hbl. non-perthitic
H17318	✓		✓	✓	M	

** Vlasovite rims around zircon

* Vlasovite/Dalyite

C = Common

M = Moderately common

R = Rare

Table 4.14 Vlasovite 15231-6 (d spacings from Gandolfi photo) (Cu Kα 24 hrs)

S/2	Sin θ	d	Intensity	Vlasovite (Tikhonenkova and Kazakova, 1960) d	I
1.10	0.0960	8.03	w		
1.51	0.1318	5.85	w-m		
1.75	0.1527	5.05	vs	5·02	S
2.12	0.1849	4.17	s		
2.32	0.2024	3.81	m		
2.42	0.2112	3.65	m	3·68	m
2.69	0.2347	3.28	s	3·26	VS
2.79	0.2435	3.17	s		
2.98	0.2600	2.96	s	2·97	VS
3.10	0.2705	2.85	m		
3.31	0.2888	2.67	s-vs	2·72	m
4.29	0.3743	2.06	s-vs	2 17	m-s
4.65	0.4058	1.90	vs	1·99	m
4.93	0.4302	1.79	w-m		
5.13	0.4476	1.72	w-m		
5.62	0.4904	1.57	m		
6.43	0.5611	1.37	m-s		
7.26	0.6335	.22	w-m		

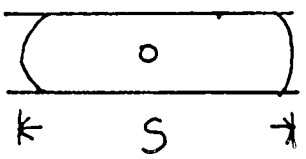
w = weak

m = moderate

s = strong

vs = very strong

Circumference of camera = 360 mm



The Bragg eqn is $n\lambda = 2d \sin\theta$

where λ = wavelength, n = integer

d = d spacing, $\theta = 10\,S/4$

hence for $n=1$ $d = \dfrac{\lambda}{2 \sin\theta}$

Table 4.15 Dalyite H30(1) (d spacings from Gandolfi photo) (Cu Kα 48 hrs)

S	10 S/4 (θ)	d	Intensity	Dalyite (van Tassel, 1952) d	Intensity
2.75	6.88	6.44	S	6.54	M
3.03	7.58	5.85	S	5.90	S
3.11	7.78	5.70	S		
4.10	10.25	4.33	S-VS	4.31	S
4.235	10.59	4.20	S-VS	4.20	VS
4.57	11.41	3.90	W		
5.05	12.63	3.53	S	3.58	VS
5.32	13.30	3.35	S		
5.79	14.48	3.08	S	3.08	VS
6.33	15.81	2.83	W		
6.84	17.09	2.62	VS	2.62	VS
10.15	25.38	1.80	W		
11.17	27.93	1.65	W		
14.38	35.95	1.31	W		

Table 4.16 Zircon, Vlasovite, Dalyite Analyses

	Zircon		Vlasovite			Dalyite		
	H30(3)		17318(i)	17318(i)	17318(ii)	H30(1)	H30(1)	H17318F
SiO_2	33.34		58.29	57.92	58.00	63.03	62.39	63.22
TiO_2	0.04		0.15	0.04	0.06	0.21	0.13	0.21
Al_2O_3	0.32		0.02	0.04	0.02	0.04	0.08	0.04
FeO	0.13		0.03	0.03	0.01	0.01	0.03	0.01
MnO	0.04		0.01	0.03	0.01	0.00	0.00	0.00
MgO	0.02		0.02	0.00	0.00	0.00	0.00	0.00
CaO	0.03		0.01	0.01	0.01	0.00	0.00	0.00
Na_2O	0.19		13.45	14.30	13.45	1.07	1.06	1.16
K_2O	0.12		0.16	0.15	0.15	14.74	14.90	15.01
ZrO_2	64.88		28.26	28.17	29.12	21.47	21.29	21.32
Total	99.11		100.40	100.69	100.83	100.61	99.89	100.48
				Cations				
K	-		0.01	0.01	0.01	1.79	1.83	1.82
Na	-		1.82	1.94	1.82	0.20	0.20	0.21
Zr	0.96		0.96	0.96	0.99	0.99	0.99	0.96
Si	1.02		4.07	4.05	4.05	4.05	5.99	6.02
O	4		11	11	11	15	15	15

Table 4.17

Chemistry and modal proportions of H30(1)

Analysis of H30)1)

Na_2O	5.01
MgO	0.04
Al_2O_3	11.48
SiO_2	74.00
P_2O_5	0.01
K_2O	4.65
CaO	0.27
TiO_2	0.21
MnO	0.16
*FeO	4.33
ZrO_2	0.12
	100.28
Y	86 ppm

REE abundances ppm

Ce	220
Nd	108
Sm	21.5
Eu	1.86
Gd	17.7
Dy	17.5
Er	7.38
Yb	1.99

Modal proportions H30(1)

Perthite	59
Quartz	30
Mafics (including aegirine arfvedsonite)	10
Dalyite	<1
Eudialyte	<1

*Total Fe as FeO

Analysis by microprobe on fused rock/flux beads by the method of Dickin and Exley, 1981.

REE analysed by std. isotope dilution techniques, Y by X.R.F.

Table 4.18 X-ray diffraction data and cell parameters for REE-rich eudialytes.

	Ascension eudialyte,			Kipawa Lake eudialyte, Edgar & Blackburn (1972)	
hkl	d(obs)	d(calc)	I(est)	d(obs)	I(est)
011	11.35	11.36	50	-	-
003	10.03	10.05	50	-	-
110	7.08	7.08	50	6.94	20
104	6.42	6.42	30	6.33	10
021	6.02	6.01	40	5.91	10
202	5.67	5.68	30	5.58	30
015	5.40	5.41	30	-	-
006	5.04	5.03	1	4.96	5
205	4.29	4.30	60	4.25	50
300	4.08	4.09	50	-	-
107	-	-	-	4.05	40
214	3.94	3.95	40	3.91	20
303	3.79	3.79	40	3.75	35
125	3.67	3.67	10	3.64	5
018	3.59	3.60	5	3.56	5
220	-	-	-	3.50	35
221	3.52	3.52	40	-	-
131	3.39	3.38	30	3.35	40
223	3.33	3.34	30	3.30	7
208	3.20	3.21	40	3.19	40
217	3.15	3.16	40	3.10	80
119	3.02	3.03	40	3.00	30
315	2.96	2.96	90	2.94	90
226	2.90	2.89	5	2.88	10
404	2.84	2.84	100	2.82	100
045	2.74	2.73	1	2.69	10
410	2.68	2.68	15	2.63	15
01,11	2.66	2.67	15	2.66	10
309	2.59	2.59	30	2.58	40
0012	2.52	2.51	20	2.51	10
Hexagonal cell dimensions		a = 14.16 c = 30.15		a = 13.95 c = 30.10	

Table 4.19 Chemical analysis of eudialyte from H30(1)

	RIM	RIM-CORE	CORE
SiO_2	49.36	47.76	46.64
Al_2O_3	0.09	0.02	0.02
*FeO	5.97	5.92	6.24
MgO	0.02	0.02	0.02
CaO	3.92	4.29	4.04
Na_2O	13.48	12.74	12.82
K_2O	0.52	0.42	0.37
TiO_2	0.50	0.43	0.41
MnO	2.19	2.45	2.69
ZrO_2	14.39	13.39	13.39
Y_2O_3	3.61	4.18	3.58
La_2O_3	1.13	1.31	1.50
Ce_2O_3	2.37	2.48	2.93
Pr_2O_3	0.27	0.25	0.25
Nd_2O_3	1.12	1.05	1.30
Sm_2O_3	0.29	0.28	0.35
Gd_2O_3	0.69	0.72	0.75
Dy_2O_3	0.52	0.68	0.69
Er_2O_3	0.48	0.45	0.45
Yb_2O_3	0.18	0.16	0.17
Total	100.96	99.03	98.62
R.E+Y	10.77	11.55	11.78
CeN/YN	1.86	1.87	2.49

* All Fe represented as Fe^{2+}

Table 4.20

Structural formula of eudialyte from H30(1) assuming 19 oxygens compared with Kipwa Lake eudialyte

Ascension (rim)	wt%	19 O
Na_2O	13.48	3.48
K_2O	0.52	
CaO	3.92	
FeO	5.97	
MnO	2.19	2.01
MgO	0.02	
Y_2O_3	3.61	
REE_2O_3	7.16	
ZrO_2	14.39	
Al_2O_3	0.09	0.96
TiO_2	0.50	
SiO_2	49.36	6.48
	100.96	12.98

Kipwa Lake Edgar & Blackburn (1972)	wt%	19 O
Na_2O	12.53	3.08
K_2O	0.43	
CaO	9.74	
FeO	2.41	
MnO	1.34	2.08
MgO	0.13	
RE+Y	6.40	
SrO	0.11	
ZrO_2	11.80	
Al_2O_3	0.44	0.87
Fe_2O_3	0.19	
TiO_2	0.38	
Nb_2O_5	0.69	
SiO_2	50.35	6.23
	99.88	12.26

Table 4.21 Partially Melted Blocks (* analysed by microprobe)

Number	Locality	Petrography	Nature of glass	wt SiO_2 in glass
*17360(1)	E. Crater	Qz, Cpx, KFsp	clear, unaltered	73-76
*17360(2)	"	Plag, Cpx, Bi, Amph	"	59-60
*17360(3)	"	Qz, Cpx	"	75-77
*H32(1)	"	Fsp, Cpx, Ol	"	50-52
H32(2)	"	Fsp, Cpx, Ol	"	
*H33(4)	"	Cpx, Fsp	"	68-70
H34(2)	"	Qz, Bi, KFsp, Cpx	"	
*H39(1)	"	Qz, KFsp, Cpx	"	65-67
*H39(2)	"	Qz, KFsp, Cpx	brown	62-76
*H7(1)	Crystal Bay	Qz, KFsp, Cpx	no glass - all quenched	-
*H83(6)	Mt. Red.	PL, Cpx, Ol, Op (Opx)	altered	50-52
*H83(10)	"	PL, Cpx, Ol, Op	altered	45-47
*H60(4)	NASA	PL, Cpx, Op	brown/black	50-52
15368a	Green Mt.	Plate 4.23	brown	
A44(1)	"	Highly broken and altered	altered	
A44(2)	"			
15243A	'	Qz, Cpx, Fsp, Op	brown	
A60(3)	NASA	Plag, Cpx, Op	altered	
H95(16)	Lady Hill	Ol, Op, Plag. Plate 4.17	fresh - brown	
*H49(16)	Crystal Bay	Qz, KFsp, Cpx	fresh	61-66

Modal percentage for East Crater xenoliths

	H32(2)	H33(4)	H34(2)	H39(1)	H39(2)	17360(1)
Glass*	8.6	28.4	3.9	14.5	5.4	9.1
Quartz	1.7	-	3.0	-	-	0.3
Feldspar	86.0	67.2	88.5	71.3	82.2	87.2
Augite	2.6	2.7	3.3	11.3	9.1	1.9
Biotite	-	-	-	0.4	-	-
Opaque	1.1	1.7	1.3	2.9	3.3	1.5
No points counted	2539	3568	846	1973	2607	2689

Table 4.22

* includes all products of partial melting e.g.

Quench xtals etc.

Whole rock analyses East Crater Lava and Blocks, 5 Mile Post Granite and Little White Hill Comendite

	Lava		Blocks			Granite	Comendite
	H31L	H39L	H33(3)	H34(1)	H39(4)	H30(1)	A35
SiO_2	60.88	59.61	65.03	63.59	62.35	74.00	74.05
TiO_2	1.35	1.61	0.44	0.45	0.59	0.21	0.13
Al_2O_3	16.14	15.84	18.29	18.33	18.73	11.48	12.44
*FeO	5.88	7.39	3.43	3.16	3.53	4.33	2.53
MnO	0.22	0.25	0.10	0.11	0.13	0.16	0.06
MgO	1.68	2.22	0.38	0.46	0.47	0.04	0.04
CaO	3.51	4.42	1.95	2.13	2.53	0.27	0.19
Na_2O	5.88	4.94	6.32	7.45	7.24	5.01	5.53
K_2O	3.88	2.80	3.55	3.29	3.08	4.65	4.60
P_2O_5	0.58	0.95	0.49	0.98	1.33	0.01	0.02
Zr (ppm)	469	n.d.	356	292	269	1538	871
Tot.	99.56	100.06	100.03	99.98	100.01	100.16	99.70
					K_2O/Na_2O	0.93	0.832

Table 4.23

n.d. = not determined

*All Fe as FeO. Analyses by the method of Dickin & Exley 1981.

TABLE 4.24

Microprobe analyses of opaque Fe-silicate

	H33(4)	H33(4)	H39(1)	H39(1)	*17360(1)	17360(1)
SiO_2	32.01	40.33	31.30	31.36	32.98	31.18
TiO_2	0.11	0.34	0.06	0.05	0.03	0.05
Al_2O_3	0.42	1.16	0.47	0.37	1.04	0.79
FeO	51.21	40.88	55.11	55.74	52.77	52.81
MnO_2	2.70	2.12	3.84	3.94	3.36	3.18
MgO	7.50	6.77	3.00	3.20	3.28	4.55
CaO	0.45	0.31	0.05	0.08	0.20	0.19
Na_2O	0.07	0.22	-	-	0.29	0.17
K_2O	0.08	0.41	-	-	-	-
	94.55	92.54	93.83	94.74	93.95	92.98

All analyses from small opaques associated with melted pyroxene except * core of altered fayalite.

Table 4.25

East Crater Glasses by microprobe

	17360(1)	17360(1)	17360(2)	17360(2)	17360(3)	17360(3)
SiO_2	73.27	76.47	60.41	59.32	75.81	77.32
TiO_2	0.30	0.18	1.20	1.19	0.50	0.32
Al_2O_3	13.01	12.81	17.12	16.45	12.15	11.84
*FeO	4.22	3.30	8.26	10.21	3.52	3.31
MnO	0.18	0.15	0.18	0.22	0.31	0.25
MgO	0.15	0.15	1.26	1.41	0.27	0.21
CaO	0.69	0.48	3.74	4.46	0.73	0.69
Na_2O	3.25	1.42	2.60	3.07	1.84	1.73
K_2O	5.38	5.21	4.54	4.04	4.61	4.80
Tot.	100.35	100.86	99.31	100.37	99.79	100.50

	H39(2)	H39(2)	H33(4)	H33(4)	H39(1)	H39(1)
SiO_2	62.66	76.15	68.46	69.71	65.01	67.25
TiO_2	0.53	0.04	0.59	0.67	0.26	0.11
Al_2O_3	11.46	13.79	13.86	13.92	15.68	17.67
FeO	10.35	2.25	8.05	7.11	6.21	4.03
MnO	0.46	0.10	0.44	0.34	0.24	0.18
MgO	3.08	0.11	0.50	0.41	0.26	0.14
CaO	5.84	0.37	1.51	1.34	1.51	0.95
Na_2O	1.68	3.10	1.90	2.37	5.21	4.68
K_2O	3.68	5.93	5.05	5.17	5.06	5.66
Tot.	99.74	101.84	100.36	101.04	99.44	100.67

*All Fe as FeO

Analysed area = 10μm to avoid volatile loss

Fig 4.1

MINERALOGY OF DARK SLOPE XENOLITHS

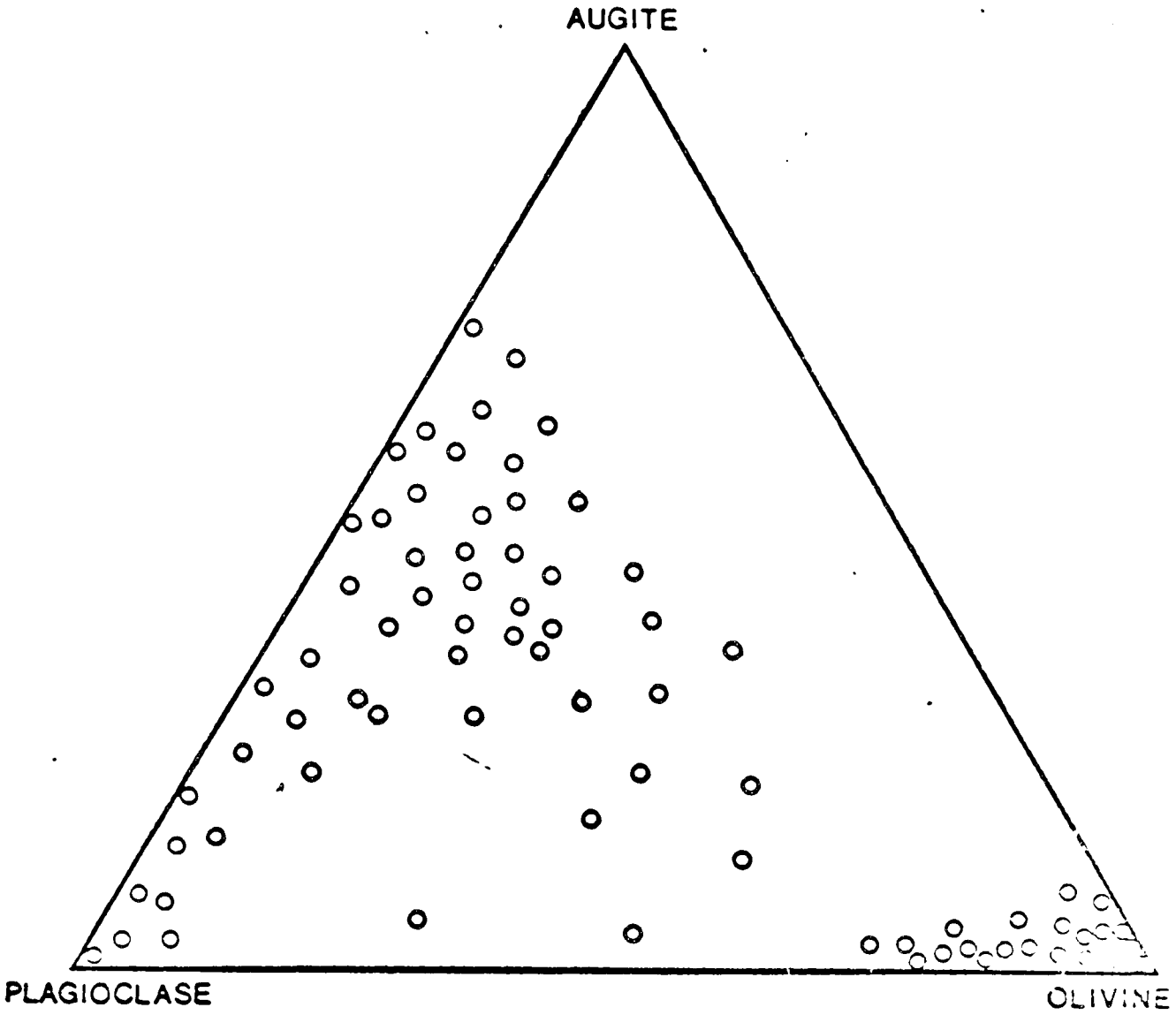


Fig 4.2 Composition of feldspars from Dark Slope Crater gabbros

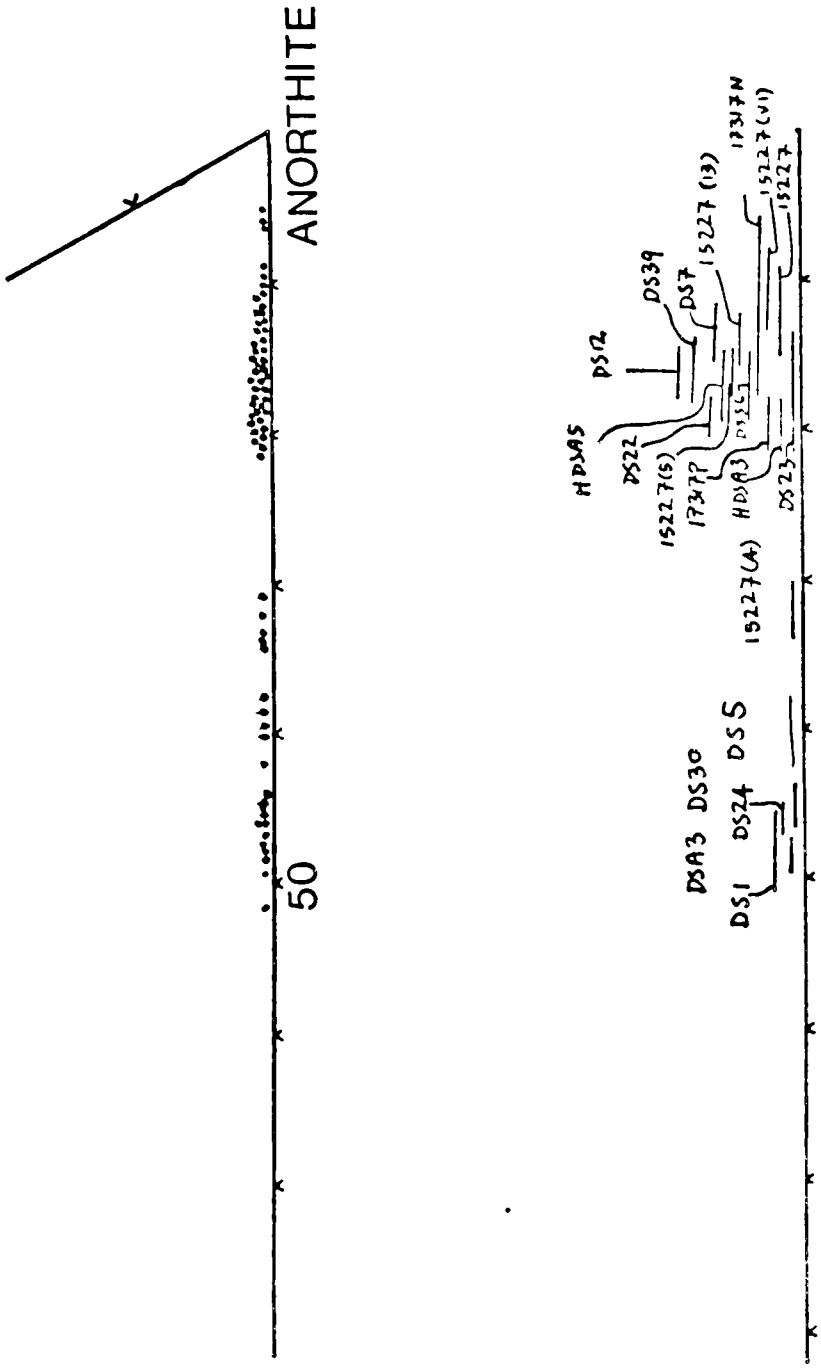


Fig 4.3 Variation in composition of pyroxenes from Dark Slope Crater blocks

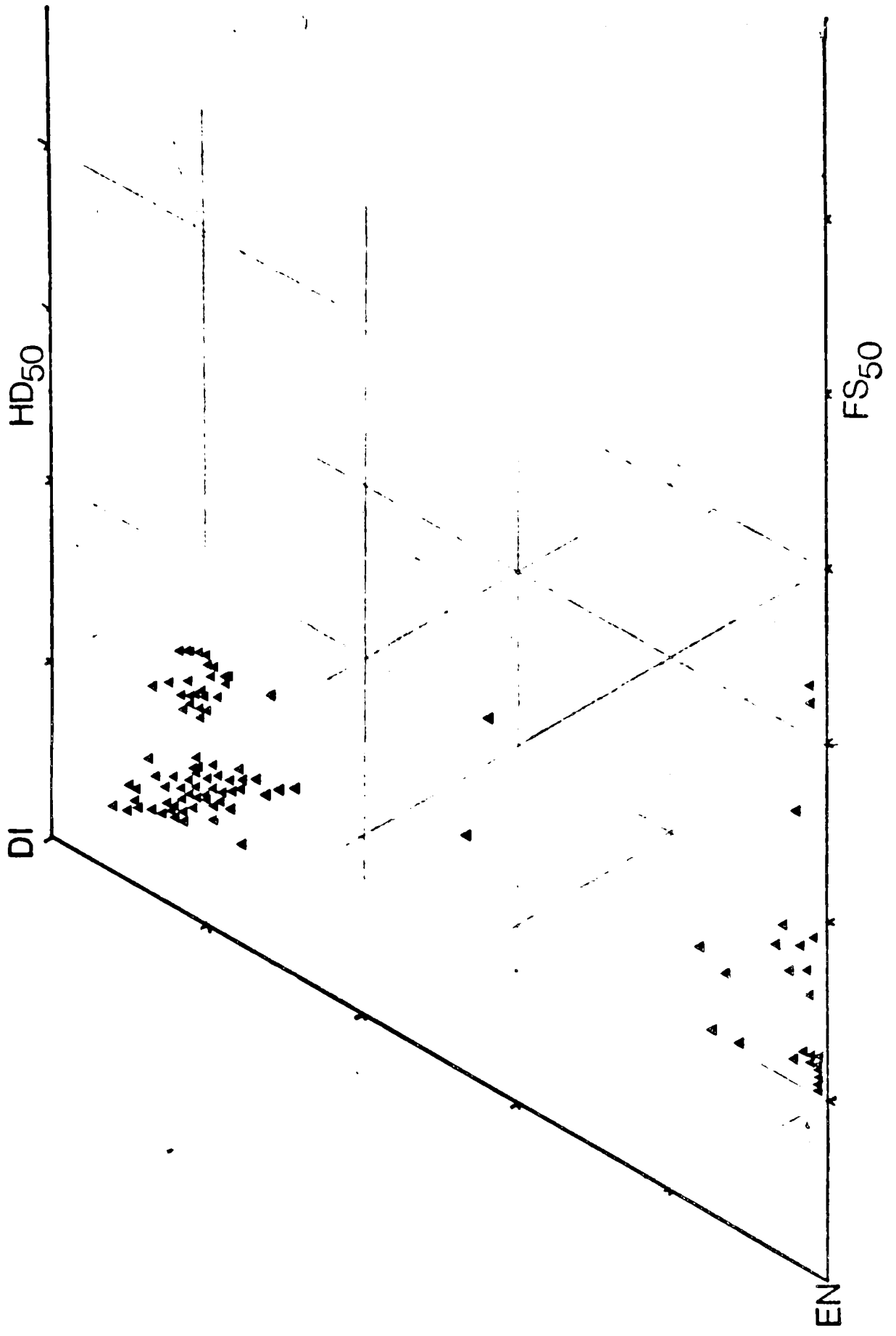


Fig 4.4 Dark Slope Crater pyroxene analyses - intrasample variation

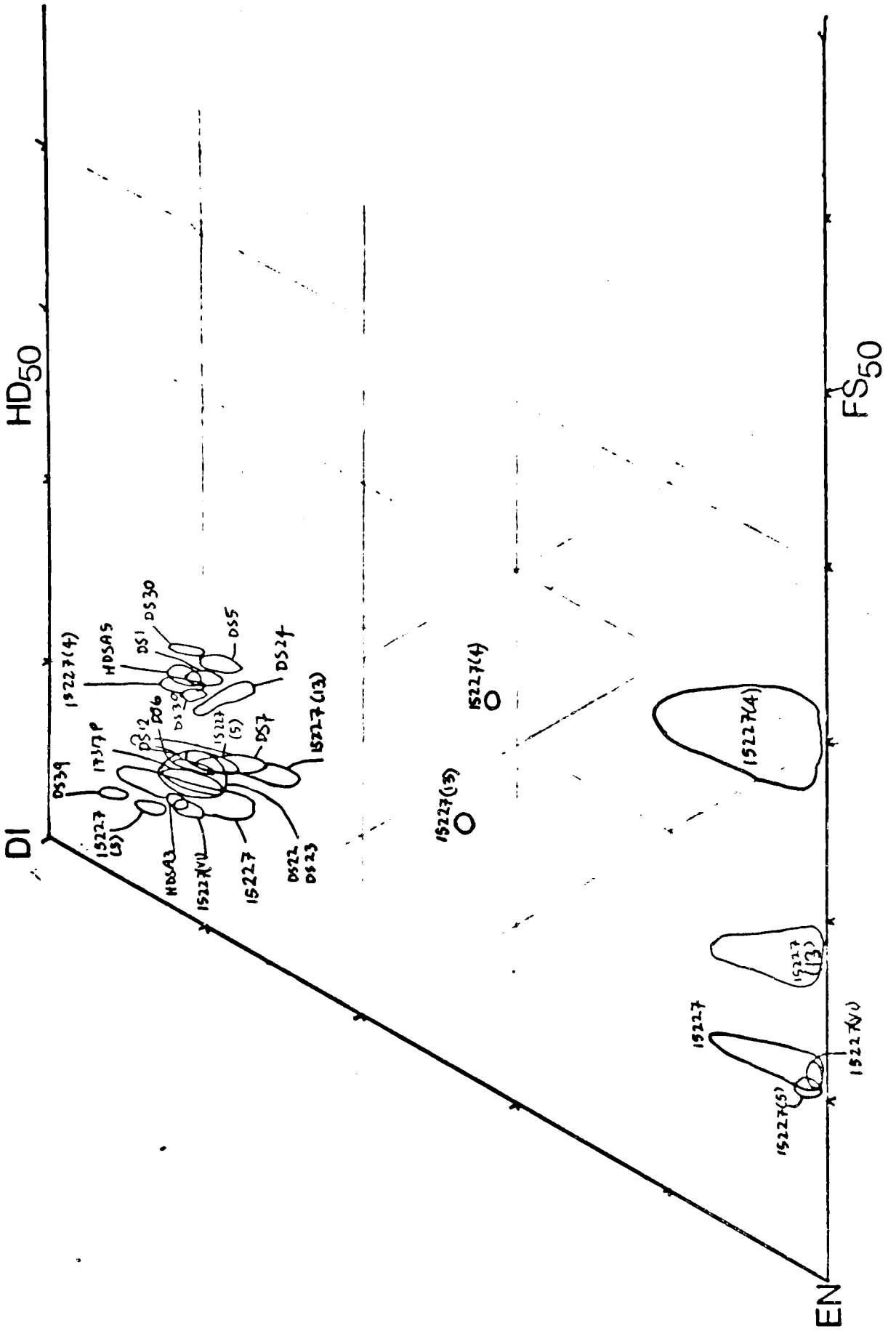


Fig 4.5a Variation in Pyroxene Composition (rocks 15227(13)&15227(4))

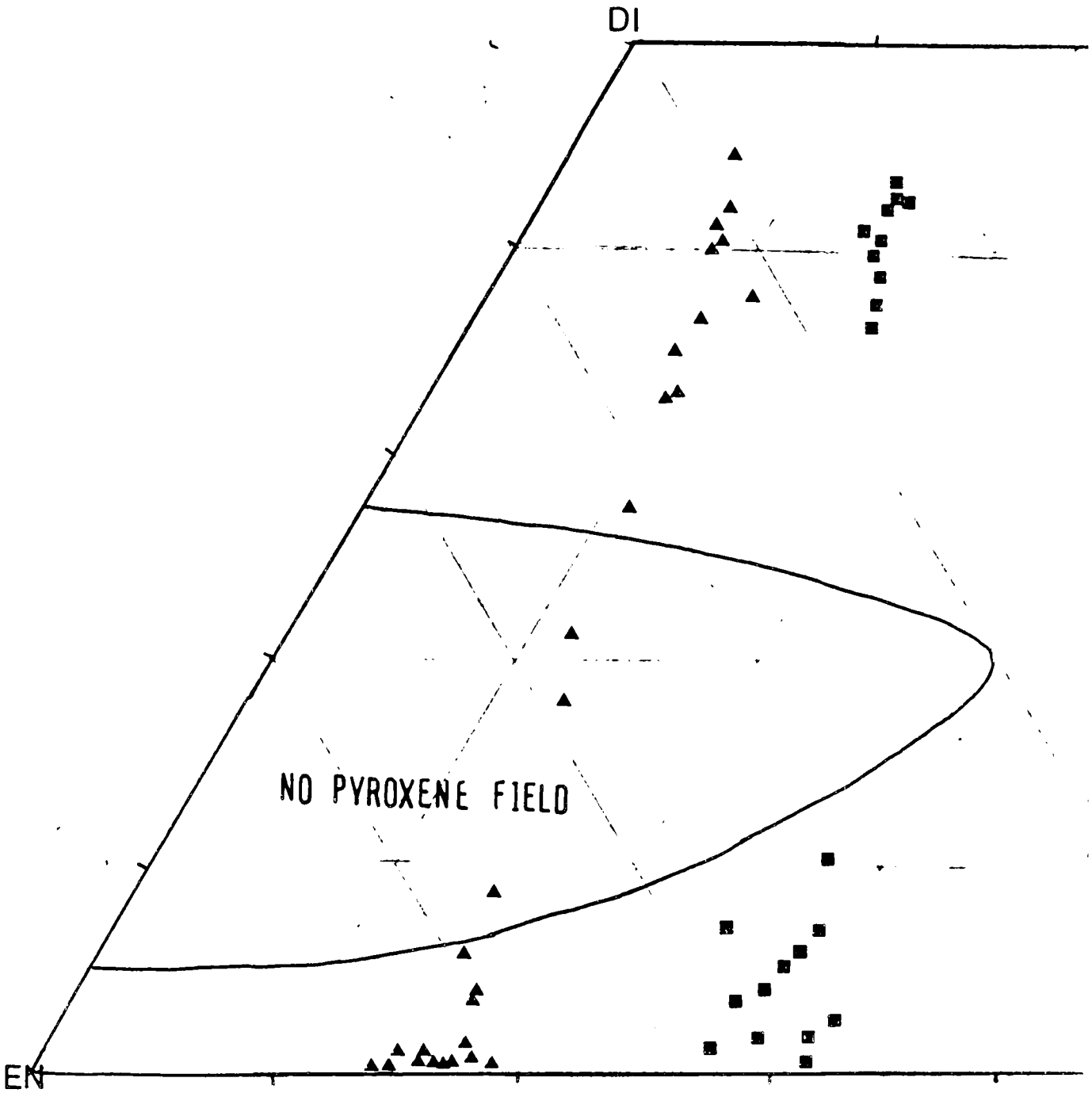


Fig 4.5b Variation in Olivine Composition in 15227(13)

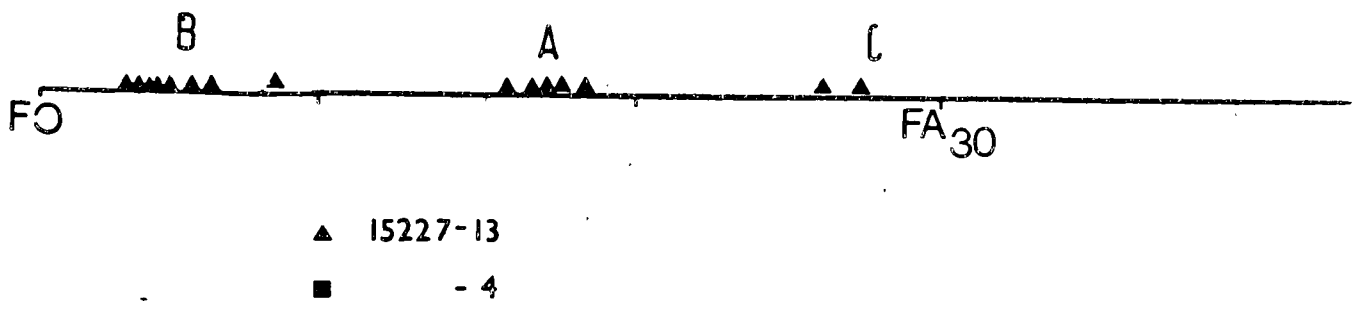


Fig 4.6 Olivine Analyses from Dark Slope Crater and Intrasample Variation

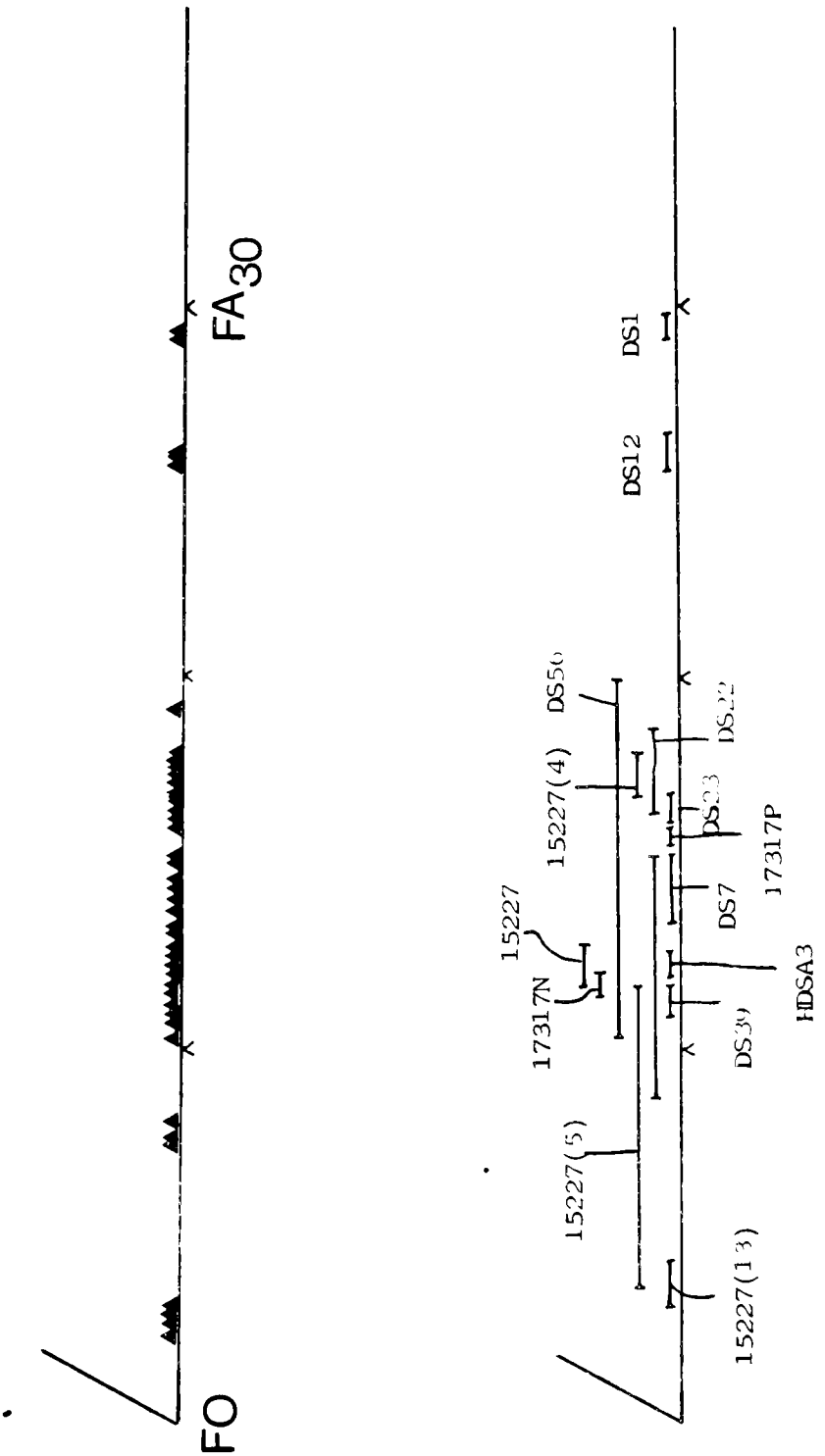
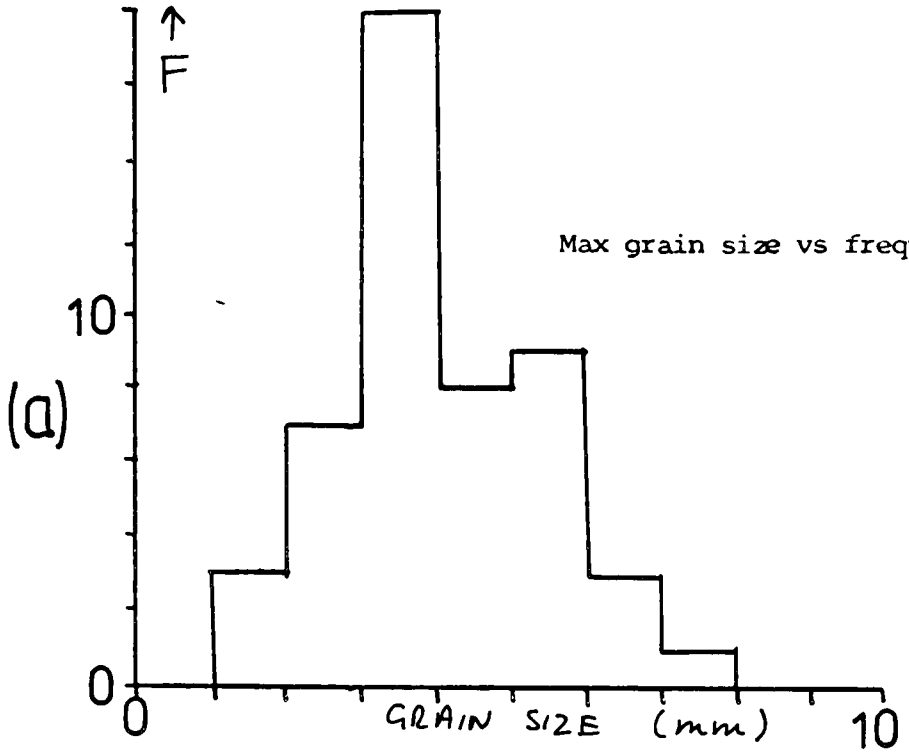
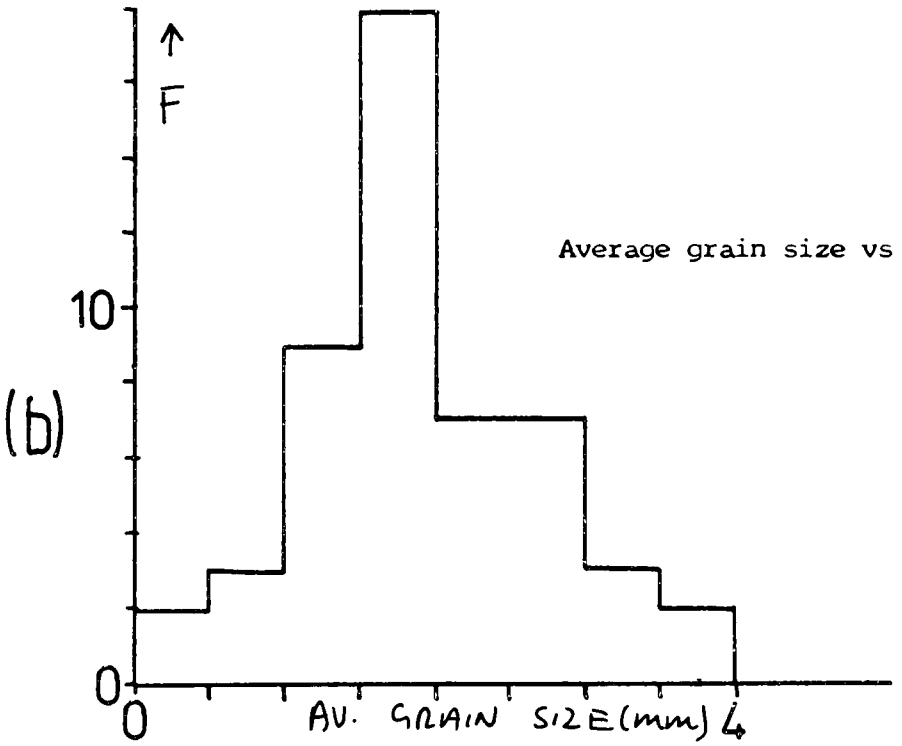


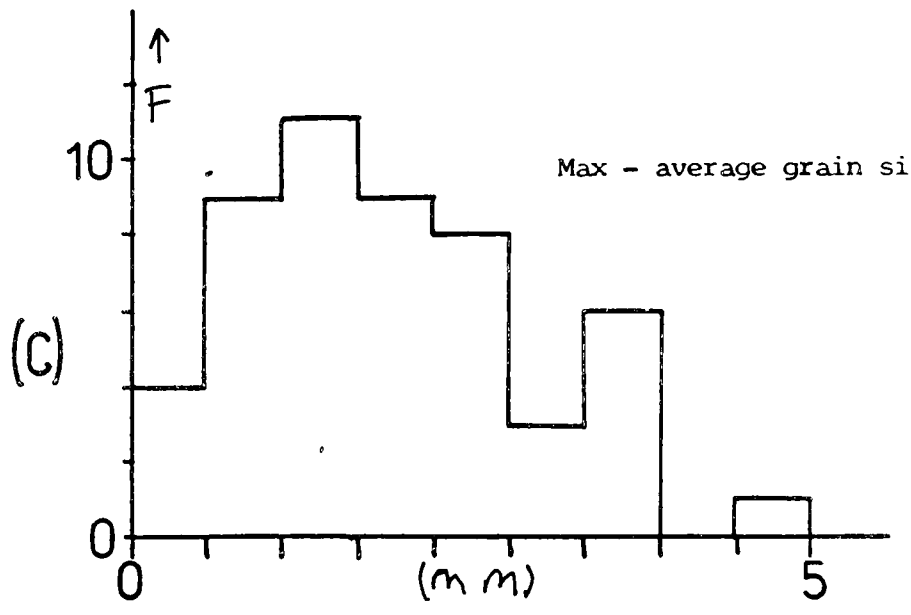
Fig 4.7 Grain vs frequency histograms for blocks from Dark Slope Crater.



Max grain size vs frequency (F)



Average grain size vs frequency (F)



Max - average grain size vs frequency (F)

Fig 4.8 Types of cumulate texture (after Wager et al,1960)

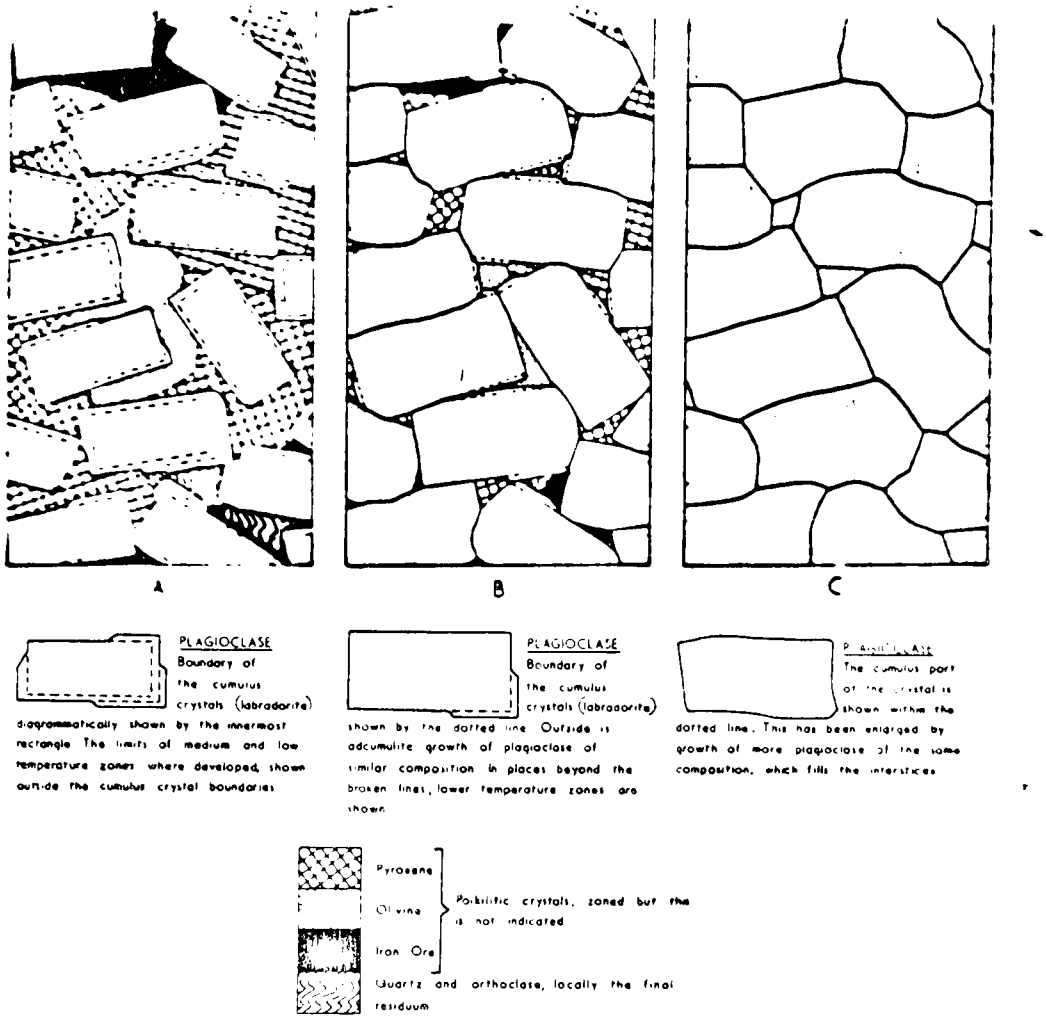


FIG. 1. Diagrammatic representation of plagioclase cumulates formed from a gabbroic magma. A, extreme plagioclase orthocumulate. B, plagioclase mesocumulate. C, extreme plagioclase adcumulate.

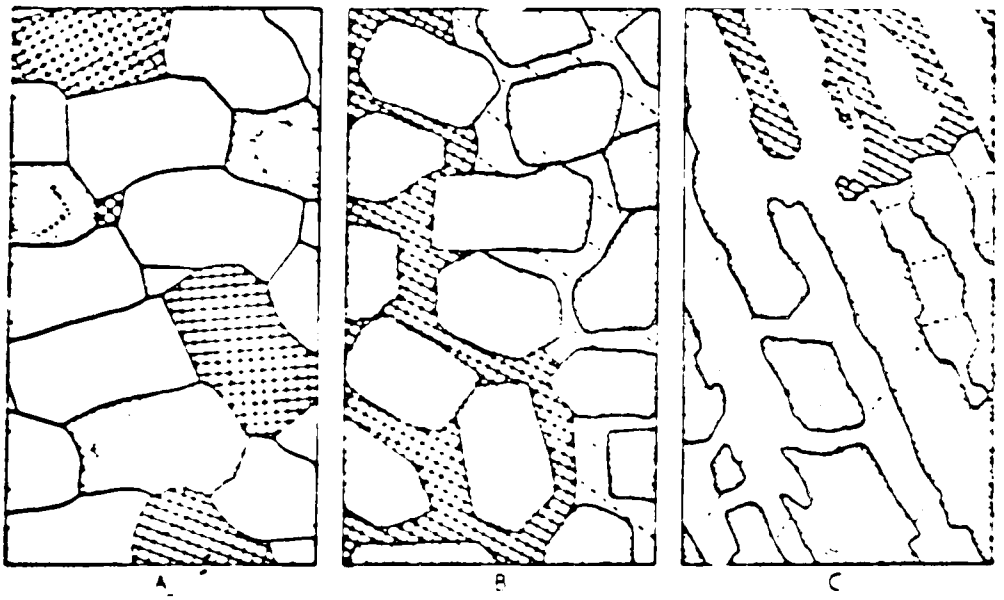


FIG. 2. Diagrammatic representation of an adcumulate, heteradcumulate, and harrisitic cumulate formed from gabbroic magma. Plagioclase, white; olivine, stippled; pyroxene, cross-hatched. A, plagioclase–olivine-augite adcumulate in which the three types of cumulus crystals are considered to have been enlarged by the adcumulus process until all the intercumulus liquid has been eliminated (cf. Fig. 1C). The boundaries of the cumulus crystals of plagioclase, olivine, and pyroxene are indicated diagrammatically by dotted lines. The material inside and outside the dotted lines has the same composition B, olivine heteradcumulate. Large poikilitic augite and plagioclase crystals, essentially unzoned, are shown surrounding cumulus olivines. Adcumulus growth of the olivines is not indicated on the diagram. In this diagram it is assumed that there was no trapped liquid. C, olivine harrisitic cumulate. All olivine shown has the same orientation and is essentially unzoned. The surrounding plagioclase and pyroxene are also essentially unzoned and are considered to have been formed as in the heteradcumulates.

Fig 4.9 Layering in gabbroic block DS36
(approximately three times actual size)

numbers refer to modal % olivine, clinopyroxene and feldspar respectively

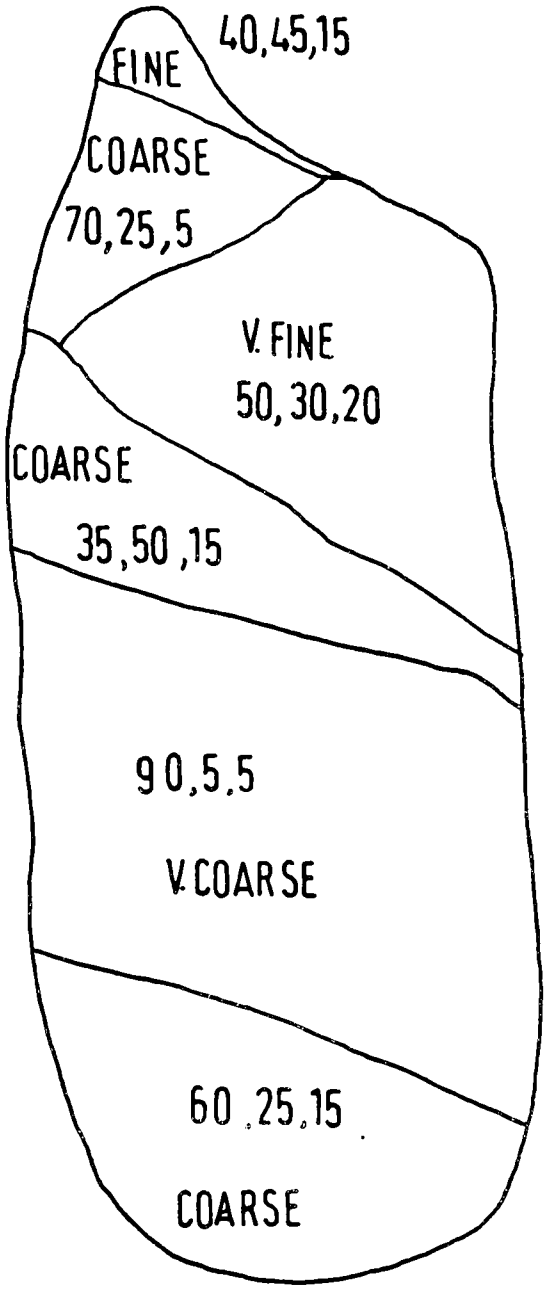


Fig 4.10 Sketch of layering in gabbroic block DS23
(approximately three times actual size)

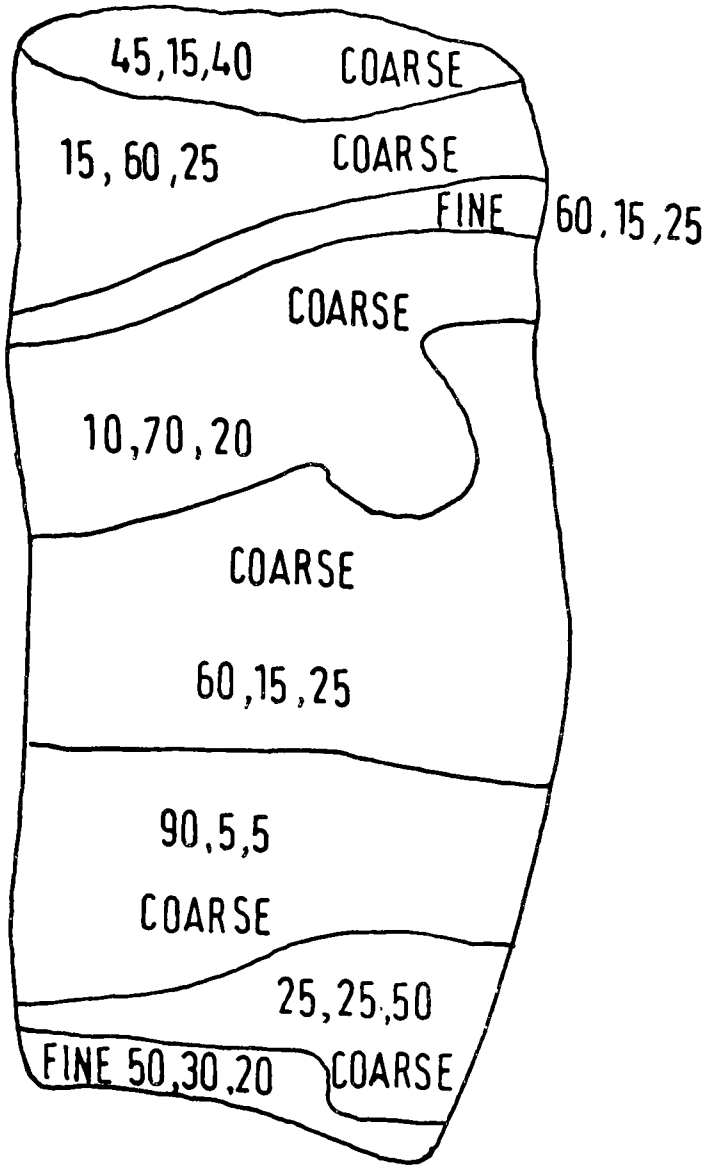


Fig 4.11 Intervariation of coexisting olivine, plagioclase and clinopyroxene in gabbroic blocks from Dark Slope Crater.

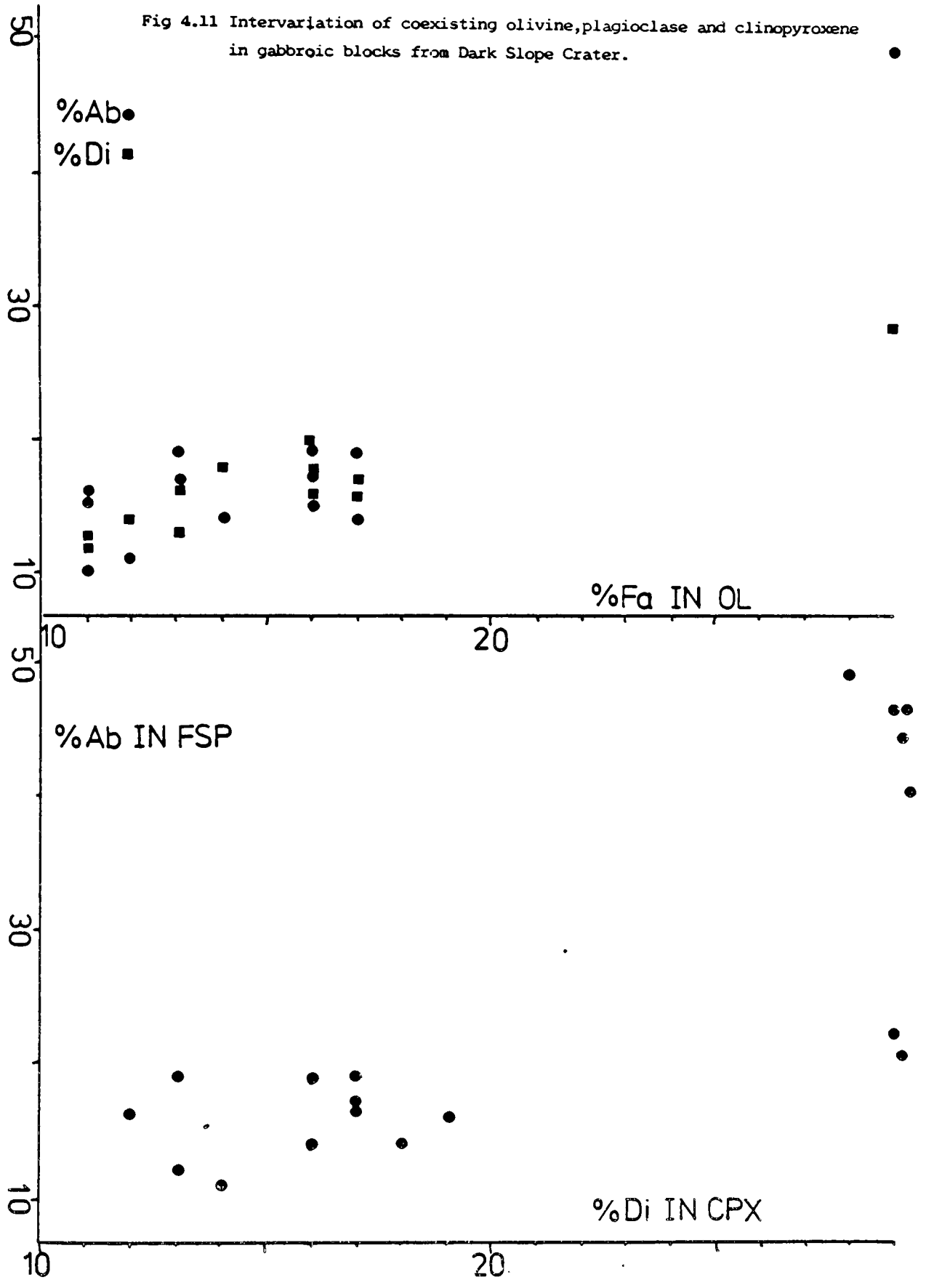
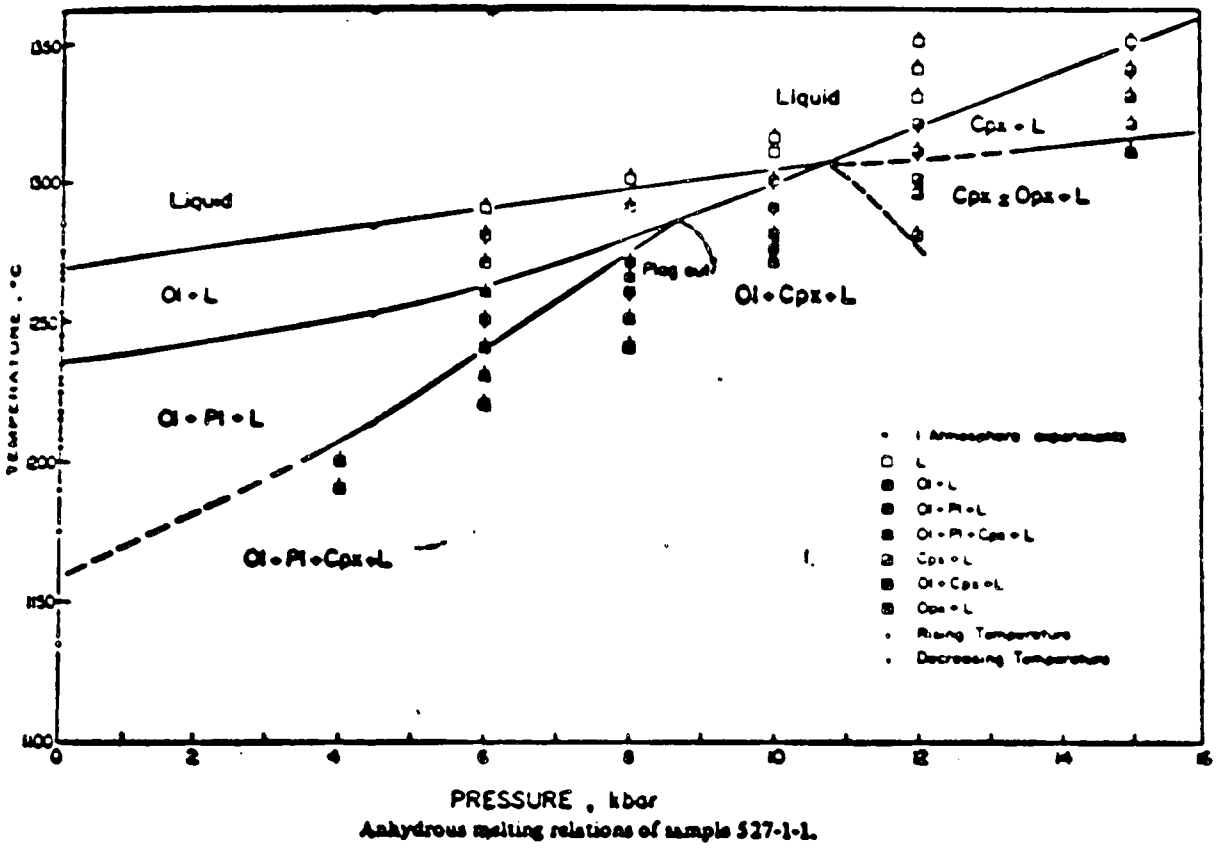


Fig 4.12 Melting relations of tholeiitic basalt (from the M.A.R.) from Bender et al (1978).



Anhydrous melting relations of sample 527-1-1.

Fig 4.13 Schematic reconstruction of original Dark Slope Crater intrusion . Height up the intrusion for a block estimated from relative abundance of block types.

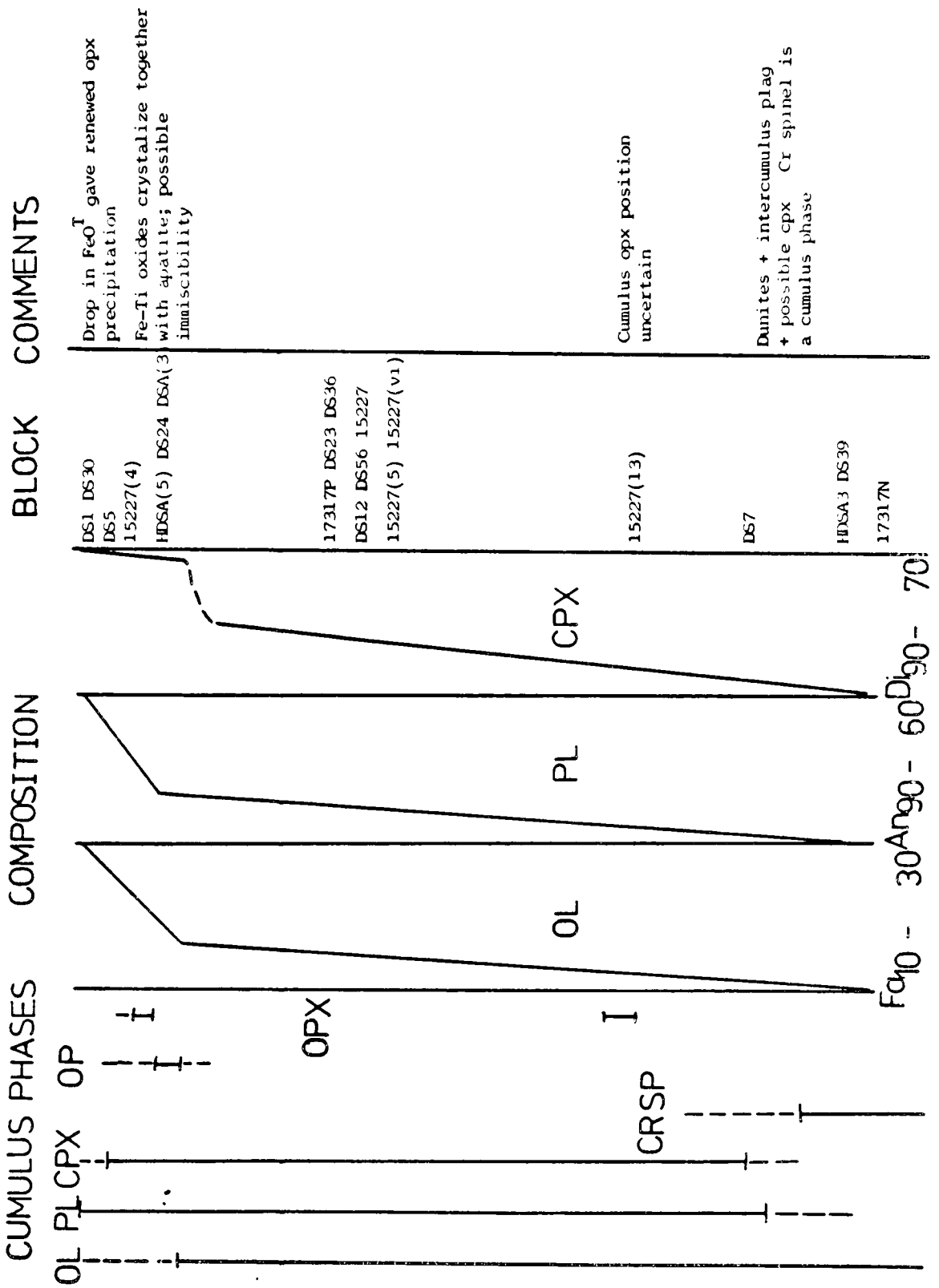


Fig 4.14 Modal proportions of Middleton's gabbro blocks .
Area of square is proportional to the volume of mesostasis in each block

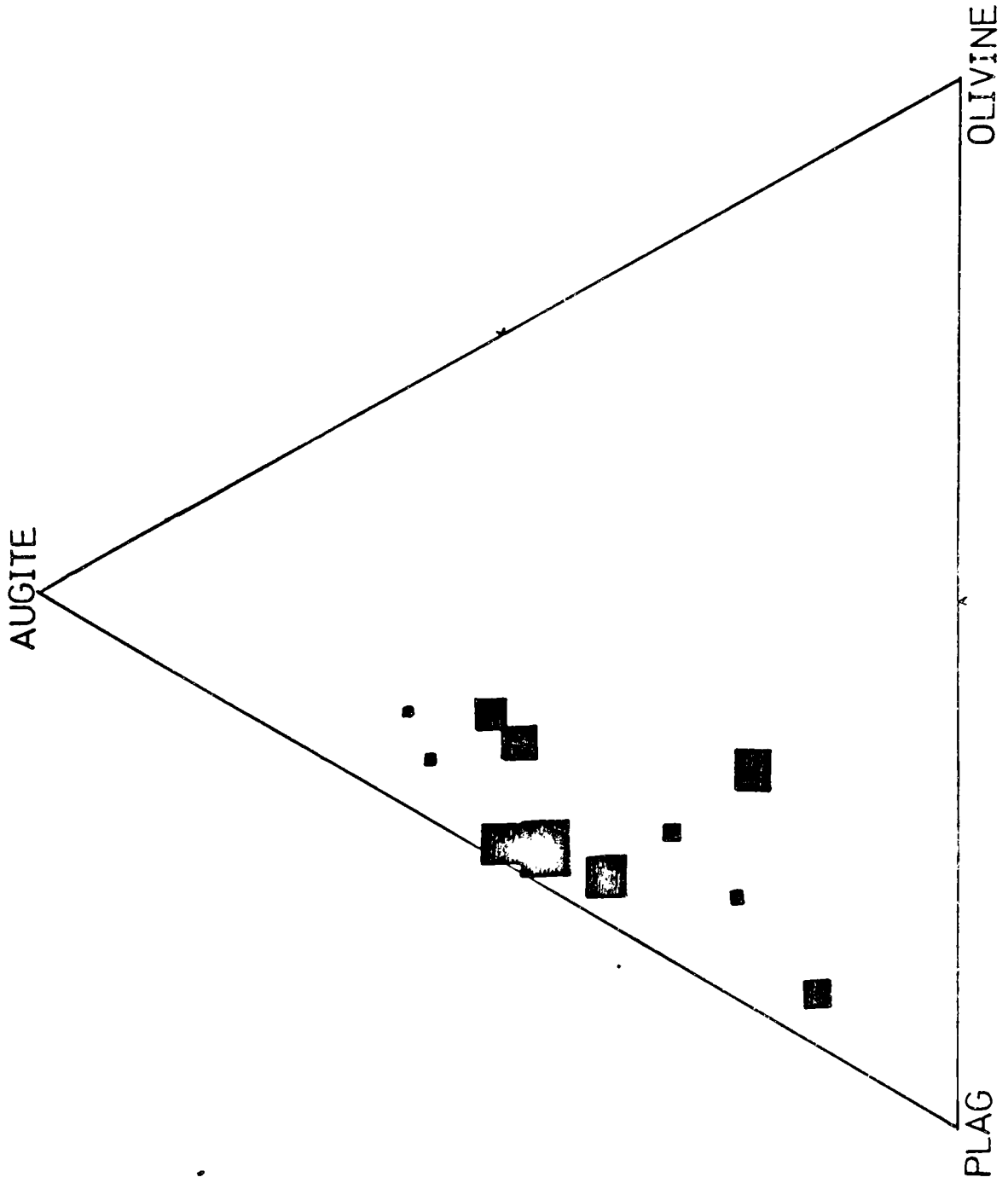


Fig 4.15 Variation in composition of feldspars from Middleton's gabbro blocks

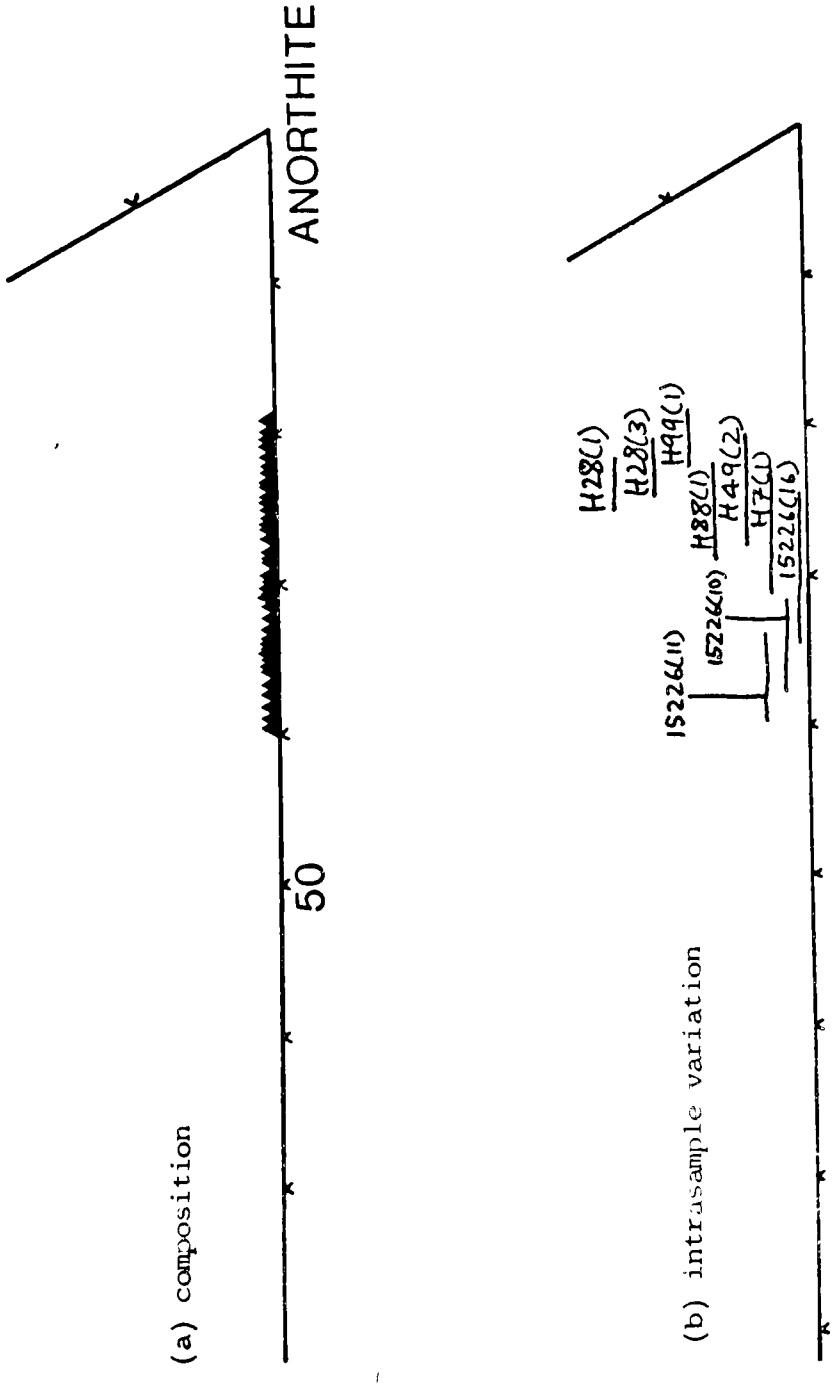


Fig 4.16 Variation in composition of olivine and pyroxene from Middleton's gabbroic blocks

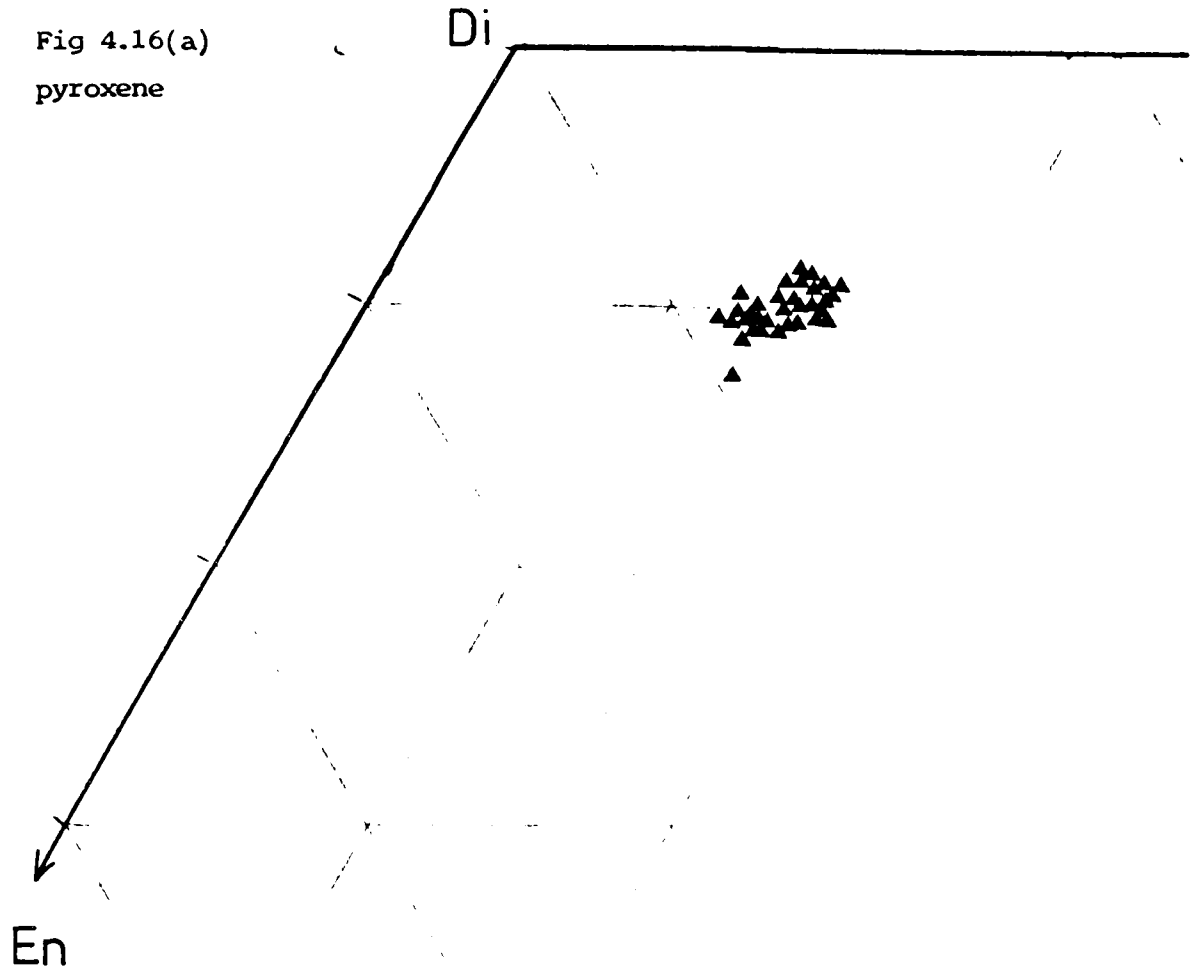


Fig 4.16(a)
pyroxene

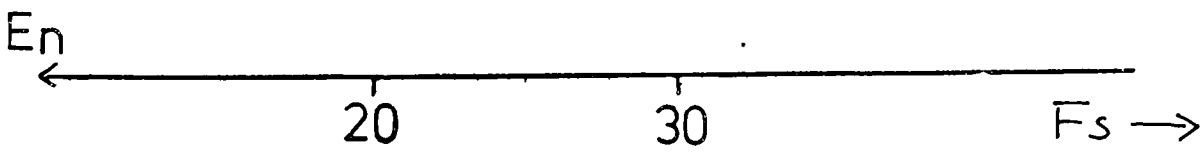


Fig 4.16(b)
olivine

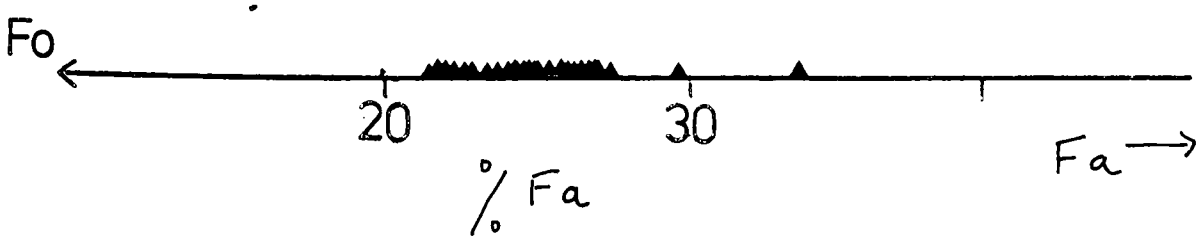
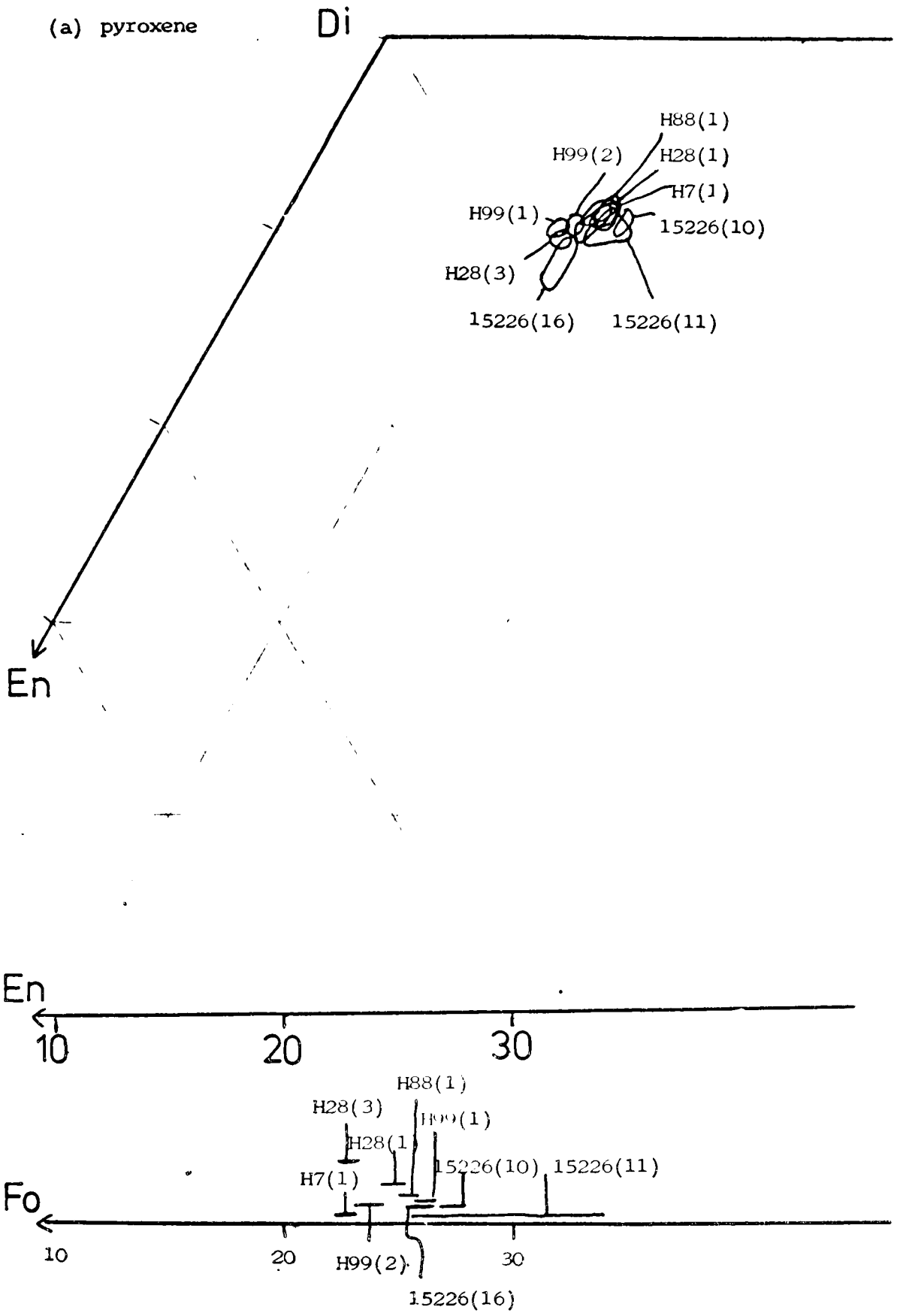


Fig 4.17 Intrasample variation of pyroxenes and olivines from Middleton's Ridge gabbros



(b) Intrasample variation of olivines from Middleton's Ridge gabbros

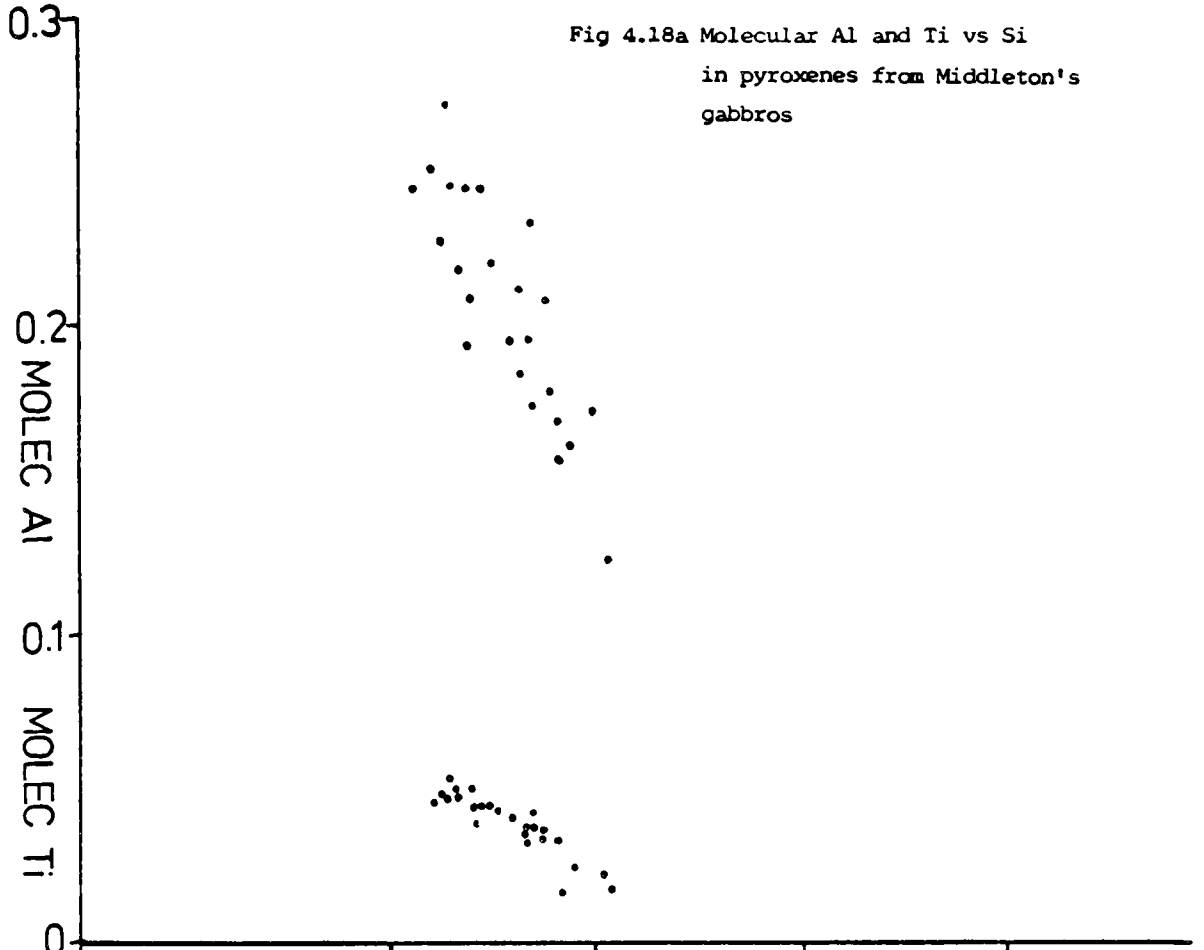


Fig 4.18a Molecular Al and Ti vs Si in pyroxenes from Middleton's gabbros

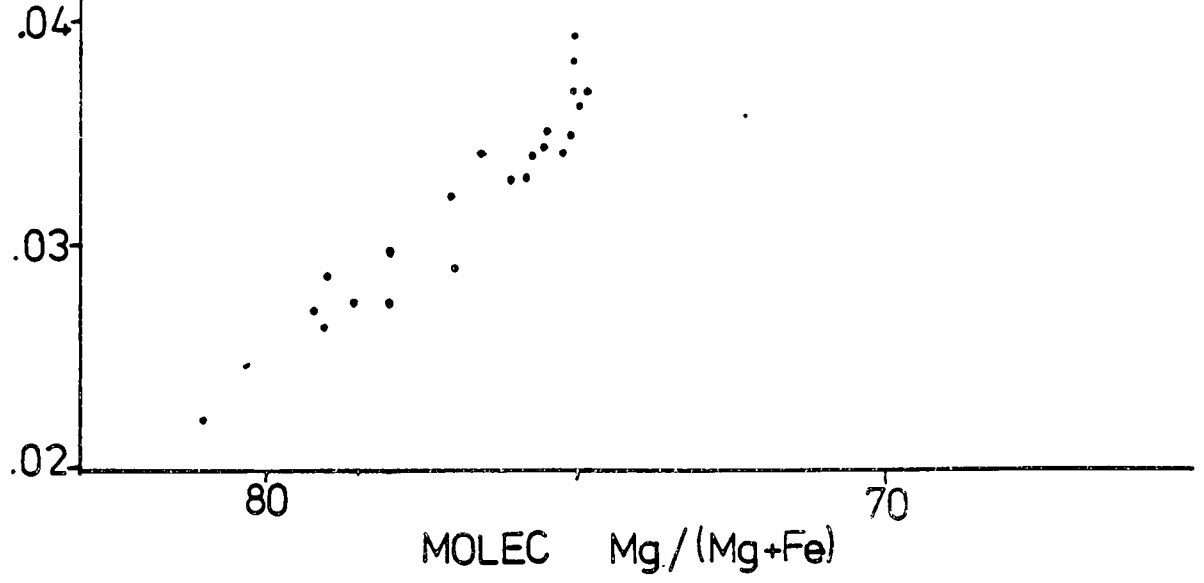


Fig 4.18b Molecular Na vs Mg (Mg+Fe) in pyroxenes from Middleton's gabbro blocks

Fig 4.19 Composition of feldspars of gabbroic blocks from Mountain Red Hill and Lady Hill

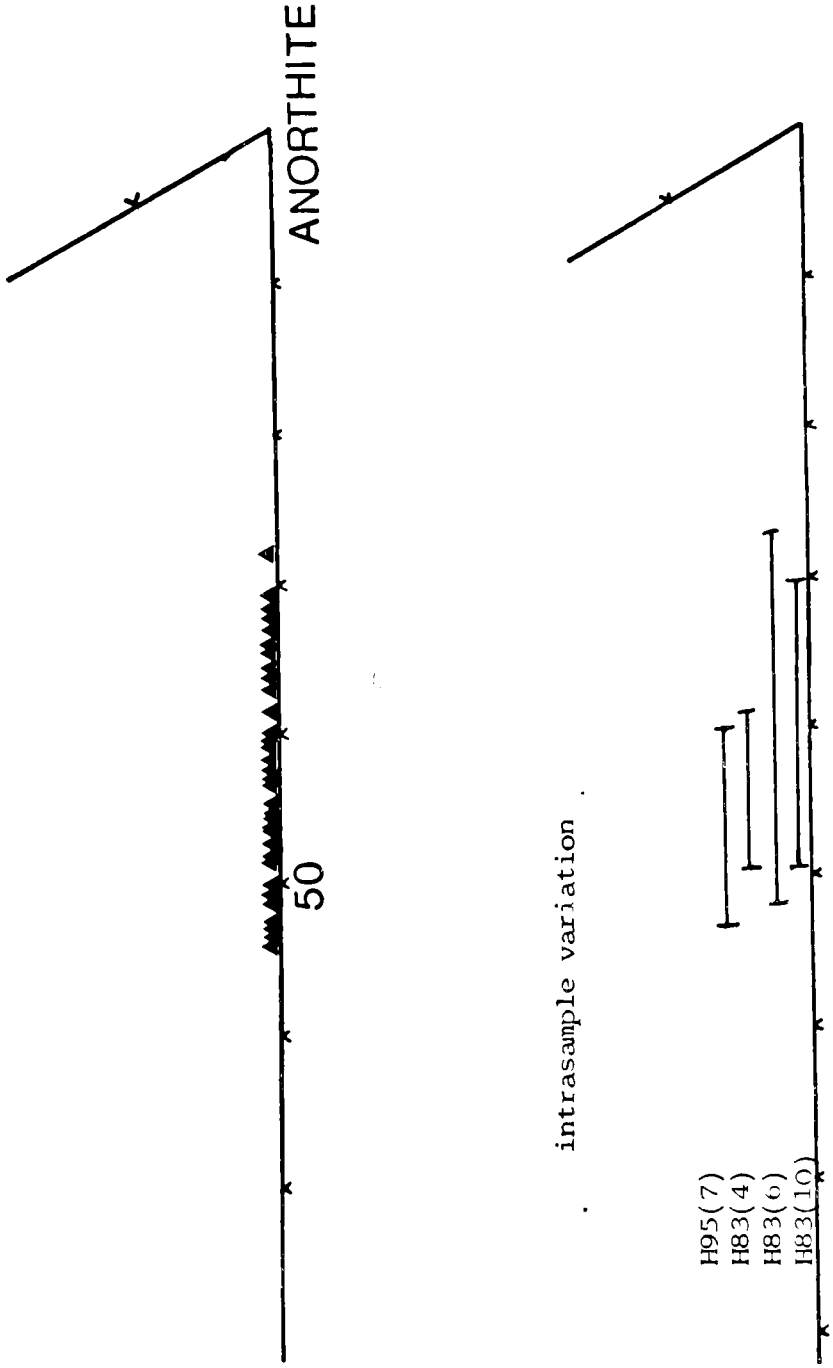
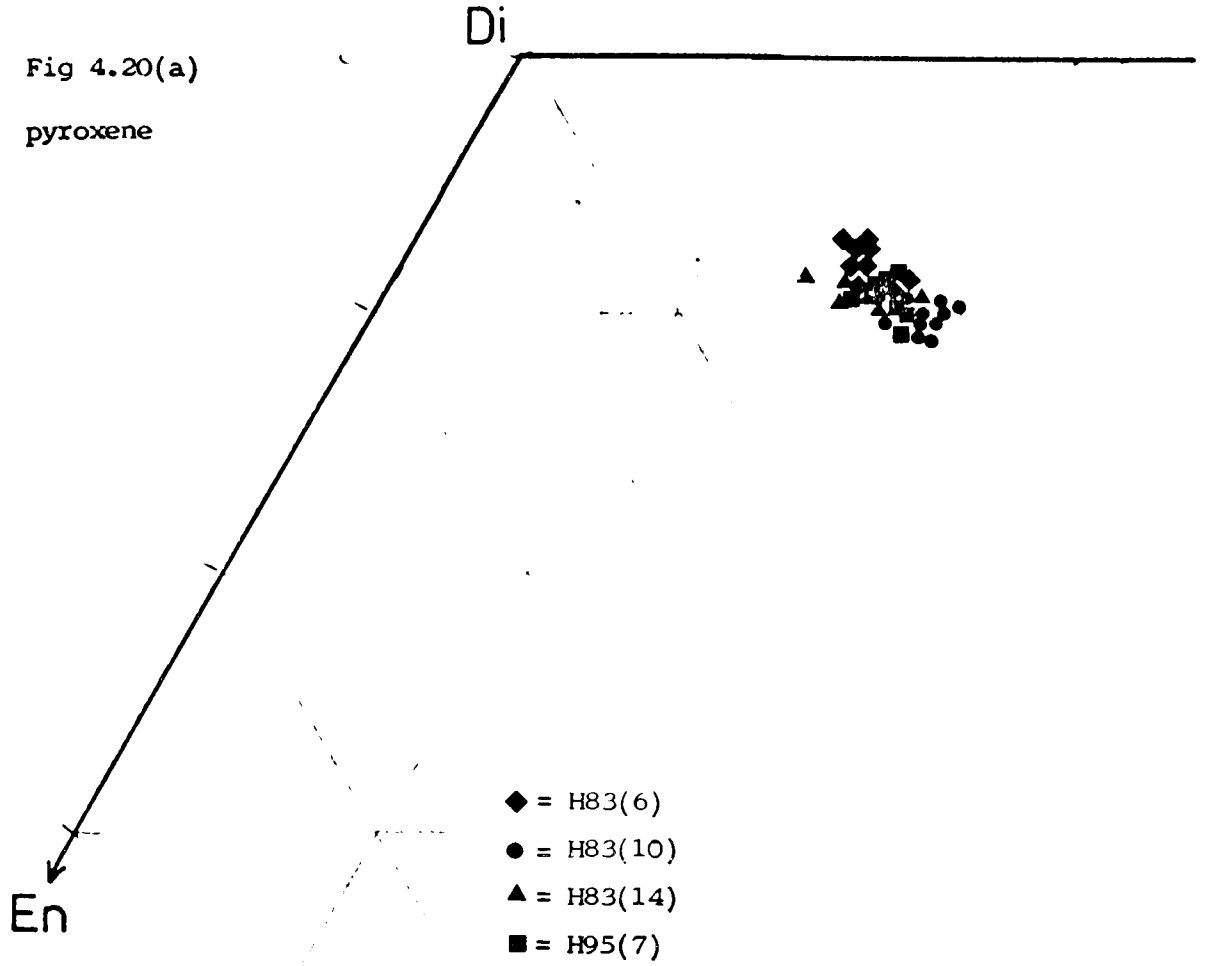


Fig 4.20 Variation in composition of pyroxene and olivine in Mt Red Hill and lady Hill gabbroic blocks

Fig 4.20(a)
pyroxene



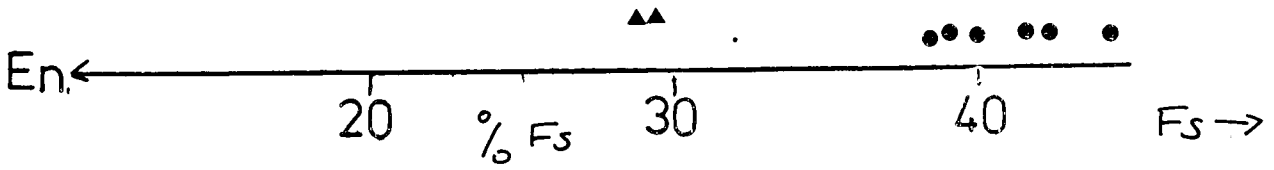


Fig 4.20(b)
olivine

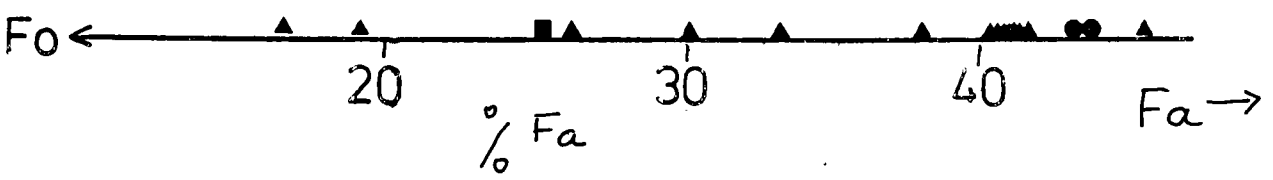


Fig 4.21 Al vs Ti in pyroxenes from Mountain Red and Lady Hill gabbros (assuming 6 oxygens).

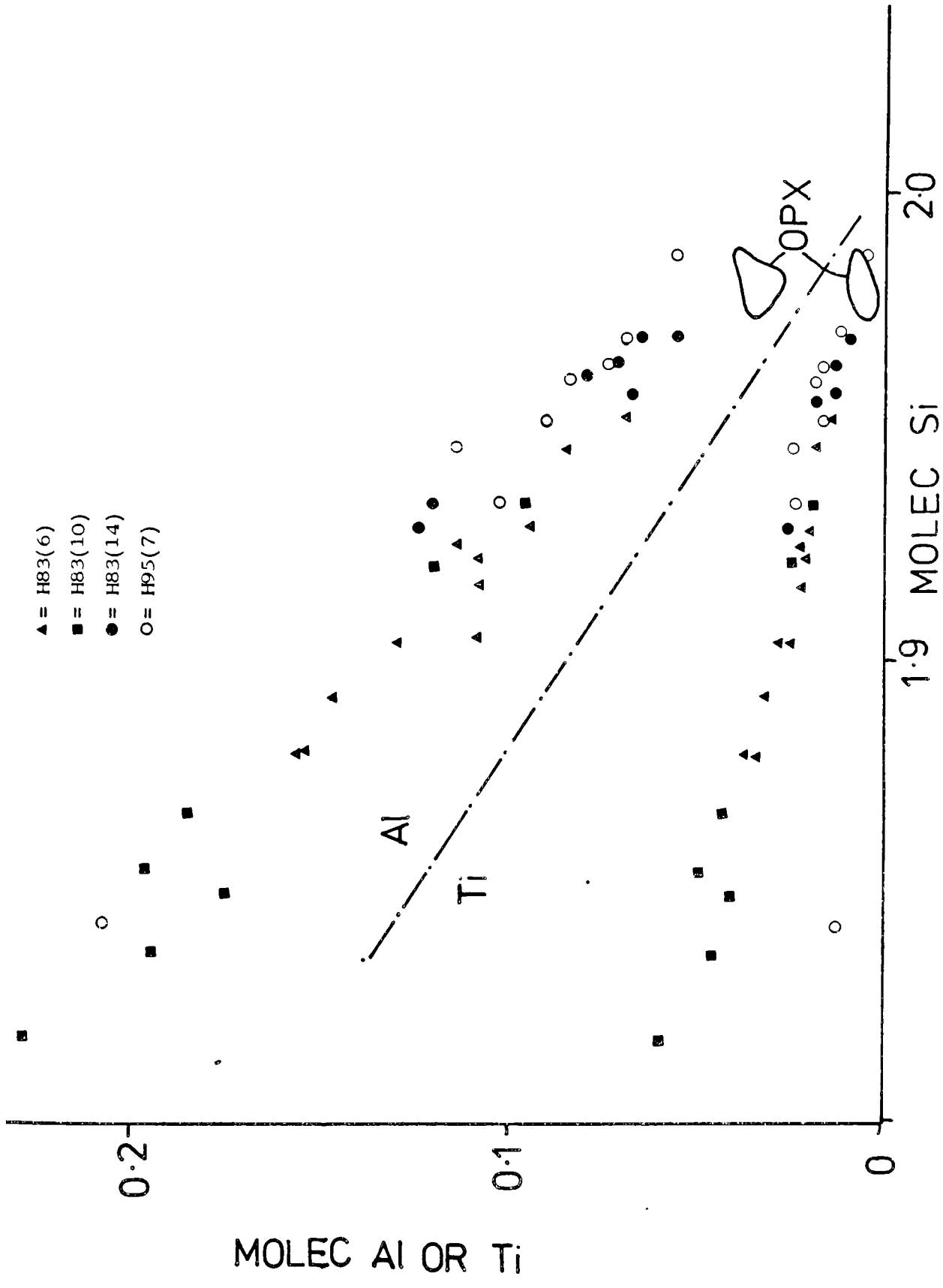
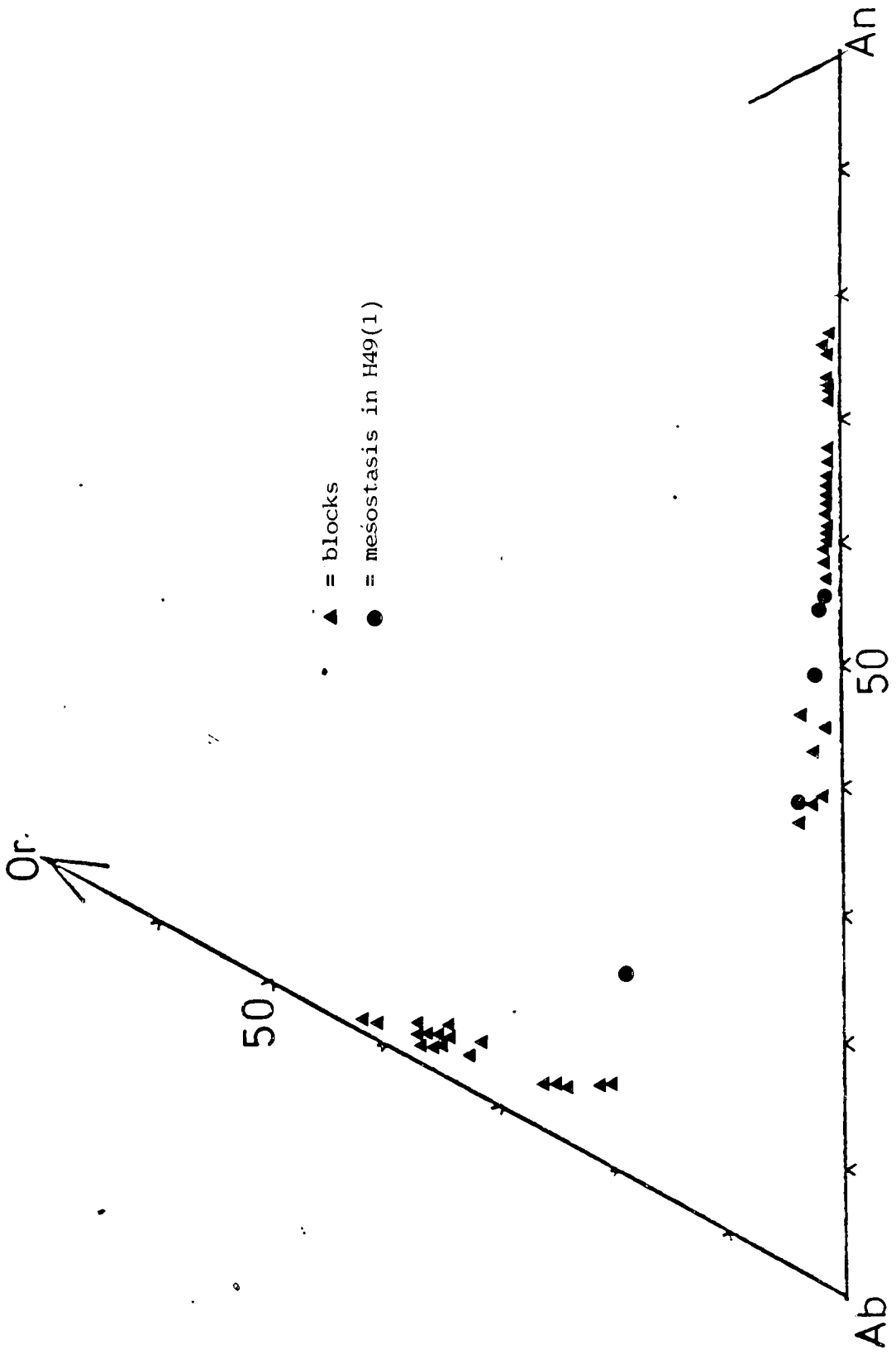
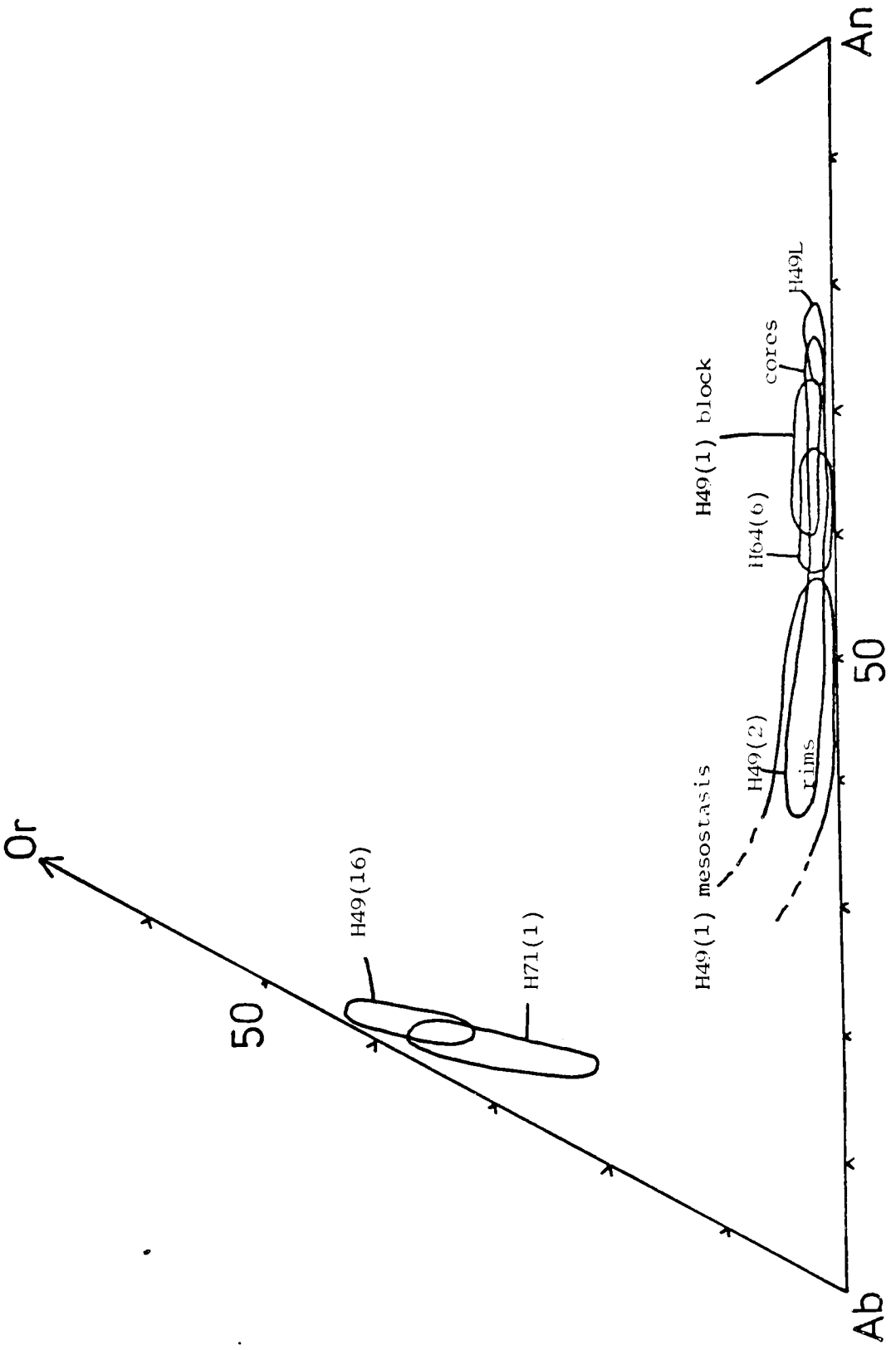


Fig 4.22 Variation in feldspar composition in blocks from the south coast lavas



variation in feldspars from south coast lava blocks



composition of pyroxenes in blocks from the south coast lavas

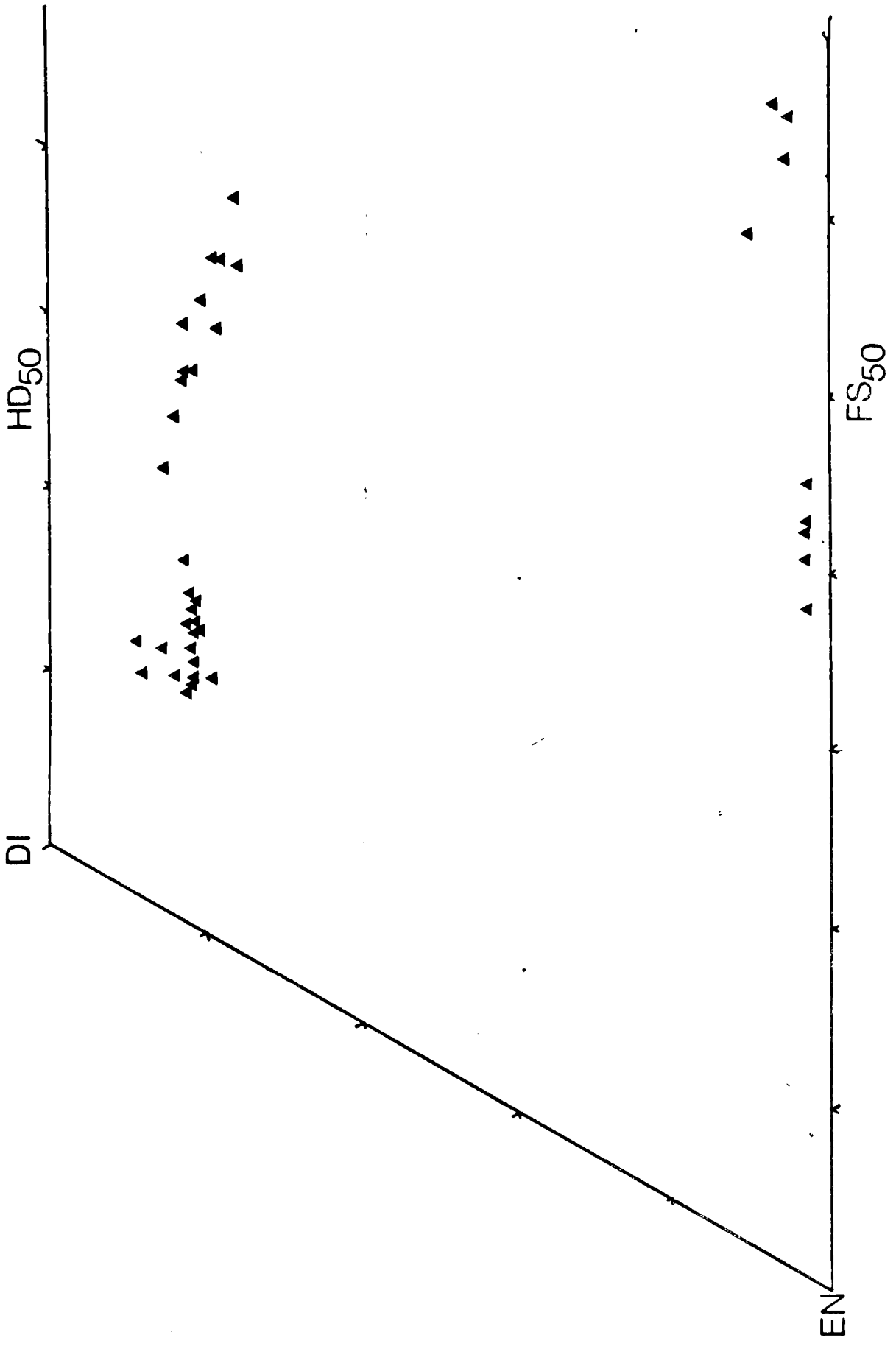


Fig 4.25 Intrasample variation of pyroxene analyses from south coast lava blocks

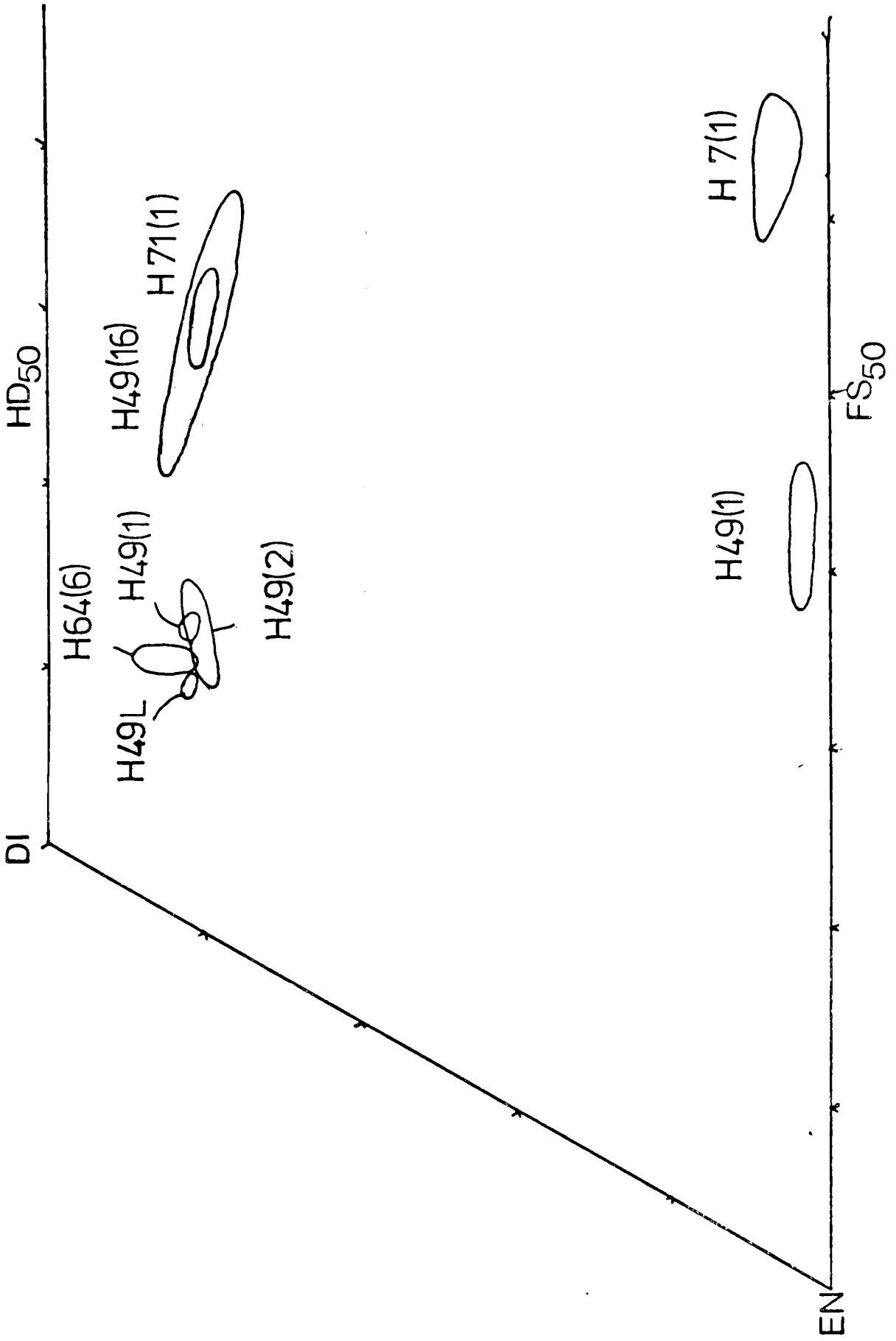


Fig 4.26 Al and Ti vs Si in pyroxenes from gabbroic-inter mediate blocks from south coast lavas (assuming 6 oxygens).

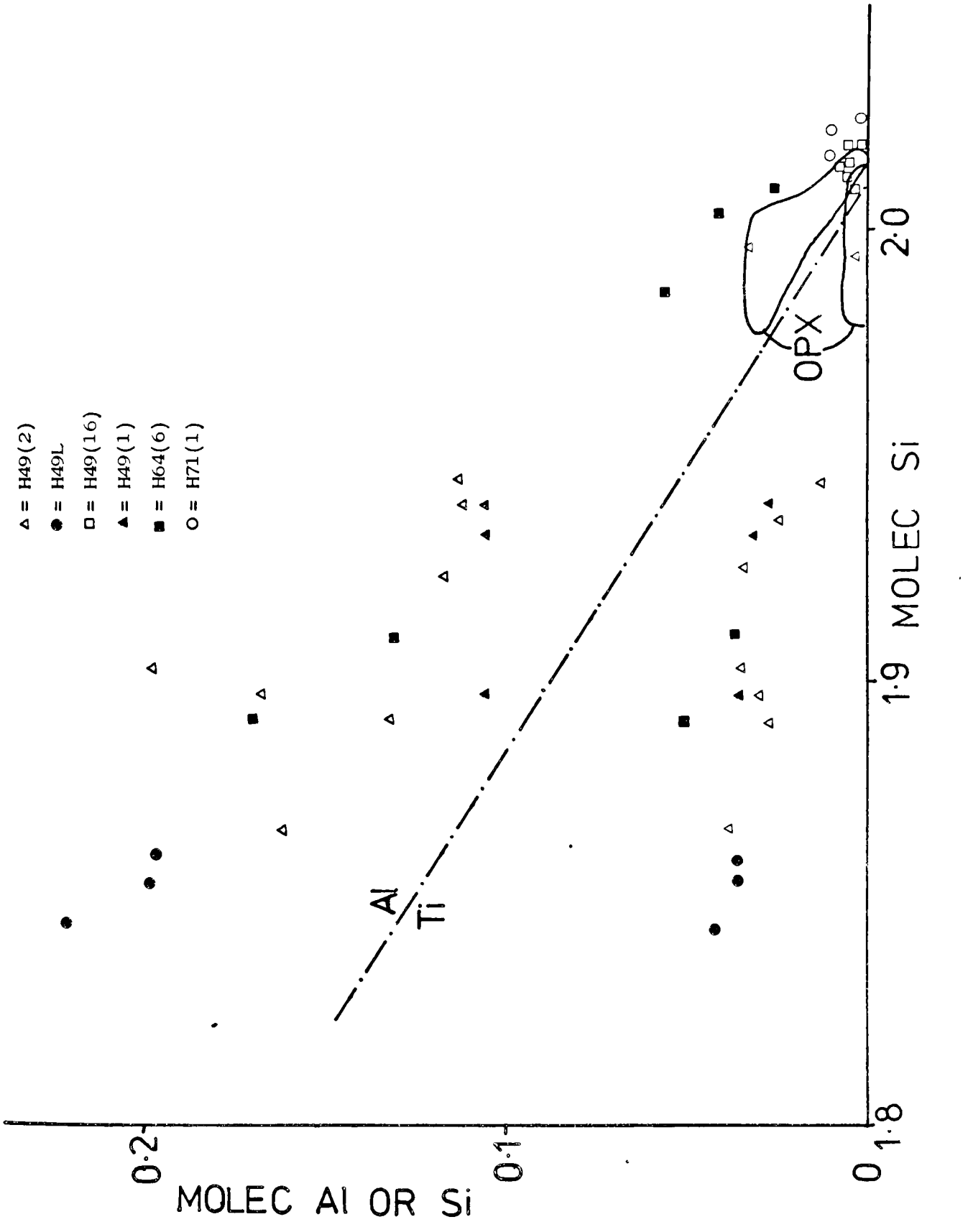


Fig 4.27 Composition of olivine in blocks from the south coast lavas

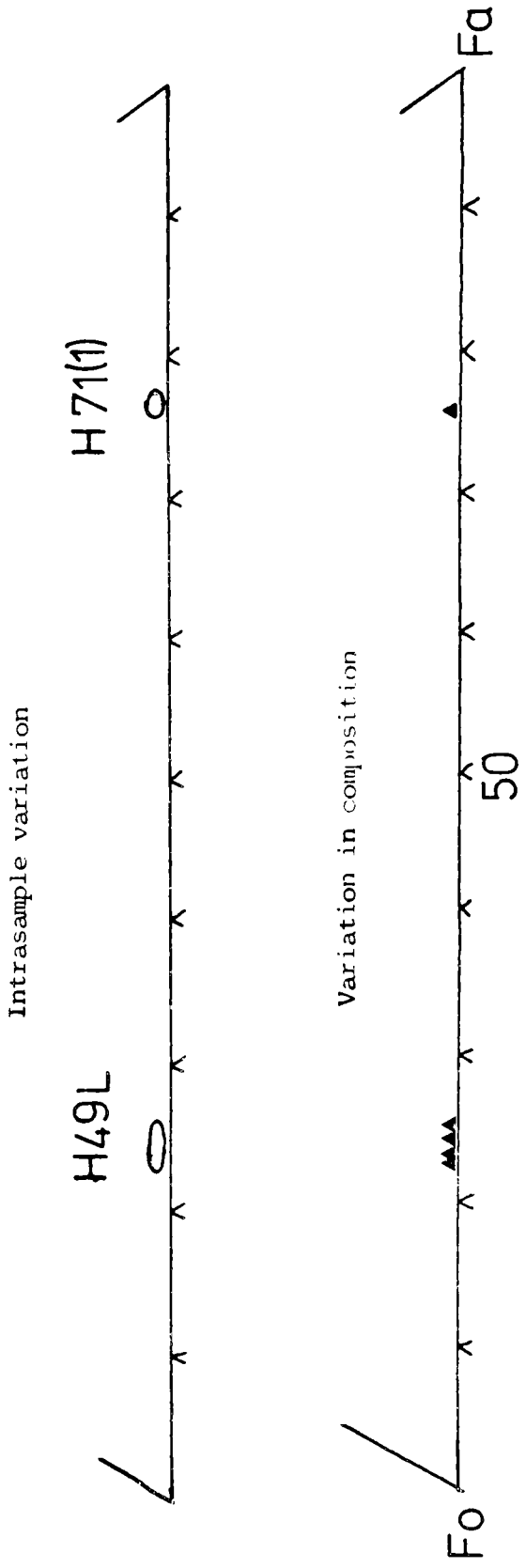


Fig 4.28 Composition of feldspars in blocks from the NASA facies

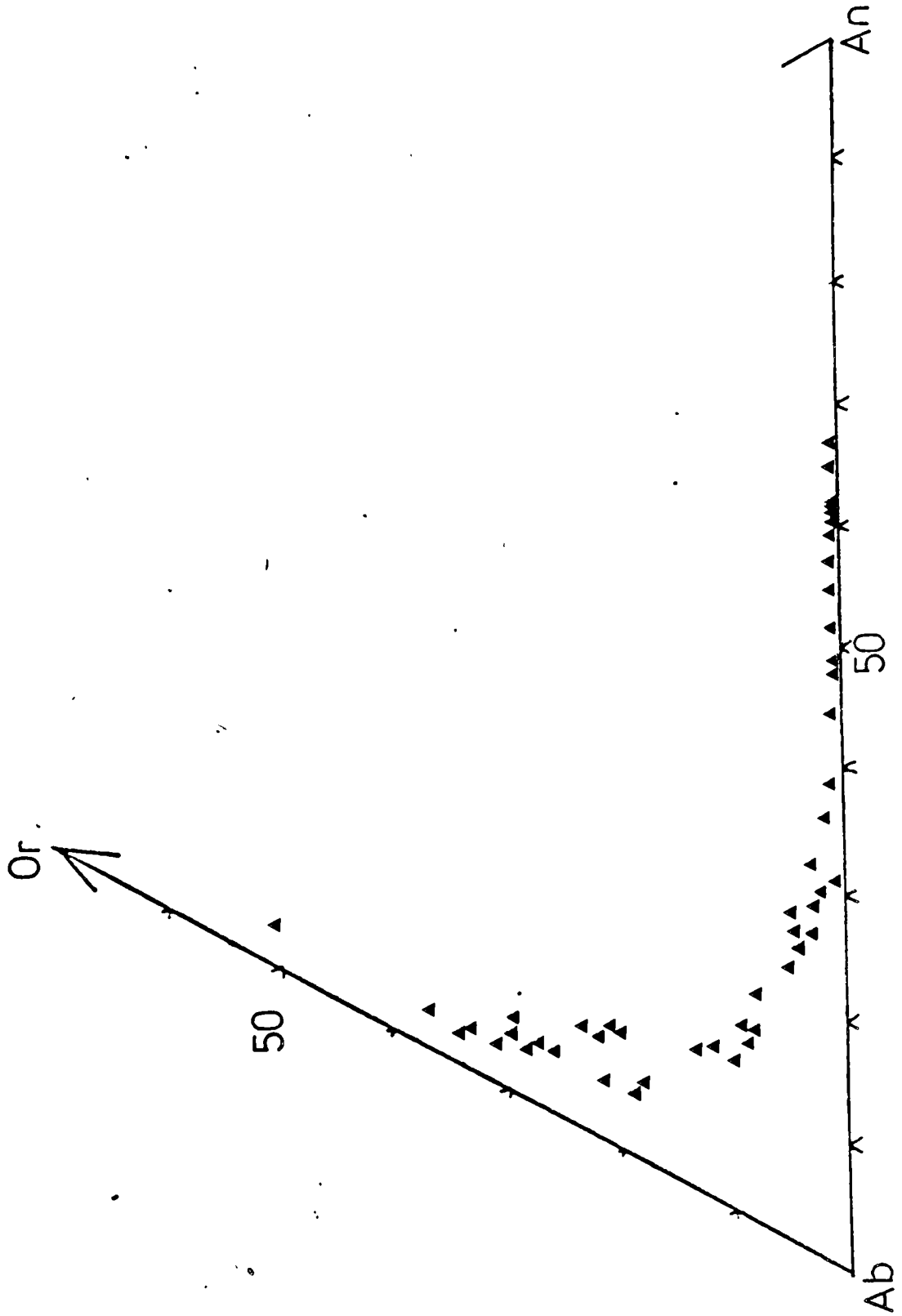


Fig 4.29 Intrasample variation of feldspar analyses from blocks of the NASA facies

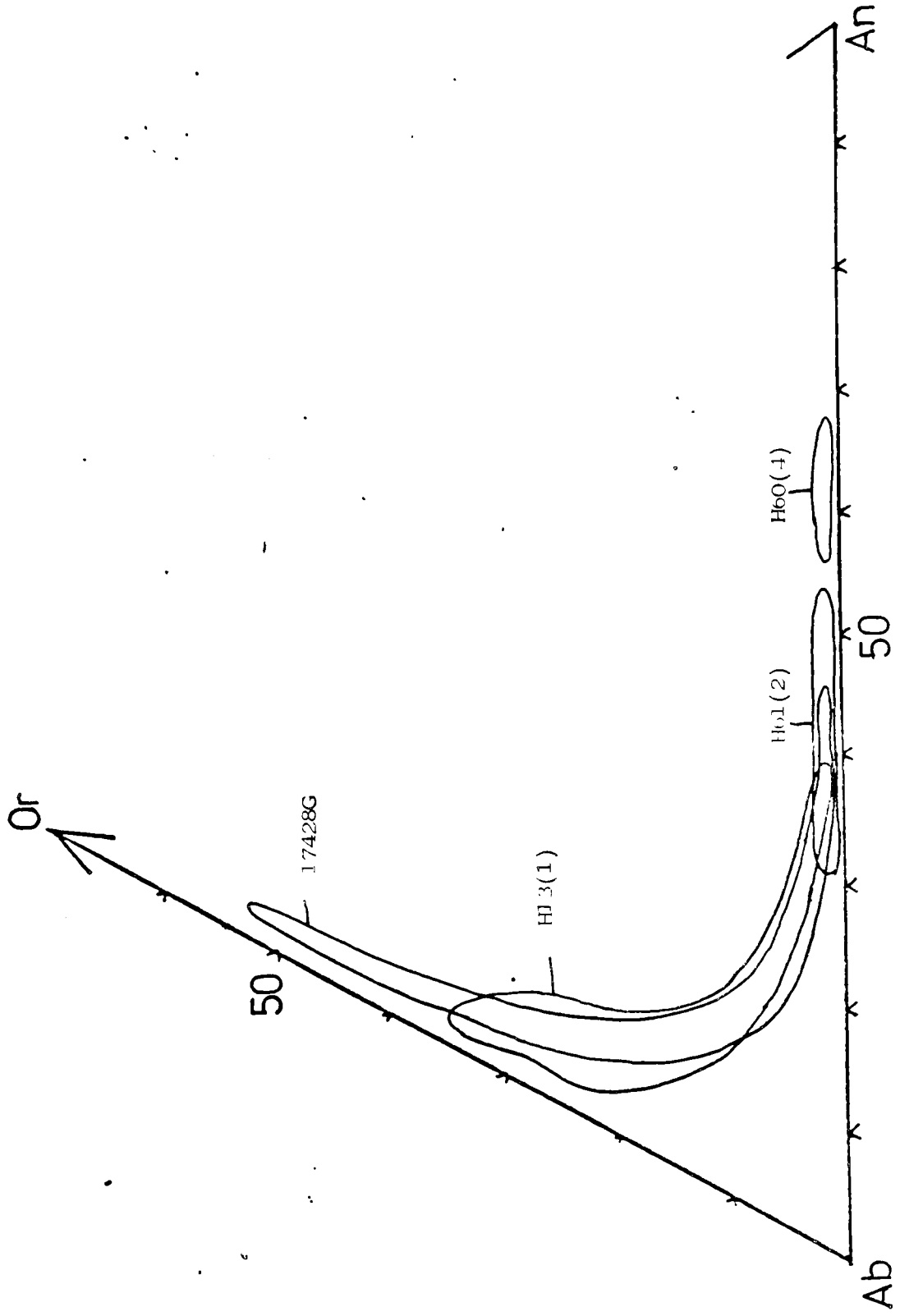


Fig 4.30 Composition of pyroxenes in blocks from the NASA facies

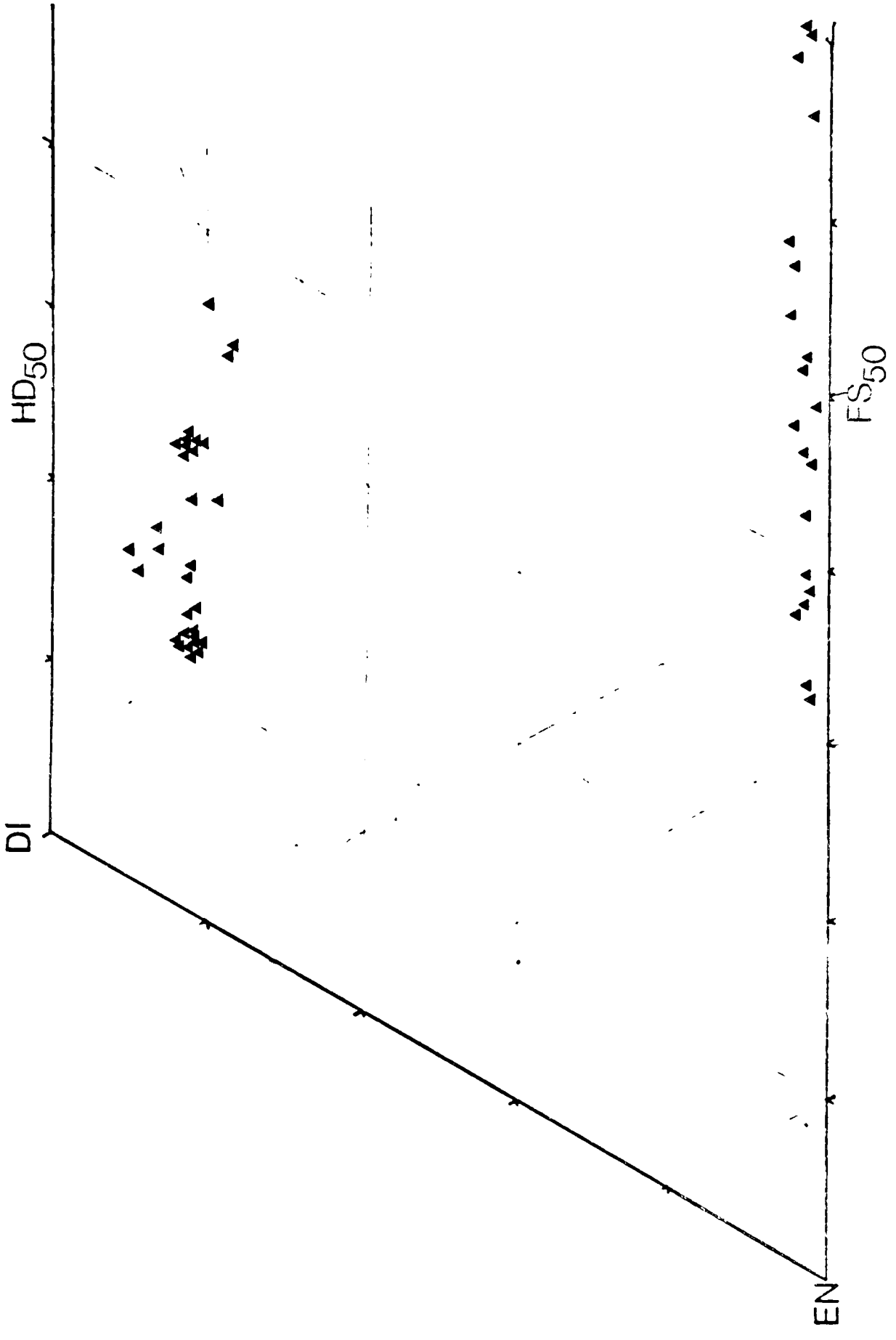


Fig 4.31 Intrasample variation of pyroxene analyses from NASA facies blocks

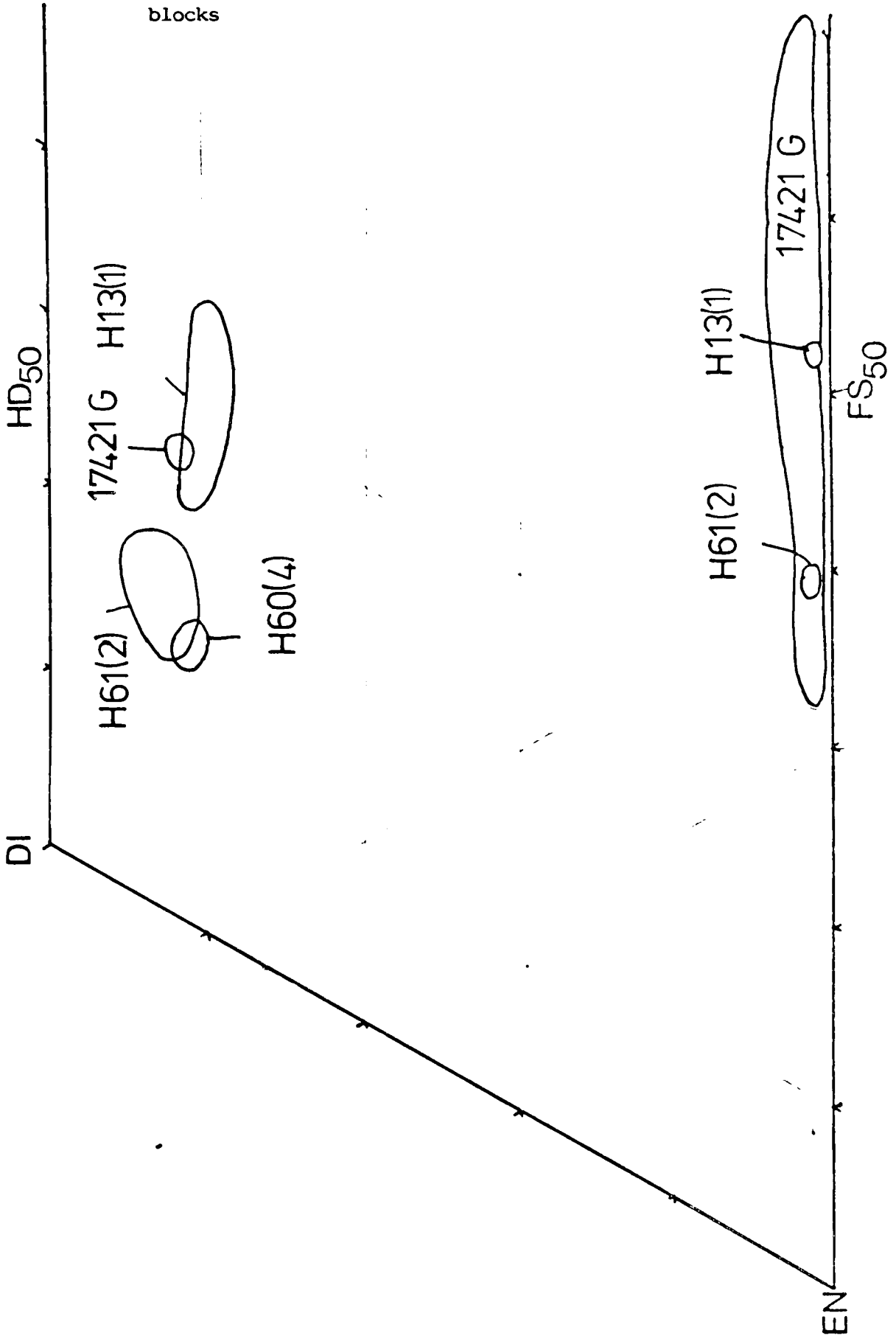


Fig 4.32 Composition of feldspars in blocks from Upper Valley Crater area

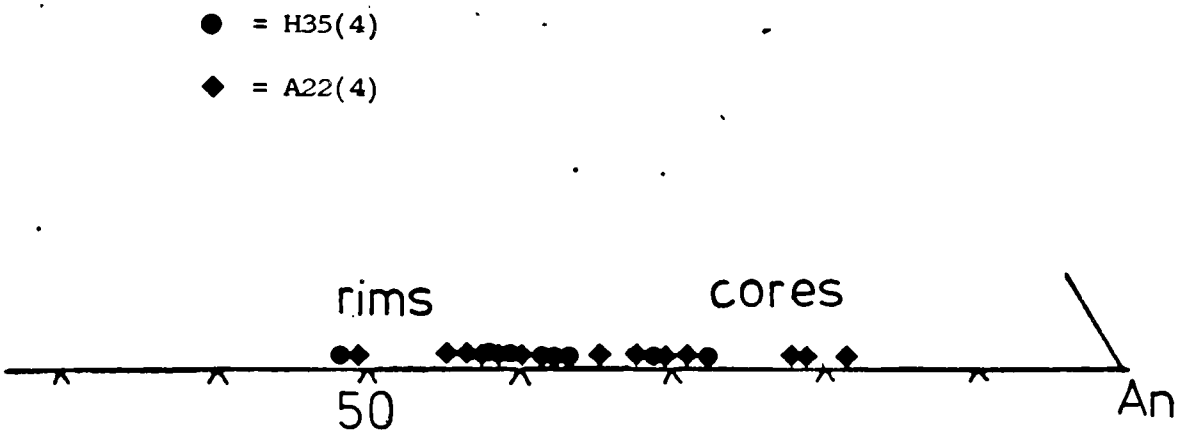
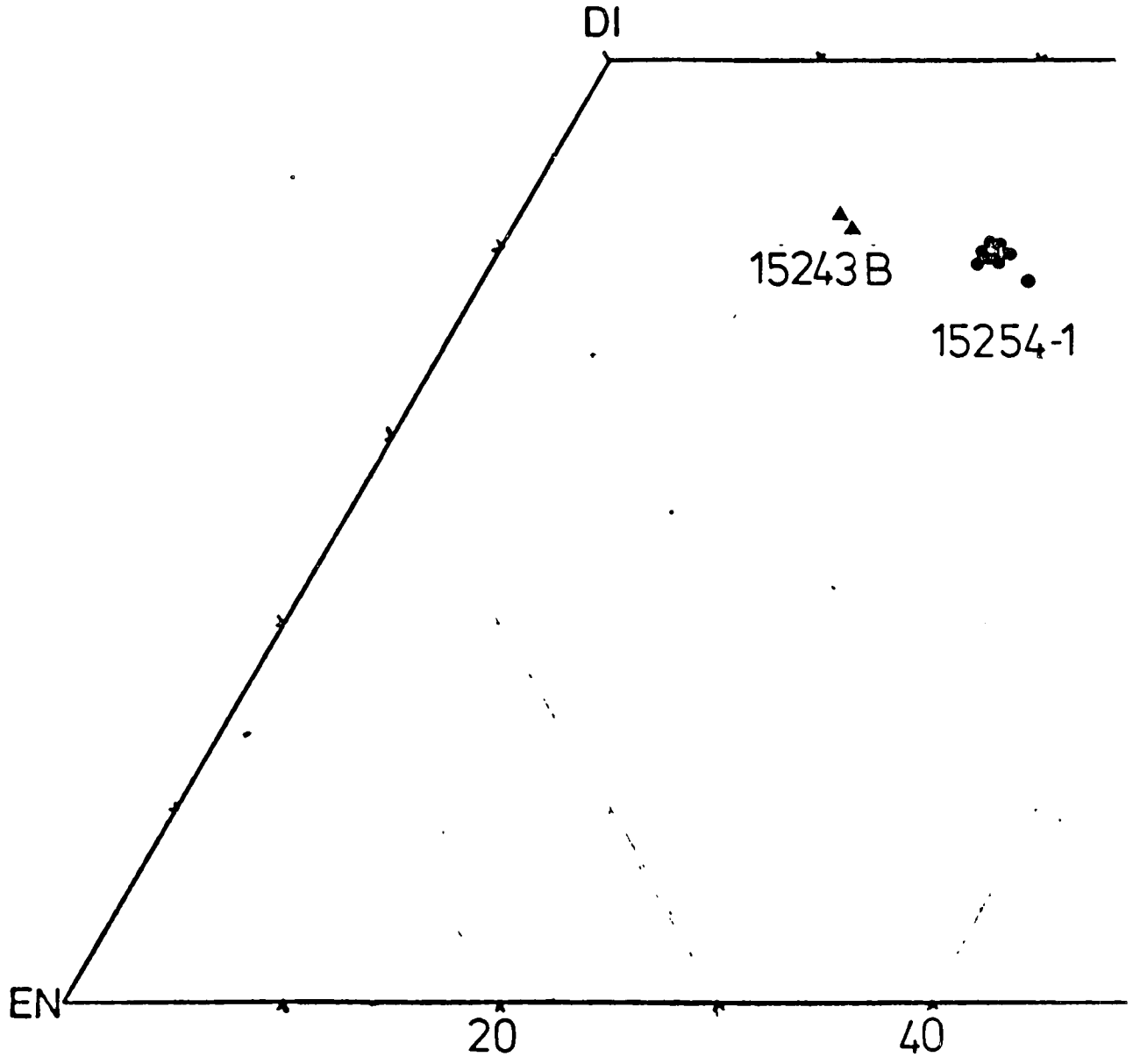


Fig 4.37 Composition of pyroxenes in blocks from Green Mountain



Figs 4.33 and 4.34 Composition of pyroxenes and olivines in blocks from the Upper Valley Crater area

Fig 4.33 pyroxene

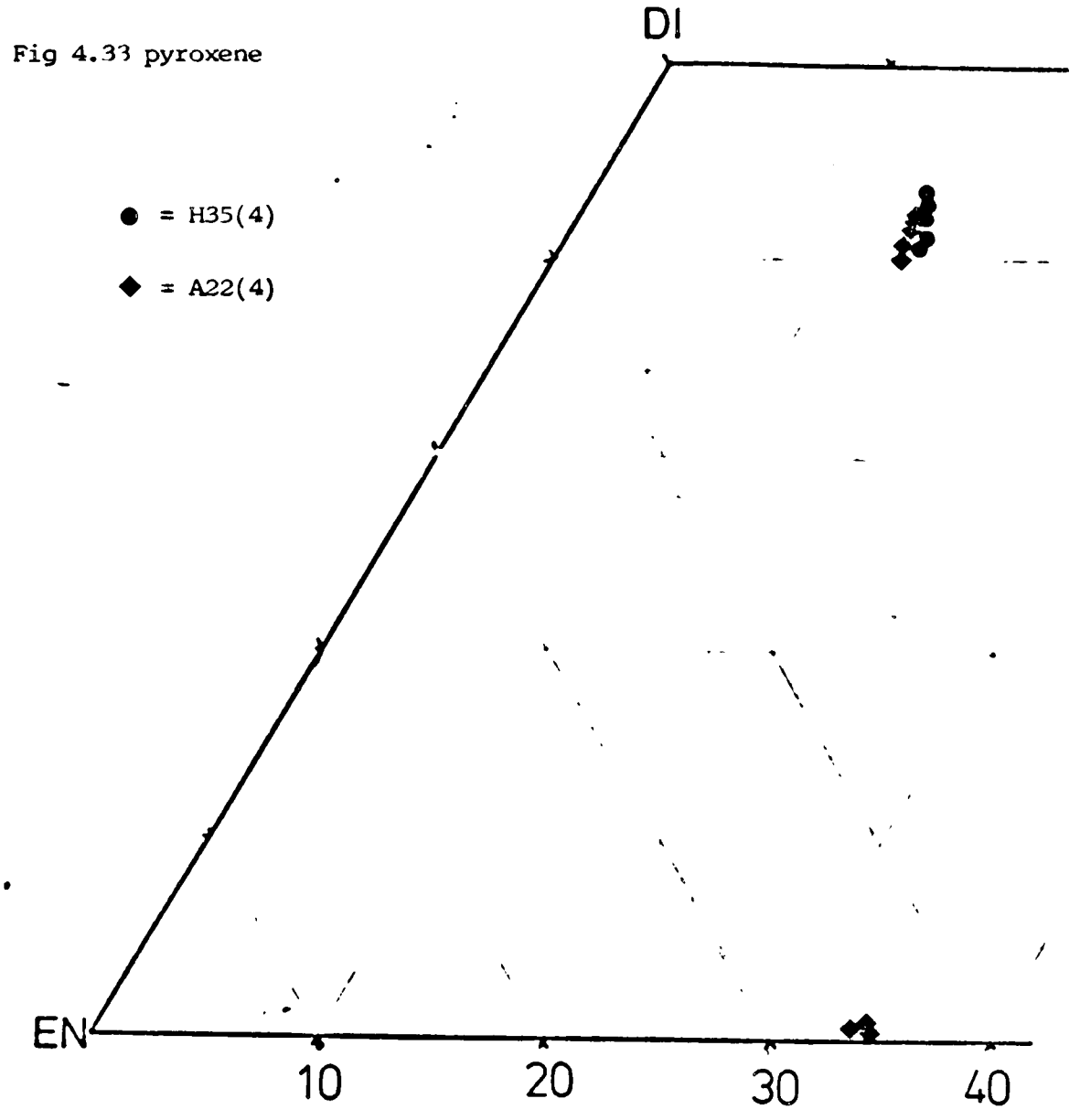
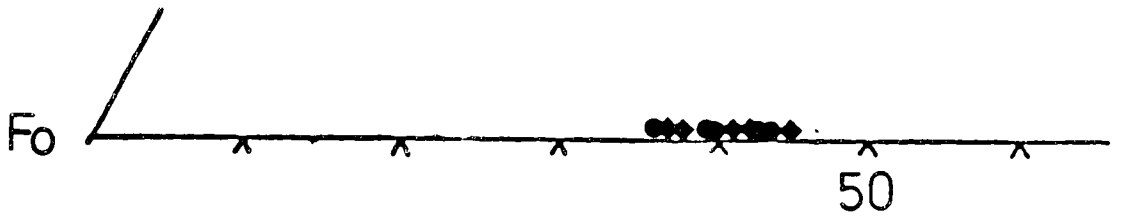


Fig 4.34 olivine



Figs 4.35 and 4.36 Composition of feldspar and olivine in blocks from Green Mountain

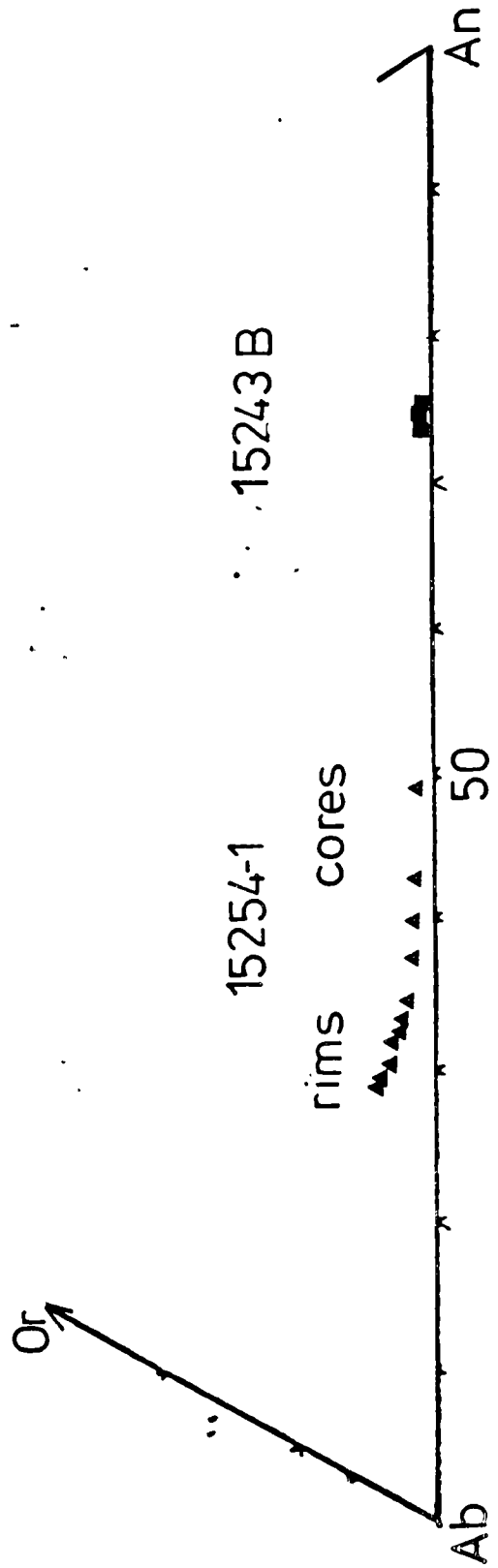


Fig 4.35 feldspar

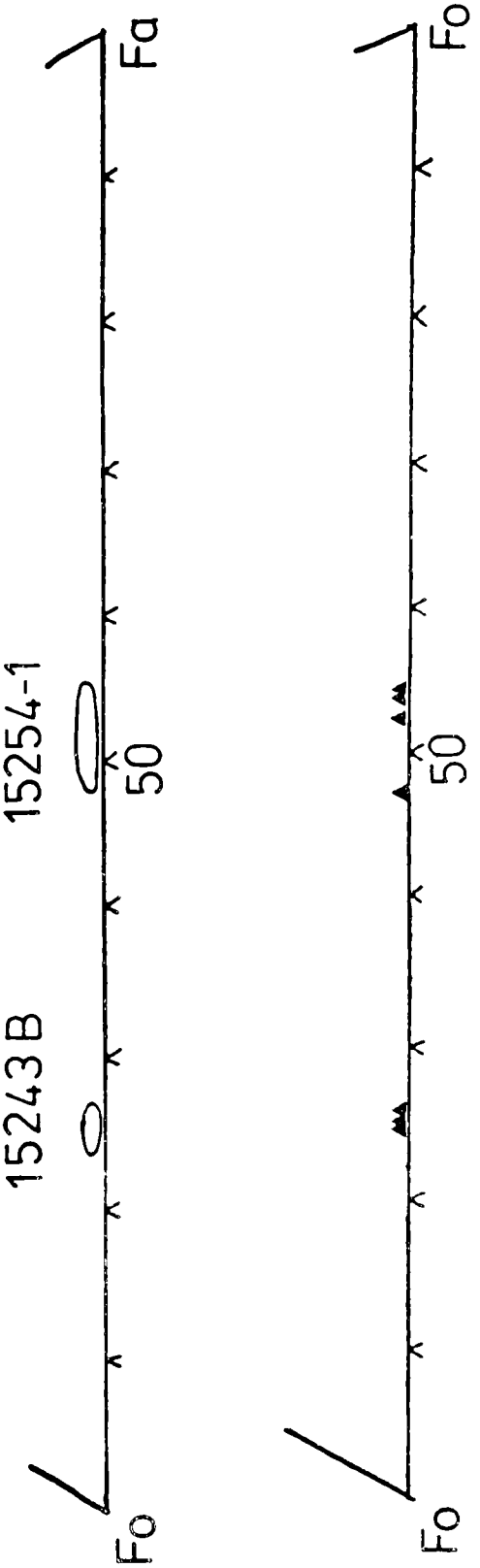


Fig 4.36 olivine

intersample variation

Fig 4.38 Composition of feldspars from acid blocks

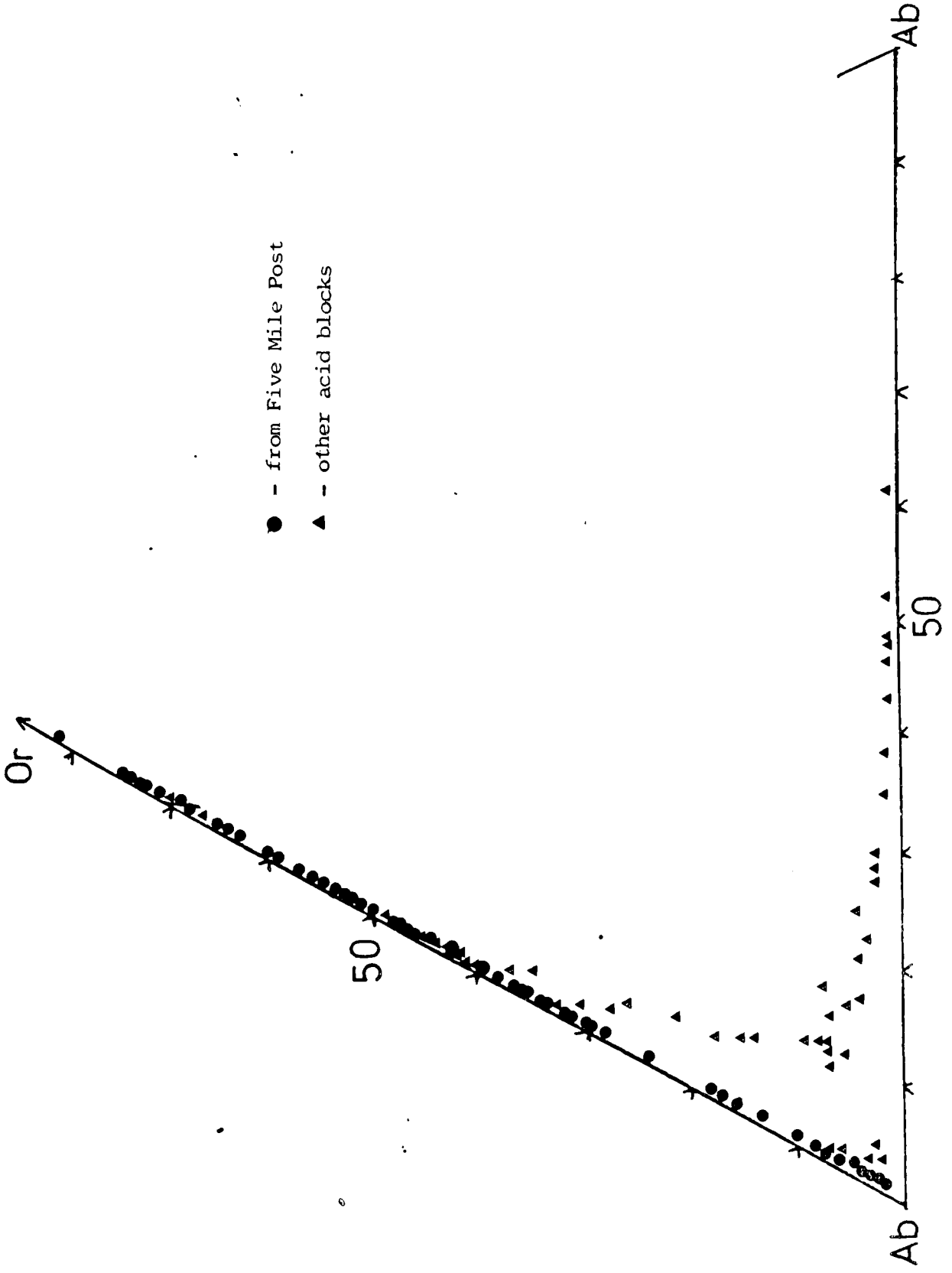


Fig 4.39 Intrasample variation of acid block feldspars

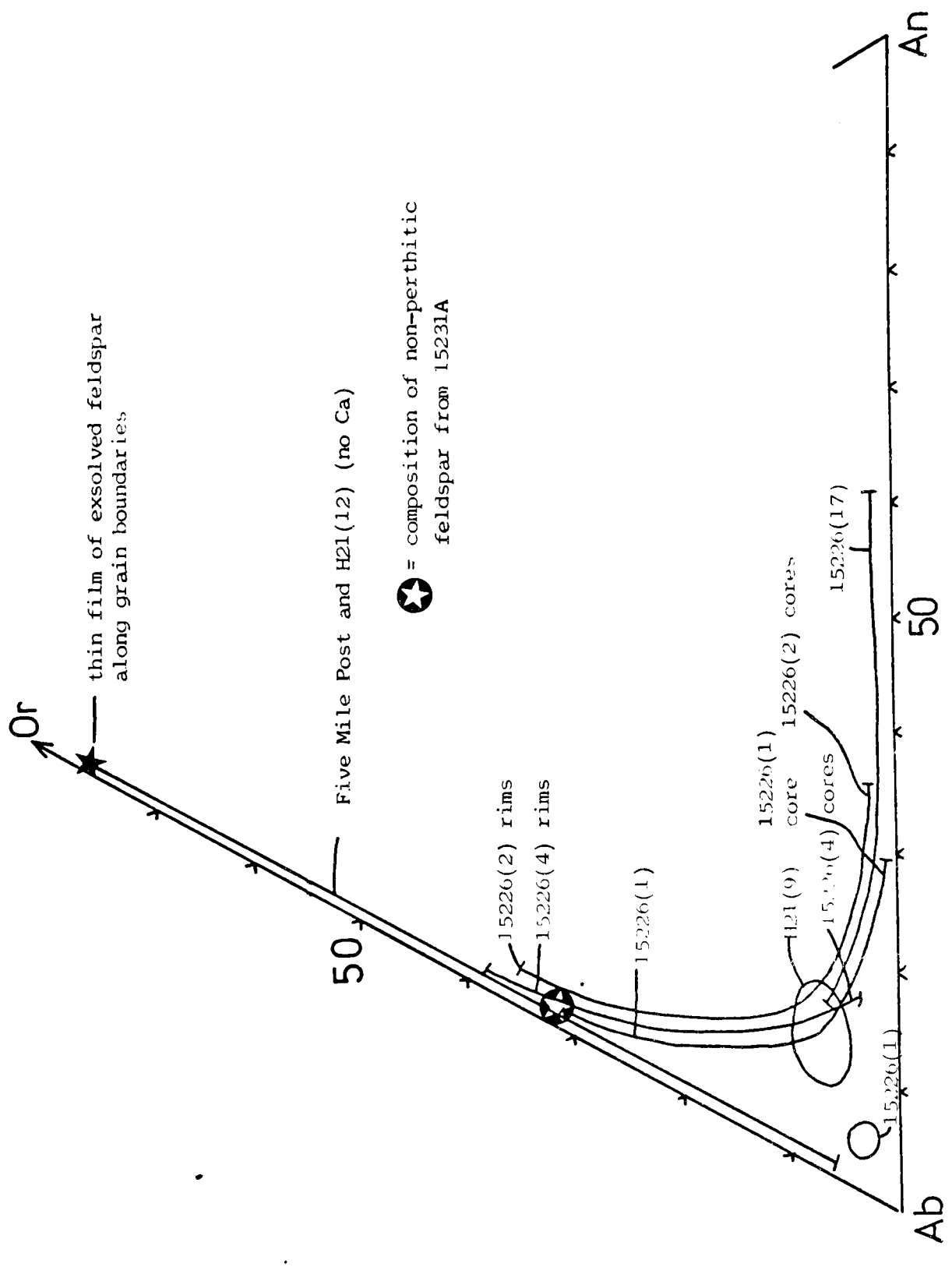


Fig 4.40 Composition of Ca - Mg - Fe pyroxenes in acid blocks

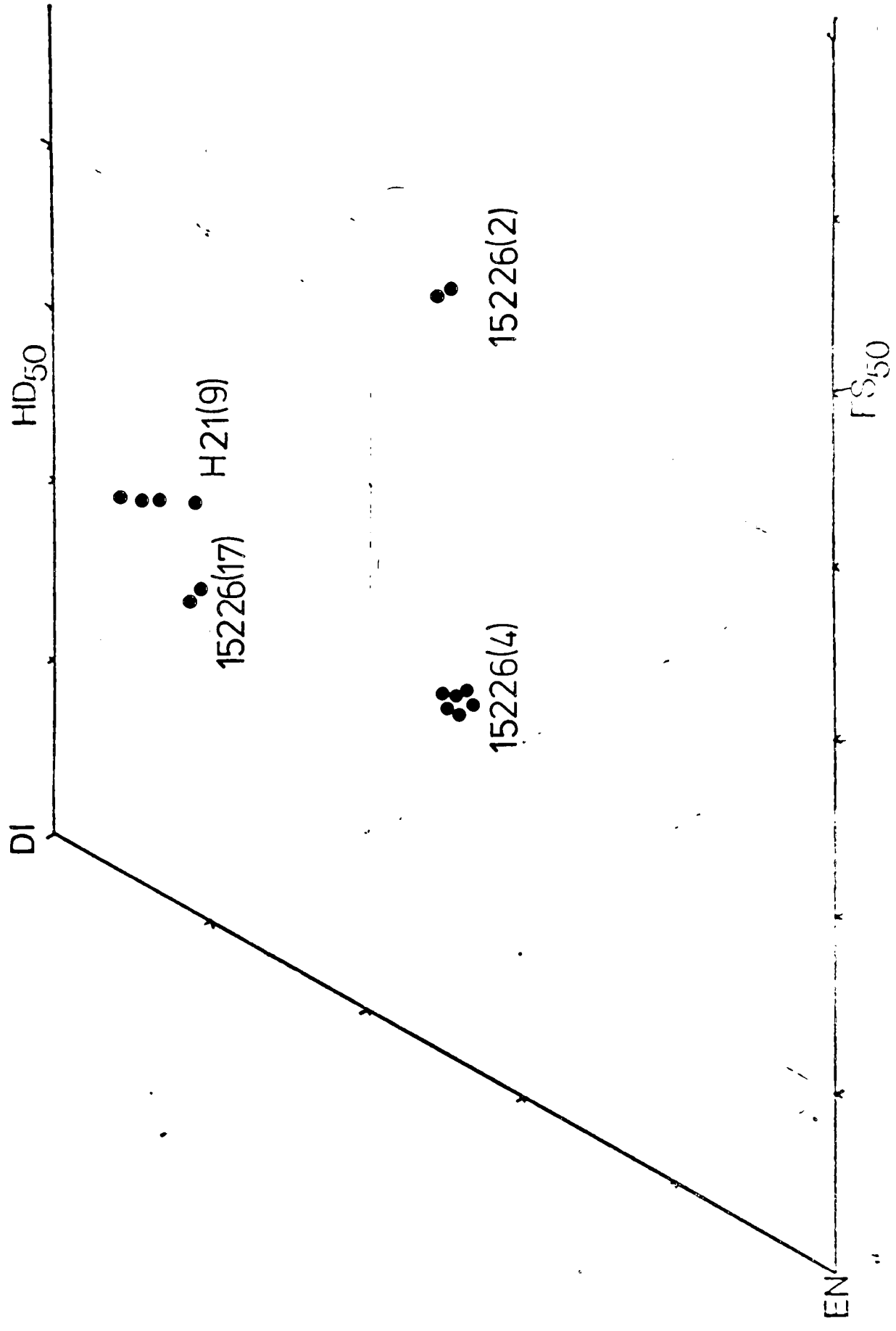


Fig 4.41 Composition of pyroxenes and amphiboles from acid blocks plotted on Na+K, Mg^{2+}, Fe^{2+} triangle

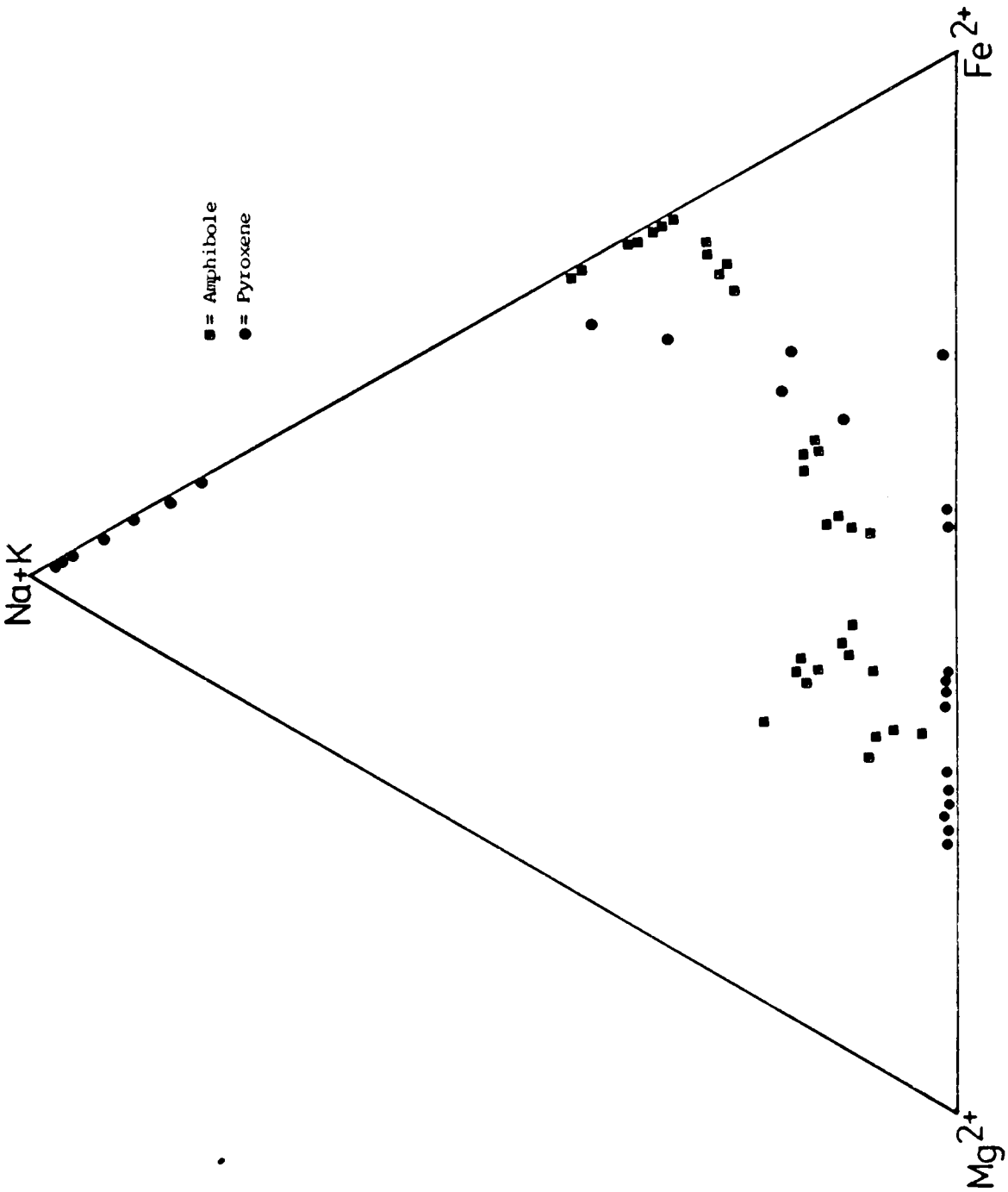


Fig 4.42 Pyroxenes and amphiboles from acid blocks; intrasample variation

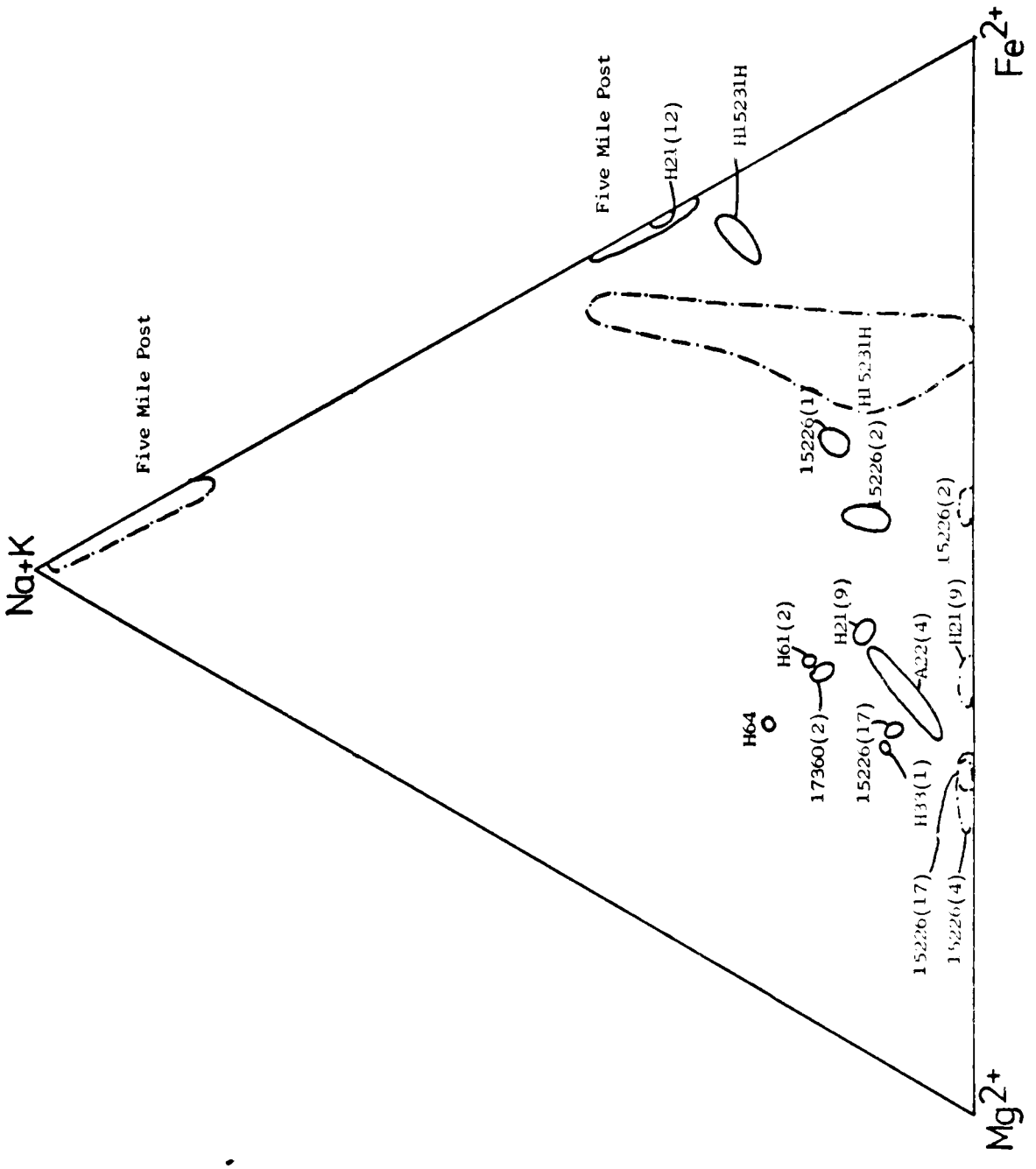


Fig 4.43 Molecular Ca and Ti vs Na (ten oxygens) in pyroxenes from granite blocks

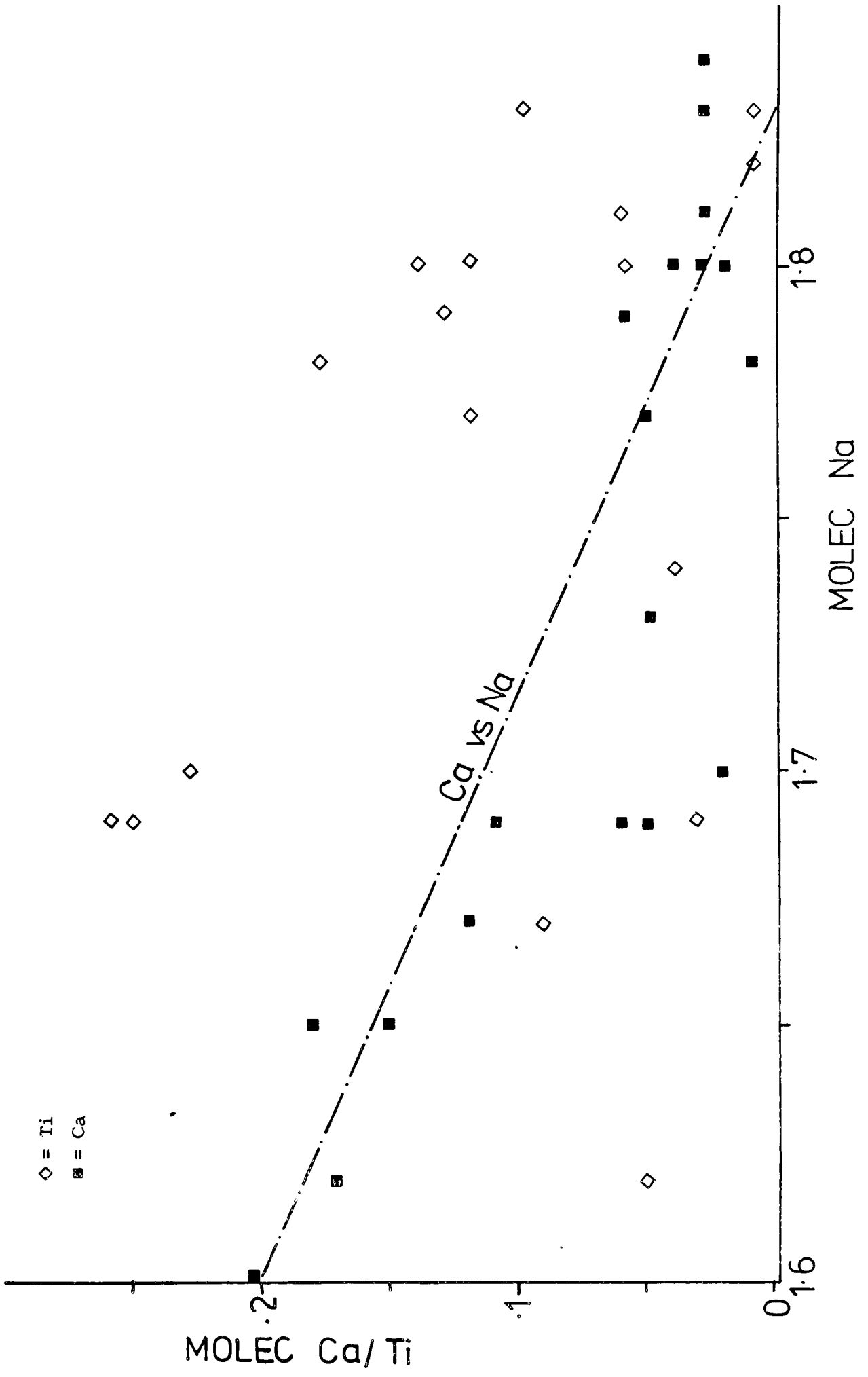


Fig 4.44 Molecular Ti vs Si and Fe in aegirine from granite blocks (assuming ten oxygens in pyroxene)

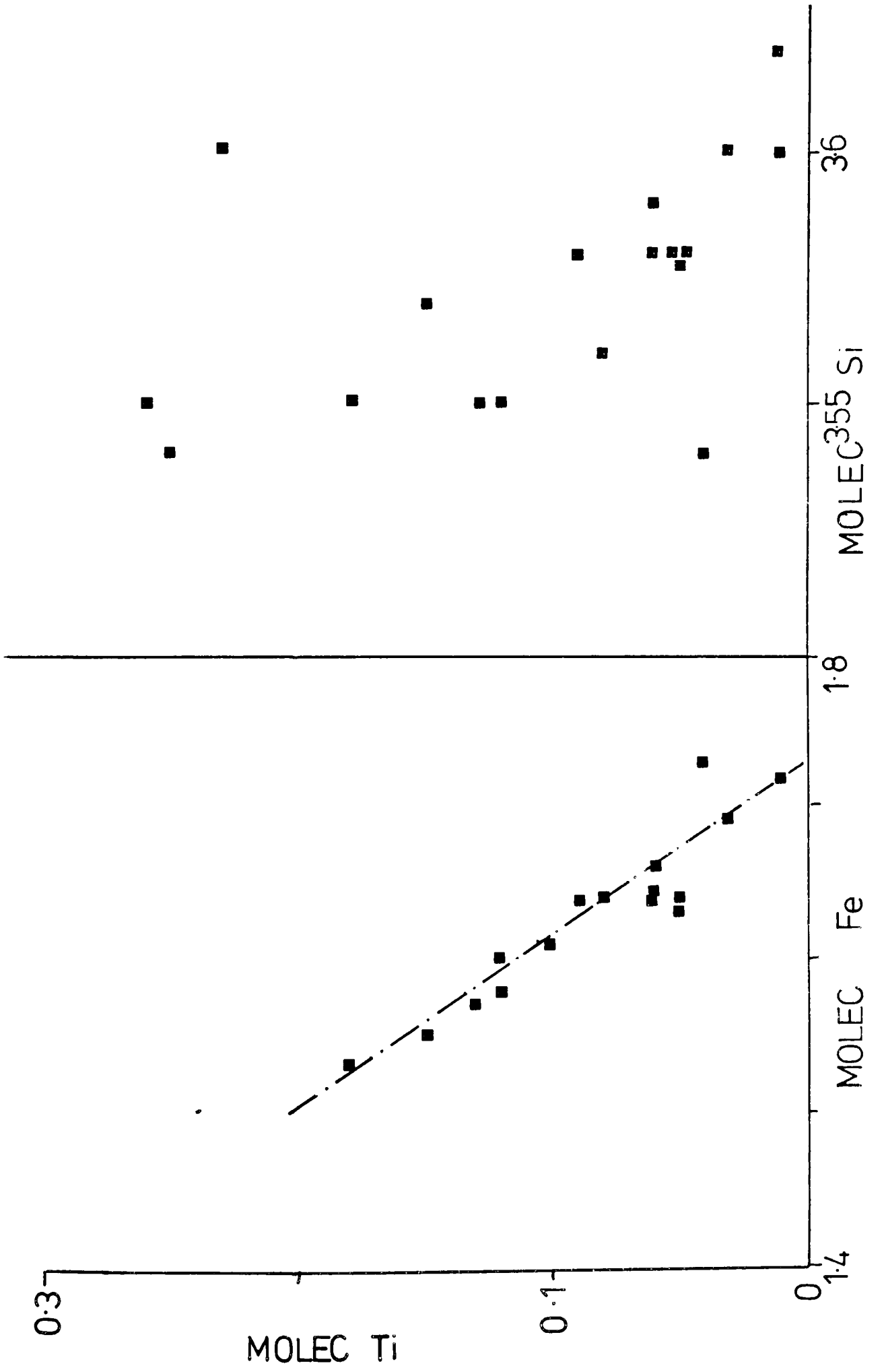


Fig 4.45 Modal proportions of acid blocks from Middleton's Ridge and Five Mile Post.

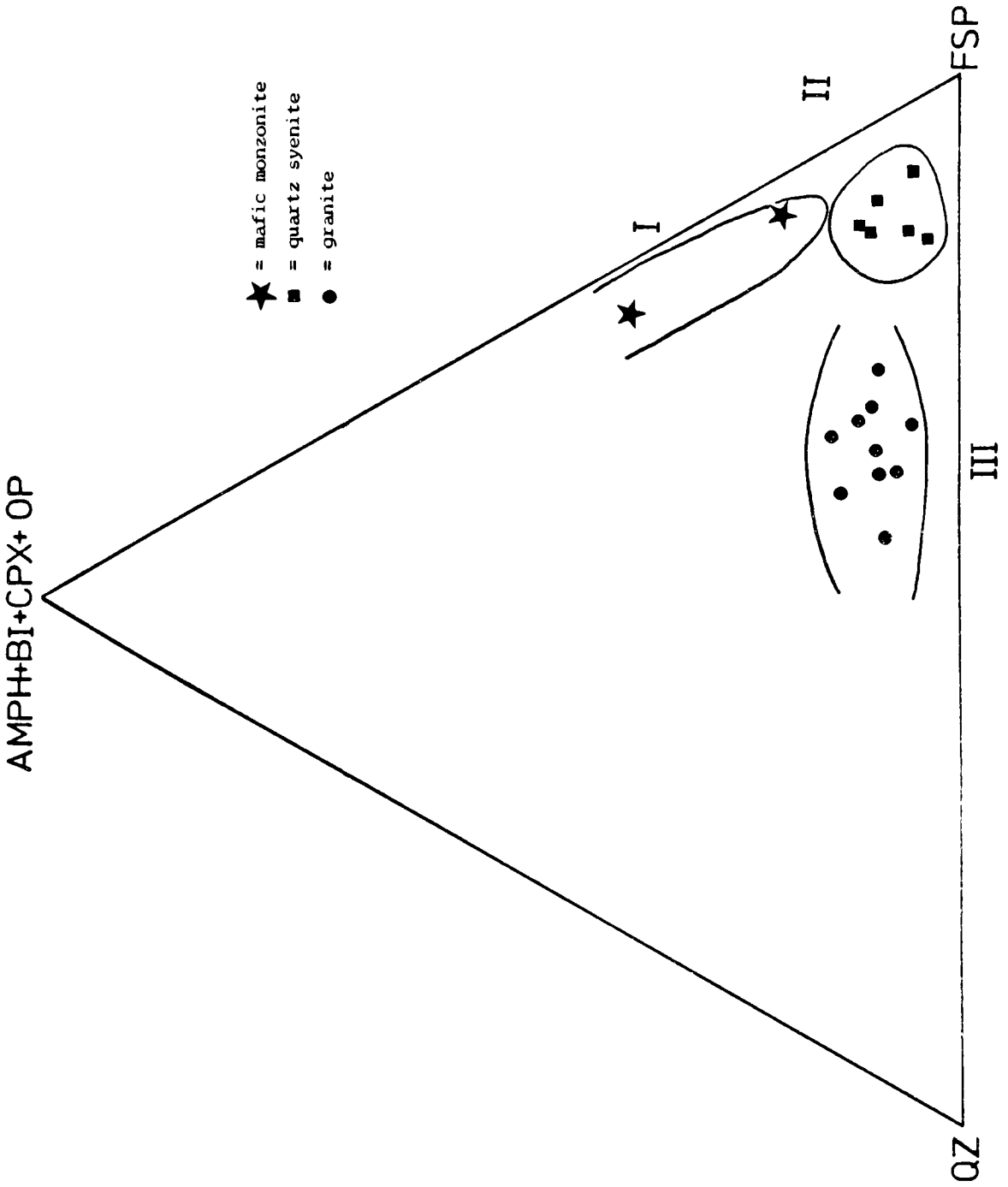


Fig 4.46 Microprobe analyses of feldspar from the pegmatoid.
P= spread of analyses from host lava (H81L) phenocrysts.

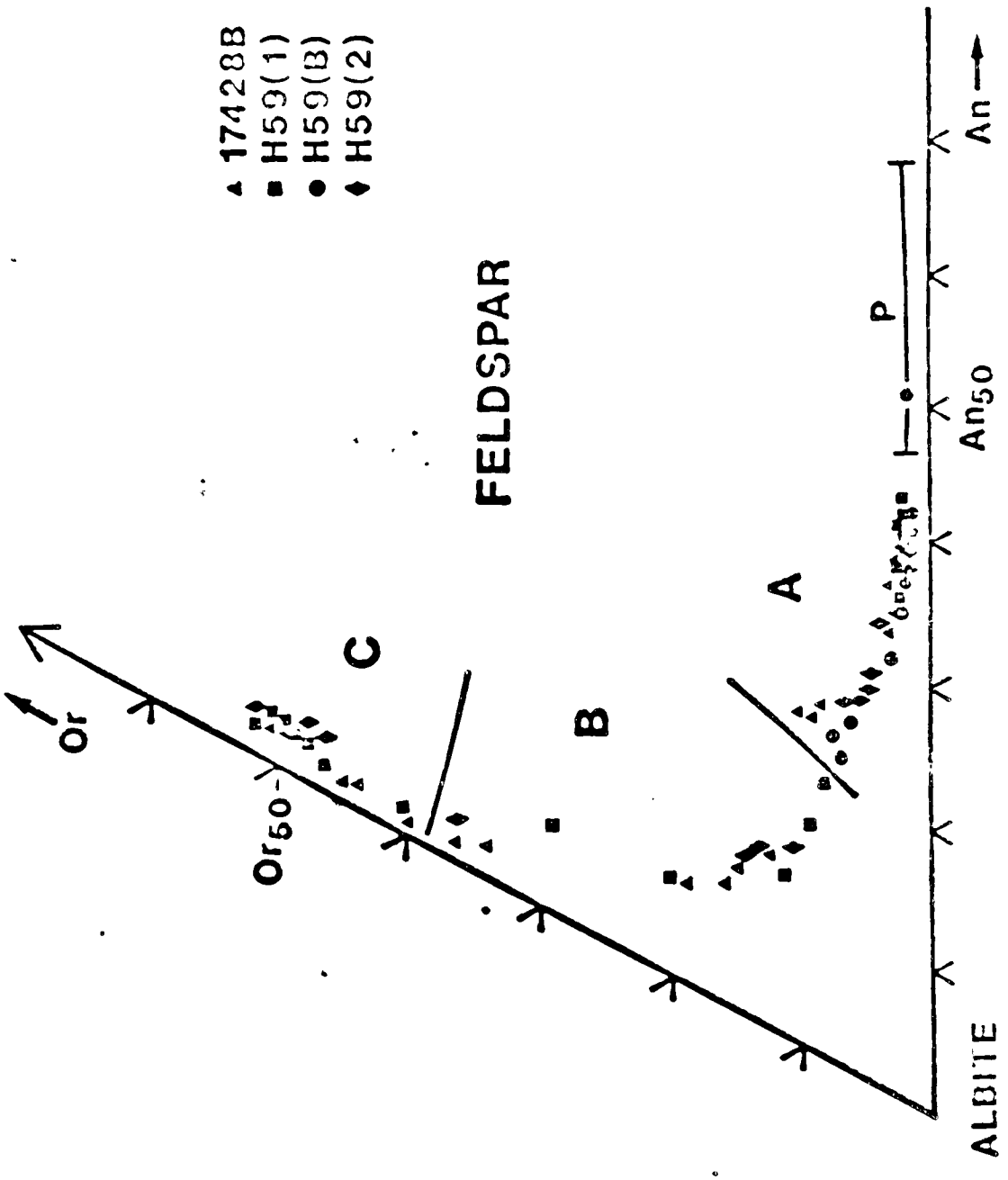


Fig 4.47 Microprobe analyses of pyroxenes and olivines from the pegmatoid

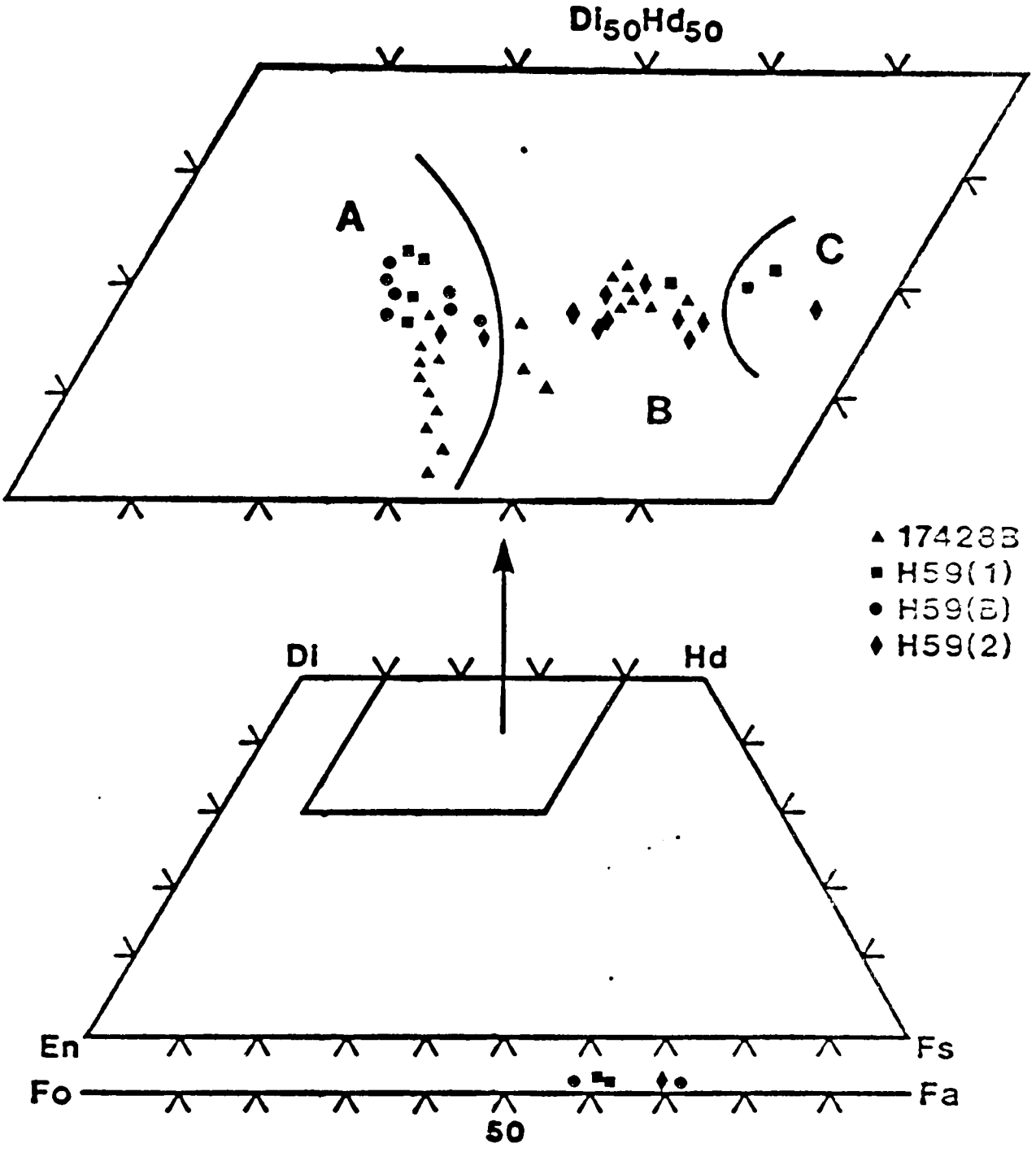


Fig 4.48 Change in composition towards sodic rims of pyroxenes in the pegmatoid. Auvergne trend from Varet (1969), Picture Gorge from Lindsley et al (1971) and Nandewar from Abbott (1969)

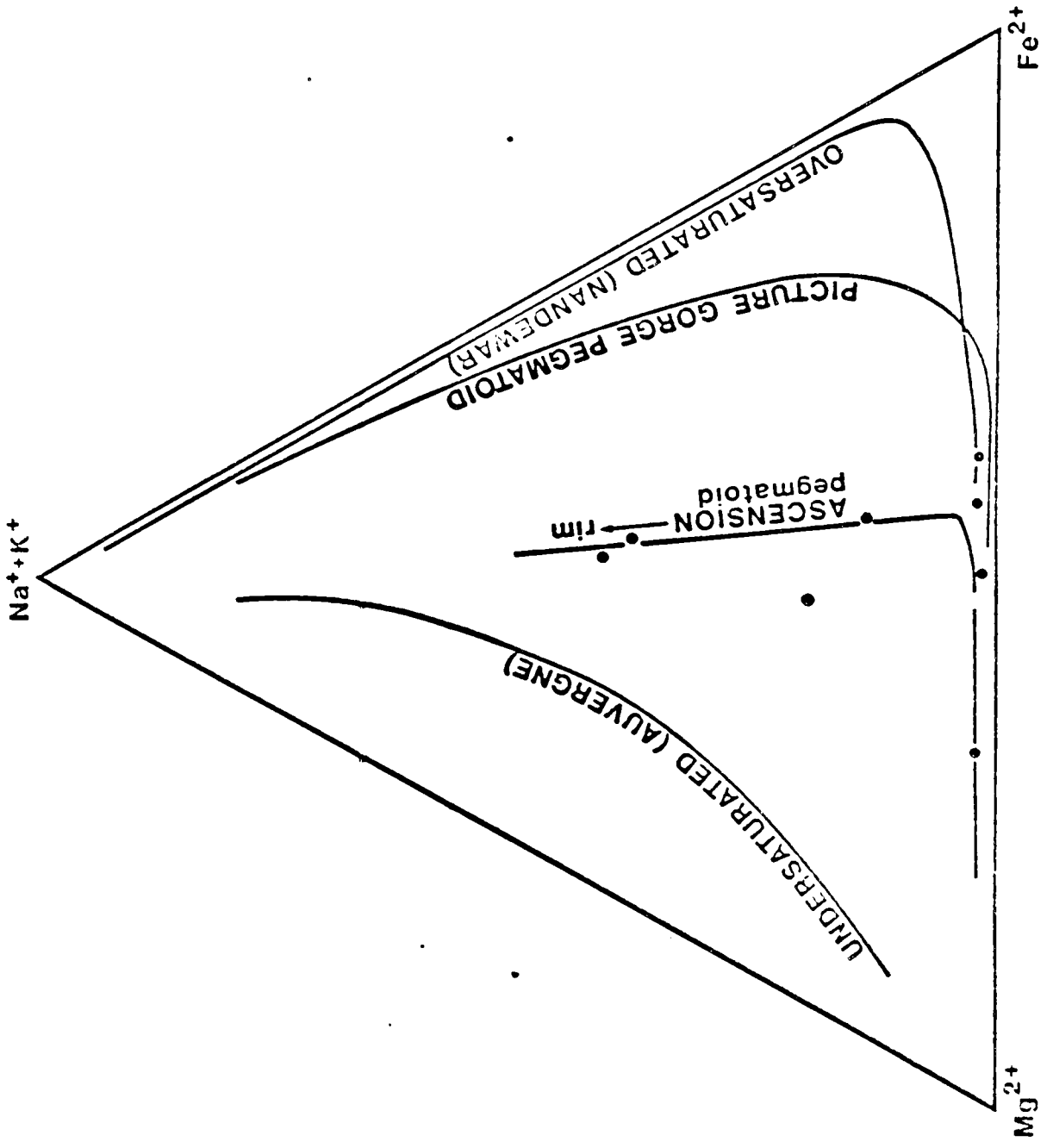


Fig 4.49 ln η (viscosity) and density vs temperature for the pegmatoid and its enclosing lava between 1200 and 1600°c

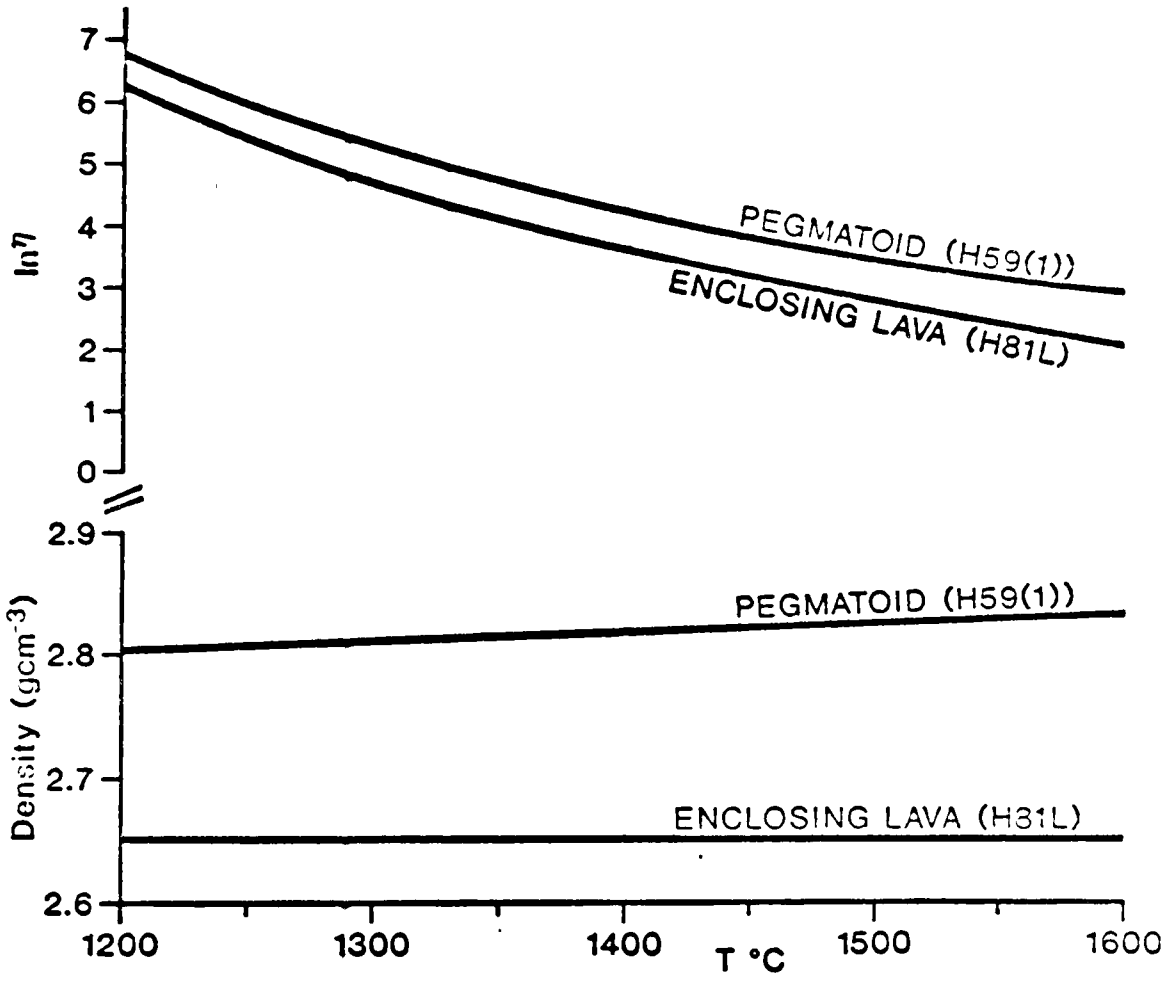


Fig 4.50 Chondrite normalized REE profiles of eudialyte from H 30(1). Shown for comparison are REE profiles of sphene and allanite from Skye granites, (Exley 1980). Circle = Eu detection unit.

Chondritic values from Nakamura (1974), Y & Pr from Frey et al. (1968) .

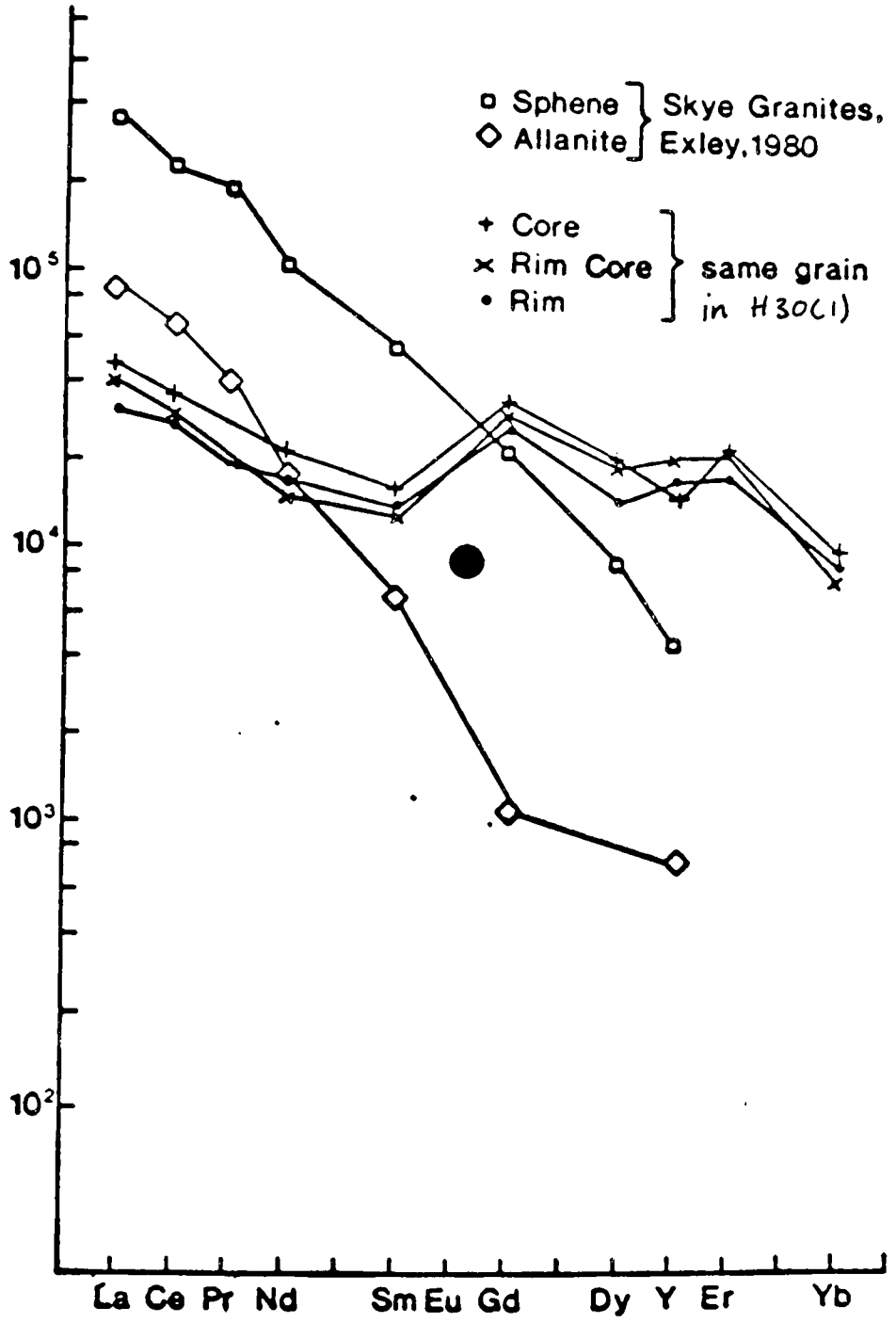


Fig 4.51 Chondrite normalised REE profile of H 30(1) whole rock. REE values obtained by standard isotope dilution methods, Y by X.R.F.

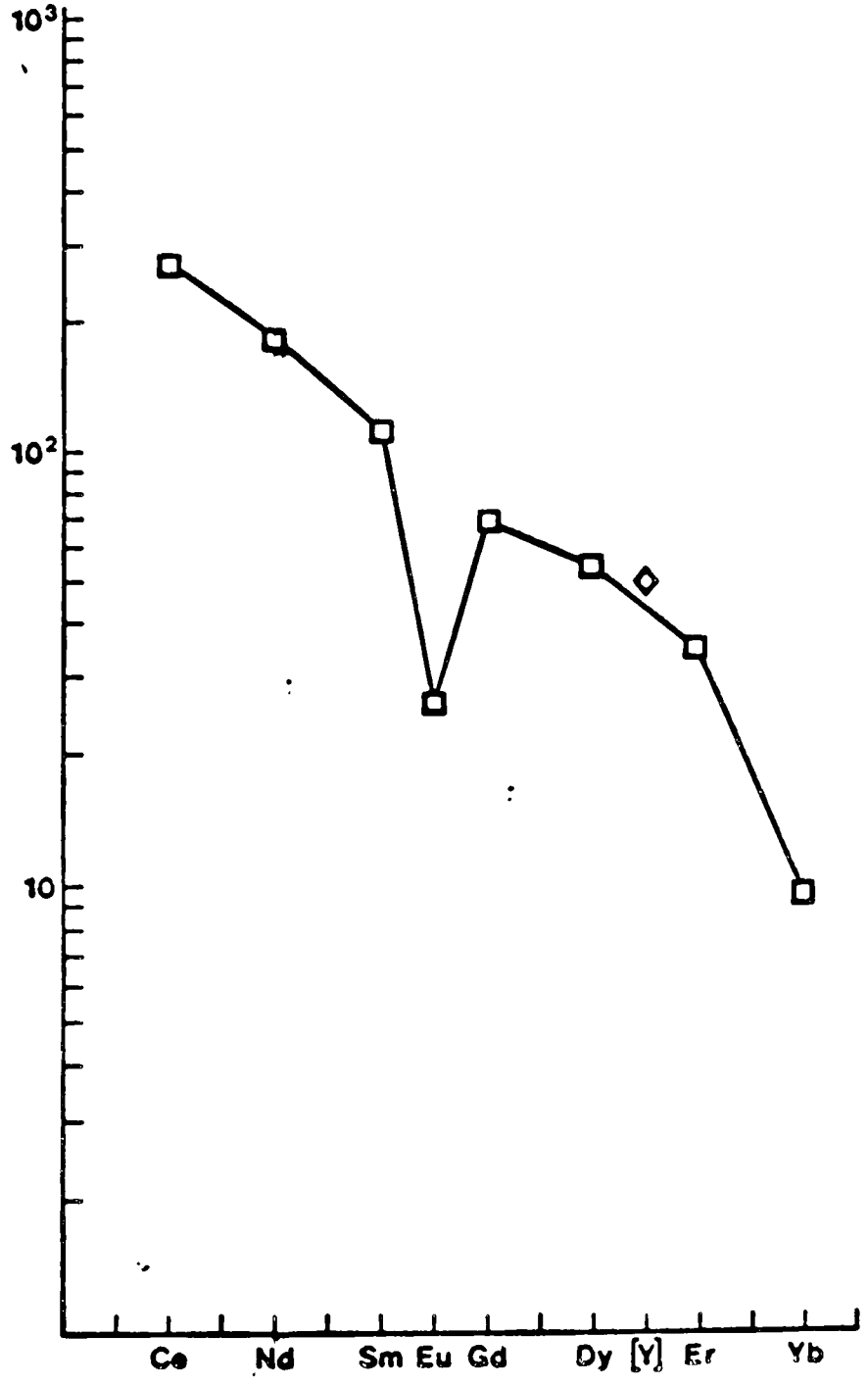
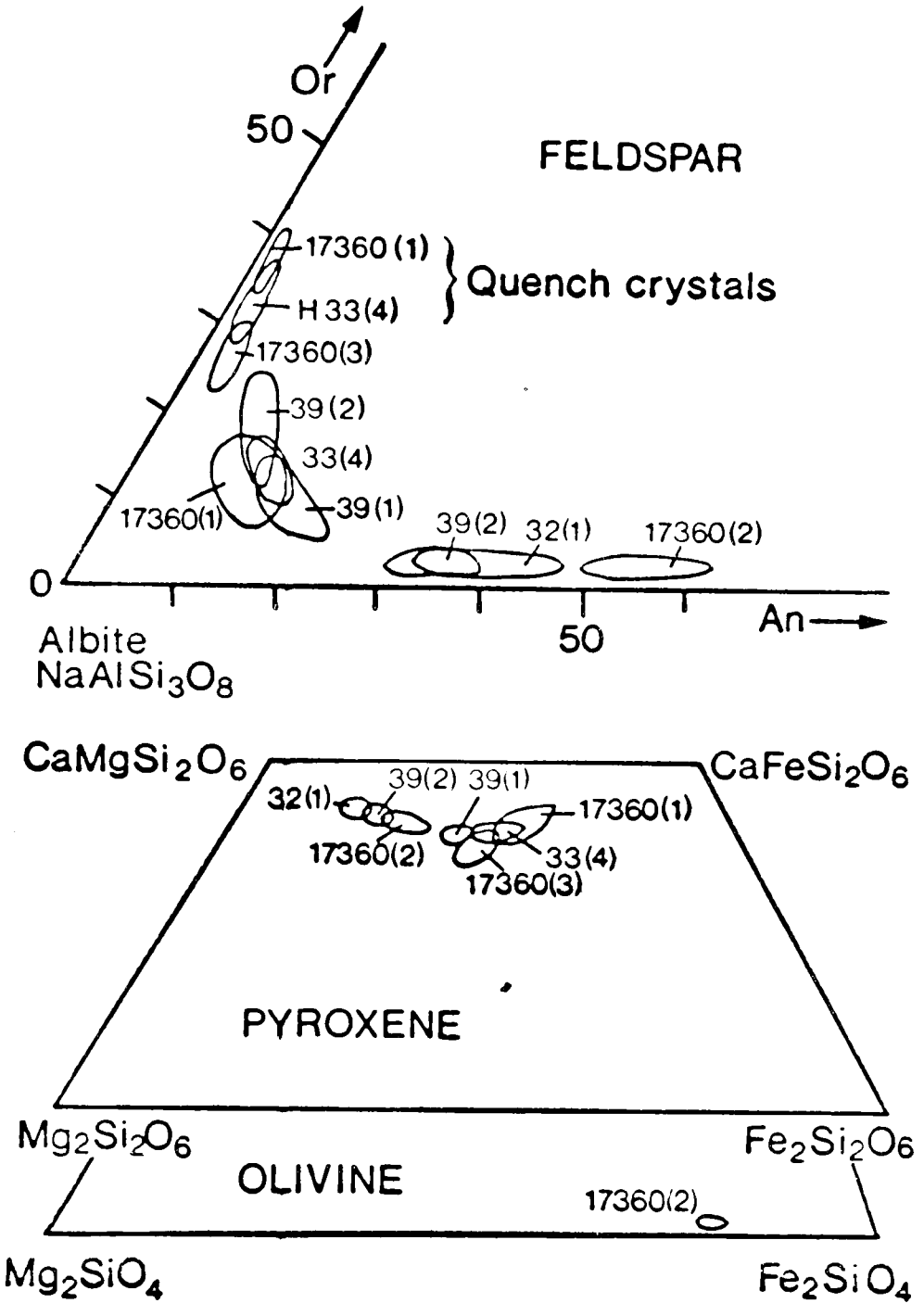
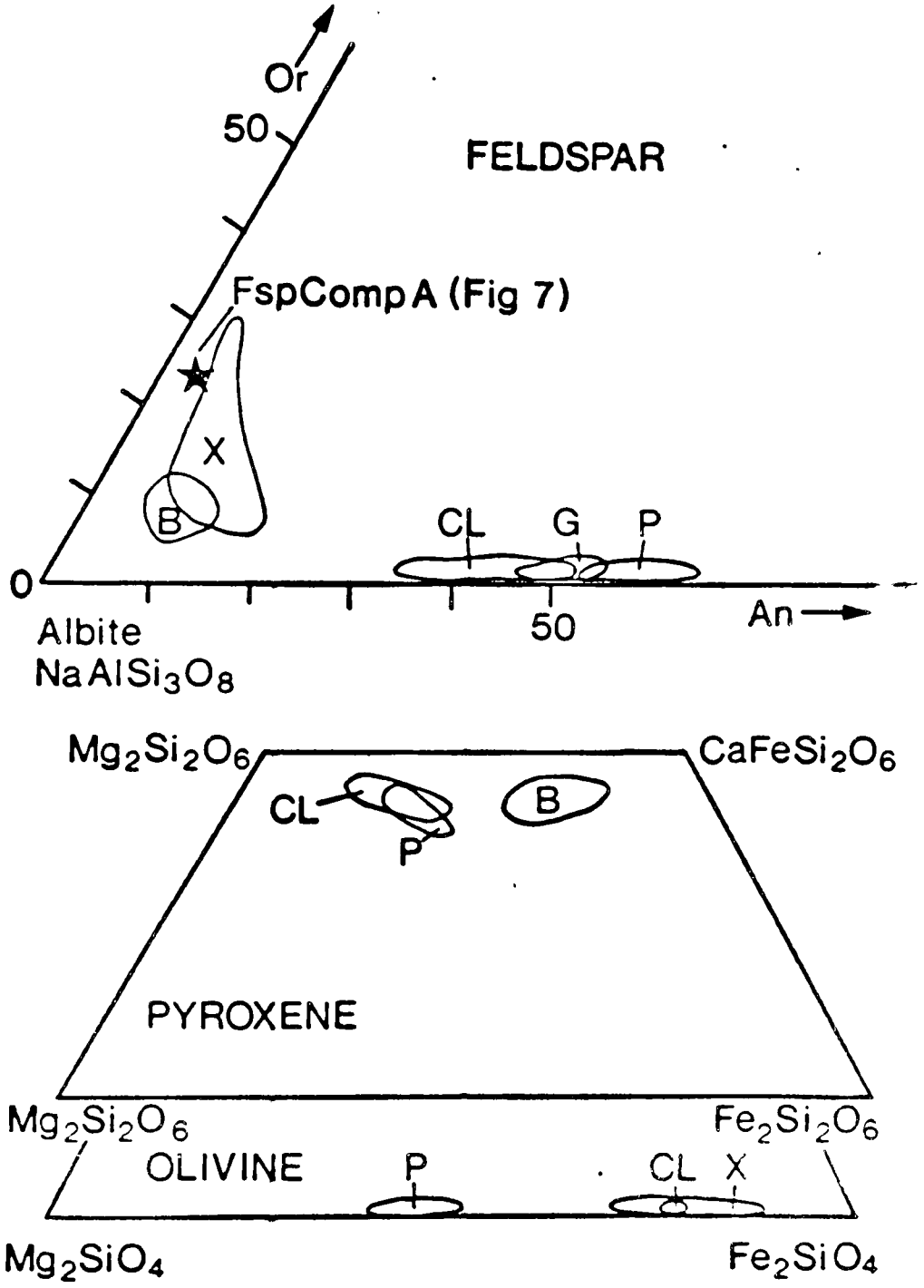


Fig 4.52



Microprobe analyses of major phases in East Crater blocks. Enclosed rings represent at least five analyses.



Microprobe analyses of major phenocryst and some ground mass phases in the East Crater lava.

X = embayed xenocrysts; B = block (fragment of coarse grained block)

CL = glomeroporphyritic cluster; G = ground mass; P = euhedral phenocrysts of plagioclase. Enclosed rings represent at least five analyses.

Fig 4.54 Simple mixing diagram showing the relationship between the two lava analyses (H31L and H39L). For detail see text

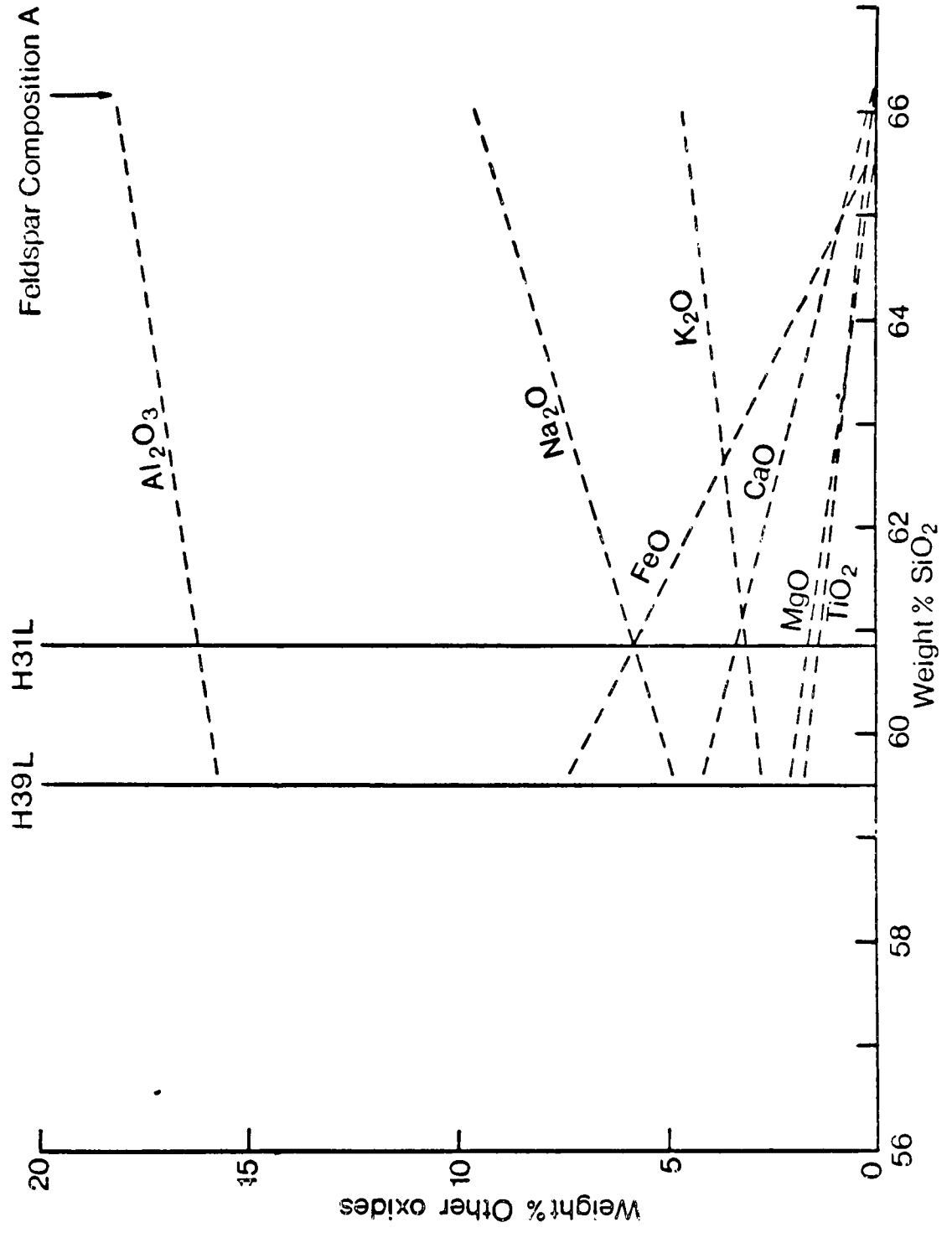


Fig 4.55

K_2ONa_2O vs SiO_2 for analysed glasses from East Crater and other Ascension localities. Also shown are Ascension granite and the trend for the volcanic analyses (from Daly, 1925)

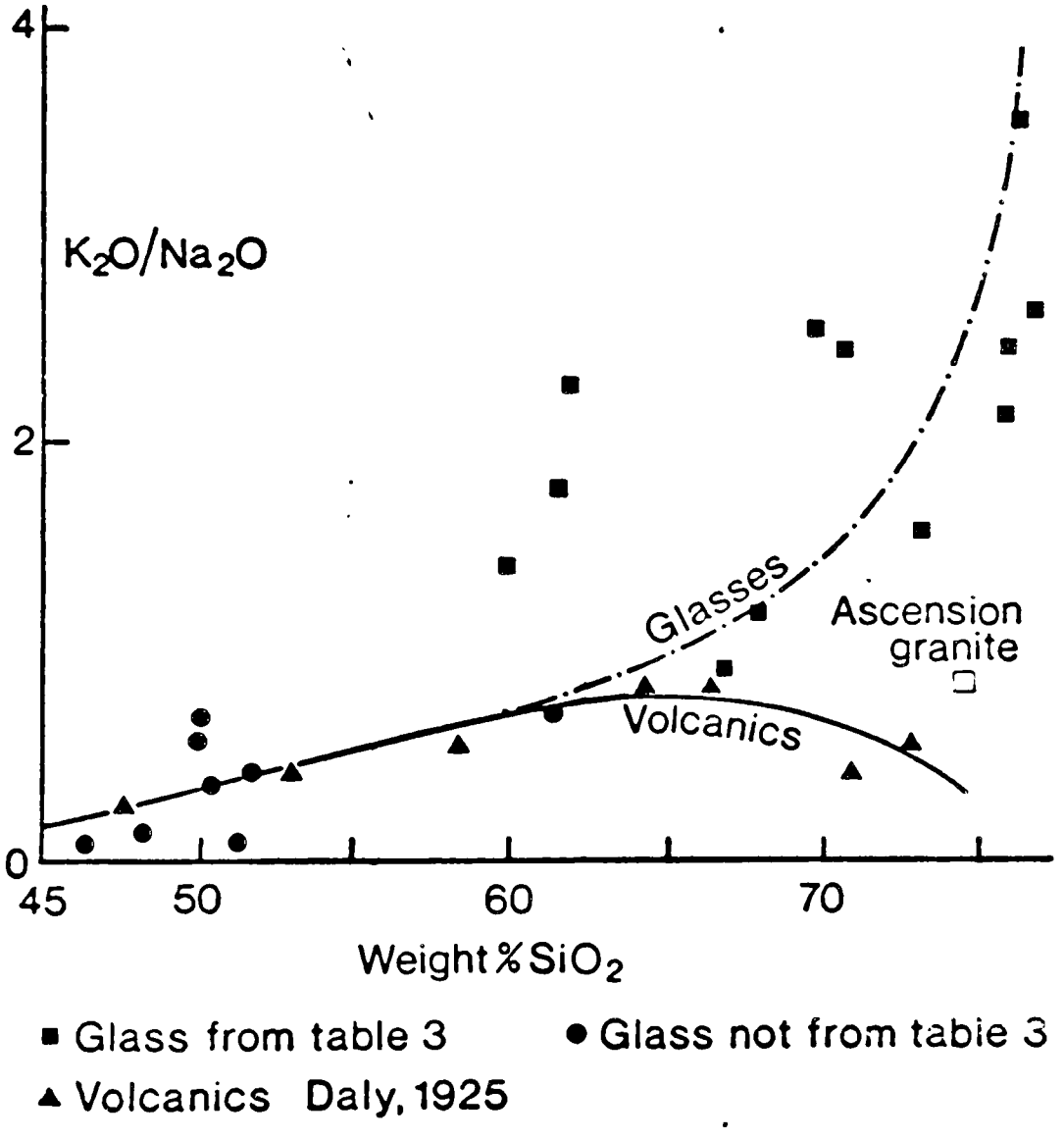


Fig 4.56 Schematic 1420°C isothermal section through the system magnetite - apatite - diorite, showing the extent of the postulated two and three liquid fields of immiscibility (after Philpotts, 1967)

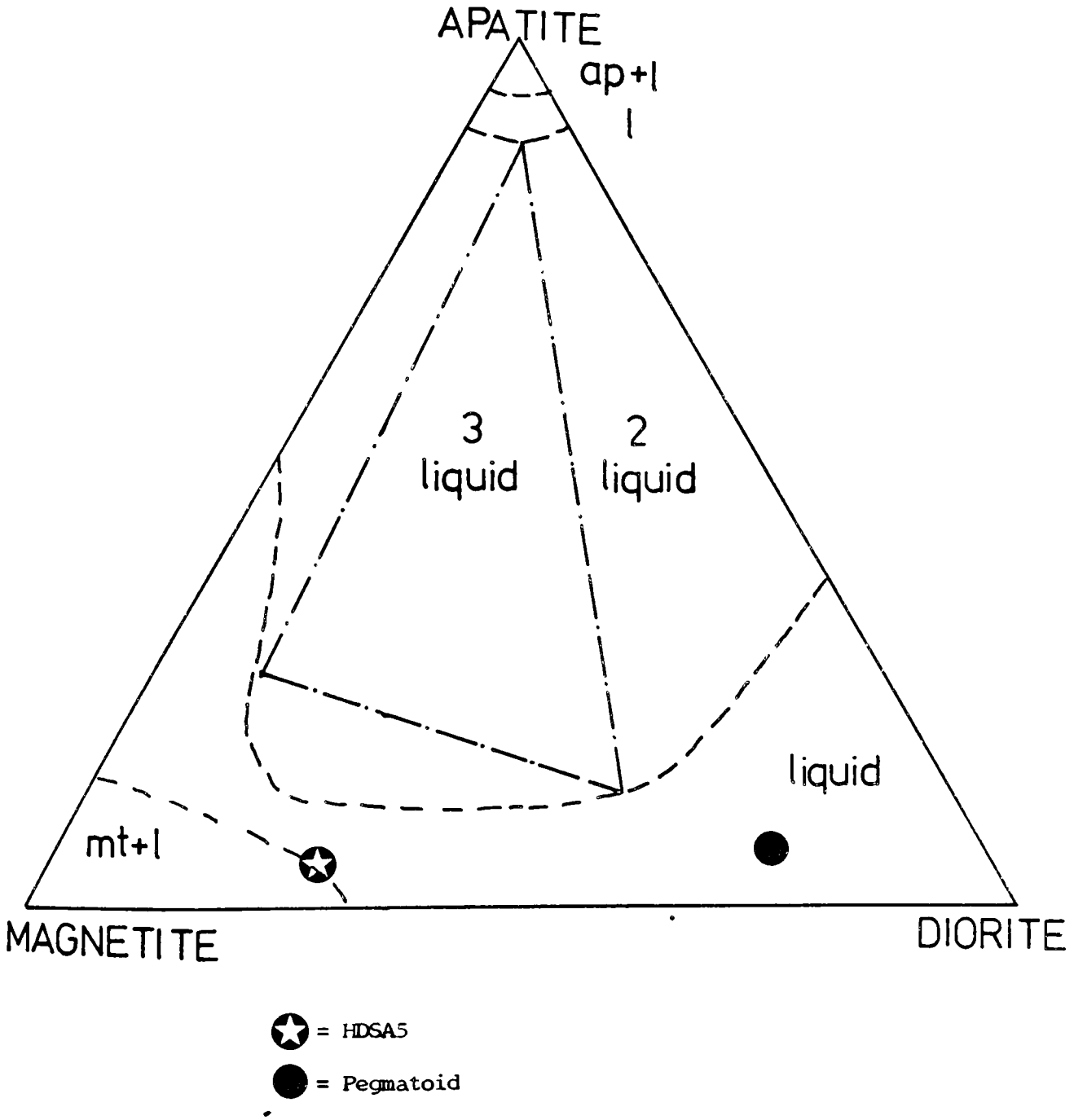


Fig 4.57 Clinopyroxene - olivine tie lines for blocks and lavas (using core compositions).

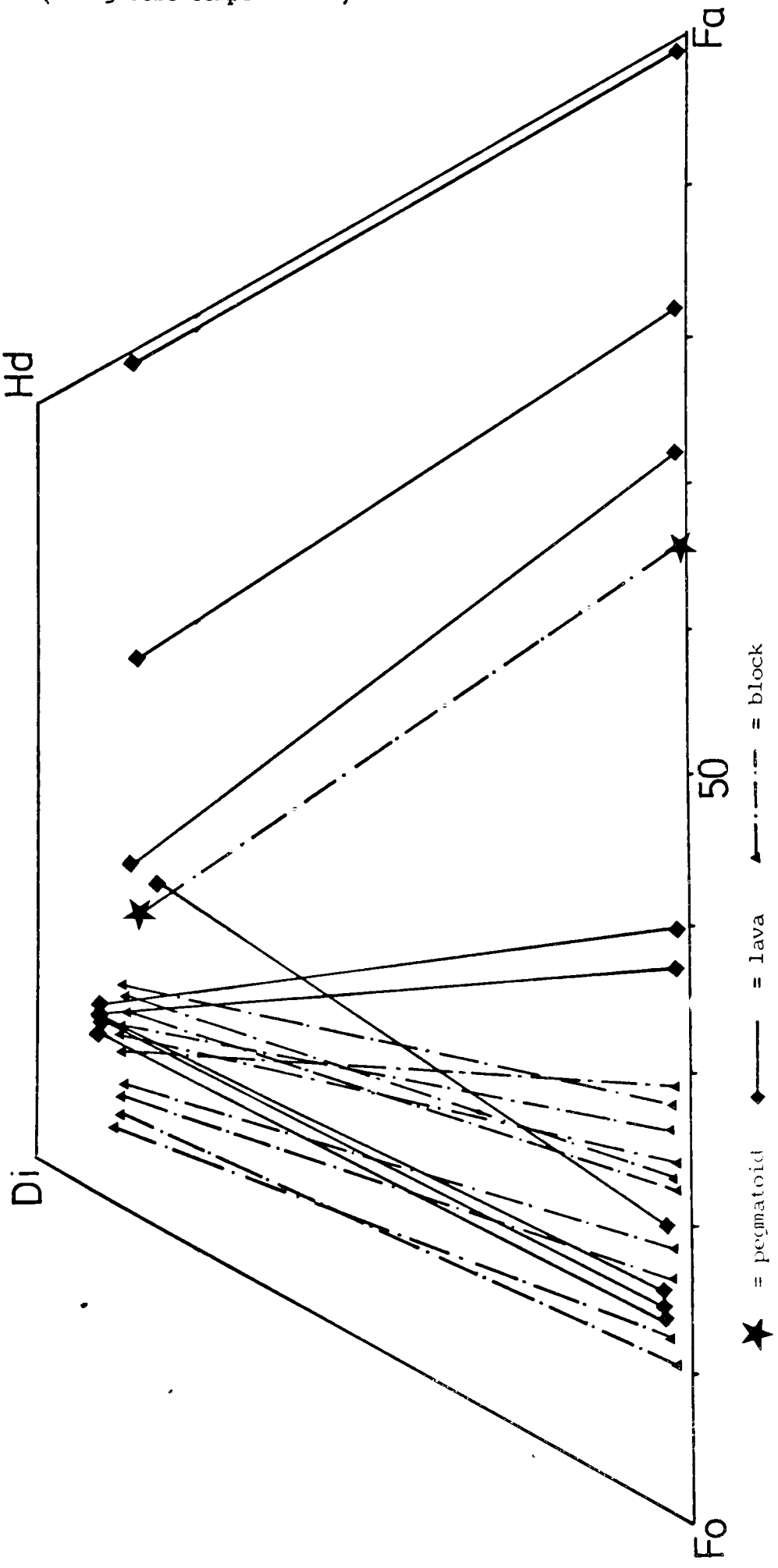


Fig 4.58 Feldspar-olivine composition tie lines for blocks and lavas (using core compositions).

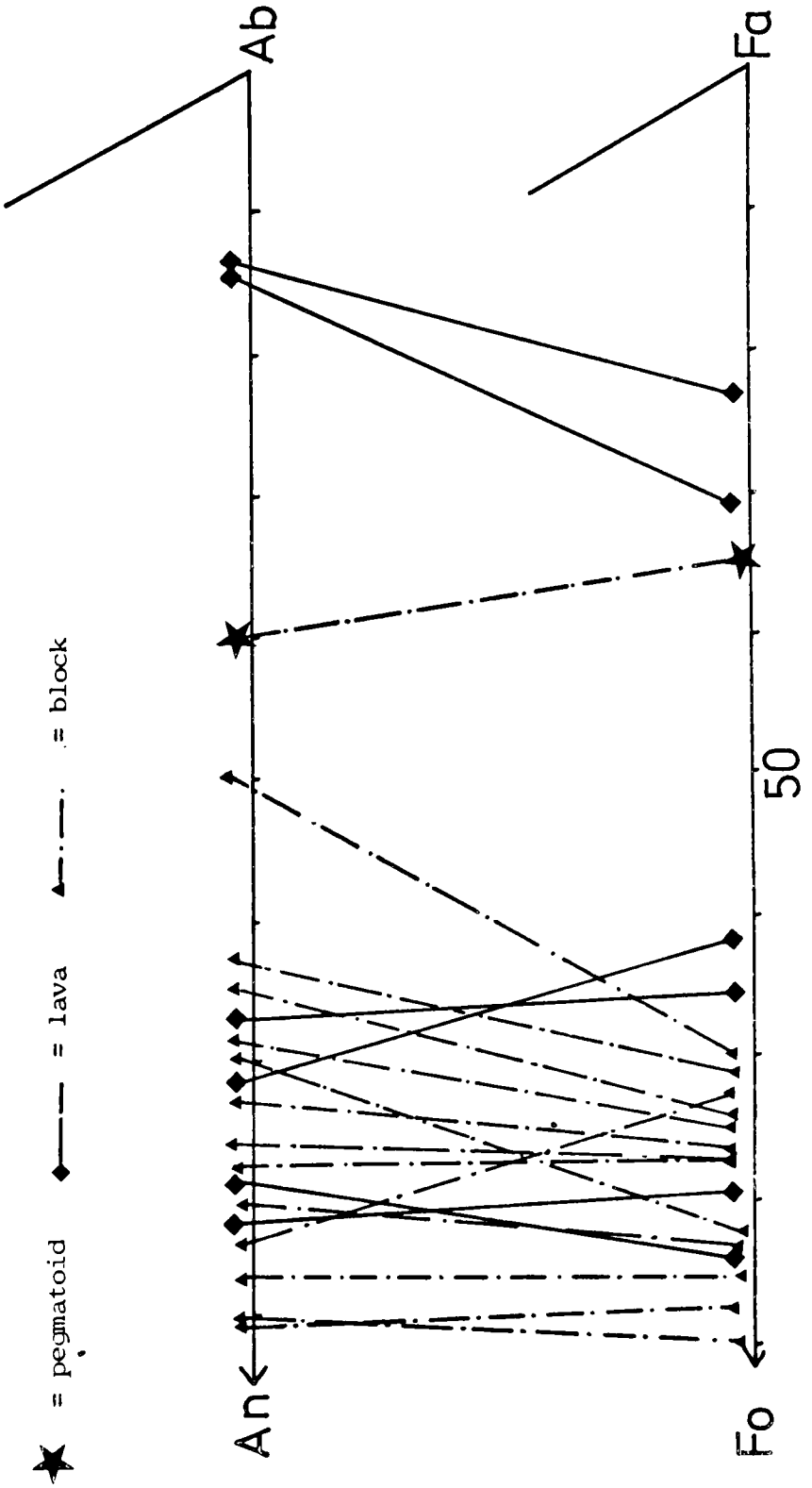


Plate 4.1 OPX as a reaction rim around olivine in a plagioclase -olivine adcumulate (15227). PPL

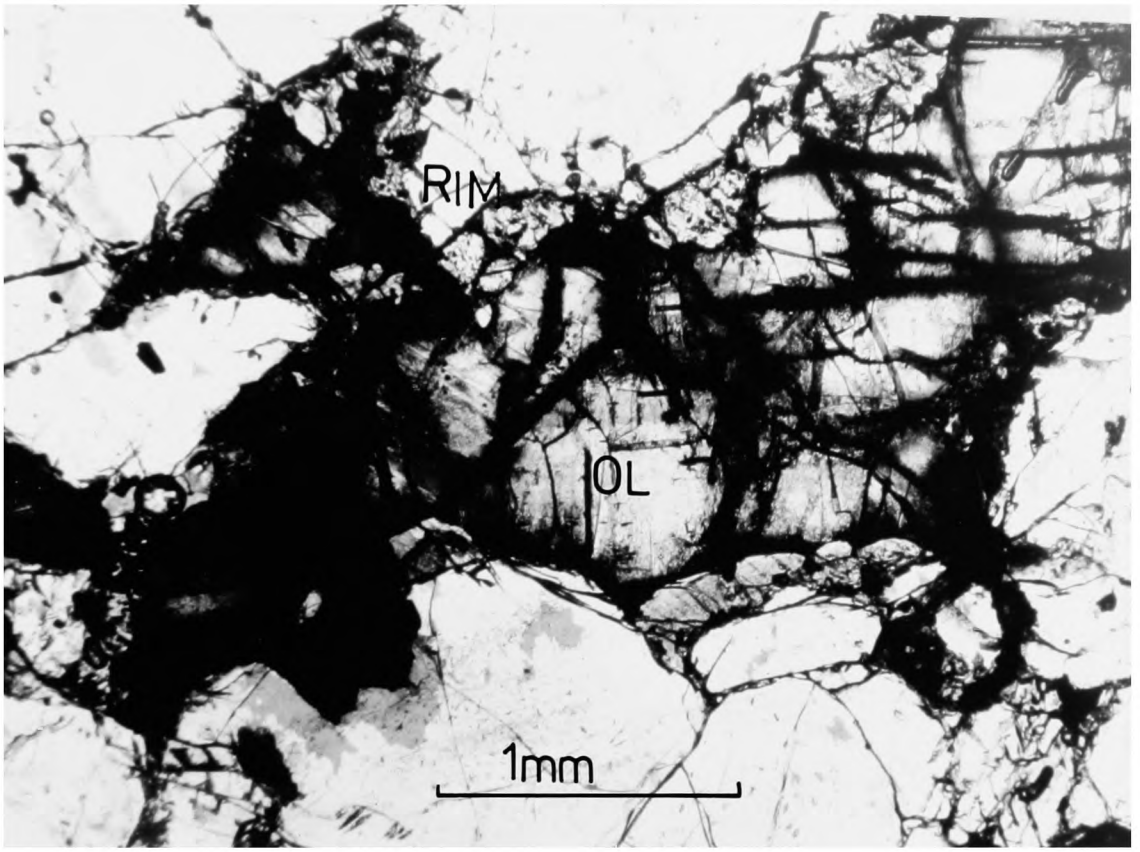


Plate 4.2 Olivine from the edge of block 15227(13) showing opaque blebs along cleavage. PPL

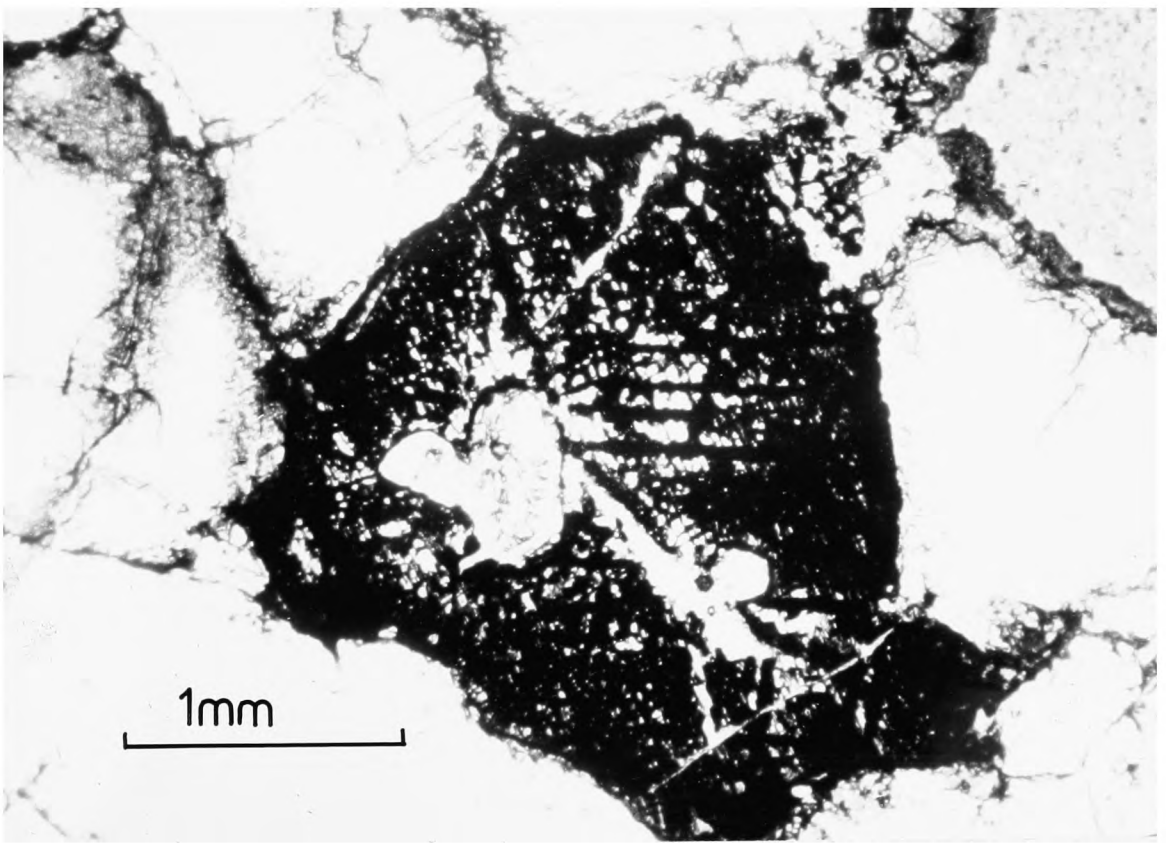


Plate 4.3 Cumulus OPX in block 15227(13) with exsolved lamellae of CPX . PPL

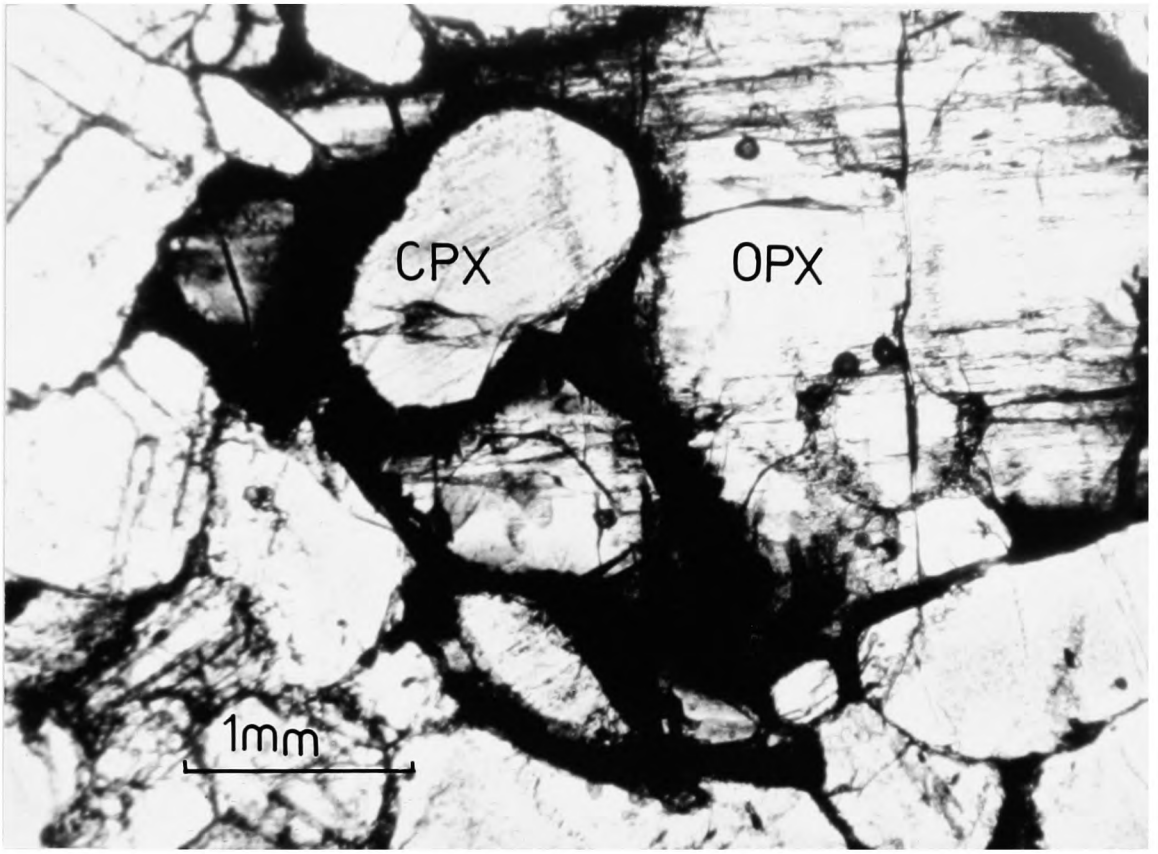


Plate 4.4 DS46 -chrome spinel in an olivine adcumulate with intercumulus plag. PPL

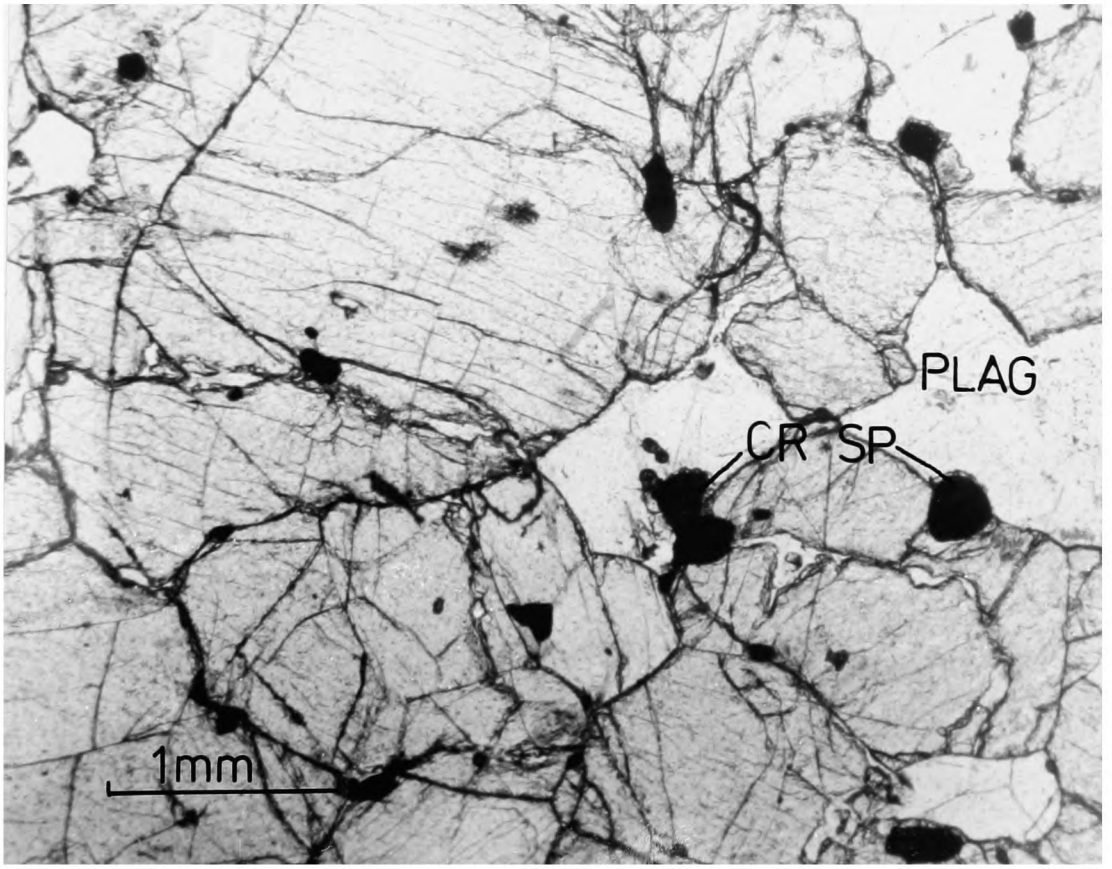


Plate 4.5 Plagioclase adcumulate (HDSC2) Xpolars.

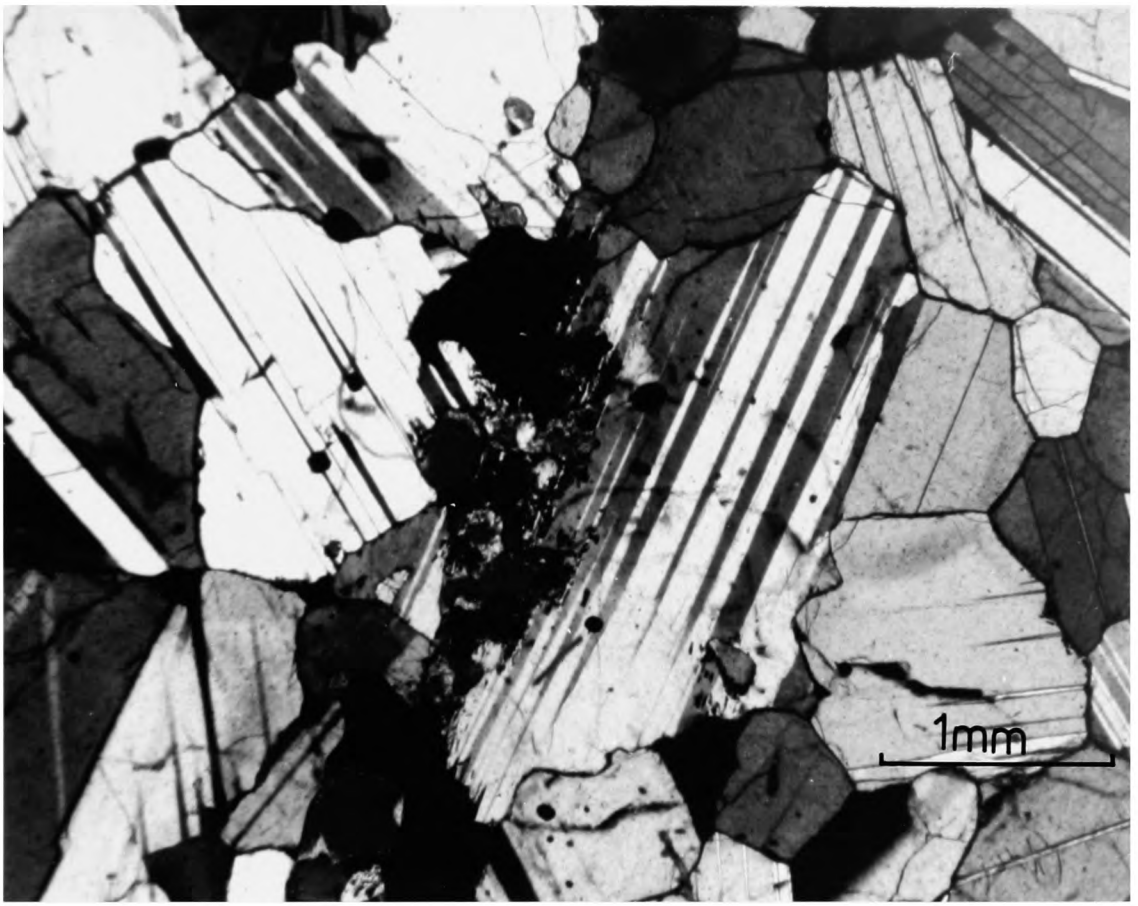


Plate 4.6 Plagioclase - pyroxene adcumulate (17317Y);slide cut parallel to orientation of CPX . Xpolars

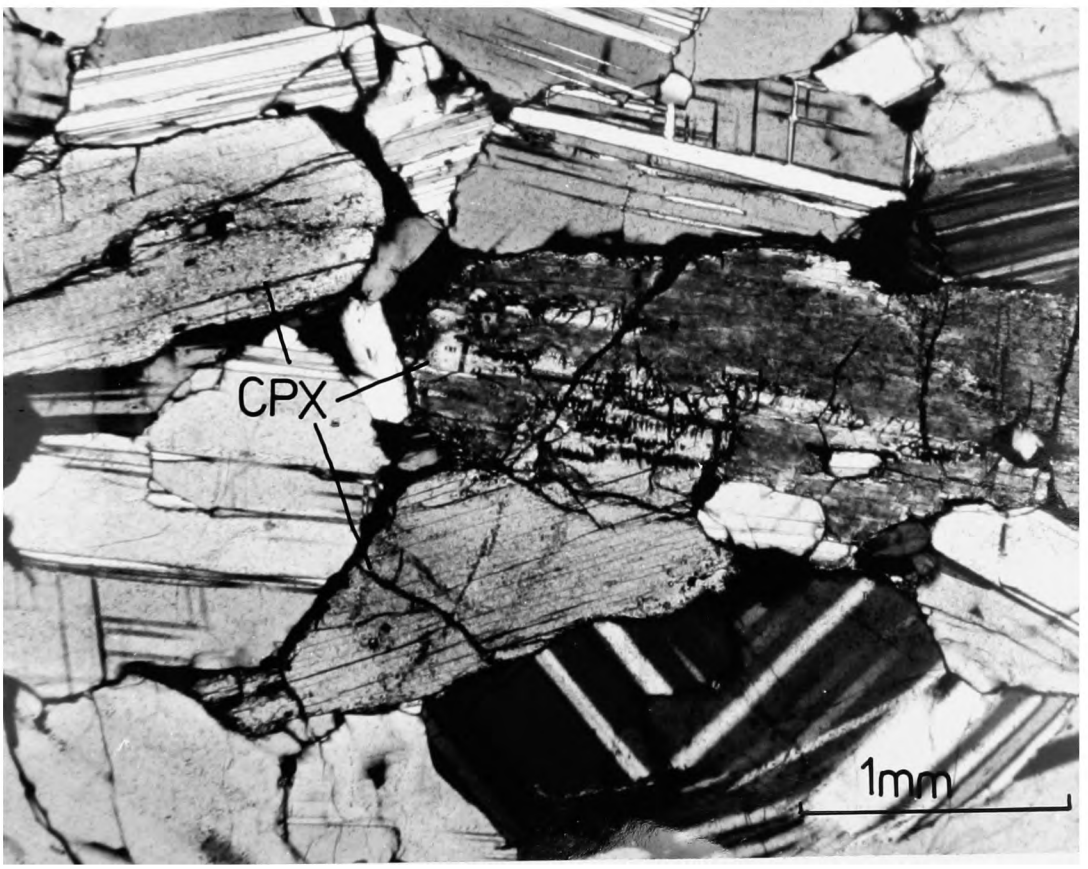


Plate 4.7 17317Y cut perpendicular to orientation of pyroxene. X polars

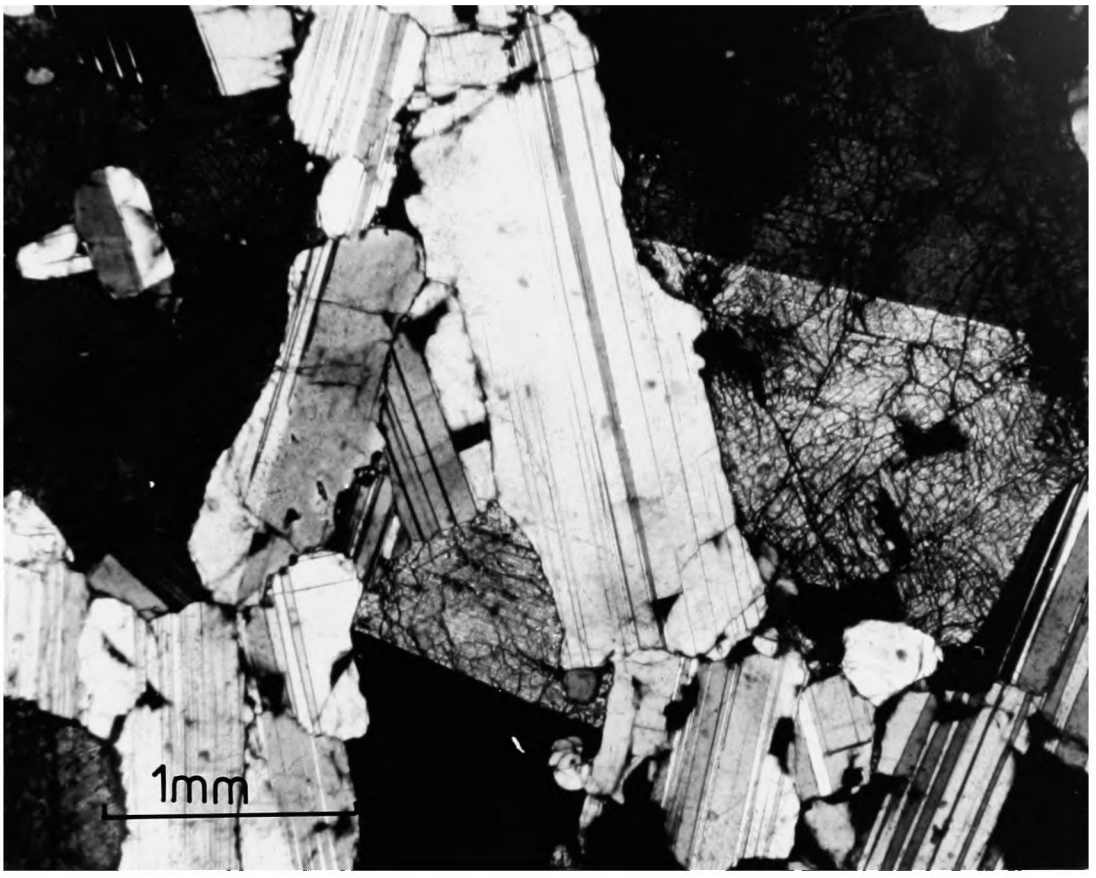


Plate 4.8 Plag. adcumulate with a vein of pyroxenes crossing it along joints (?). P is a single grain of plagioclase cut by the vein (HDSC2). ppl

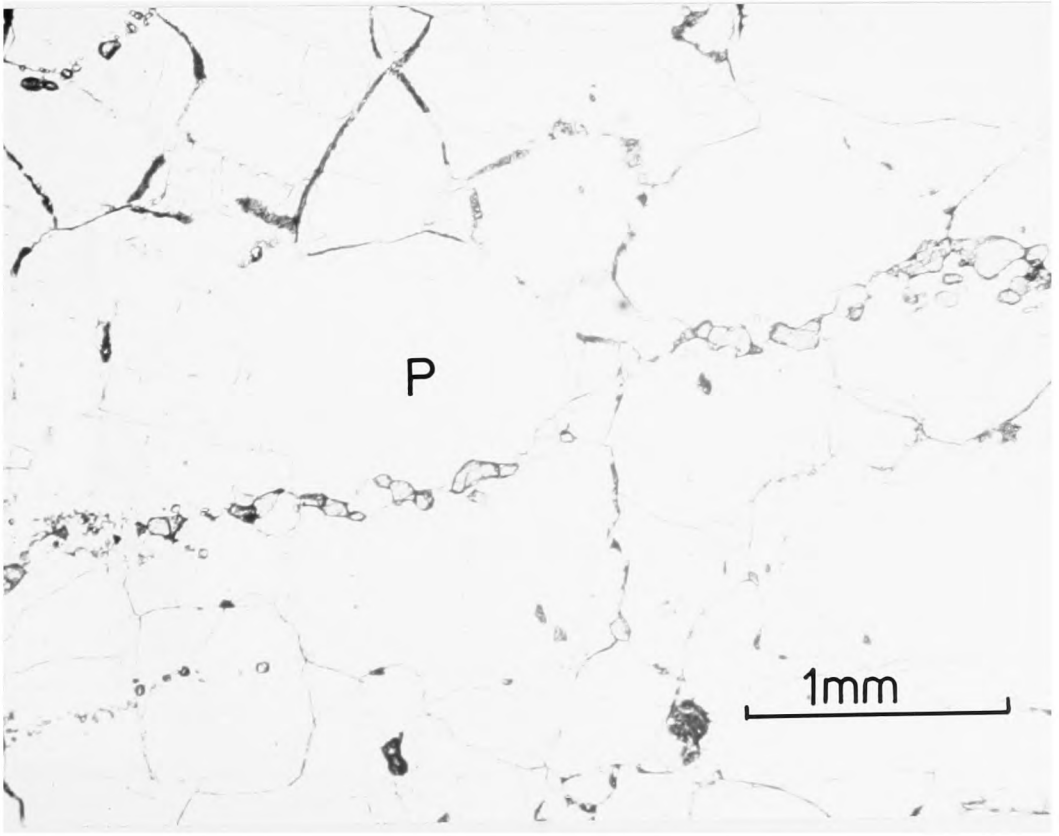


Plate 4.9 As 4.8 With crossed polars.

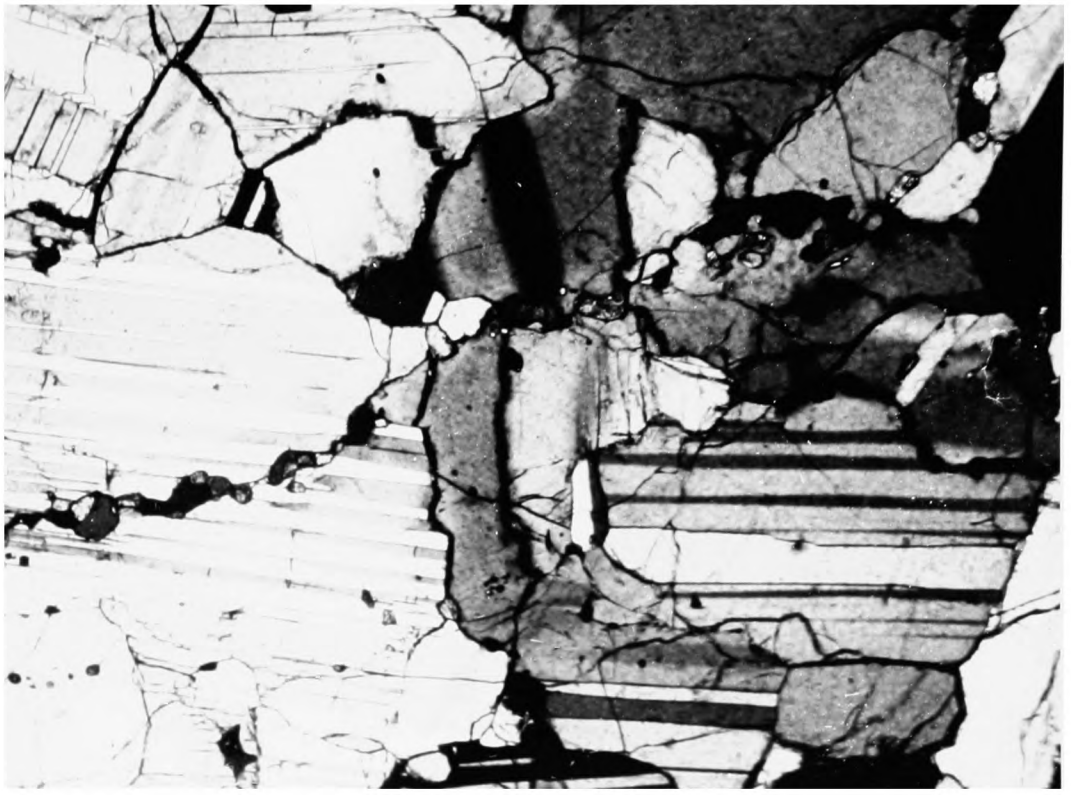


Plate 4.10 Zoning in plag. next to pyroxene vein in HDSC(2).
Point A is more sodic than point B. X polars

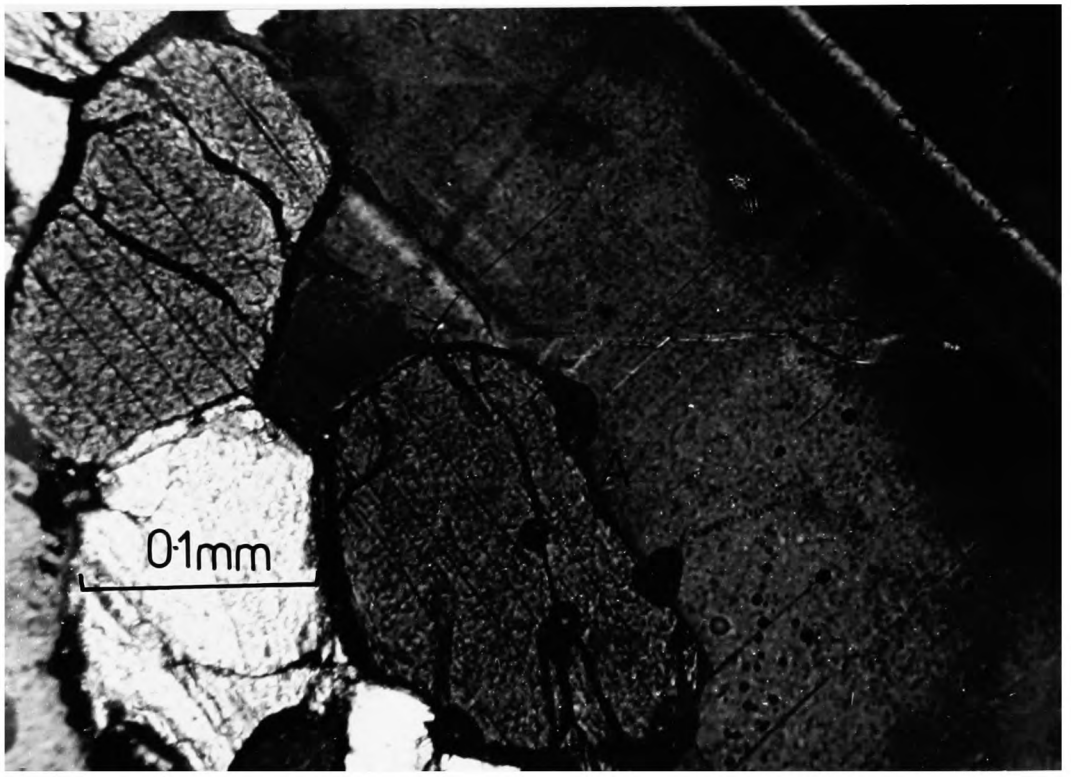


Plate 4.11 Mesostasis inclusion in pyroxene of H28(2) .PPL

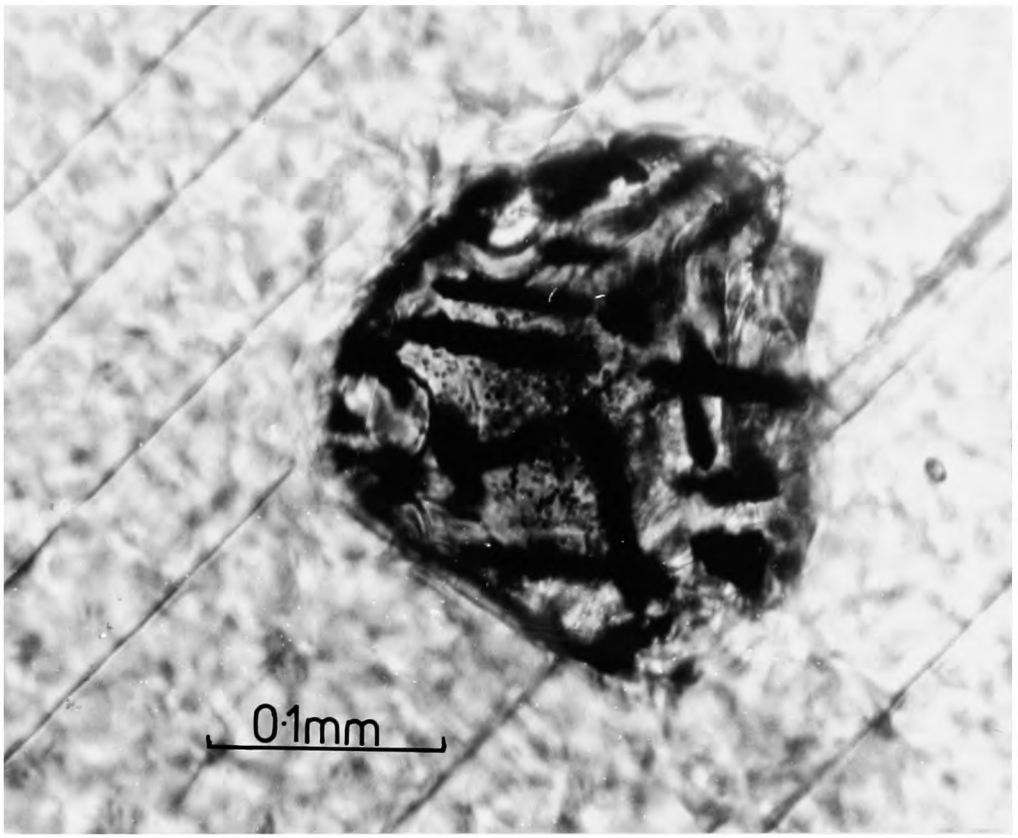


Plate 4.12 Mesostasis between euhedral plag and cpx . Note incomplete crystalization of plag and small inclusion of mesostasis in cpx (M). PPL

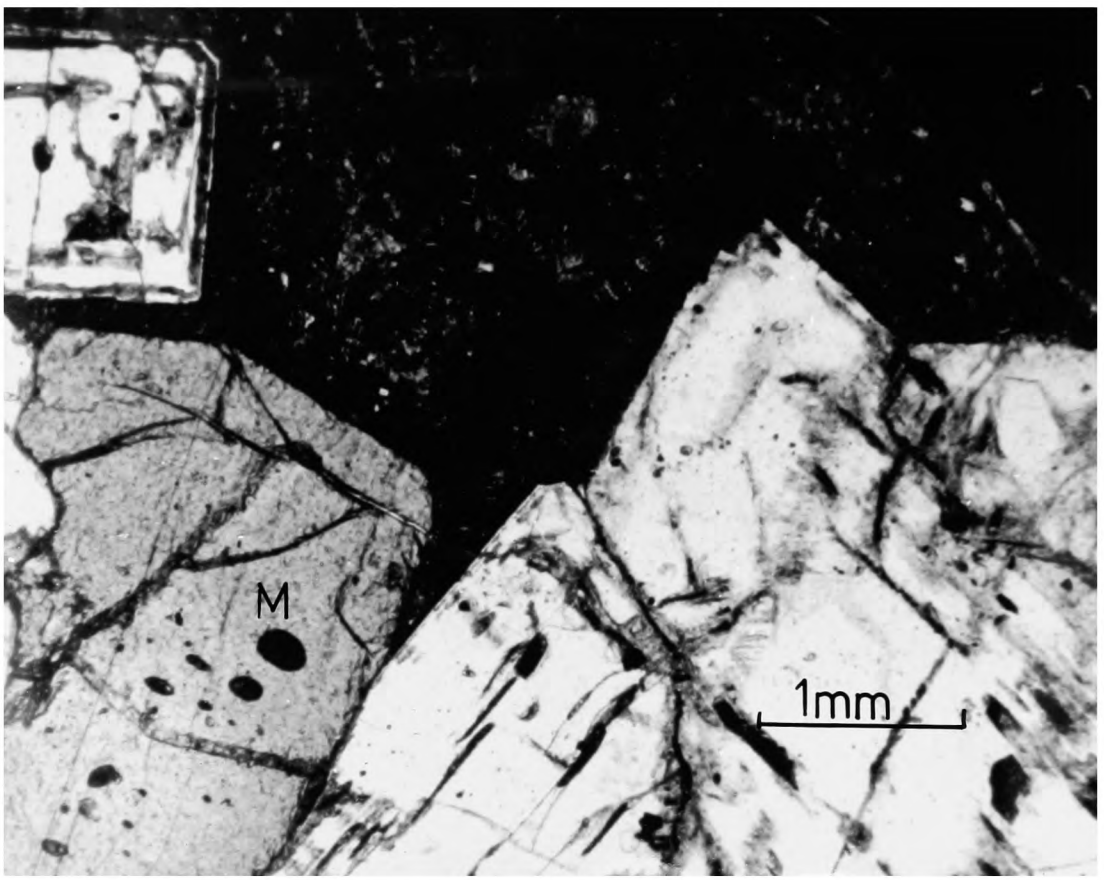


Plate 4.13 Plag + ol orthocumulate with intercumulus cpx H28(1). PPL

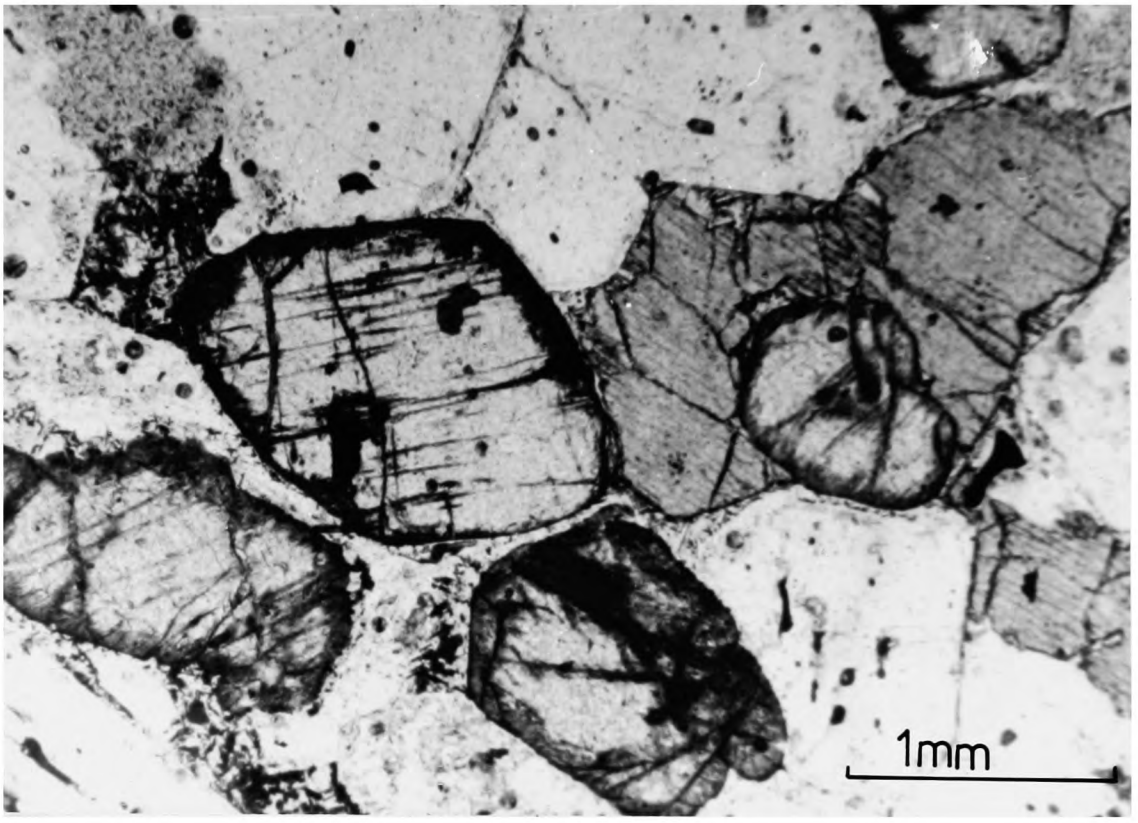


Plate 4.14 Plagioclase mesocumulate (15226(18)) with highly poikilitic pyroxene + accessory opaques . N.B. the low percentage of mesostasis. PPL

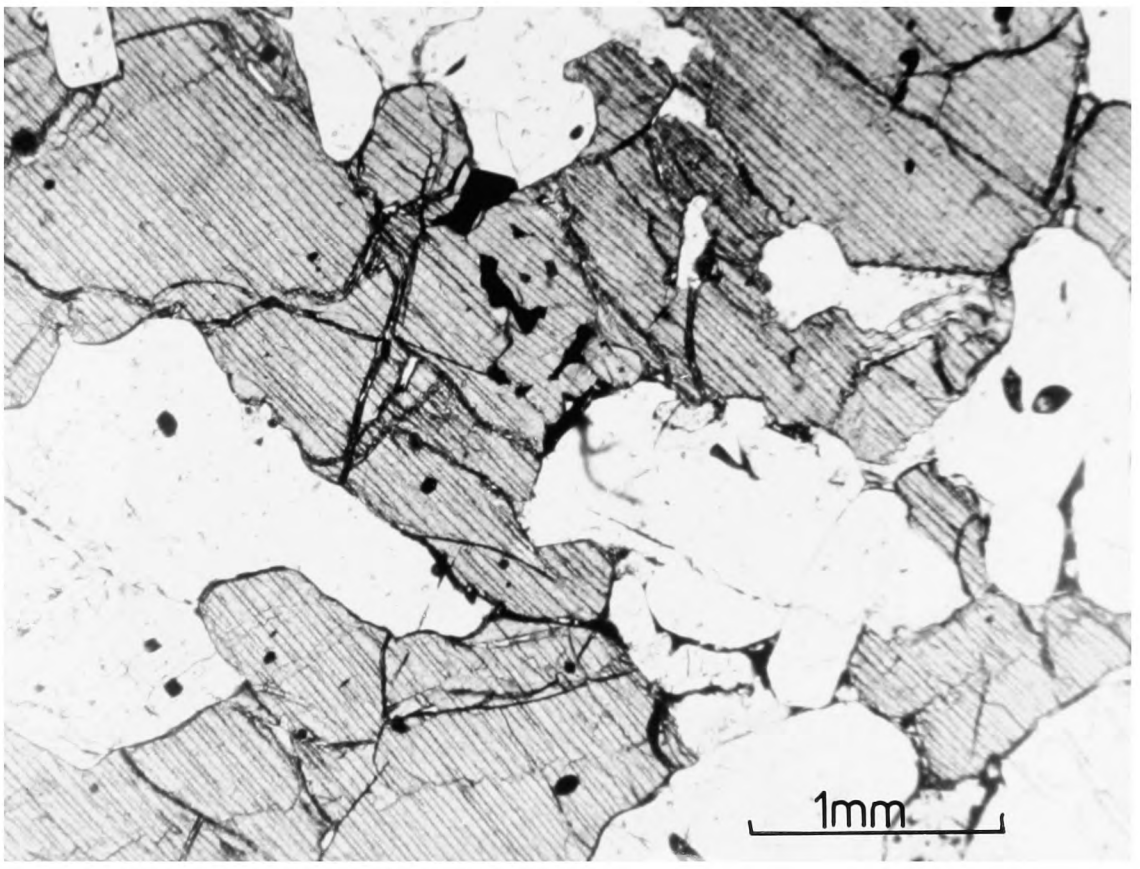


Plate 4.15 Mesostasis in H28(2) showing crisscrossed opaques and a swallowtailed feldspar set in glass. PPL

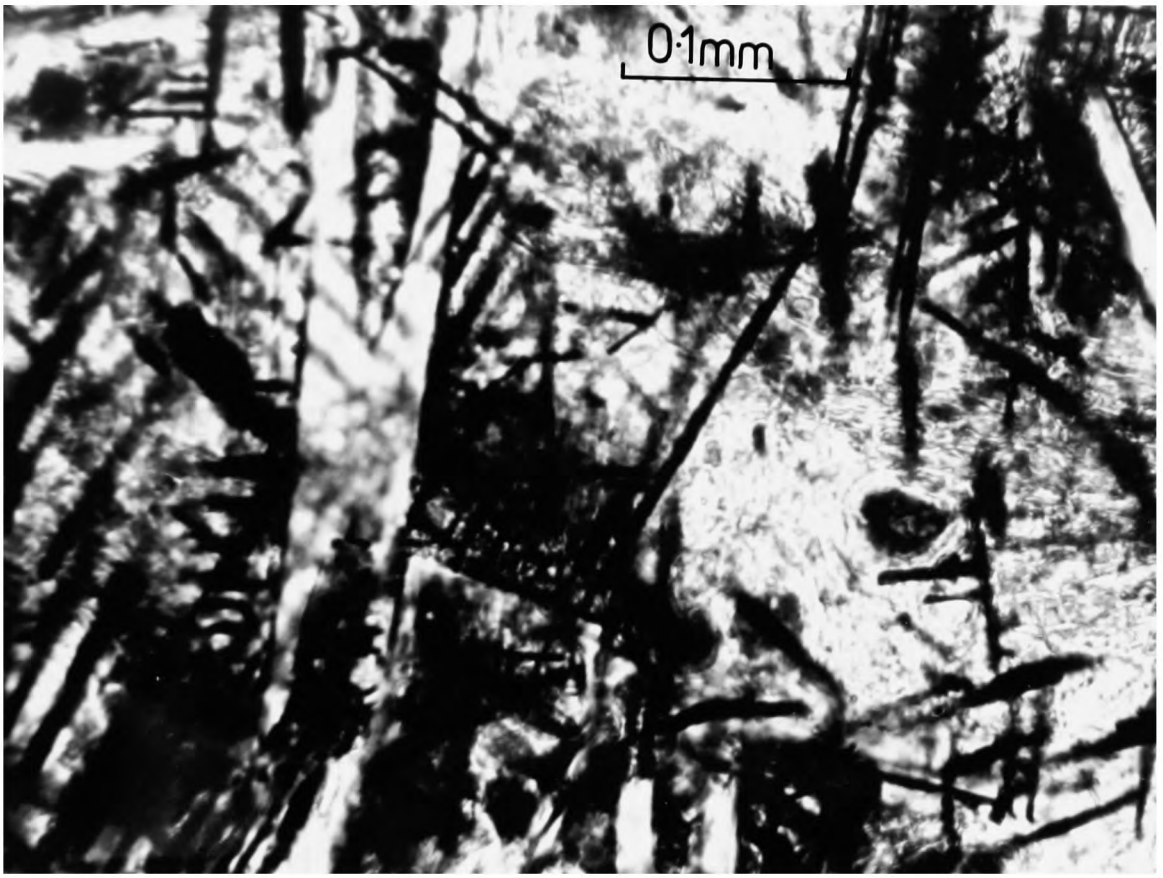


Plate 4.16 Mesostasis in H28 (2) showing typical crisscrossed opaques . PPL

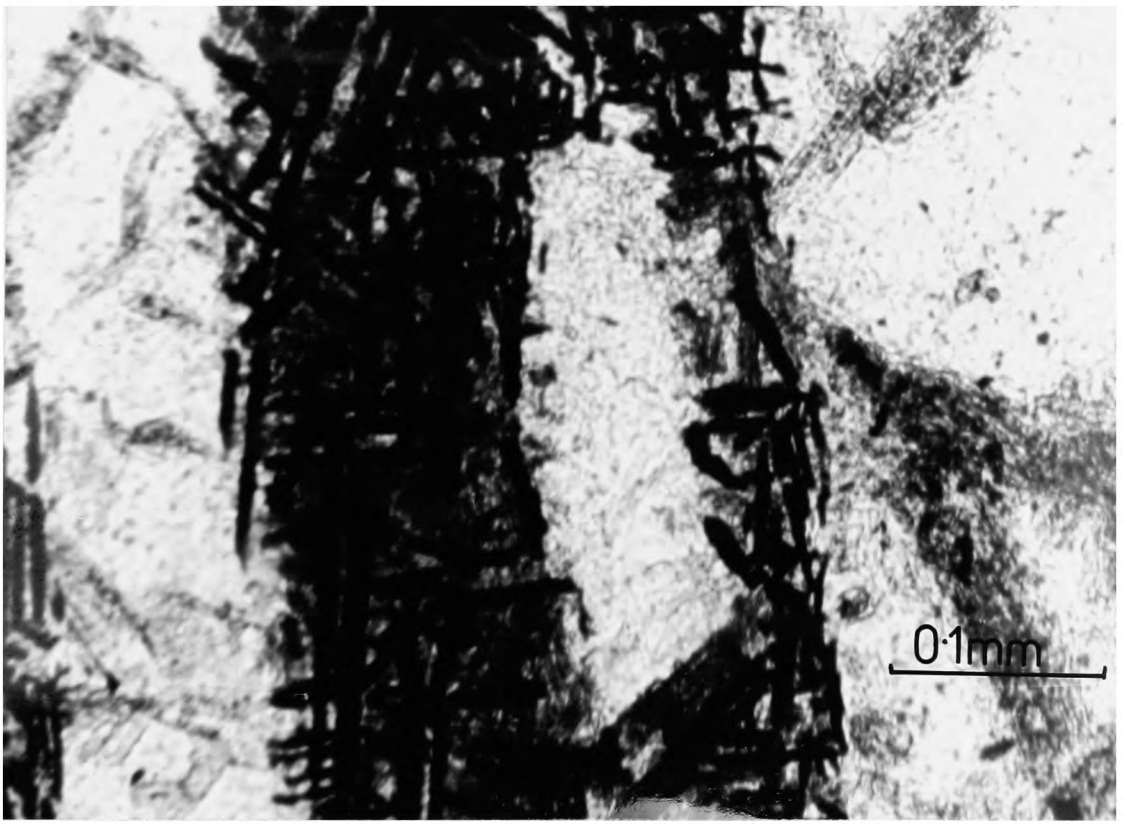


Plate 4.17 Plag orthocumulate with intercumulus olivine and incipient partial melting. PPL

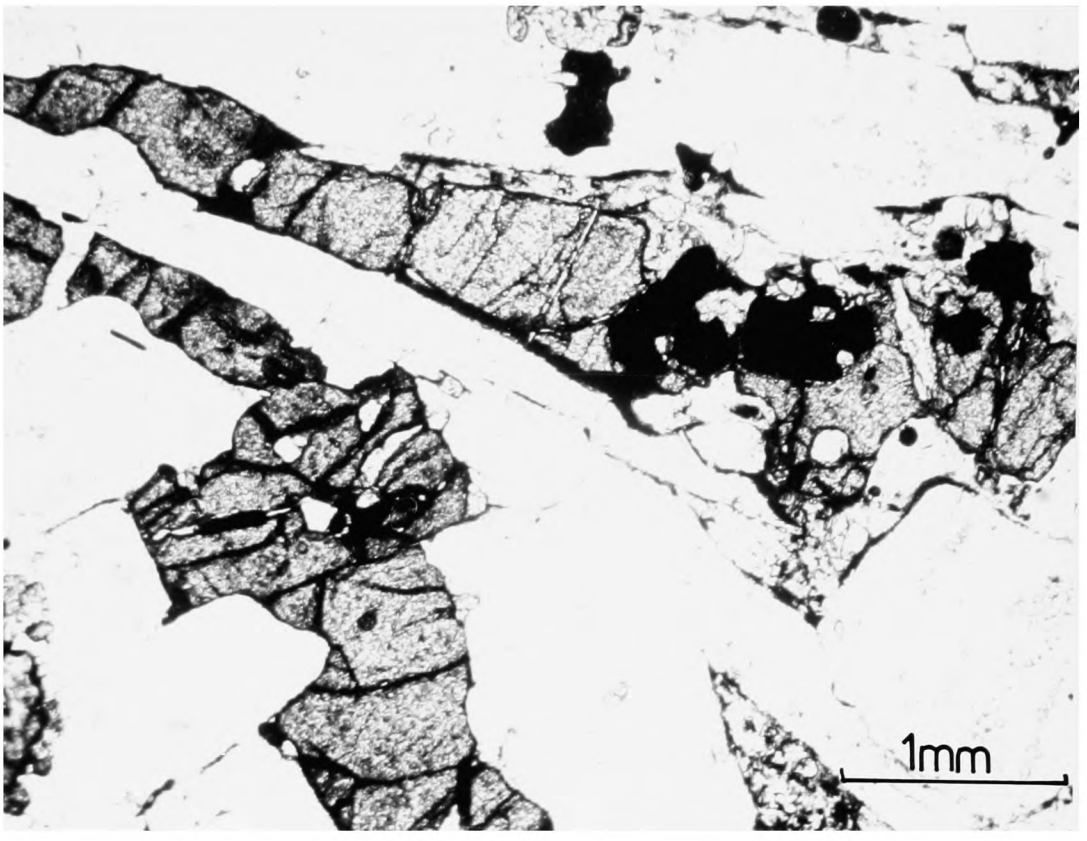


Plate 4.18 Plag orthocumulate with cumulus(?) apatite (ap). PPL

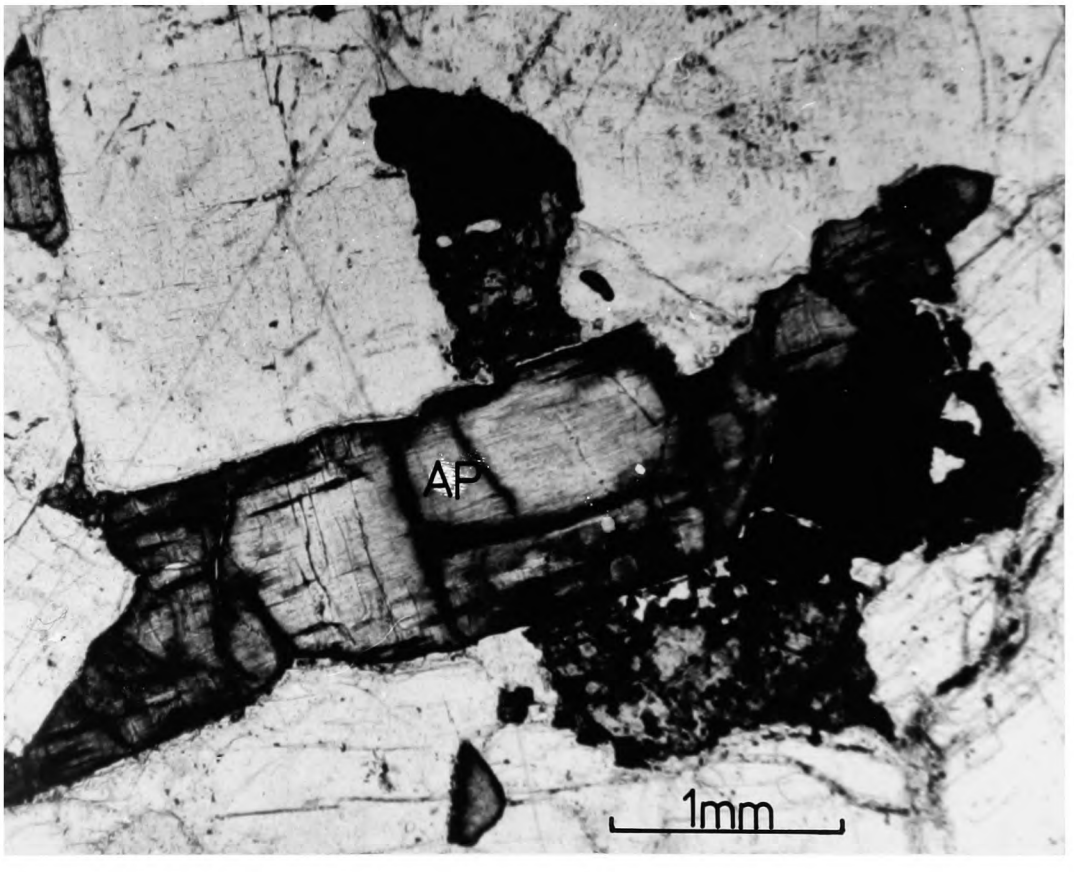


Plate 4.19 K feldspar adcumulate (H13(1)) from Cricket Valley identical to those of Crytal Bay. XPolars

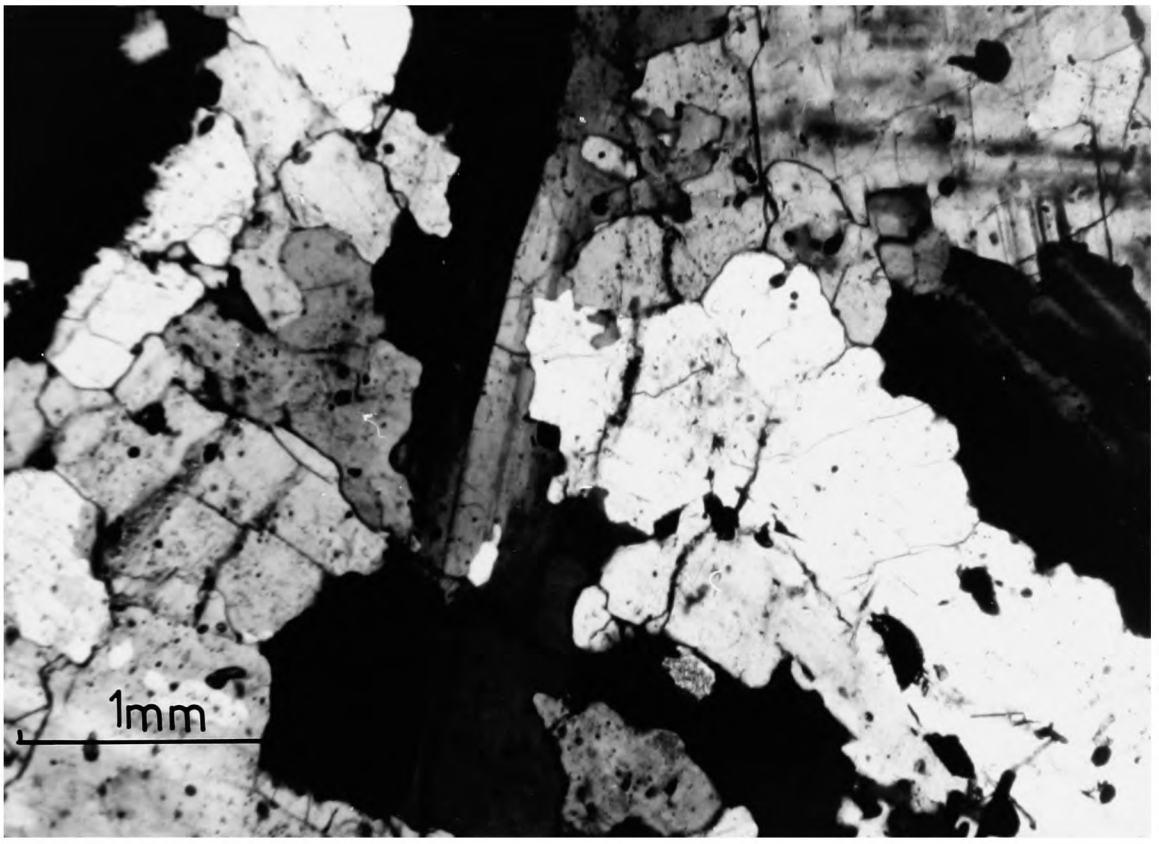


Plate 4.20 Possible mesostasis in "embryo" K feldspar adcumulate (H47(1)) . PPL

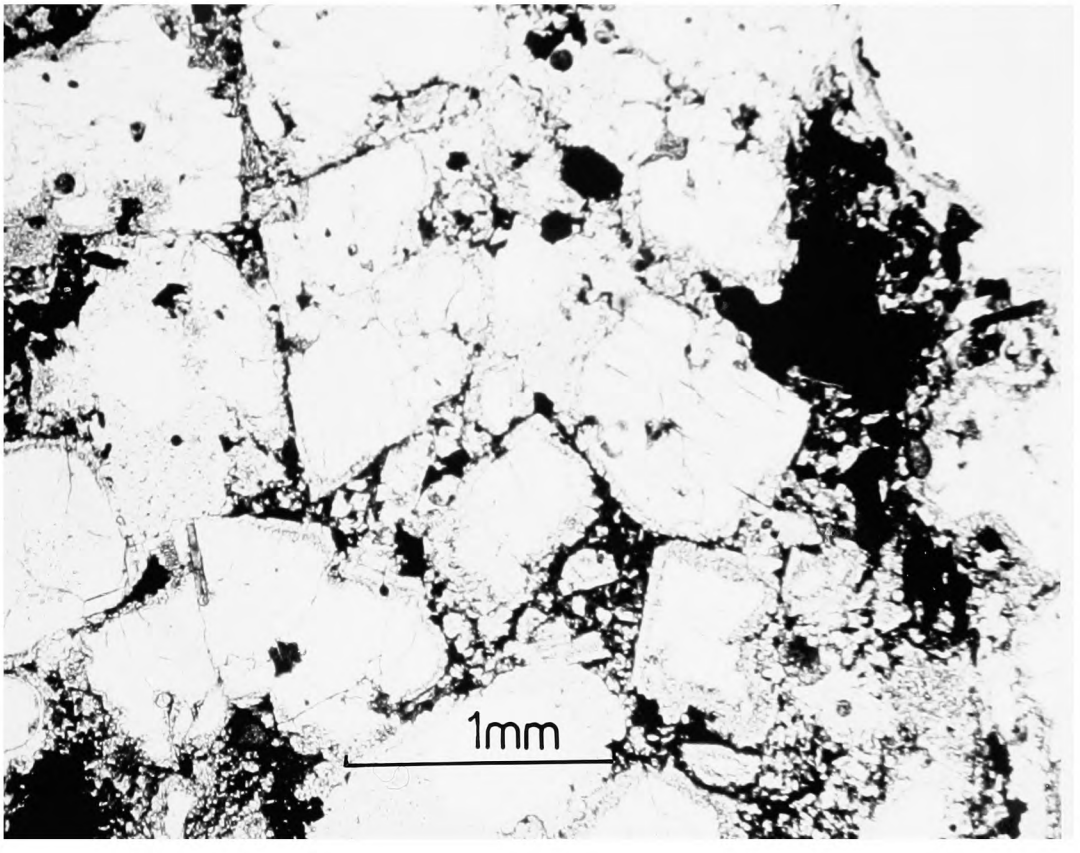


Plate 4.21 Kink bands in K feldspar (H67(1)) . PPL

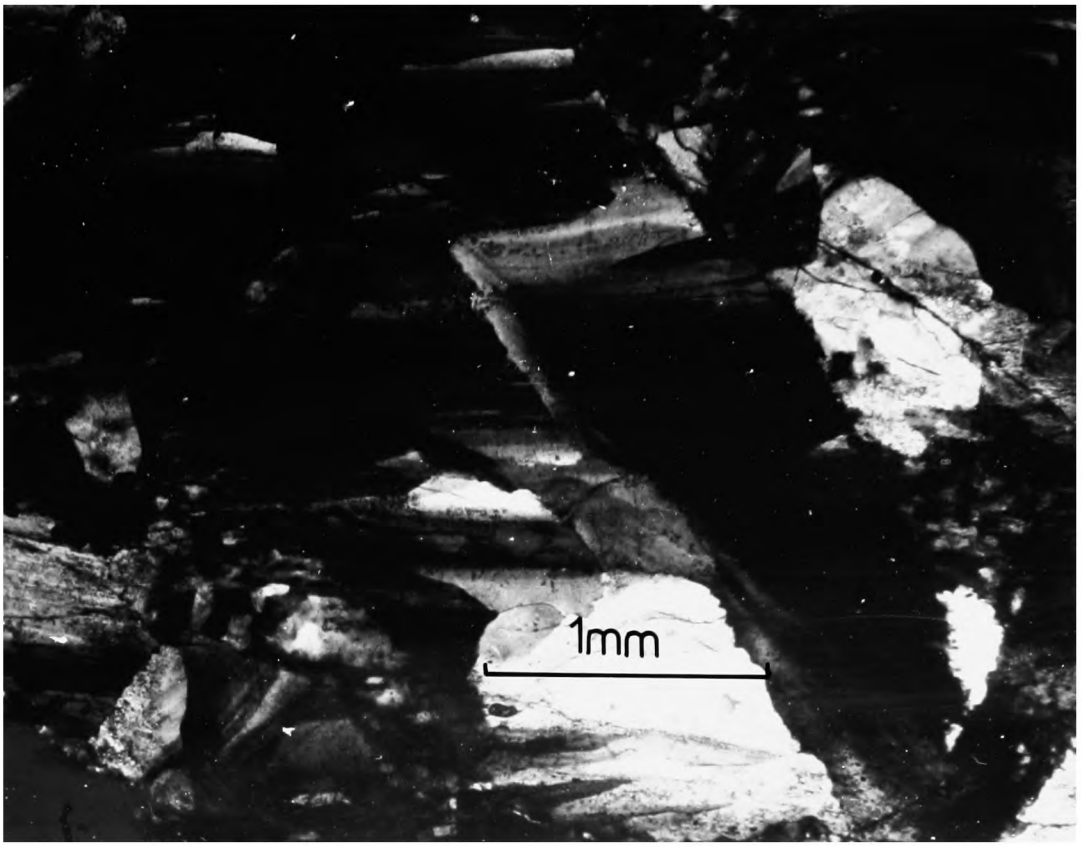


Plate 4.22 Mesostasis of gabbroic block 15243B with glass patches (gl) large enough to permit probe analysis. PPL

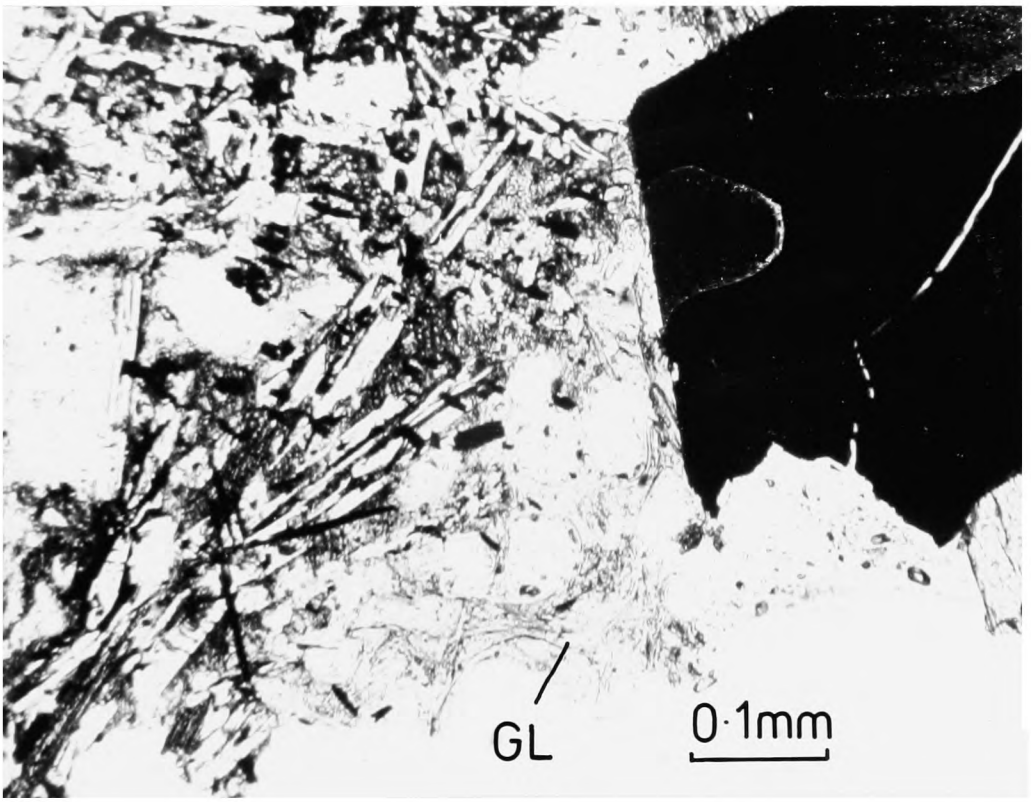


Plate 4.23 Incipient partial melting in olivine plag gabbro 15208(a) N.B. glass around olivine and the sieved edges to the plag. PPL

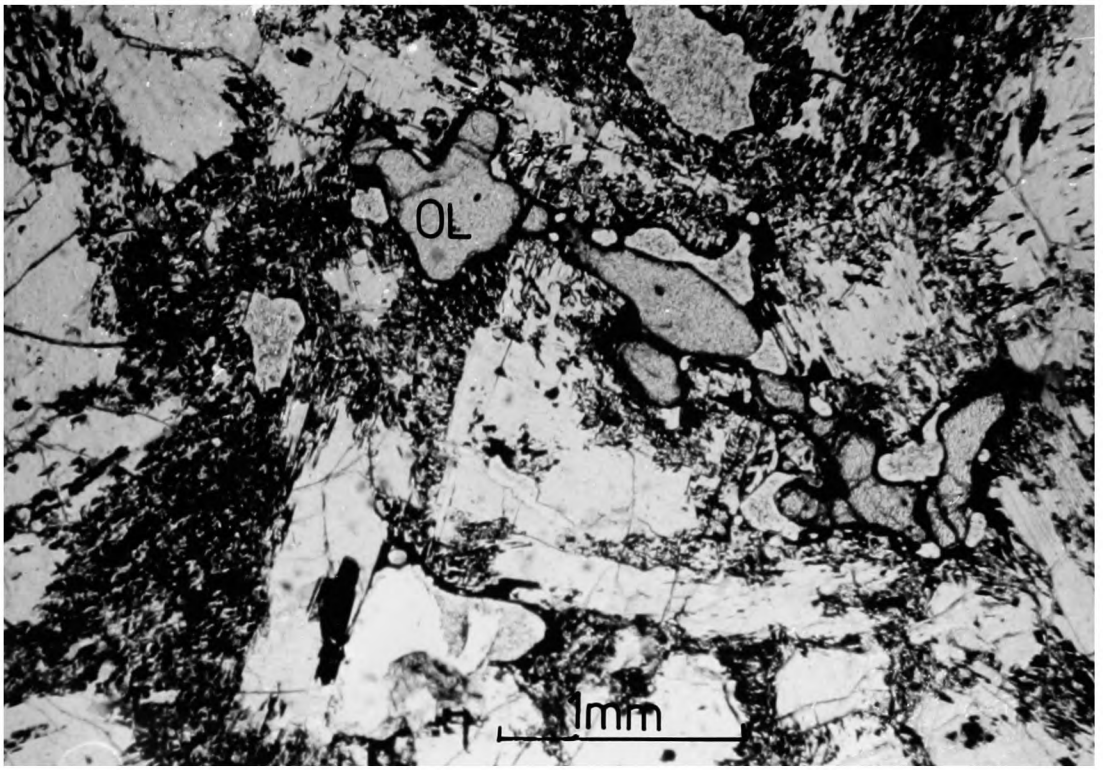


Plate 4.24 As above with crossed polars.

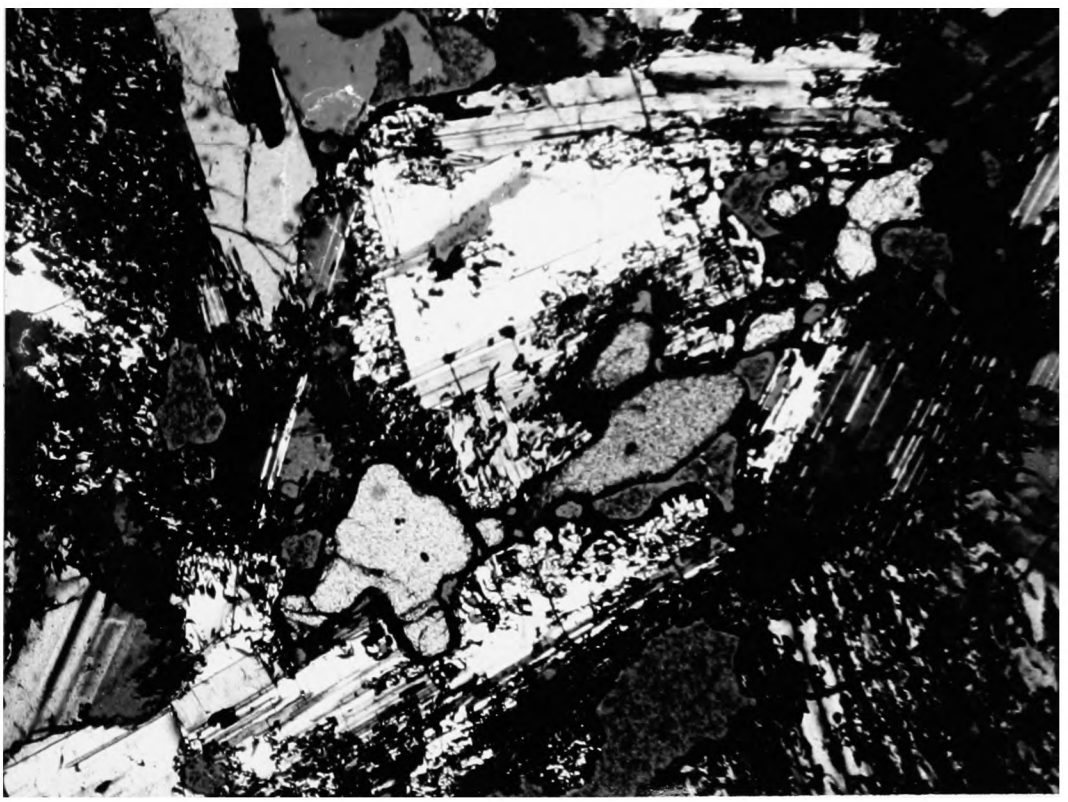


Plate 4.25 Alteration of augite (PX) to amphibole (A) in plag orthocumulate A22(1). PPL

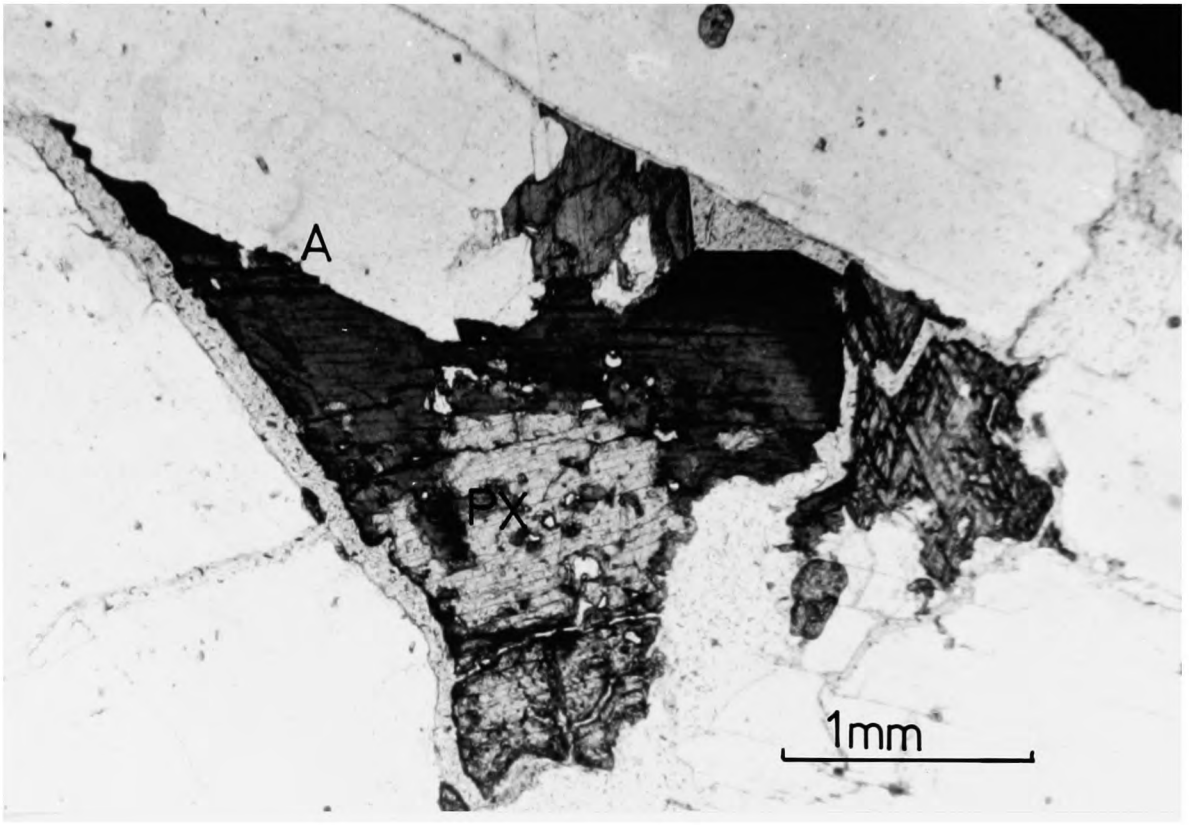


Plate 4.26 Altered gabbro H57(16) from Cricket Valley showing the reaction cpx/amph + opaque → biotite . PPL

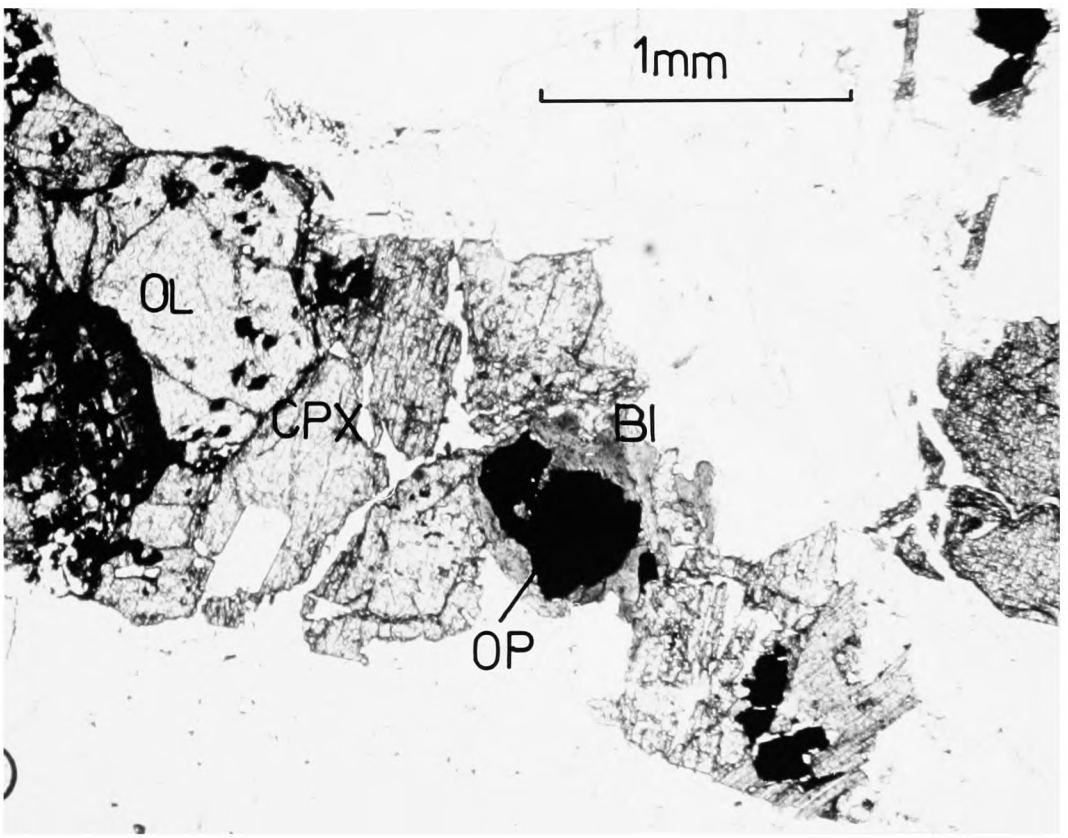


Plate 4.27 Augite rimmed by green ferroaugite or aegirine-augite in quartz syenite from Middletons Ridge. PPL

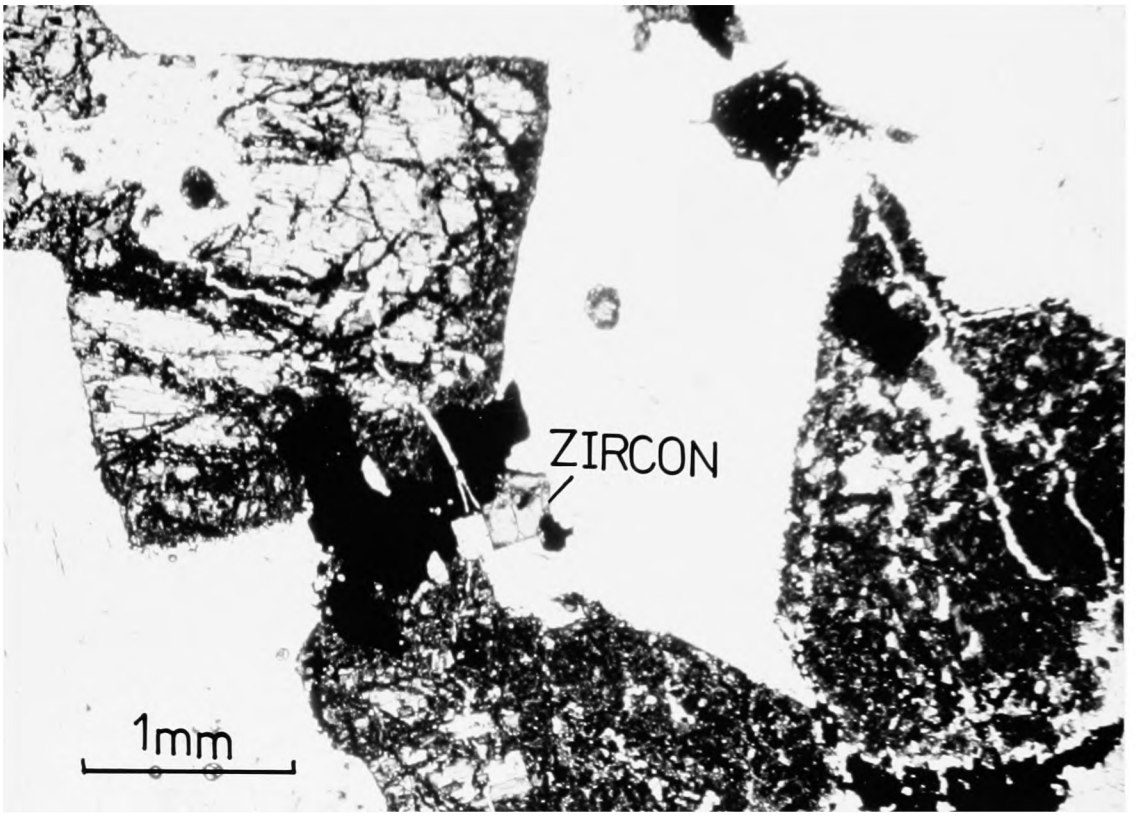


Plate 4.28 Aenigmatite(a) surrounded by aegirine (p) in a perthite granite H15231B. PPL

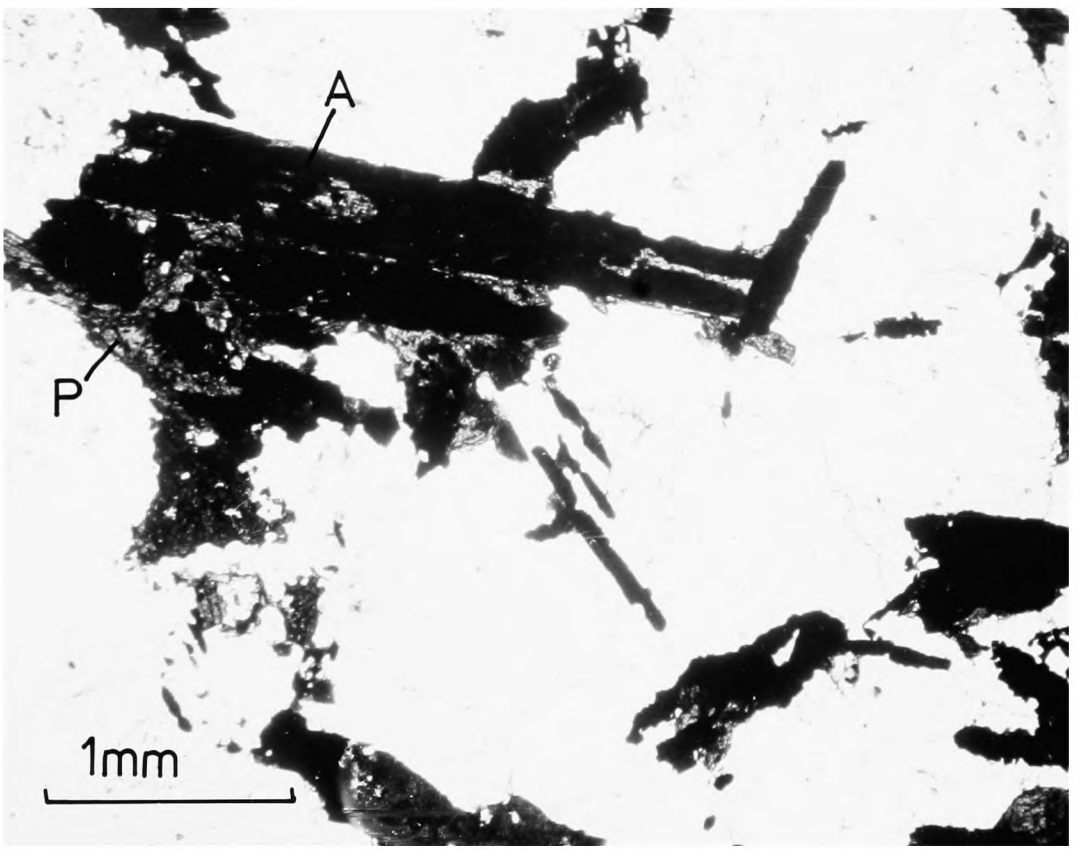


Plate 4.29 The reaction opaque +amphibole biotite in mafic monzonite 15226(17) . N.B. apatite (ap). PPL

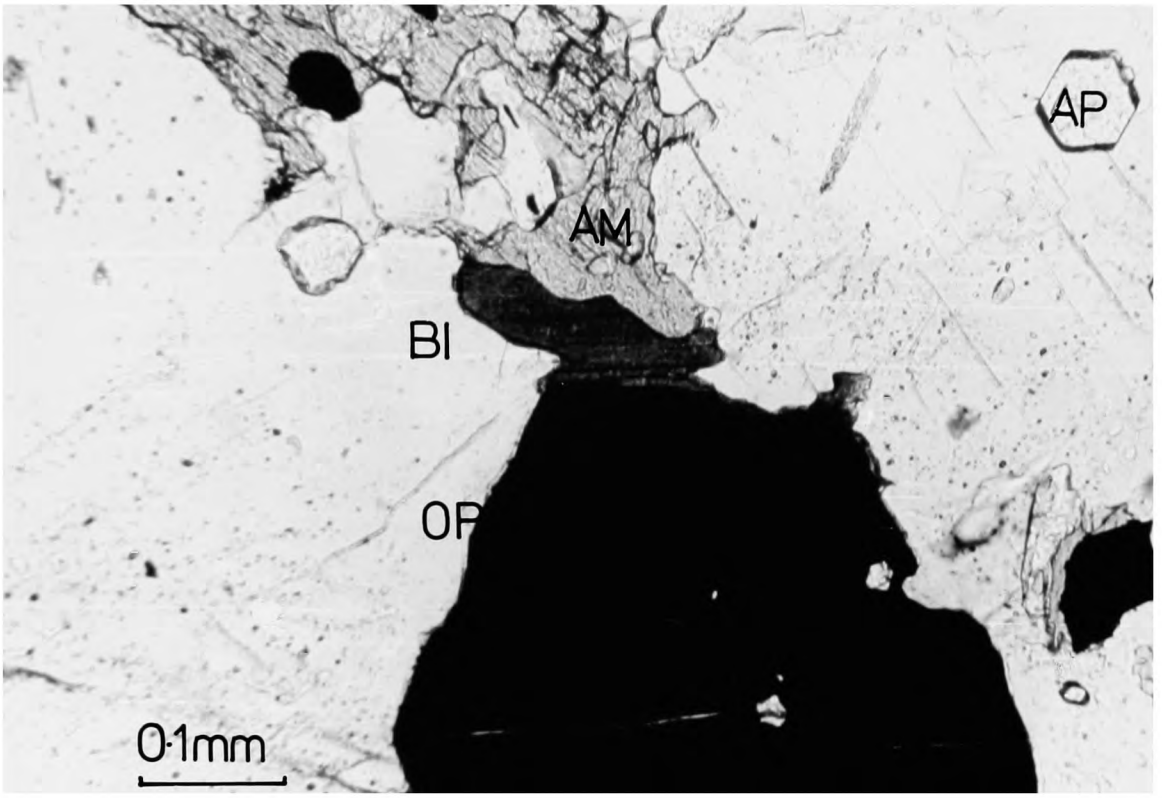


Plate 4.30 Mafics in mafic monzonite 15226(17). Cpx, biotite, amphibole, opaques + apatite and zircon. PPL

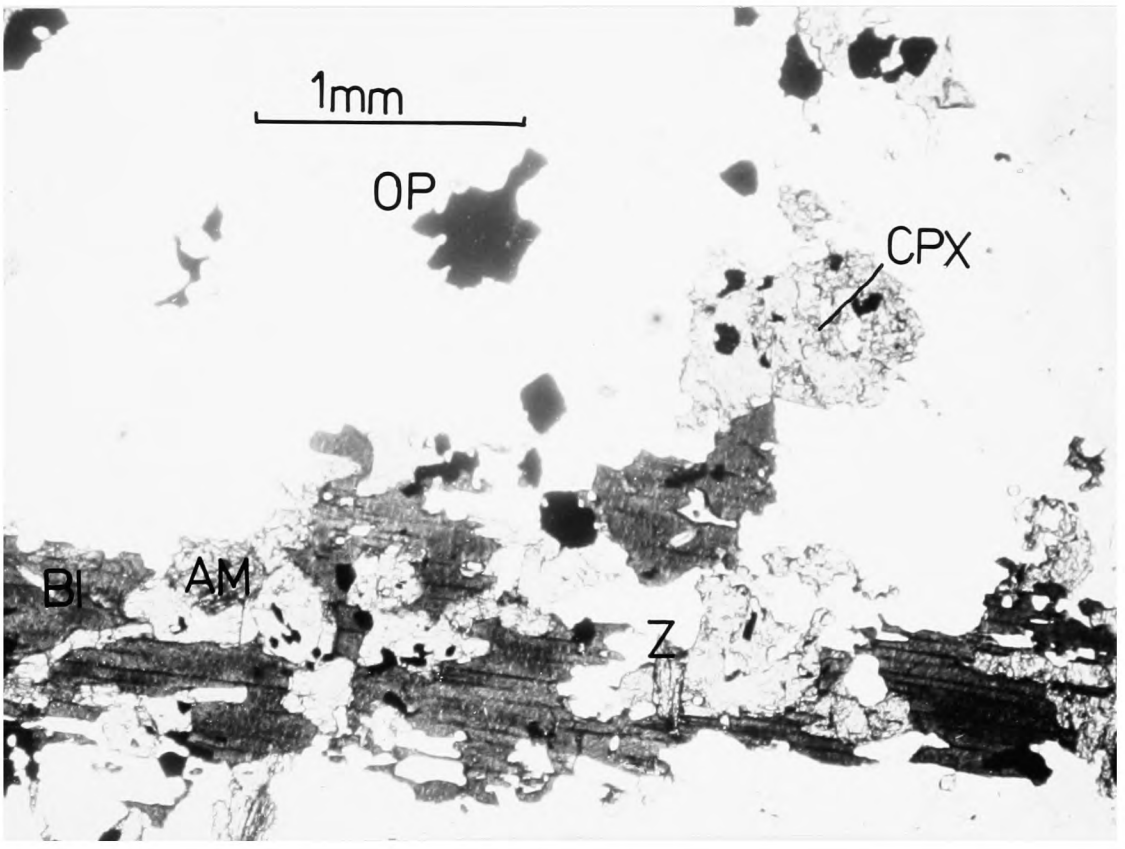


Plate 4.31 Quartz syenite (79949) with K feldspar having inclusion filled rims and clear euhedral cores. PPL

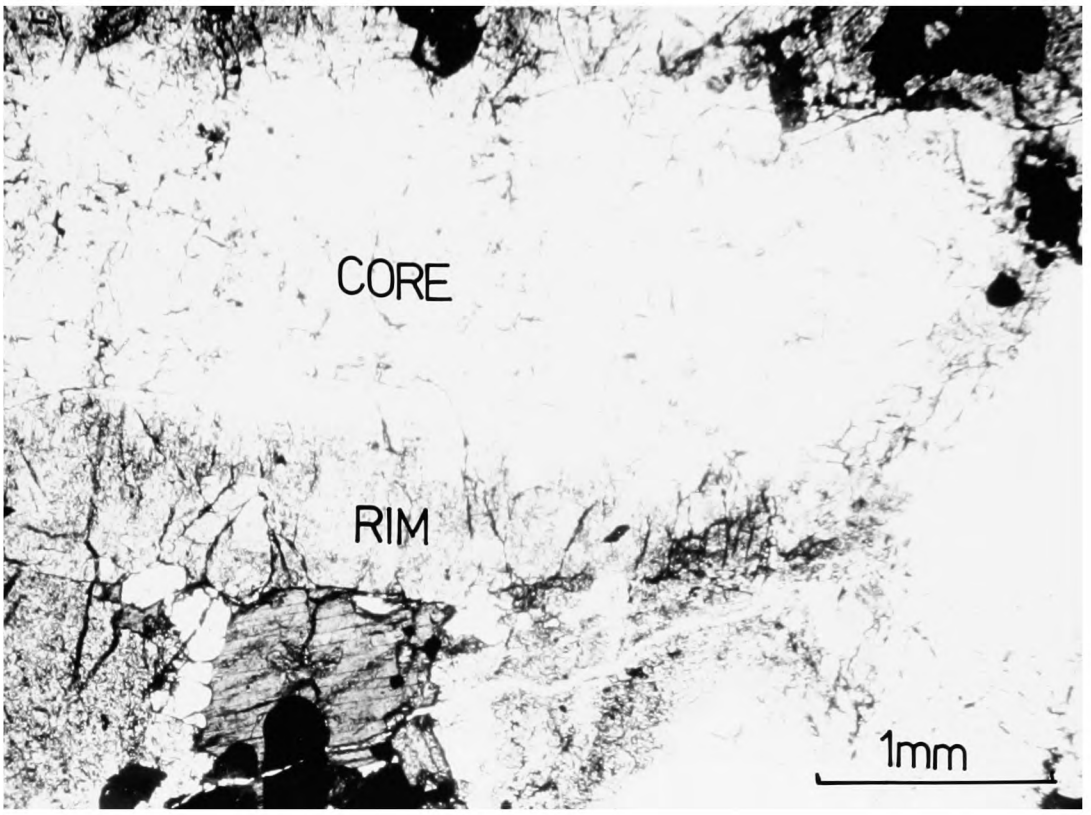


Plate 4.32 Augite zoned to aegirine - augite in quartz syenite 15226(7). PPL

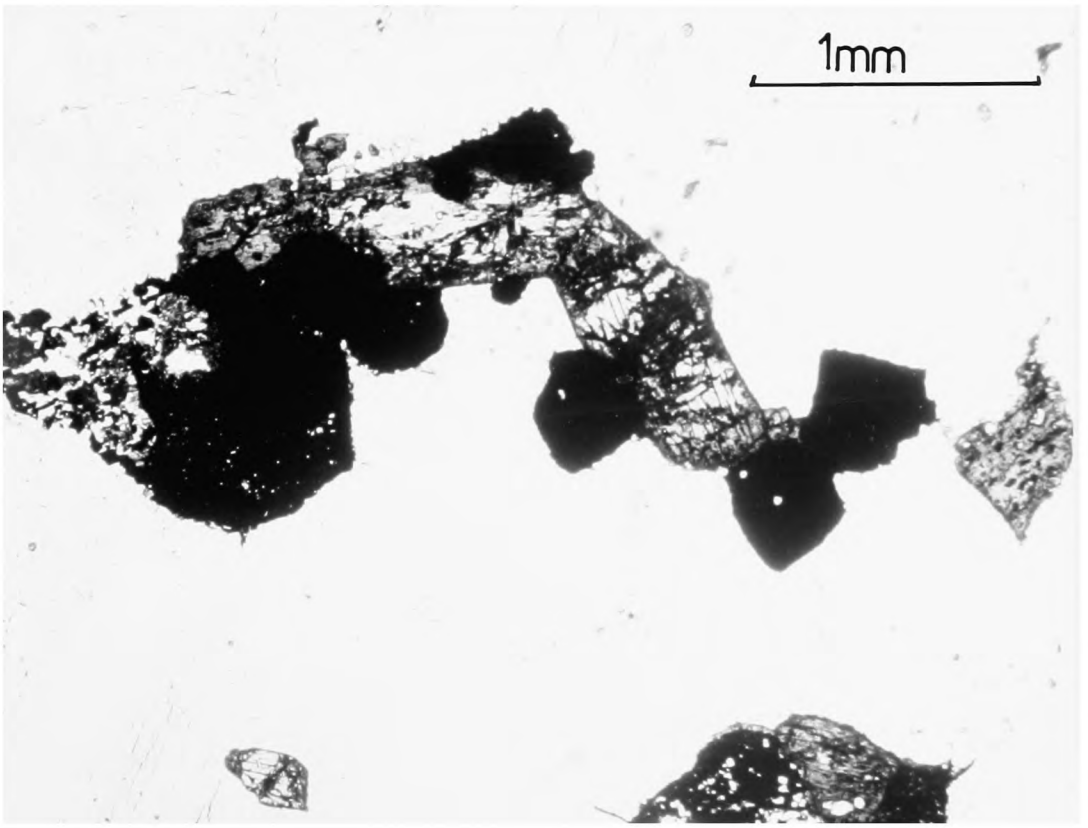


Plate 4.33 15226(4) Biotite replacing amphibole in quartz syenite. The biotite itself has been affected by reheating -see text. PPL

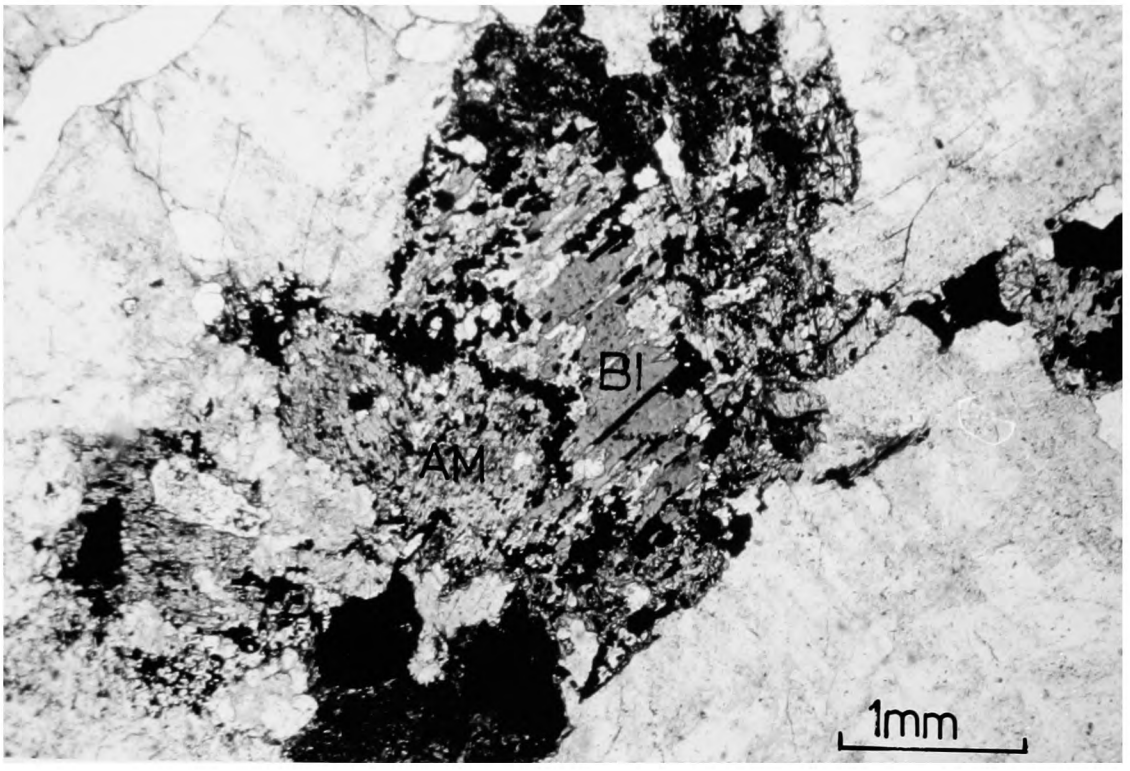


Plate 4.34 Granophyric vein in quartz syenite (15226 12b). Grain A is a feldspar cut by the vein. XPolars

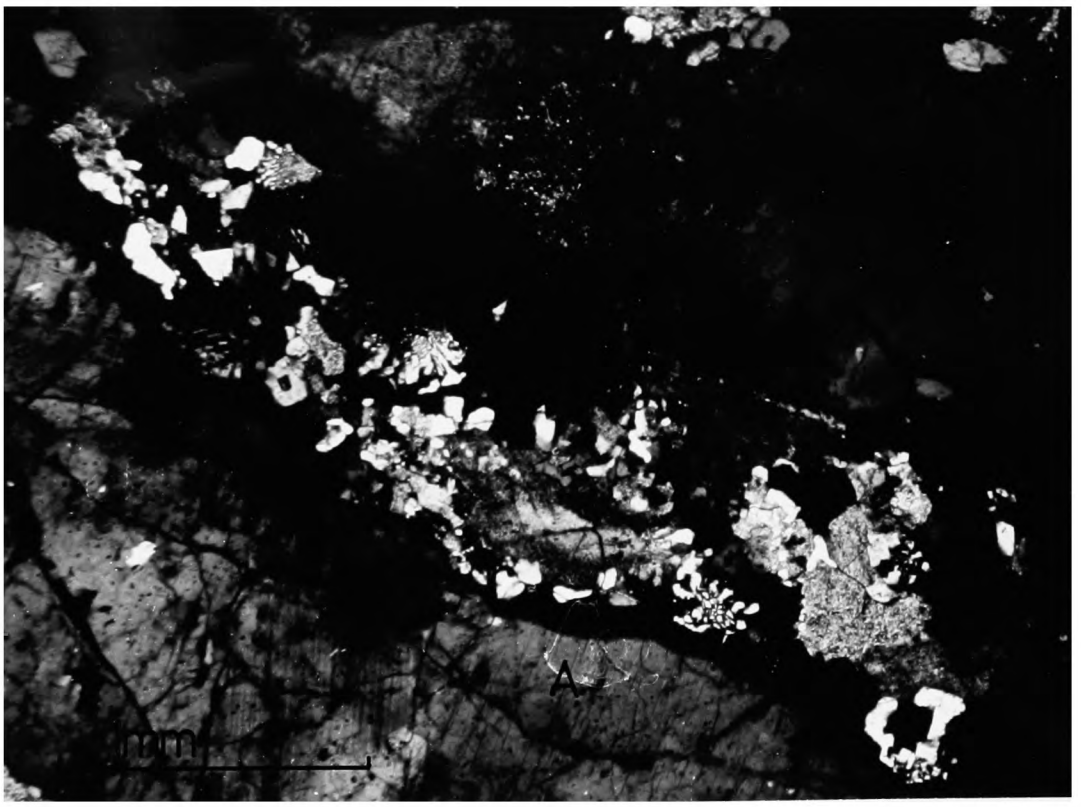


Plate 4.35 Exsolution of albite from Kfeldspar in discrete patches; granite block H30(1) . X Polars

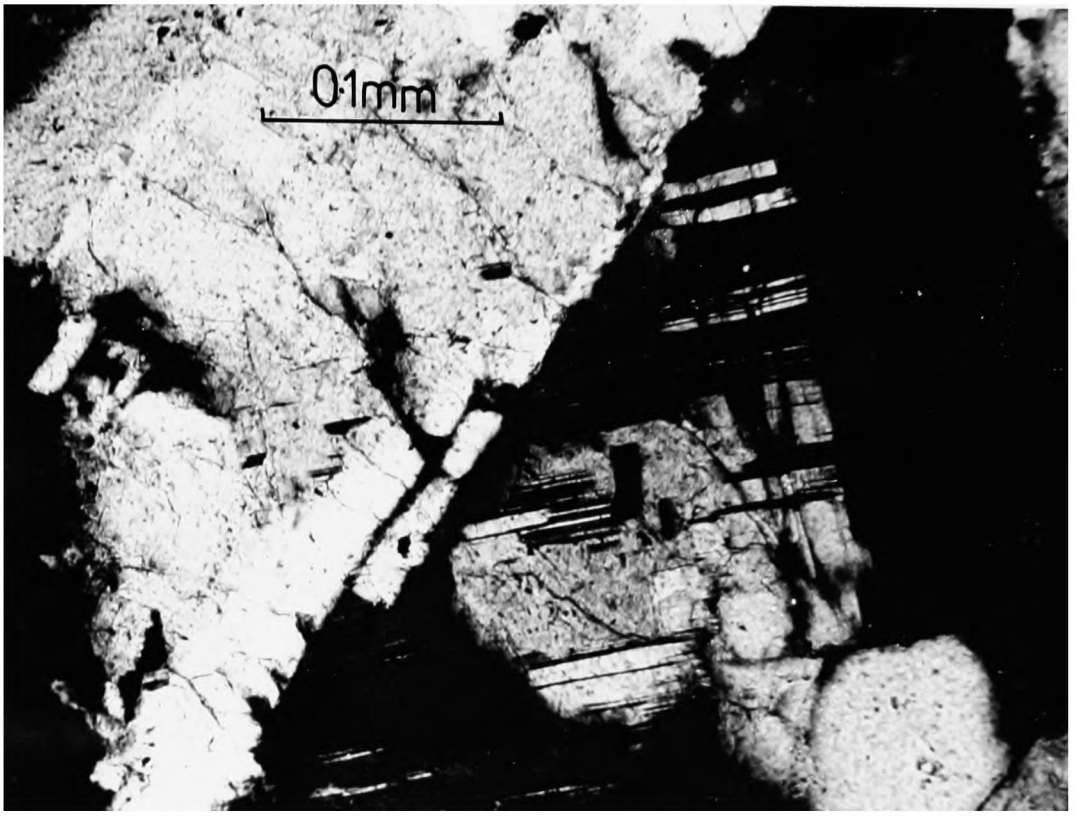


Plate 4.36 Exsolution in feldspar showing rod type pattern (H30(1))

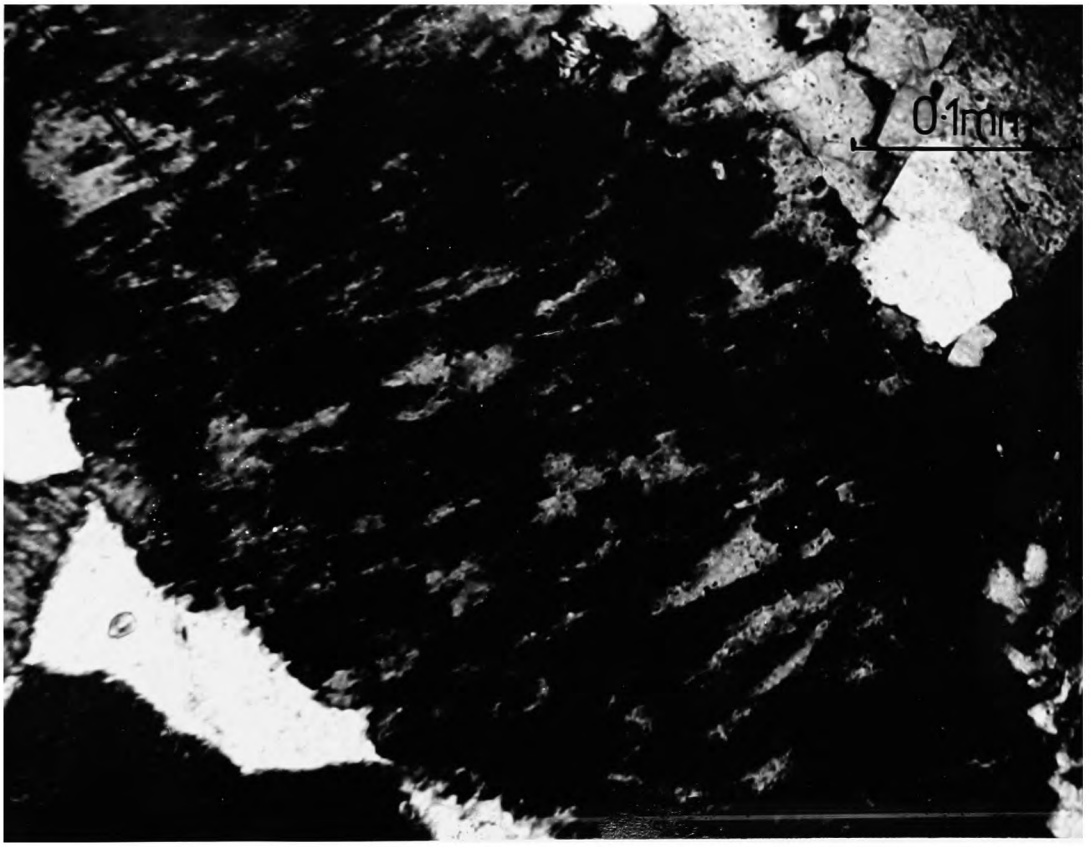


Plate 4.37 Aegirine replacing arfvedsonite (?) in perthite granite H17318(b) . PPL

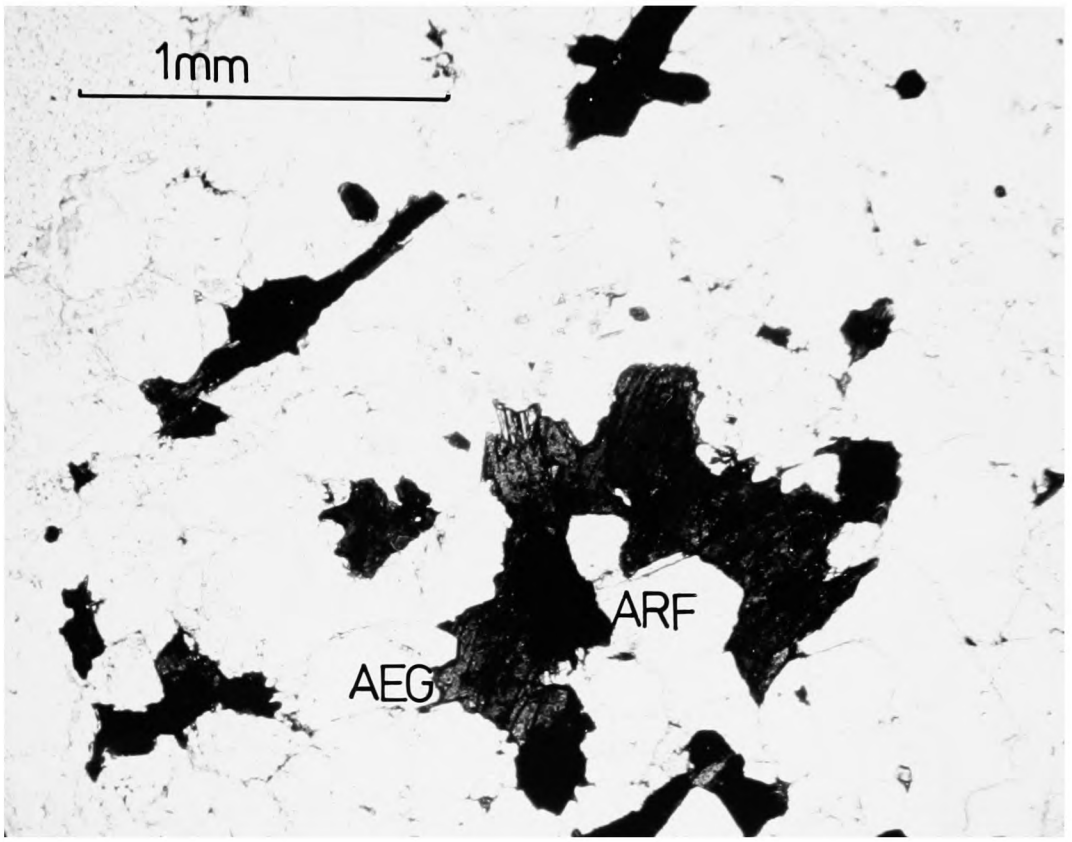


Plate 4.38 Arfvedsonite possibly replacing aegirine in perthite granite H30(1). PPL

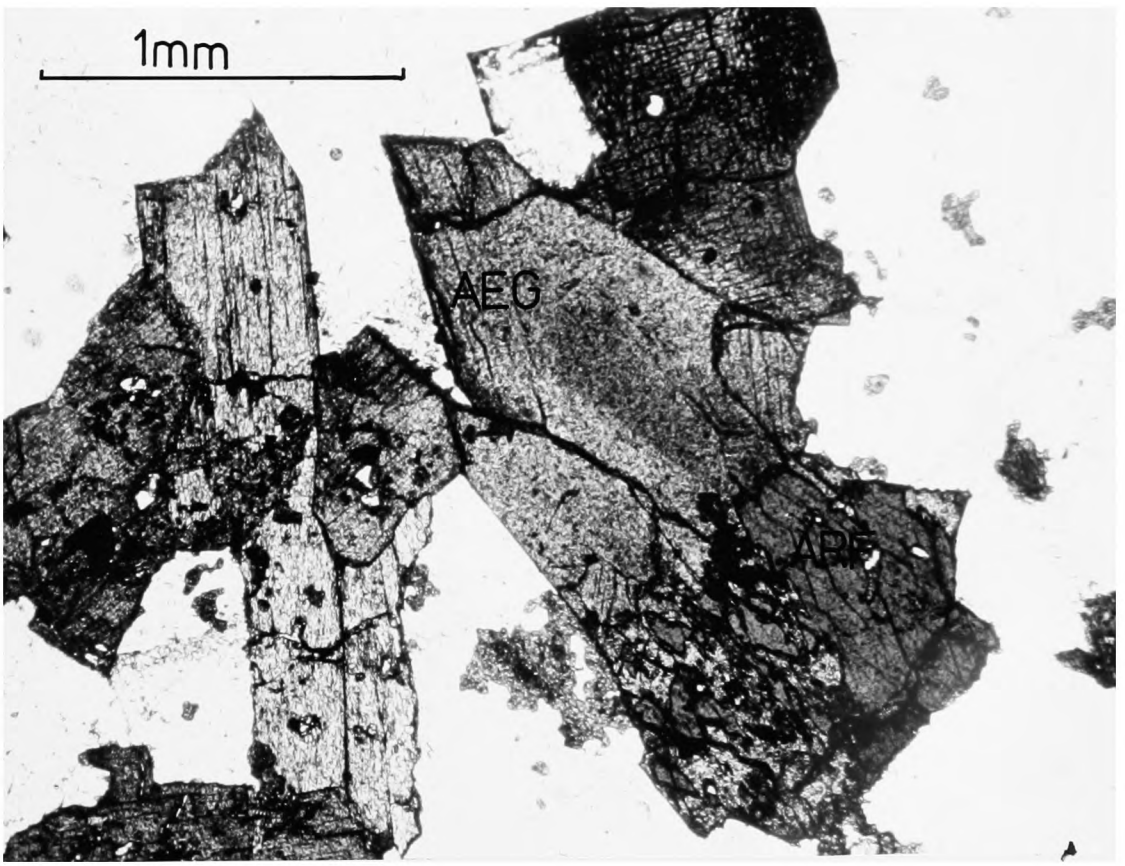


Plate 4.41 Granophyric rim to K feldspar from Devil's Riding School granophyre block H21(12). PPL

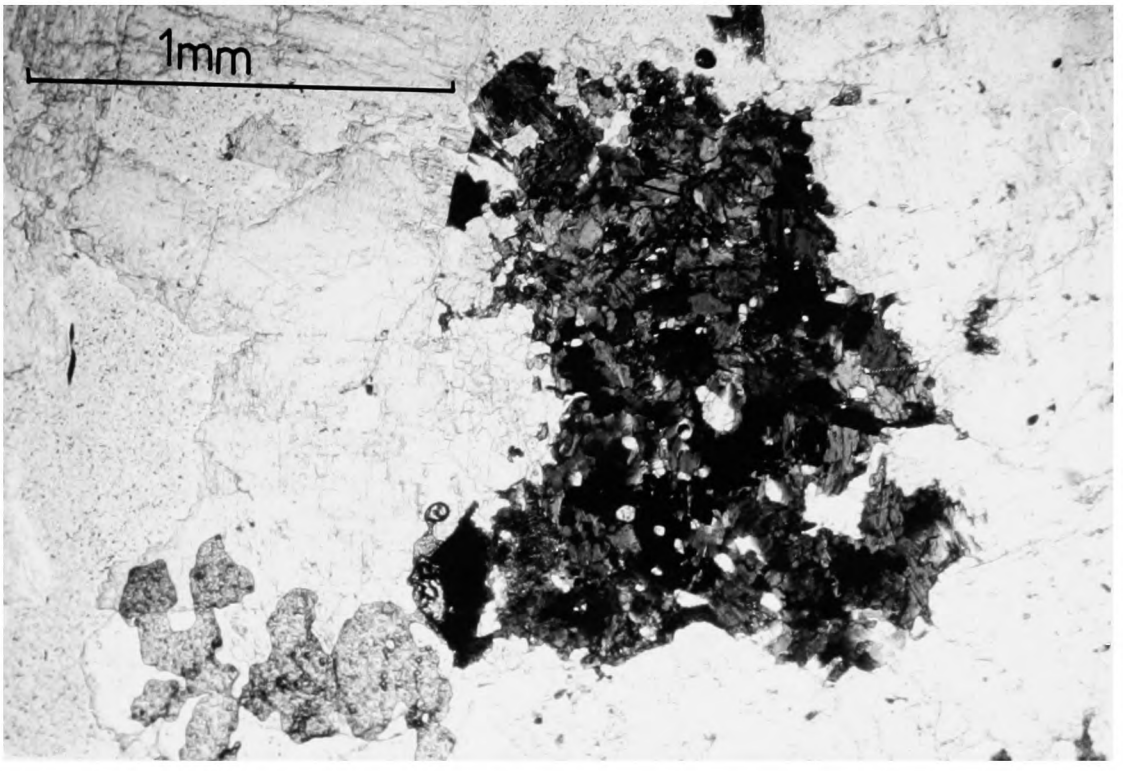


Plate 4.42 Photomicrograph of pegmatoid showing skeletal form of magnetite and early formed pyroxene, feldspar and apatite (A). PPL

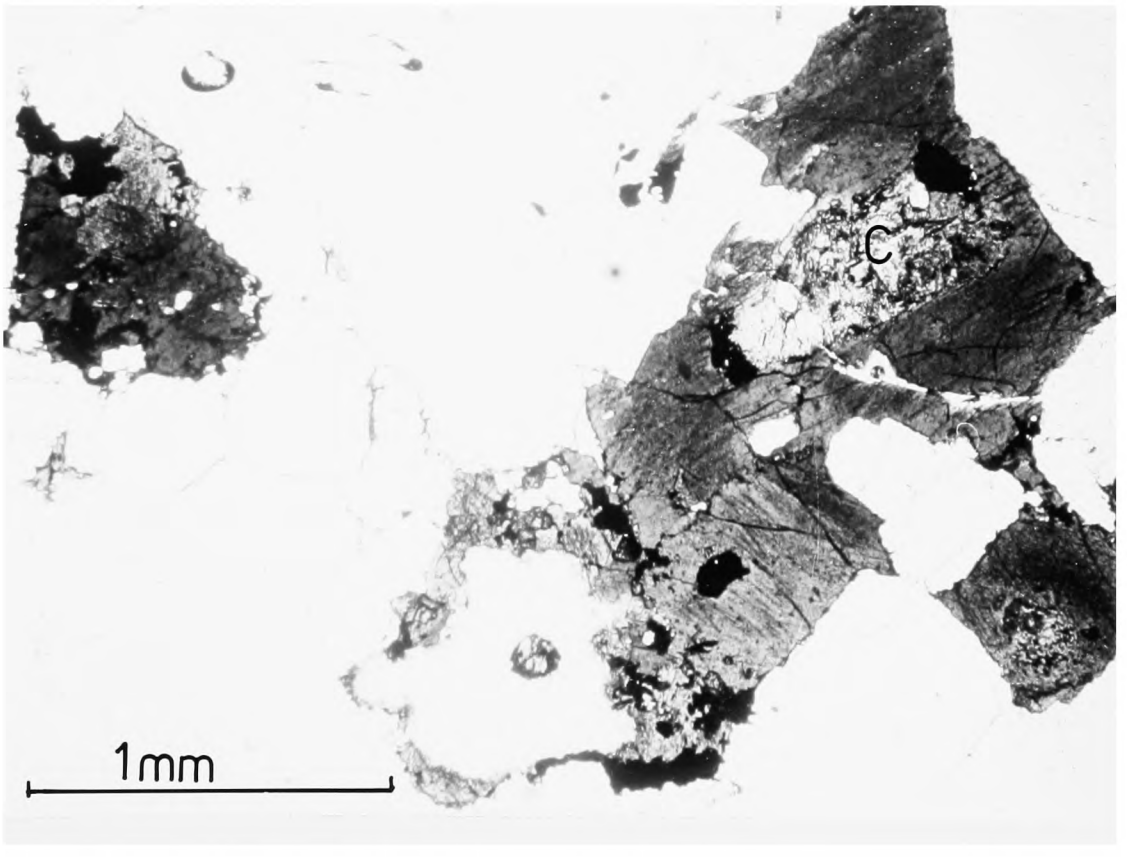


Plate 4.39 Mafic clot in non-perthitic granite (15231D). The only biotite bearing block from this suite. PPL

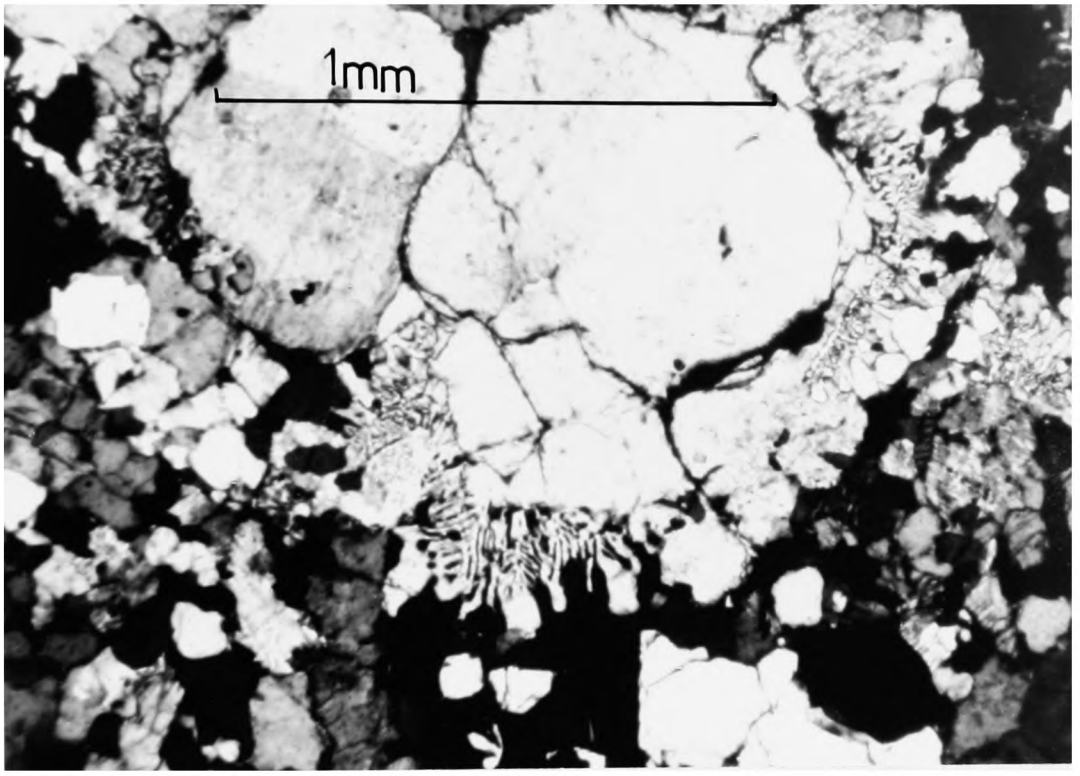


Plate 4.40 Hornblende non-perthitic granite (15231A). Amphibole has an augite core (C). PPL

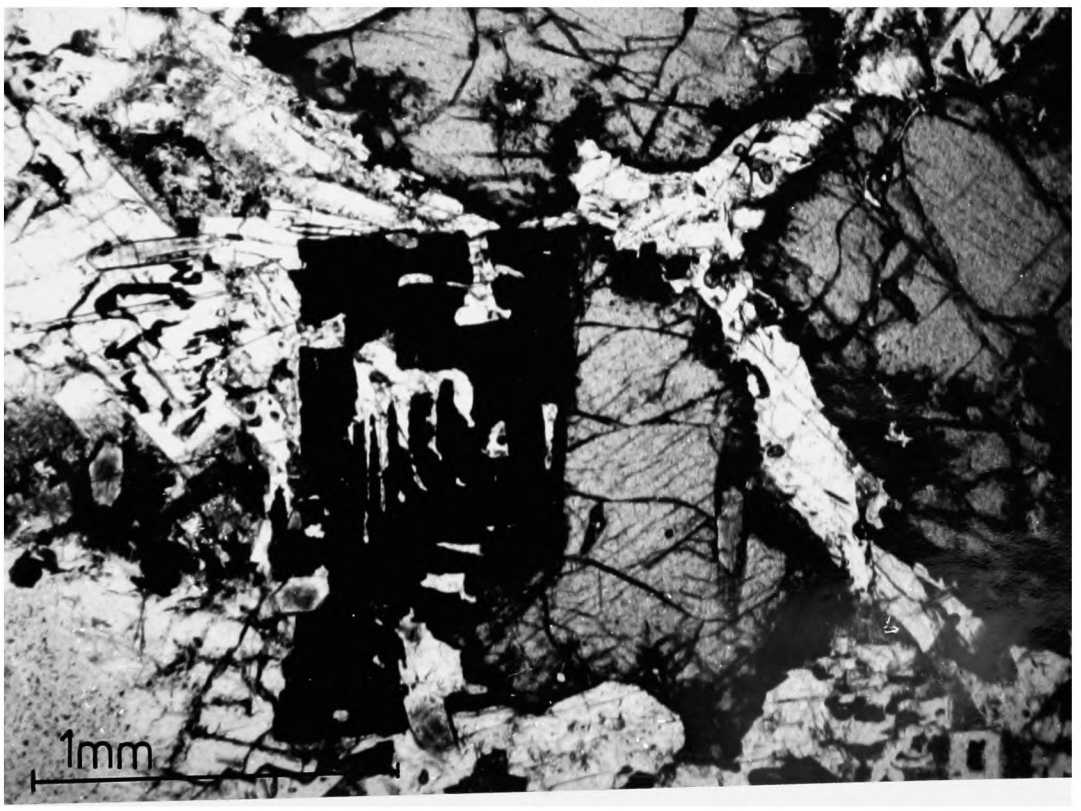


Plate 4.43 K feldspar silica intergrowth interstitial between feldspar grains 17428B. PPL

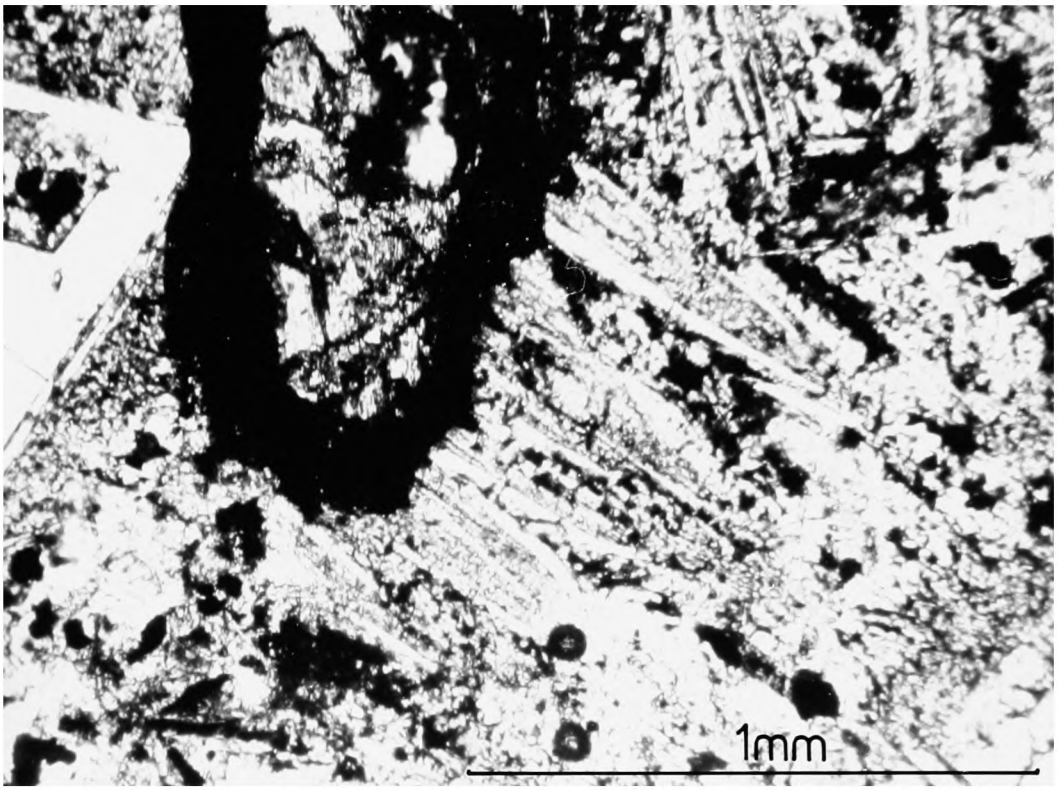


Plate 4.44 Miarolitic cavity in pegmatoid with later formed K feldspar (K) and pyroxene (P). Cryptocrystaline silica (S) partially infills the cavity. PPL

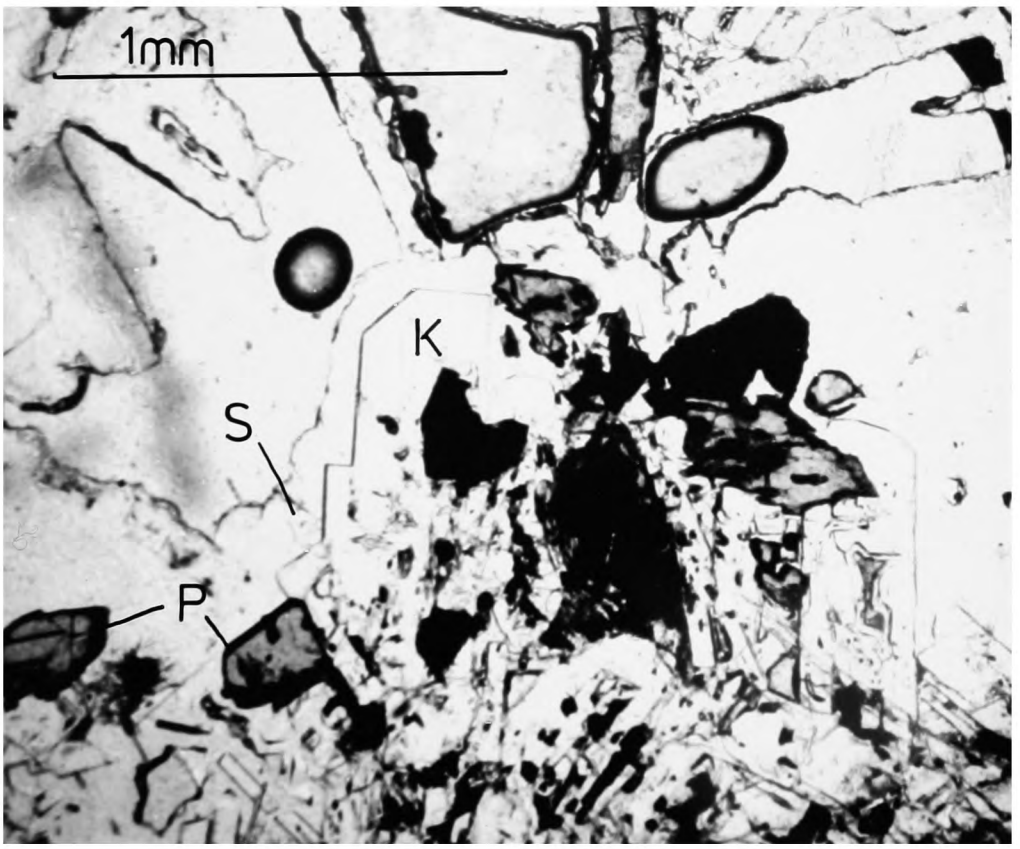


Plate 4.45 Close up of Plate 4.44 . Euhedral K feldspar (K) projects into silica infill (S). H= subhedral hollows due to incomplete crystallization of the feldspar. PPL

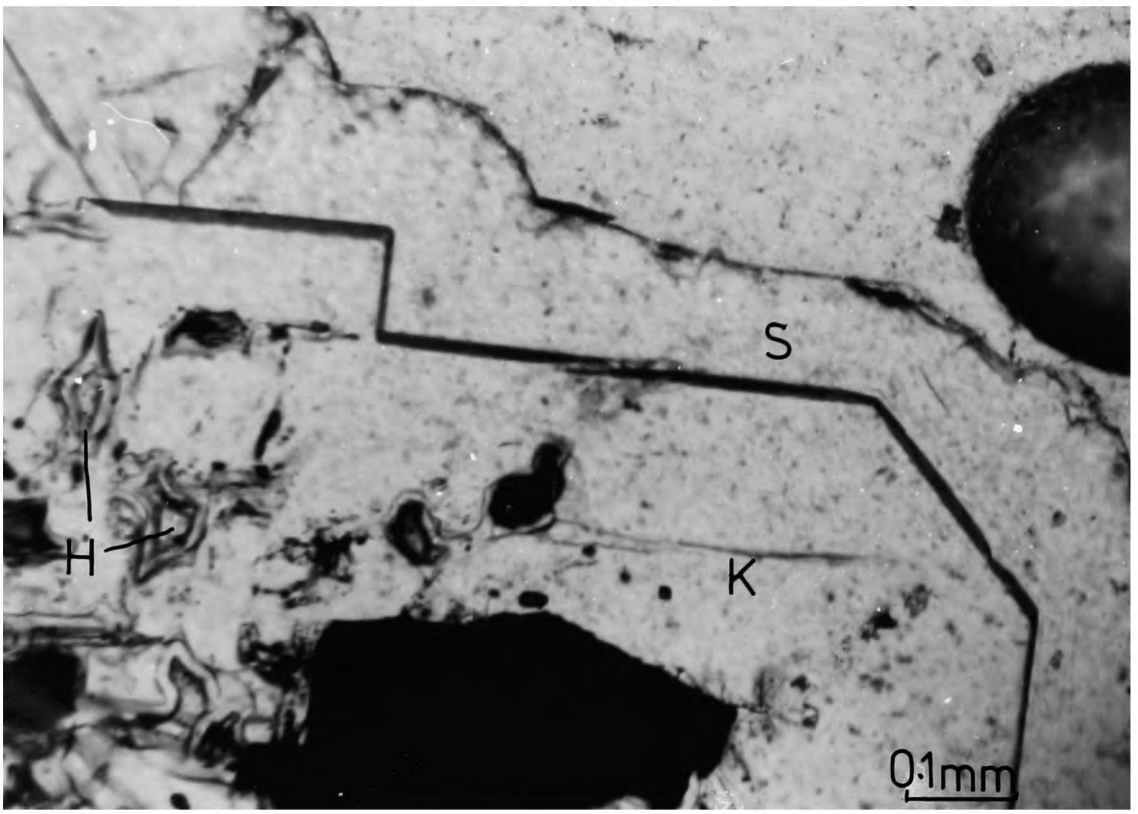


Plate 4.46 Aegirine-augite rims to augite in pegmatoid (17428B). PPL

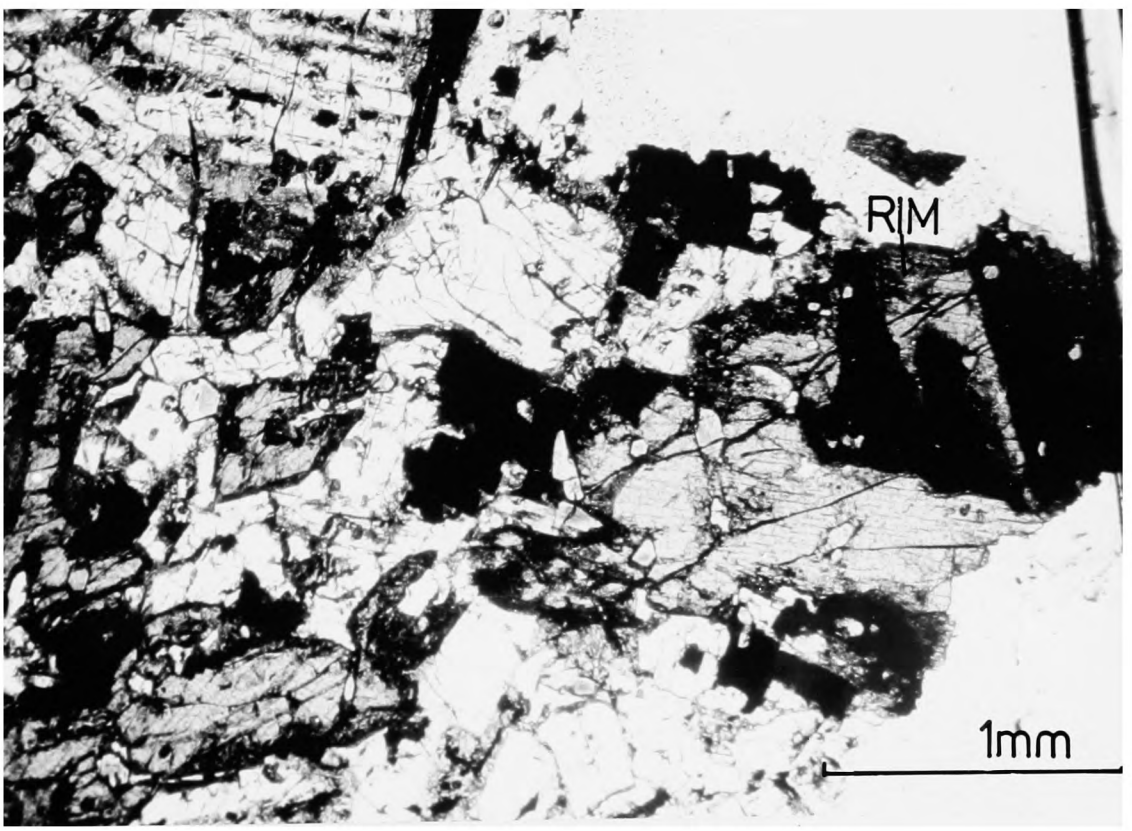


Plate 4.47 Pyroxene-feldspar intergrowth in pegmatoid. PPL

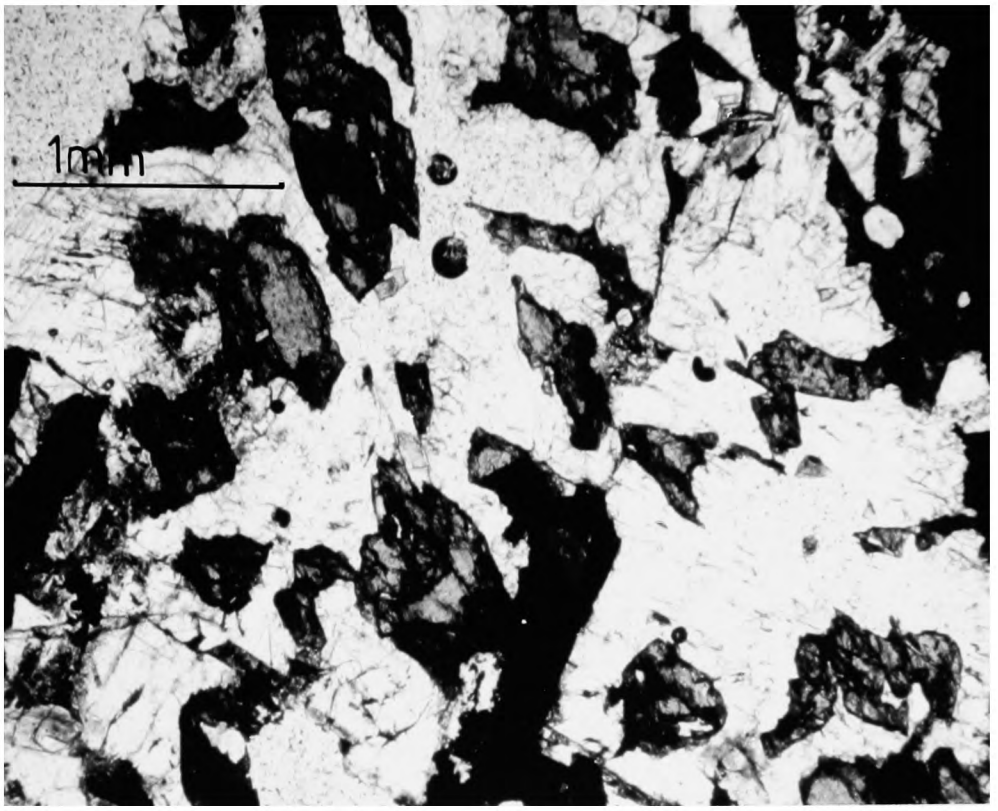


Plate 4.48 Vlasovite in perthite granite 15231-6 N.B. cleavage. PPL

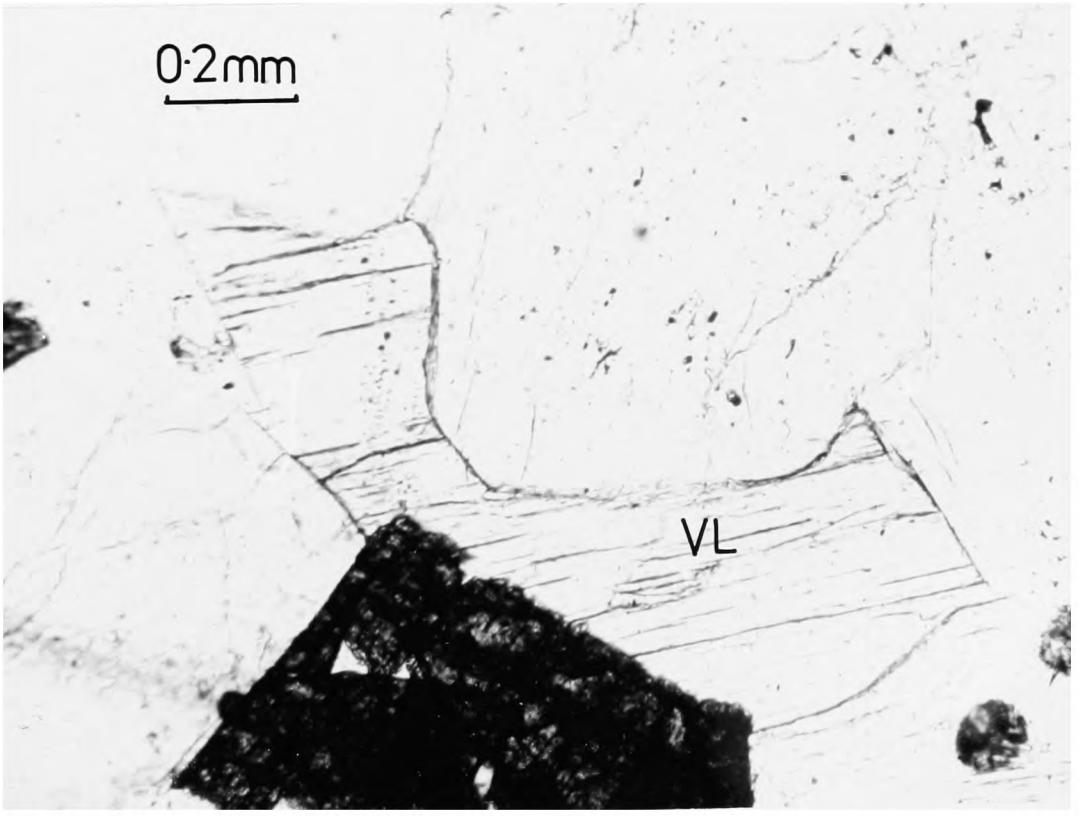


Plate 4.49 Zircon rimmed by vlasovite in perthite granite 15231-6 PPL

Z = Zircon, V = Vlasovite

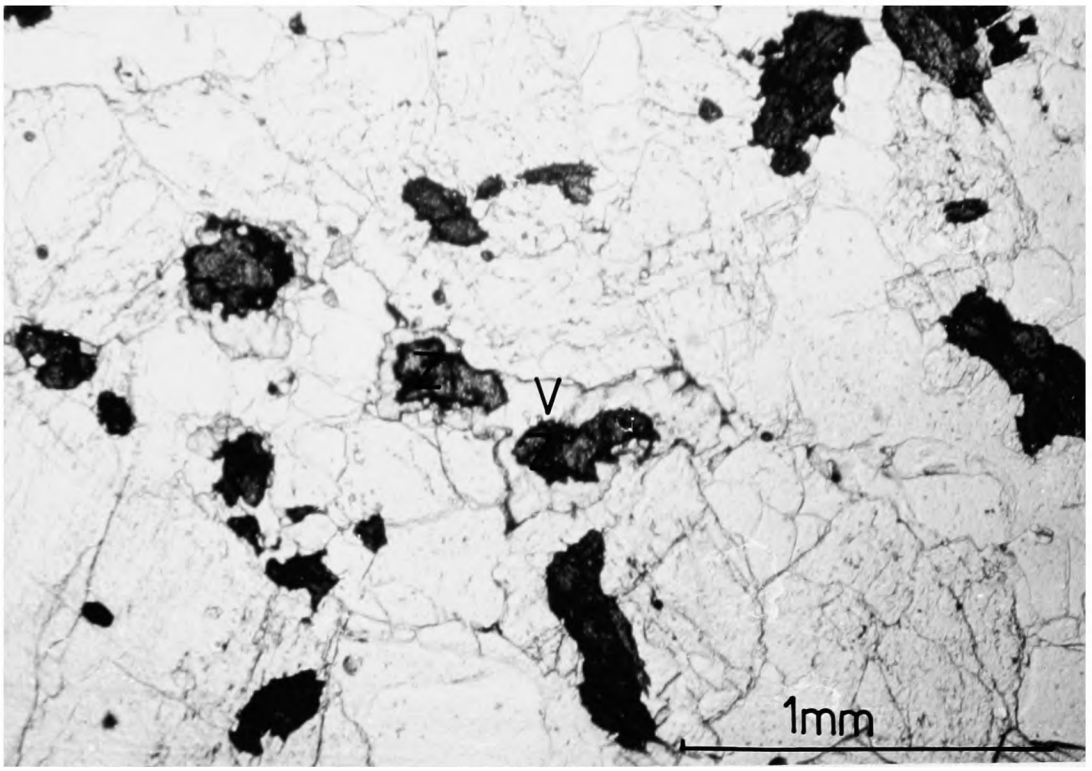


Plate 4.50 As Plate 4.49 with polariser at 45°.

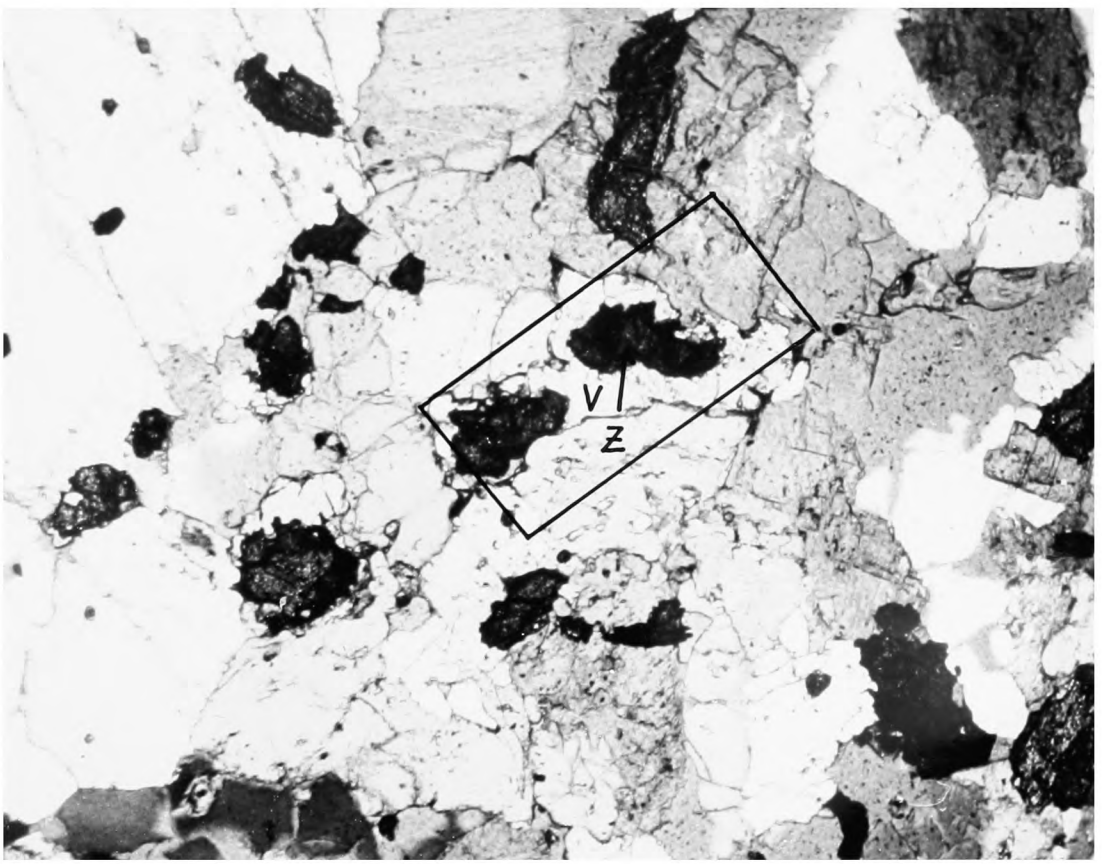
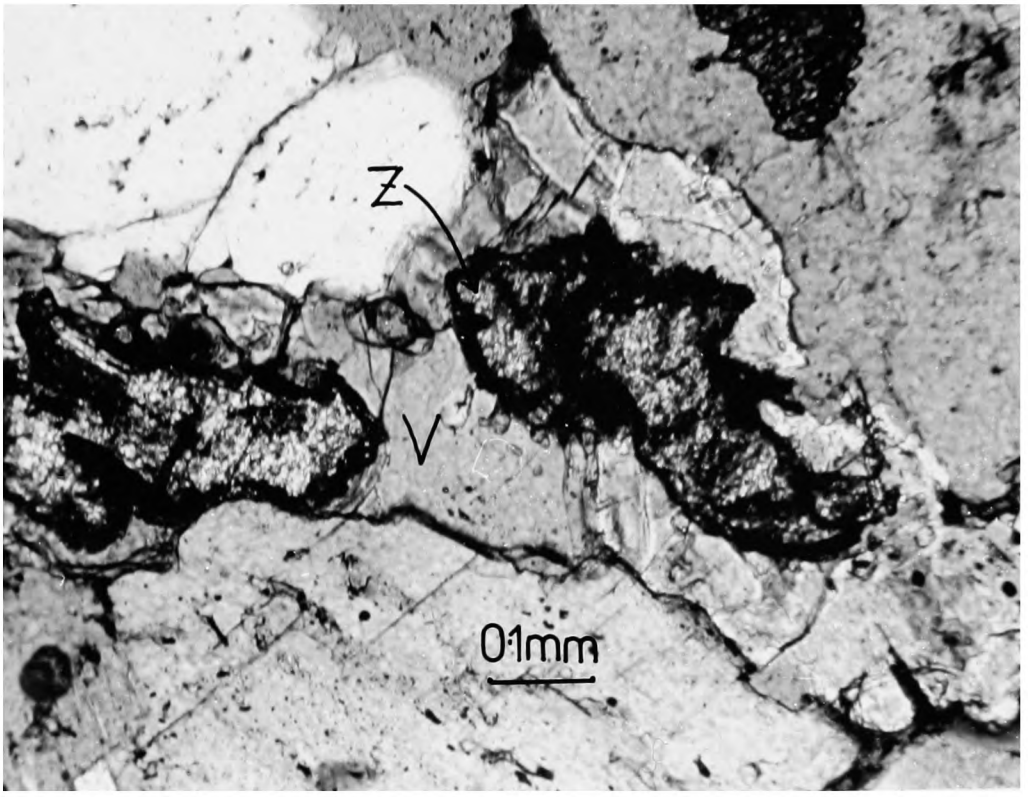


Plate 4.51 As Plate 4.50 ,close up; see Plate 4.50 for location.
X Polars



Z = ZIRCON

V = VLASOVITE

Plate 4.52 Eudialyte and dalyite in perthite granite HDD(1). PPL

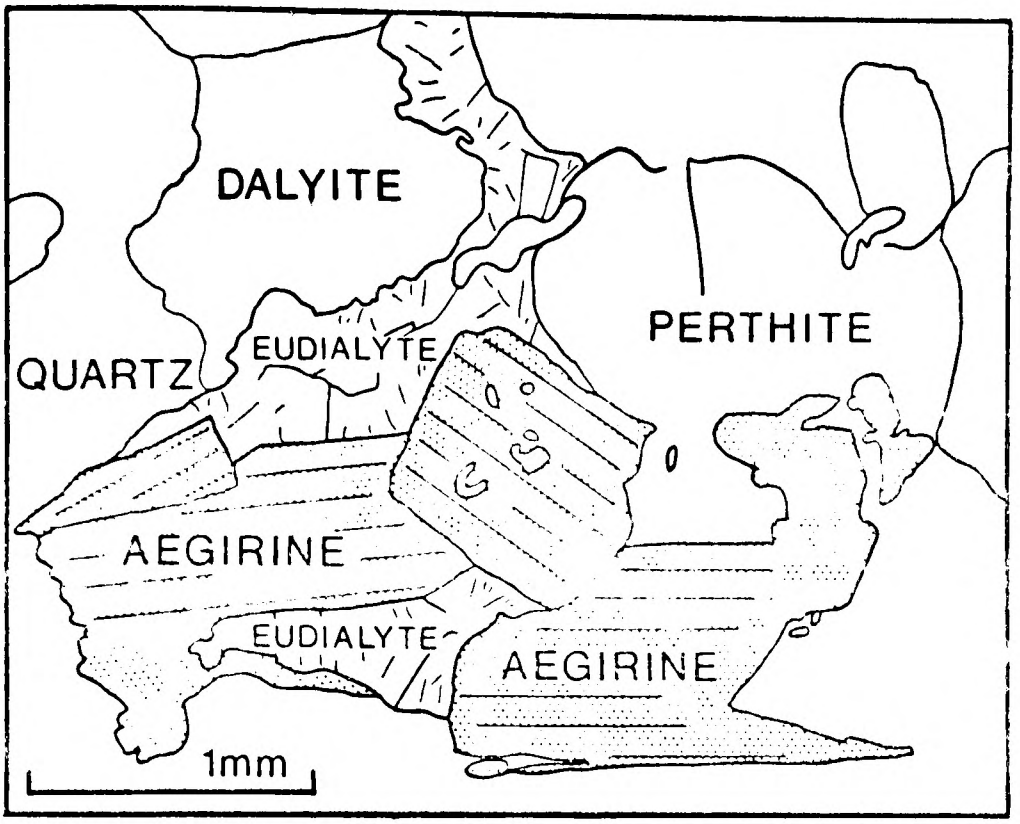
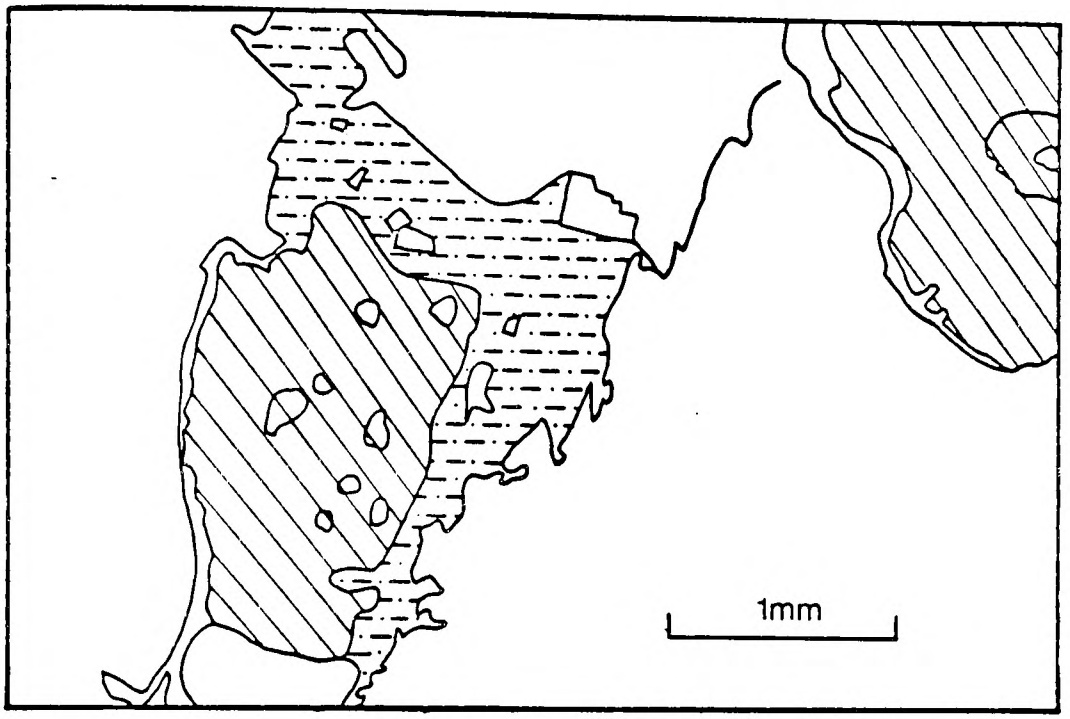




Plate 4.53 Pyroxene and feldspar. pyroxene is surrounded by brown glass and opaques. N.B. the euhedral quench crystals and the slight clouding of the anorthoclase due to reheating.



Feldspar

Pyroxene

Glass

Opaques

Brown glass & opaques

Quartz

Zircon

V Vesicle

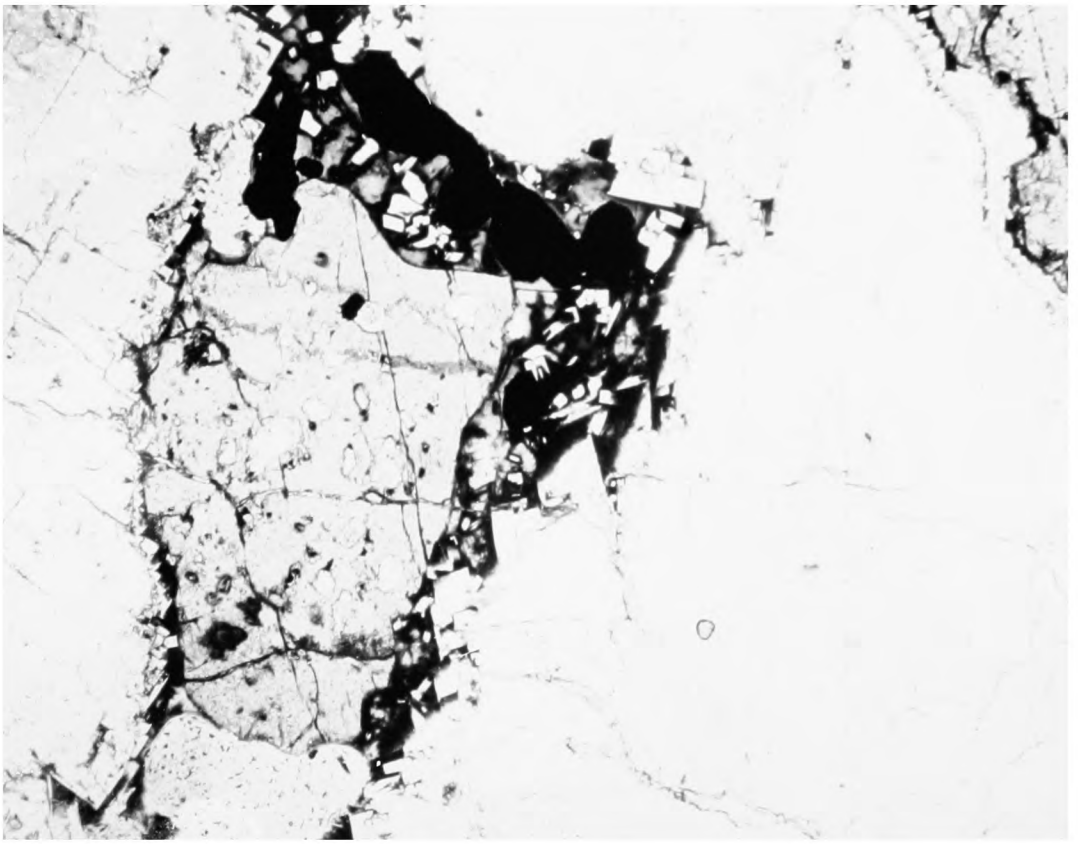
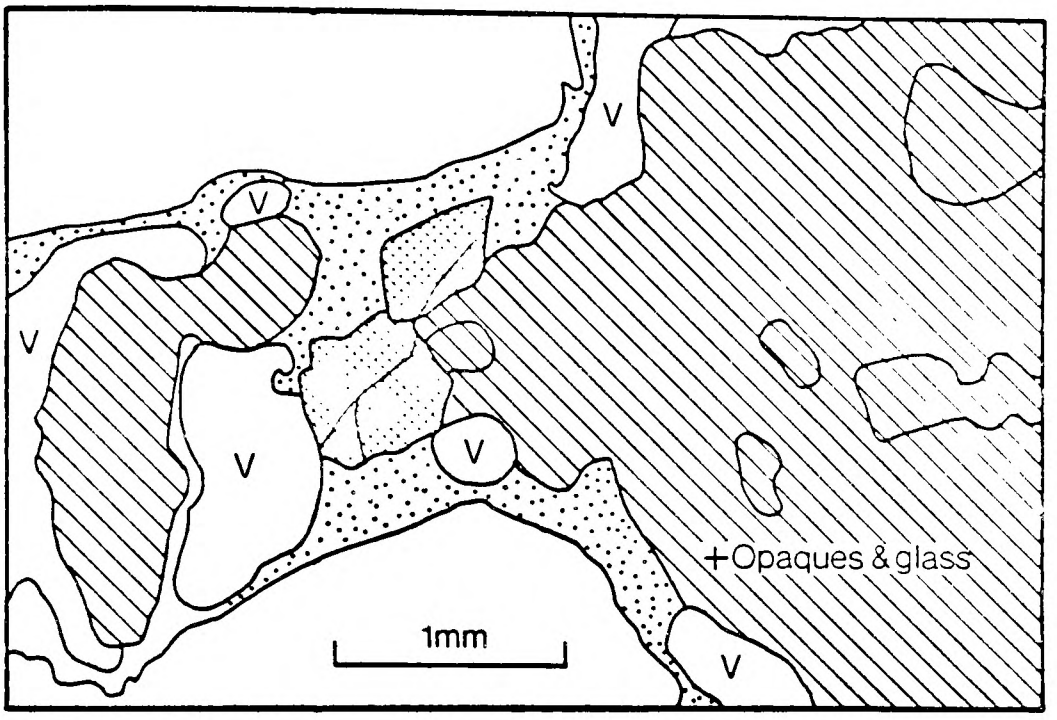


Plate 4.54 Euhedral zircon in partially melted pyroxene-feldspar area. N.B. the replacement of the original pyroxene by a pyroxene-opaque-glass mass.



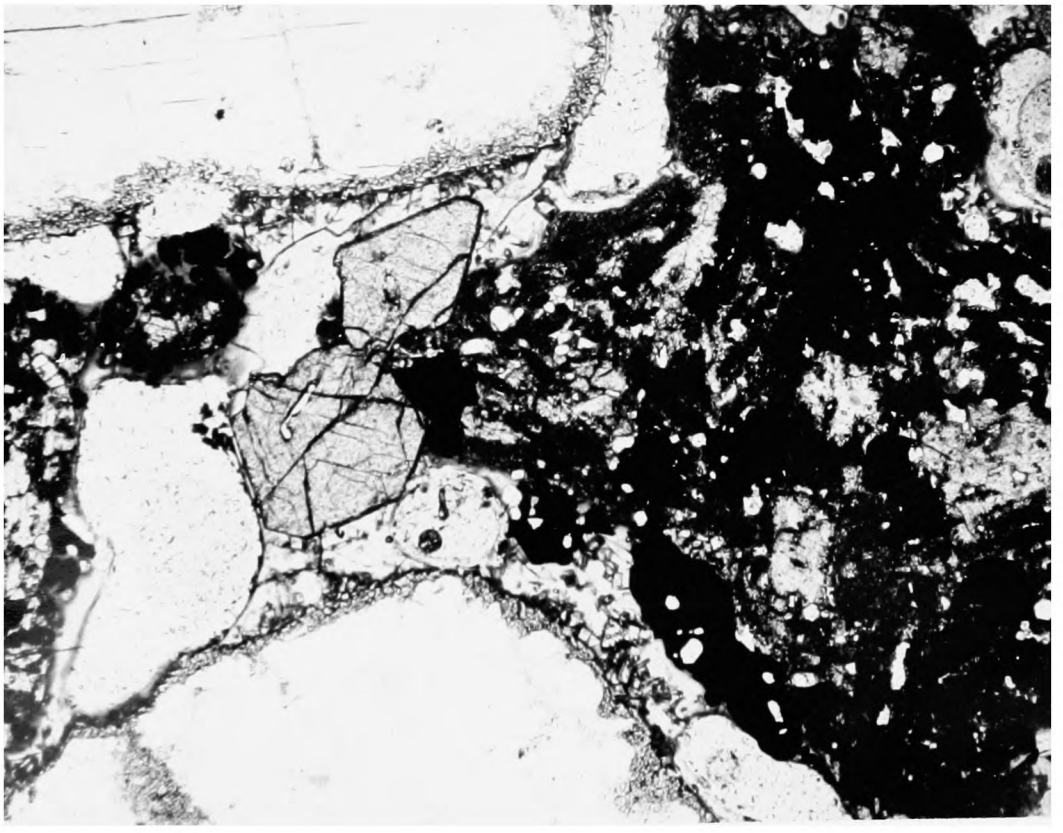
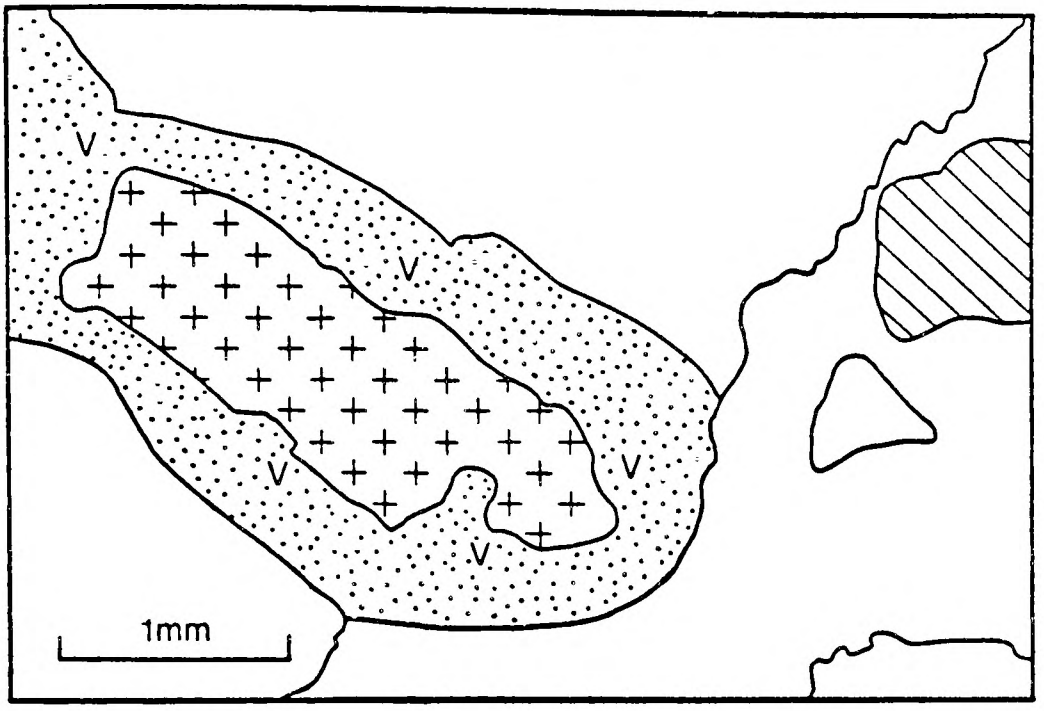


Plate 4.55 Quartz and feldspar contact with large, vesicular glass rim around the quartz (polariser at 45°).



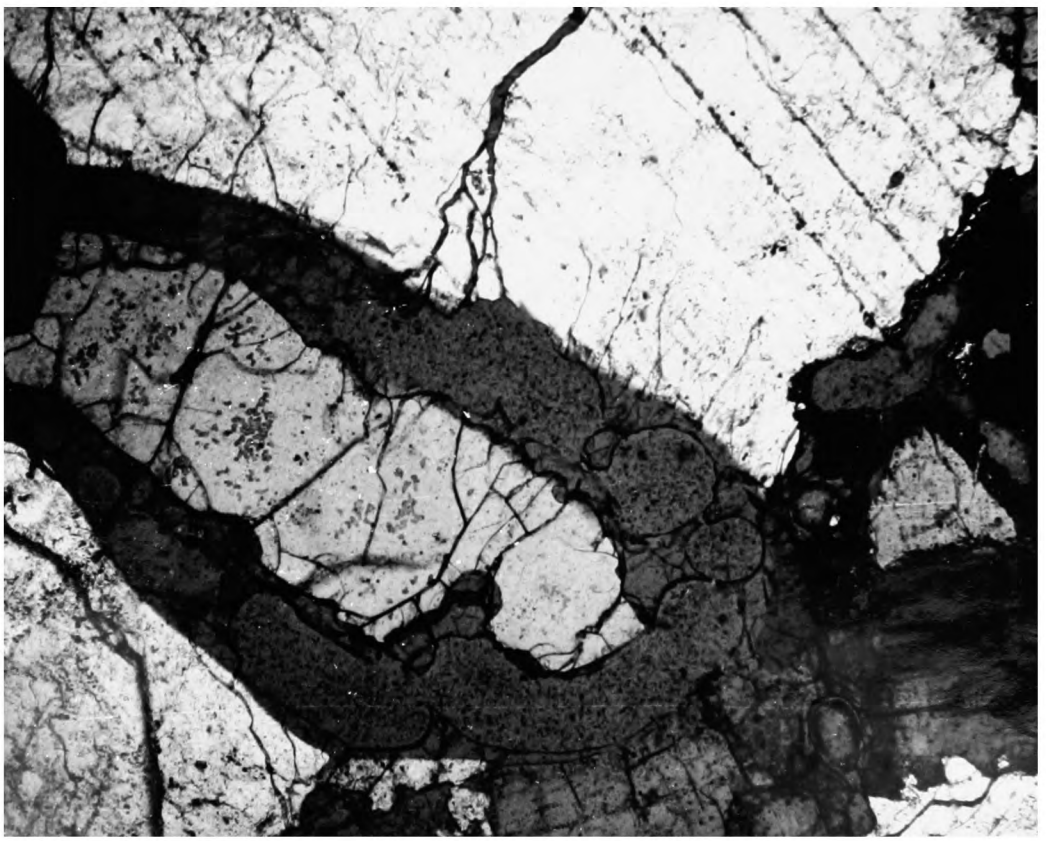


Plate 4.56 Melted pyroxene-feldspar contact (H30(3)). Plate 4.58 is a close up of the marked area. PPL

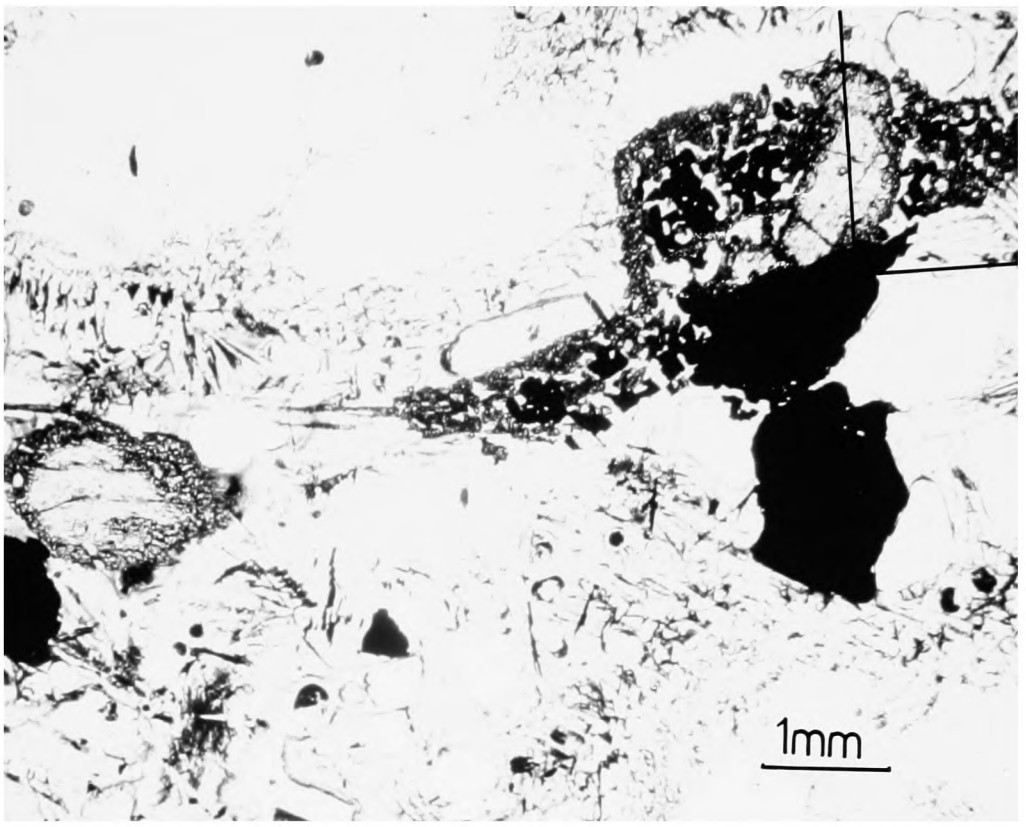
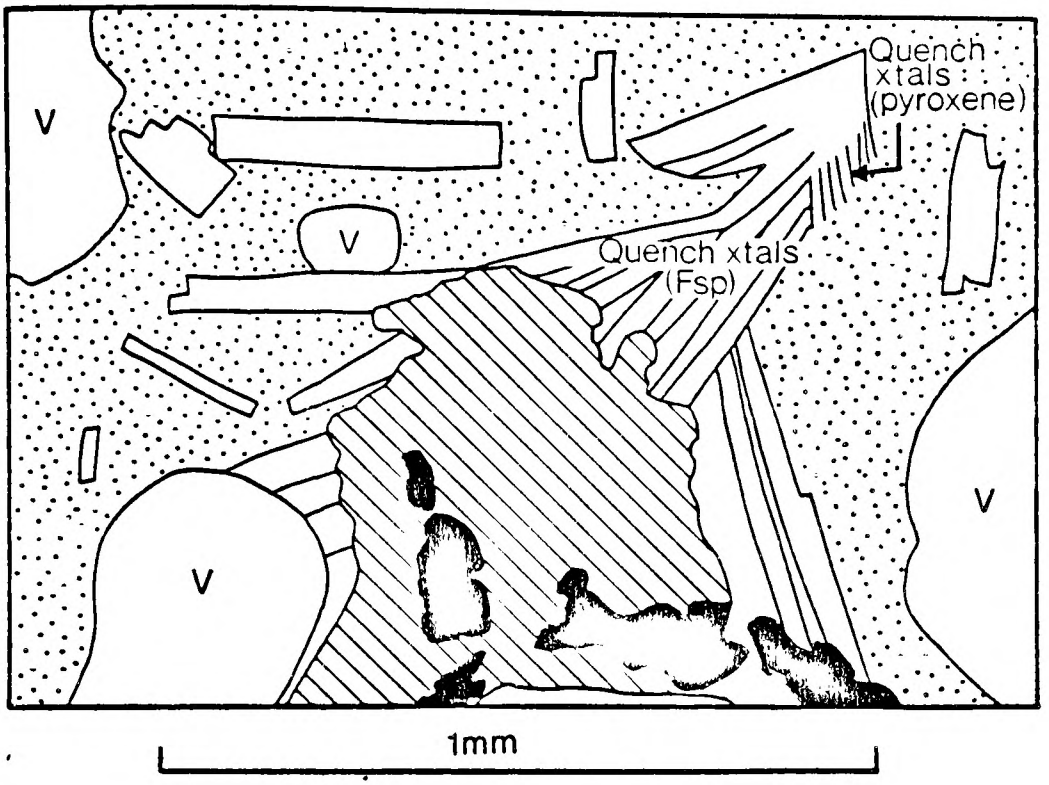


Plate 4.57 As Plate 4.56 with polariser at 45°. N.B. presence of euhedral K feldspar quench crystals adhering to the original K feldspar.



Plate 4.58 Glass containing vesicles, small radiating quench crystals of feldspar and hair-like quench crystals of pyroxene. Small disjointed patches remain of the original pyroxene. (E. Crater)





CHAPTER FIVE

TABLES AND FIGURES

Table 5.1

LAVAS	15209	15019	15176	17464	17364	15062	15367	15001	17409	15090	15113	15007	H5L	15085	DS19L	14997	H48L
SiO_2	47.16	48.15	48.19	48.38	48.45	48.71	48.73	48.77	49.05	49.21	49.70	49.74	49.83	49.94	50.31	50.49	51.38
TiO_2	3.08	3.13	3.03	2.94	3.48	3.58	2.54	2.11	2.50	2.65	2.95	2.57	1.92	3.09	2.89	2.50	2.65
Al_2O_3	15.96	15.14	17.28	16.17	14.71	15.45	16.31	16.80	16.81	14.22	16.44	15.46	17.18	15.35	16.83	18.37	16.00
Fe_2O_3	7.77	4.97	1.86	5.62	5.01	2.89	5.00	4.00	5.40	5.70	4.21	3.66	-	2.50	-	4.16	-
FeO	4.38	7.62	9.84	7.04	7.32	9.26	6.74	6.29	6.43	8.18	7.96	8.31	9.48	8.90	12.09	5.27	10.66
MnO	0.19	0.18	0.23	0.23	0.25	0.21	0.19	0.16	0.18	0.23	0.21	0.81	0.15	0.23	0.20	0.15	0.20
MgO	4.99	5.99	4.24	4.35	4.52	4.62	5.56	4.75	4.73	5.09	3.79	3.55	6.65	4.37	4.91	3.12	5.14
CaO	8.18	9.72	7.90	9.87	8.40	8.60	8.49	10.66	9.64	9.37	7.45	9.90	10.92	7.85	8.52	9.35	8.36
Na_2O	3.92	3.10	4.28	3.30	4.22	3.92	2.92	4.18	3.44	3.36	4.25	3.79	2.78	4.20	1.91	3.75	3.68
K_2O	1.82	0.90	1.54	0.95	1.48	1.48	1.14	0.84	0.78	0.81	1.63	1.17	0.65	1.60	1.58	1.30	1.35
P_2O_5	1.00	0.54	1.02	0.35	1.99	1.01	0.33	0.55	0.41	0.50	0.85	0.58	0.35	1.26		0.77	0.59
Total	99.96	99.77	99.46	99.43	100.02	100.04	99.98	99.11	99.37	100.22	100.50	99.54	99.95	99.77	99.24	99.77	100.03
Nb															64		
Zr															294		
Y															37		
Rb															33		
Sr															755		
SOURCE	1	1	1	1	1	1	1	1	1	1	1	1	2	1	2	1	2
METHOD	A	A	A	A	A	A	A	A	A	A	A	A	C	A	C	A	C

Table 5.1 (cont'd)

LAVAS	H81L	15279	15020	H90L	15121	A30L	15274G	H53L	15009	17308	14975	15083	A63L	H31L	H39L	15318	15039
SiO_2	51.42	51.69	52.03	52.06	52.90	53.19	53.30	53.60	53.97	54.87	55.78	56.19	59.42	60.88	59.61	61.35	61.51
TiO_2	2.61	2.44	2.52	2.03	2.24	2.52	2.55	1.55	2.04	2.00	1.57	1.68	1.34	1.35	1.61	0.40	0.87
Al_2O_3	15.66	15.24	15.55	16.50	17.15	16.11	14.98	19.23	18.25	16.17	16.80	17.31	17.04	16.14	15.84	15.28	15.89
Fe_2O_3		6.51	6.60		3.46		9.71		1.34	3.47	2.58	2.21				2.32	2.49
FeO	11.04	5.97	4.46	9.39	6.37	9.66	3.83	8.10	7.86	5.84	4.88	5.70	6.79	5.88	7.39	2.90	3.95
MnO	0.21	0.21	0.24	0.15	0.24	0.29	0.26	0.31	0.23	0.25	0.21	0.23	0.27	0.22	0.25	0.26	0.27
MgO	5.30	5.01	3.01	5.63	3.14	3.55	3.96	2.54	2.22	2.85	2.49	2.29	2.22	1.68	2.22	0.37	1.36
CaO	8.60	7.77	7.34	8.50	6.75	6.44	6.02	4.64	5.68	5.49	5.08	5.72	4.38	3.51	4.42	0.72	3.18
Na_2O	3.67	3.37	5.23	3.66	5.10	4.89	2.32	6.62	4.89	5.48	5.49	5.65	5.38	5.88	4.44	4.61	6.00
K_2O	1.36	1.22	1.69	1.36	2.22	1.91	1.43	2.79	2.20	2.14	2.66	2.45	2.45	3.88	2.80	5.00	2.80
P_2O_5	0.43	0.43	0.84	0.66	0.24	1.15	0.37	0.74	0.64	0.62	1.09	0.17	0.66	0.58	0.95	0.04	0.36
Total	100.3	99.86	99.51	99.98	99.81	99.71	98.73	100.12	99.79	99.76	99.35	99.93	99.95	99.56	100.06	100.25	100.63
Nb	42					74							96	81			
Zr	219					367							489	469			
Y	36					51							56	55			
Rb	31					39							55	51			
Sr	389					653							413	234			
SOURCE	2	1	1	2	1	2	1	2	1	1	1	1	2	2	2	1	1
METHOD	C	A	A	C	A	C	A	C	A	A	A	A	C	C	C	A	A

Table 5.1 (cont'd)

LAVAS	15220	15006	17453	A29L	15175	15050	17345	15303	15068	15217	15296B	15103	15035	14926	15296A	15298	15095
SiO_2	62.26	62.67	63.46	64.78	65.01	65.14	65.17	65.25	65.28	65.74	65.48	66.09	66.48	66.62	67.28	67.30	68.34
TiO_2	0.79	0.68	0.76	0.61	0.41	0.40	0.42	0.39	0.36	0.34	0.37	0.35	0.38	0.24	0.42	0.39	0.23
Al_2O_3	15.95	17.15	16.67	16.84	16.41	15.82	16.14	15.84	15.95	16.21	14.37	16.33	15.29	15.37	18.44	14.95	13.97
Fe_2O_3	3.64	4.20	2.51		1.84	4.69	3.15	5.86	4.02	3.04	6.60	2.10	4.53	2.66	7.18	3.48	1.56
FeO	2.52	0.61	3.13	4.48	2.26	0.06	1.52	0.42	0.87	2.01		1.67	0.06	1.02		2.71	2.12
MnO	0.20	0.14	0.18	0.22	0.20	0.16	0.23	0.23	0.20	0.12	0.03	0.14	0.15	0.15	0.12	0.27	0.07
MgO	0.52	0.55	0.14	6.53	0.35	0.26	0.39	0.16	0.49	0.69	0.31	0.58	0.33	0.60	0.37	0.15	0.11
CaO	2.88	2.20	2.08	1.54	0.77	1.87	1.59	0.24	0.77	0.32	0.42	0.98	0.82	0.98	0.49	0.53	0.56
Na_2O	5.84	6.74	6.55	6.53	6.70	6.50	6.65	5.83	7.15	5.28	6.34	6.65	6.67	6.21	0.99	5.02	6.43
K_2O	2.94	4.24	4.02	3.63	4.75	3.60	3.66	4.76	4.60	4.72	4.72	4.55	4.85	5.18	3.34	4.99	4.96
P_2O_5	0.60	0.17	0.14	0.66	0.05	0.24	0.13	0.90	0.06	0.02	0.30	0.05	0.12	0.04	0.03	0.11	0.32
Total	99.74	99.63	99.95	99.95	99.65	98.74	99.05	99.88	100.39	100.15	98.94	99.67	100.52	100.17	98.66	99.90	99.74
Nb				115													
Ar				631													
Y				60													
Rb				73													
Sr				96													
SOURCE	1	1	1	2	1	1	1	1	1	1	1	1	1	1	1	1	1
METHOD	A	A	A	C	A	A	A	A	A	A	A	A	A	A	A	A	A

Table 5.1 (cont'd)

LAVAS	14944	Ob3	15146	A53L	Ob4	15373	Ob1	Ob5	15255	Ob2	A35
SiO_2	68.46	70.51	70.61	71.28	72.08	72.22	72.77	73.02	73.06	73.56	74.05
TiO_2	0.29	0.15	0.14	0.27	0.16	0.24	0.23	0.18	0.20	0.17	0.13
Al_2O_3	13.64	12.03	13.22	13.99	12.20	12.91	12.39	12.52	12.43	12.54	12.44
Fe_2O_3	4.27		0.45			1.32					
FeO	0.06	2.90	1.38	3.28	2.82	2.38	3.24	2.97	3.39	2.94	2.53
MnO	0.16	0.14	0.08	0.15	0.12	0.14	0.13	0.12	0.11	0.12	0.06
MgO	0.29	0.02	0.11	0.22	0.02	0.31	0.02	0.03	0.04	0.02	0.04
CaO	0.35	0.29	0.43	0.43	0.36	0.43	0.32	0.26	0.22	0.31	0.19
Na_2O	6.19	5.31	5.71	5.87	5.91	4.77	5.68	5.47	5.58	5.38	5.53
K_2O	4.67	5.21	4.77	4.63	5.71	4.75	4.68	5.37	4.70	5.12	4.60
P_2O_5	0.17	0.00		0.04	0.02	0.01	0.01	0.01	0.02	0.02	0.02
Total	99.75	96.70	99.97	100.16	99.60	99.83	99.58	100.08	99.90	100.35	99.70
Nb				189					228		205
Ar				106					1517		871
Y				63					124		114
Rb				127					159		152
Sr				13					1.3		0.9
SOURCE	1	2	1	2	2	1	2	2	2	2	2
METHOD	A	B	A	C	B	A	B	B	C	B	C

SOURCE

1. Bell et al., unpubl.
2. C. Harris
3. J.R. Cann Unpubl.

METHOD

A XRF

B PROBE (SEE APPENDIX)

C PROBE-GLASS BEAD (SEE APPENDIX)

ALL TRACE ELEMENTS BY XRF

Table 5.1 (cont'd)

BLOCKS	DS24	DS4	DS36	DS9	DSA3	17317Q	DS3	DS44	173175	H99(2)	DS30	H56(1)	H59(2)	H13(1)	79951	H39(4)	79949
SiO_2	36.77	40.00	41.07	42.63	43.55	47.69	47.87	48.30	49.27	49.54	51.61	52.41	53.57	54.84	60.12	62.35	62.67
TiO_2	10.33		0.10	5.92	6.66	0.24	0.14	0.13	0.15	0.72	0.92	3.33	3.20	1.09	1.02	0.59	0.83
Al_2O_3	12.34		0.92	12.42	14.20	19.48	24.07	25.24	20.00	22.12	26.77	12.39	12.83	19.81	18.71	18.73	18.11
Fe_2O_3															2.53		2.18
FeO	18.89		10.78	16.52	14.54	3.31	2.83	2.43	2.70	4.55	3.31	13.13	12.64	6.98	2.48	3.53	2.28
MnO	0.24		0.17	0.19	0.21	0.05	0.45	0.10	0.08	0.06	0.31	0.30	0.31	0.26	0.15	0.13	0.16
MgO	6.57		46.31	7.53	6.93	11.26	7.62	6.57	8.42	6.55	0.88	3.18	2.80	1.61	1.19	0.47	0.74
CaO	11.11		0.49	12.68	11.51	16.50	15.46	15.66	18.05	14.00	10.85	6.98	6.58	3.16	3.06	2.53	2.09
Na_2O	1.98		0.08	1.91	2.11	1.28	1.42	1.52	1.26	2.04	5.20	4.23	4.49	7.92	7.26	7.24	7.29
K_2O	0.04		0.00	0.15	0.16	0.04	0.04	0.06	0.03	0.19	0.29	2.18	2.48	3.94	3.01	3.08	2.82
P_2O_5	1.56		0.04	0.15	0.34	0.04	0.04	0.01	0.05	0.20	0.06	1.75	1.30	0.44	0.20	1.33	0.19
Total	99.77		99.98	100.10	100.21	99.89	99.94	100.05	100.01	100.02	99.93	99.77	100.23	100.05	100.33	100.01	99.88
Nb		0						0				68			—	39	
Zr		2						2				396			618	266	730
Y		3						3				72			33	22	68
Rb		0						0				59			68	24	56
Sr		45						171				352			457	306	276
SOURCE	2	2	2	2	2	2	2	2	2	2	2	2	2	2	3	2	3
METHOD	C	C	C	C	C	C	C	C	C	C	C	C	C	C	A?	C	A?

Table 5.1 (cont'd)

BLOCKS	71727	79934	H34(1)	H33(3)	15226(1)	15226(2)	69525	17318P	H30(1)	H30(2)	H30(3)	15231(5)	17318B
SiO_2	62.99	63.73	64.04	65.03	67.34	67.44	72.57	73.80	74.00	75.42	75.76	77.30	77.92
TiO_2	0.71	0.74	0.45	0.44	0.40	0.71	0.24	1.61	0.21	0.20	0.21	0.21	0.18
Al_2O_3	16.31	16.92	18.46	18.29	16.88	15.81	12.26	11.83	11.48	10.75	10.85	10.77	10.28
Fe_2O_3	1.95	1.78					1.48						
FeO	4.00	2.45	3.18	3.43	3.13	3.42	2.58	3.84	4.33	4.28	3.99	4.28	3.78
MnO	0.15	0.16	0.11	0.10	0.14	0.13	0.17	0.17	0.16	0.14	0.17	0.17	0.12
MgO	0.40	0.79	0.46	0.38	0.22	0.62	0.02	0.02	0.04	0.13	0.01	0.04	0.04
CaO	1.45	2.00	2.14	1.95	1.26	1.29	0.23	0.18	0.27	0.18	0.22	0.11	0.17
Na_2O	7.07	6.67	7.50	6.32	6.24	6.40	5.56	4.57	5.01	4.43	3.79	3.68	4.01
K_2O	4.08	3.78	3.31	3.55	4.28	3.99	4.57	4.28	4.65	4.07	4.56	3.16	3.55
P_2O_5	0.28	0.28	0.33	0.49	0.04	0.02	0.02	0.02	0.01	0.04	0.01	0.05	0.01
Total	99.84	99.85	100.01	100.03	99.93	99.83	100.12	100.32	100.16	99.98	99.57	99.77	100.06
Nb		-	42	46	79	115	-	177	223	242	393	318	202
Zr	772	682	292	356	664	582	1134	1045	1538	2145	2888	2294	1514
Y	79	69	24	26	31	30	110	81	86	68	174	160	83
Rb	34	81	34	37	75	131	96	107	139	122	83	139	114
Sr	36	259	273	224	51	190	2	0	2	2	1	0.8	0
SOURCE	3	3	2	2	2	2	3	2	2	2	2	2	2
METHOD	A?	A?	C	C	C	C	A?	C	C	C	C	C	C

Table 5.2 Norms of Acid Blocks and Lavas

	BLOCKS						LAVAS								
	H30(1)	H30(2)	H30(3)	15213(5)	17318P	17318B	Ob1	Ob2	Ob3	Ob4	Ob5	15373	15146	A35	15255
Quartz	28.42	32.98	33.65	40.04	28.37	38.13	24.77	25.37	23.83	24.04	24.65	22.59	20.27	26.80	24.99
Corundum	-	-	-	1.22	-	-	-	-	-	-	-	-	-	-	-
Orthoclase	-	24.05	26.95	18.67	25.29	20.48	27.65	30.25	30.79	33.74	31.73	28.07	28.19	27.18	27.77
Albite	33.16	32.63	30.42	31.14	37.02	33.11	37.67	35.99	32.87	30.46	34.50	39.96	41.44	38.38	37.77
Anorthite	-	-	-	0.22	-	-	-	-	-	-	-	-	-	-	-
Acmite	-	-	-	-	-	-	-	-	-	-	-	-	2.75	-	-
Na-meta-silicate	2.15	1.13	0.38	-	0.38	0.19	2.42	2.24	2.81	4.43	2.74	0.09	0.87	1.96	2.20
K-meta-silicate	-	-	-	-	-	-	-	-	-	-	-	-	-	-	-
Diopside	0.02	-	-	-	0.01	0.01	0.01	0.01	0.01	0.02	0.02	0.21	0.21	0.02	0.02
Hedenbergite	1.12	-		-	0.67	0.68	1.34	1.24	1.27	1.46	1.07	1.60	1.66	0.70	0.84
Enstatite	0.09	0.31	0.02	0.10	0.05	0.09	0.04	0.04	0.04	0.04	0.07	0.67	0.18	0.09	0.09
Ferrosilite	7.31	7.51	6.81	7.83	6.71	6.50	4.36	4.68	4.66	4.36	4.81	5.81	1.57	4.17	5.65
Ilmenite	0.40	0.38	0.40	0.40	0.34	0.34	0.30	0.32	0.28	0.30	0.34	0.46	0.27	0.25	0.38
Apatite	0.02	0.09	0.02	0.12	0.05	0.02	0.05	0.05		0.05	0.02	0.02	-	0.05	0.05
Water	-	-	-										2.86	-	-
Total	100.16	99.64	99.57	99.77	98.89	100.06	99.48	100.18	96.56	99.48	99.95	99.48	99.96	99.59	99.75

Table 5.3 Analyses of Mesostasis in 15243B

	A	A	A	B	B	B	C	C	C	H99(2)
SiO_2	54.22	54.69	56.96	50.84	50.54	50.50	55.52	55.70	54.38	49.59
TiO_2	1.74	1.26	1.87	3.30	1.50	1.52	1.75	1.86	1.80	0.72
Al_2O_3	17.83	18.88	19.84	16.94	17.49	17.62	16.61	16.69	16.21	22.12
FeO^T	7.29	6.59	4.78	7.36	8.12	7.77	9.57	9.46	10.55	4.55
MnO	0.16	0.16	0.11	0.15	0.16	0.15	0.24	0.20	0.23	0.06
MgO	1.94	1.40	2.05	2.77	2.49	2.56	2.36	2.28	2.51	6.55
CaO	7.21	7.16	6.07	10.57	9.52	9.45	6.06	5.61	6.02	14.00
Na_2O	3.86	2.74	2.54	2.21	3.43	4.26	2.16	2.75	2.82	2.04
K_2O	2.82	2.80	1.97	1.94	1.96	2.19	3.51	3.66	3.43	0.19
P_2O_5	1.11	1.17	0.94	1.42	1.13	1.13	N.D.	N.D.	N.D.	0.20
	98.20	96.87	97.12	97.52	96.40	97.21	98.76	98.21	97.45	100.02

A = inclusion in cpx

B = inclusion in olivine

C = intergranular mesostasis

N.D. = not detected

Mesostasis by routine microprobe analysis (beam diam. 10 μm)

H99(2) - Middleton's Gabbro by probe analysis of rock-flux glass

Table5.4 Analyses of Pegmatoid and enclosing lava

	Lava	Pegmatoid	
	H81L	H59(X)	H59(Y)
SiO_2	91.42	S2.41	53.57
TiO_2	2.61	3.33	3.20
Al_2O_3	15.66	12.39	12.83
*FeO^T	11.04	13.13	12.64
MnO	0.21	0.30	0.31
MgO	5.30	3.18	2.80
CaO	8.60	6.98	6.58
Na_2O	3.67	4.23	4.49
R_2O	1.36	2.18	2.48
P_2O_5	0.43	1.75	1.30
TOTAL	100.30	99.88	100.20

* FeO^T = Total iron expressed as FeO

Analyses by the method of Dickin and Exley (1981)

Table 5.5 Fractionation Test C. Valley lava → pegmatoid

Test 1 - An, Ab end members

	Weight	H59(2)	Calc.	Diff.	% Diff.
SiO_2	1	53.57	54.007	-.487	-.815
TiO_2	1	3.2	3.373	-.173	-5.409
Al_2O_3	1	12.83	12.824	6E-03	.046
Fe_2O_3	1	12.64	12.853	-.213	-1.687
MnO	1	.31	.251	.059	19.023
MgO	1	2.8	2.971	-.171	-6.11
CaO	1	6.58	7.125	-.545	-8.295
Na_2O	1	4.49	4.677	-.187	-4.174
K_2O	1	2.48	1.76	.72	29.042
P_2O_5	1	1.3	.556	.744	57.201

Sum of squares: 1.7029

	Solution
H91L	129.394
Fa	-2.04934
Fo	-6.68385
An	-20.4339
Ab	-.22657

Test 2 - H81L Phenocrysts

SiO_2	1	53.57	52.658	.912	1.702
TiO_2	1	3.2	3.687	-.437	-13.666
Al_2O_3	1	12.83	13.23	-.4	-3.117
Fe_2O_3	1	12.64	13.777	-1.137	-8.993
MnO	1	.31	.226	.084	27.228
MgO	1	2.8	2.799	1E-03	.03
CaO	1	6.58	7.411	-.831	-12.635
Na_2O	1	4.49	4.237	.253	5.639
K_2O	1	2.48	1.862	.618	24.935
P_2O_5	1	1.3	.605	.695	53.479

	Solution
H81L	140.645
Opx	-2.78145
Plag	-28.4166
Ol	-9.44669

Sum of squares: 4.10312

Table 5.6(i) Fractionation Test 15209 → H48L

	Weight	15209	Ol	Ilm	Mgt	Cpx	An70	H48L
		0	1	1	1	1	1	0
SiO_2	1	47.16	35	0	0	52.43	52.79	51.38
TiO_2	1	3.08	0	52.73	19.42	.37	0	2.65
Al_2O_3	1	15.96	0	0	0	4.16	29.89	16
Fe_2O_3	1	12.15	15	45.83	80	6.19	0	10.66
MnO	1	.19	0	0	0	.12	0	.2
MgO	1	4.99	50	0	0	18.19	0	5.14
CaO	1	8.18	0	0	0	16.56	13.78	8.36
Na_2O	1	3.92	0	0	0	0	3.43	3.68
K_2O	1	1.82	0	0	0	0	.15	1.35
P_2O_5	1	0	0	0	0	0	0	.59

Solution

	Weight	H48L	Calc.	Diff.	% Diff.
SiO_2	1	51.38	49.833	1.547	3.011
TiO_2	1	2.65	1.922	.728	27.476
Al_2O_3	1	16	15.454	.546	3.415
Fe_2O_3	1	10.66	9.894	.766	7.182
MnO	1	.2	.225	-.025	-12.354
MgO	1	5.14	4.764	.376	7.325
CaO	1	8.36	8.659	-.299	-3.573
Na_2O	1	3.68	4.172	-.492	-13.368
K_2O	1	1.35	2.091	-.741	-54.869
P_2O_5	1	.59	0	.59	100

Sum of squares: 5.17842

	Solution
15209	115.754
Ol	-3.47272
Ilm	-1.71261
Mgt	-3.88781
Cpx	3.9788
An70	-10.6597

Table 5.6(ii) Fractionation Test H48L → A63L

Input Data (Oxide Weight %)

	Weight	H48L	Ol	Mgt	Ilm	Cpx	An60	A63L
		0	1	1	1	1	1	0
SiO_2	1	51.38	35	0	0	52.43	54.47	59.42
TiO_2	1	2.65	0	19.42	52.73	.37	0	1.34
Al_2O_3	1	16	0	0	0	4.16	28.69	17.04
Fe_2O_3	1	10.66	15	80	45.83	6.19	.51	6.79
MnO	1	.2	0	0	0	.12	0	.27
MgO	1	5.14	50	0	0	18.19	0	2.22
CaO	1	8.36	0	0	0	16.56	12.3	4.38
Na_2O	1	3.68	0	0	0	0	4.6	5.38
K_2O	1	1.35	0	0	0	0	.21	2.45
P_2O_5	1	.59	0	0	0	0	0	.66

Solution

	Weight	A63L	Calc.	Diff.	% Diff.
SiO_2	1	59.42	59.089	.331	.556
TiO_2	1	1.34	1.194	.146	10.89
Al_2O_3	1	17.04	16.946	.094	.55
Fe_2O_3	1	6.79	6.64	.15	2.209
MnO	1	.27	.394	-.124	-45.92
MgO	1	2.22	2.151	.069	3.089
CaO	1	4.38	4.453	-.073	-1.677
Na_2O	1	5.38	5.468	-.088	-1.637
K_2O	1	2.45	2.873	-.423	-17.259
P_2O_5	1	.66	1.309	-.649	-98.393

Sum of squares: .795598

	Solution
H48L	221.931
Ol	-3.39049
Mgt	-15.3626
Ilm	-2.9393
Cpx	-41.5645
An60	-58.6741

Table 5.6(iii) Fractionation Test A29L → A35

Input Data (Oxide Weight %)

	Weight	A29L -1	San -1	Anor -1	Andes -1	Augite -1	Hed -1	Ol -1	A35 0
SiO_2	1	64.78	67.4	66.53	57.86	51.79	47.91	31.12	74.05
TiO_2	1	.61	.02	.06	.08	.41	.23	.03	.13
Al_2O_3	1	16.84	18.84	21.58	25.34	.86	.37	.1	12.44
Fe_2O_3	1	4.98	.38	.2	.46	15.22	29.23	57.37	2.53
MnO	1	.22	0	0	.03	1.12	1.42	3.36	.06
MgO	1	.46	0	0	.06	10.46	.36	.17	.04
CaO	1	1.59	.24	2.63	8.08	19.2	19.07	.15	.19
Na_2O	1	6.53	7.85	8.02	6.28	.5	.8	.56	5.53
K_2O	1	3.63	4.88	2.86	.52	0	0	0	4.6

Solution

	Weight	A35	Calc.	Diff.	% Diff.
SiO_2	1	74.05	73.296	.754	1.018
TiO_2	1	.13	1.94	-1.81	-1392.16
Al_2O_3	1	12.44	12.549	-.109	-.873
Fe_2O_3	1	2.53	2.323	.207	8.185
MnO	1	.06	-.074	.134	224.051
MgO	1	.04	1.351	-1.311	-3278.33
CaO	1	.19	-.426	.616	324.196
Na_2O	1	5.53	6.213	-.683	-12.354
K_2O	1	4.6	4.673	-.073	-1.577

Sum of squares: 6.4876

	Solution
A29L	332.91
San	-145.098
Anor	0
Andes	-63.7145
Augite	-.980154
Hed	0
Ol	-23.1172

Table 5.6(iv) Fractionation Test A53L → A35

Input Data (Oxide Weight %)

	Weight	A53L	San	And	Aug	Ol	A35
		0	1	1	1	1	0
SiO_2	1	71.28	67.4	57.86	51.79	31.12	74.05
TiO_2	1	.27	.02	.08	.41	.03	.13
Al_2O_3	1	13.99	18.84	25.34	.88	.1	12.44
Fe_2O_3	1	3.28	.38	.46	15.22	57.37	2.53
MnO	1	.15	0	.03	1.12	3.36	.06
MgO	1	.22	0	.06	10.46	.17	.04
CaO	1	.43	.24	8.08	19.2	.15	.19
Na_2O	1	5.87	7.85	6.28	.5	.56	5.53
K_2O	1	4.63	4.88	.52	0	0	4.6

Solution

	Weight	A35	Calc.	Diff.	% Diff.
SiO_2	1	74.05	74.163	-.113	-.152
TiO_2	1	.13	.362	-.232	-178.446
Al_2O_3	1	12.44	12.616	0.176	-1.416
Fe_2O_3	1	2.53	2.623	-.093	-3.68
MnO	1	.06	.101	-.041	-68.887
MgO	1	.04	.244	-.204	-509.559
CaO	1	.19	.21	-.02	-10.774
Na_2O	1	5.53	5.405	.125	2.264
K_2O	1	4.6	4.814	-.214	-4.647

Sum of squares: .211286

	Solution
A53L	138.319
San	-32.3223
And	-2.51598
Aug	-:515557
Ol	-2.96476

Table 5.6(v) Fractionation Test A29L → A53L

Input Data (Oxide Weight %)

	Weight	A29L	San	And	Aug	Ol	A53L
		0	-1	-1	-1	-1	0
SiO_2	1	64.78	67.4	57.86	52.798	31.12	71.28
TiO_2	1	.61	.02	.08	.41	.03	.27
Al_2O_3	1	16.84	18.84	25.34	.88	.1	13.99
Fe_2O_3	1	4.98	.38	.46	15.22	57.37	3.28
MnO	1	.22	0	.03	1.12	3.36	.15
MgO	1	.46	0	.06	10.46	.17	.22
CaO	1	1.59	.24	8.08	19.2	.15	.43
Na_2O	1	6.53	7.85	6.28	.5	.56	5.87
K_2O	1	3.63	4.88	.52	0	0	4.63

Solution

	Weight	A53L	Calc.	Diff.	% Diff.
SiO_2	1	71.28	70.699	.581	.815
TiO_2	1	.27	1.445	-1.175	-435.145
Al_2O_3	1	13.99	13.945	.045	.321
Fe_2O_3	1	3.28	3.075	.205	6.248
MnO	1	.15	.02	.13	86.908
MgO	1	.22	1.011	-.791	-359.355
CaO	1	.43	-.027	.457	106.164
Na_2O	1	5.87	6.43	-.56	-9.544
K_2O	1	4.63	4.494	.136	2.937

Sum of squares: 2.94427

	Solution
A29L	246.731
San	-86.7119
And	-44.3838
Aug	-.691639
Ol	-14.9437

Table 5.6(vi) Fractionation Test 15006 → 15146

Input Data (Oxide Weight %)

	Weight	15006	And	Aug	Ol	Volatiles	15416
		0	-1	-1	-1	-1	0
SiO_2	1	62.67	57.86	51.78	31.12	0	70.61
TiO_2	1	.68	.08	.41	.03	0	.14
Al_2O_3	1	17.15	25.34	.88	.1	0	13.22
Fe_2O_3	1	4.8	.46	15.22	57.37	0	2.33
MnO	1	.14	.03	1.12	3.36	0	.08
MgO	1	.55	.06	10.46	.17	0	.11
CaO	1	2.2	8.08	19.2	.15	0	.43
Na_2O	1	6.74	6.28	.5	.56	100	5.71
K_2O	1	4.24	.52	0	0	0	4.77

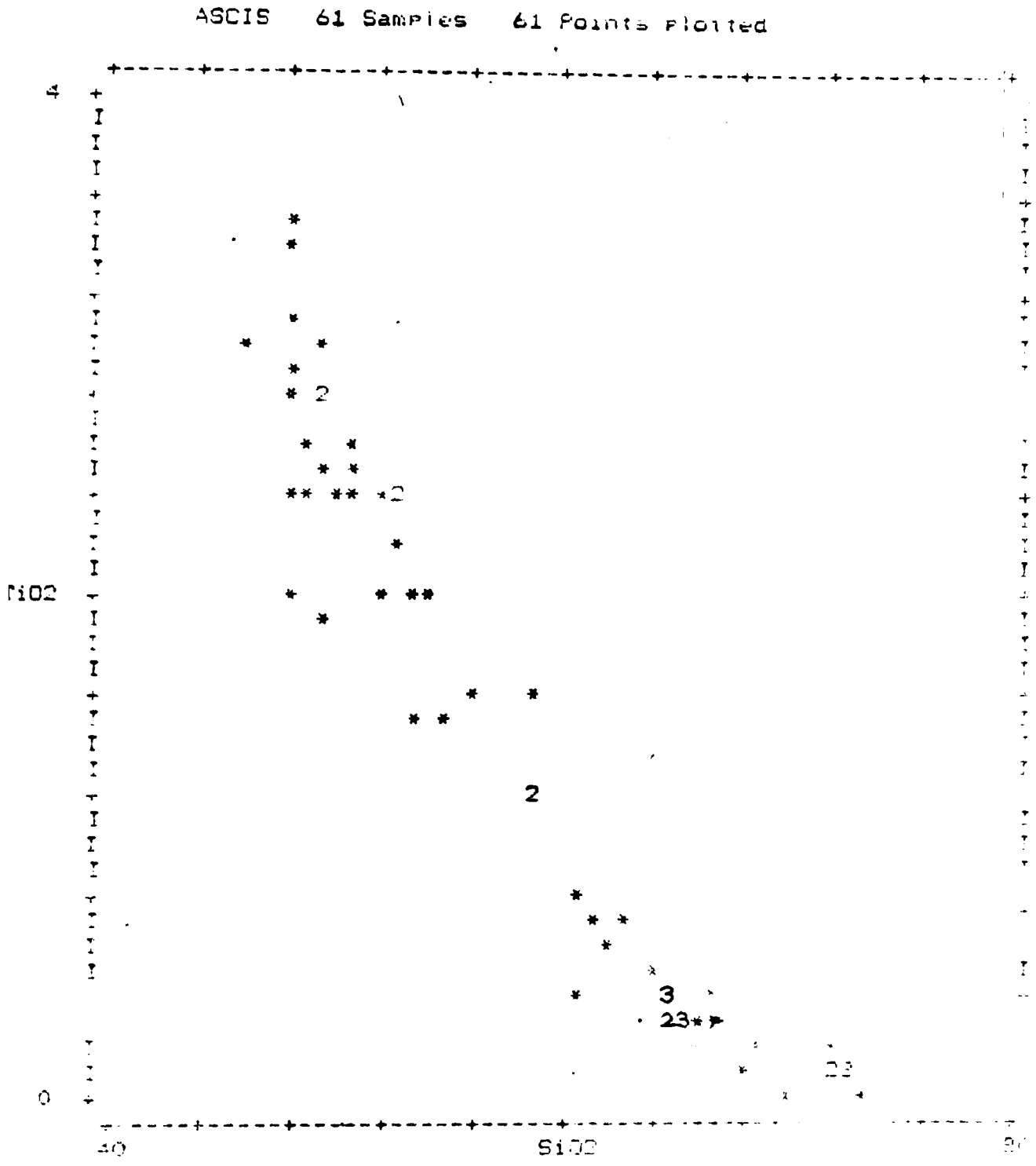
Solution

	Weight	15146	Calc.	Diff.	% Diff.
SiO_2	1	70.61	69.628	.982	1.39
TiO_2	1	.14	1.084	-.944	-674.295
Al_2O_3	1	13.22	14.629	-1.409	-10.655
Fe_2O_3	1	2.33	2.41	-.03	-3.442
MnO	1	.08	-.095	.175	218.943
MgO	1	.11	.866	-.756	-687.128
CaO	1	.43	-.781	1.211	281.583
Na_2O	1	5.71	5.482	.228	3.985
K_2O	1	4.77	6.765	-1.995	-41.821

Sum of squares: 9.94493

	Solution
15006	166.265
And	-54.7615
Aug	0
Ol	-9.27074
Volatiles	-2.23285

Fig 5.1 Wt % TiO_2 vs Wt % SiO_2 for Ascension lavas



2 = 2 analyses etc

X = > 9 analyses

Fig 5.2 Wt % Al_2O_3 vs Wt % SiO_2 in Ascension lavas
ASCIS 61 Samples 61 Points Plotted

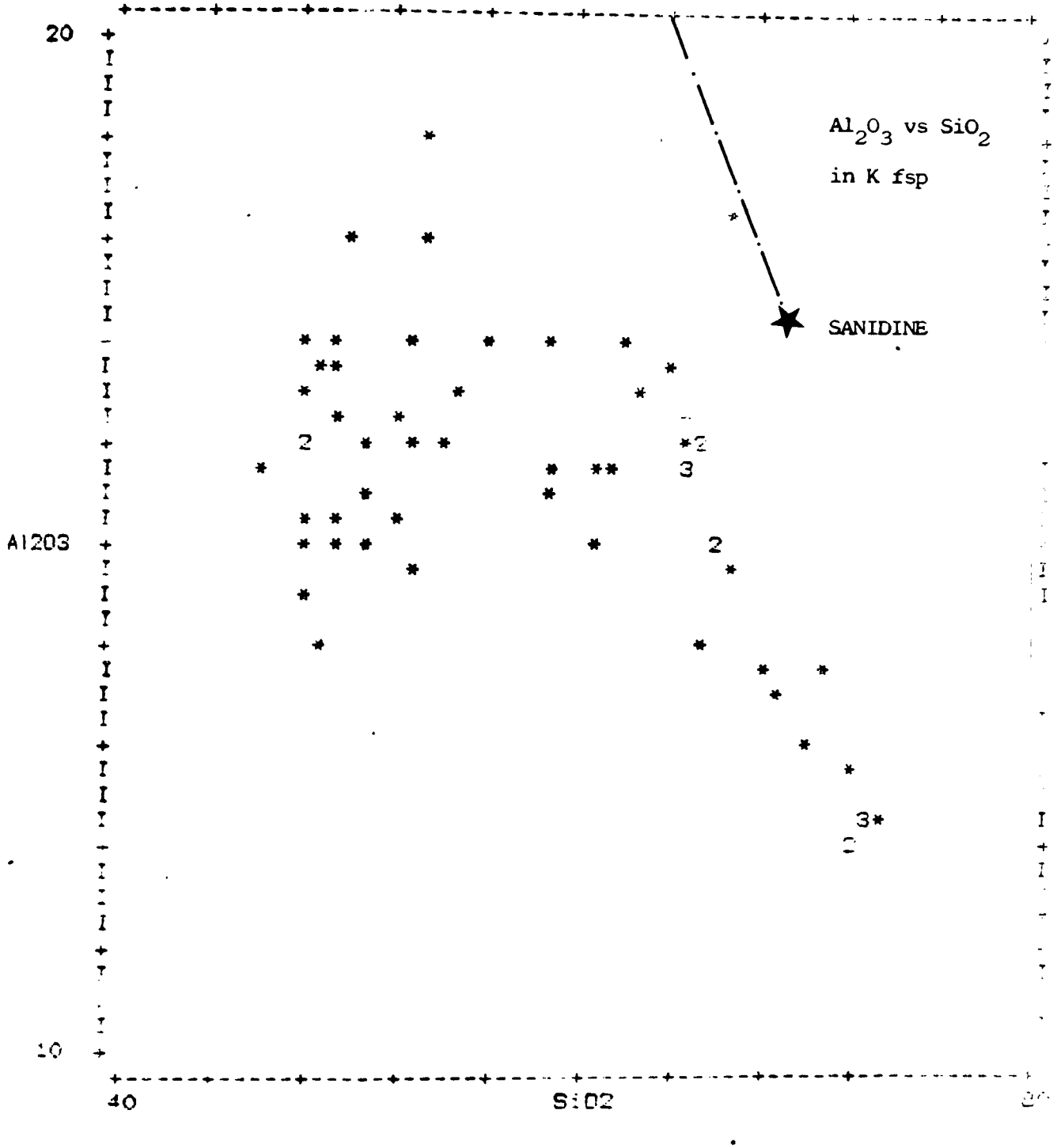


Fig 5.3 Wt% FeO^T vs SiO_2 in Ascension lavas

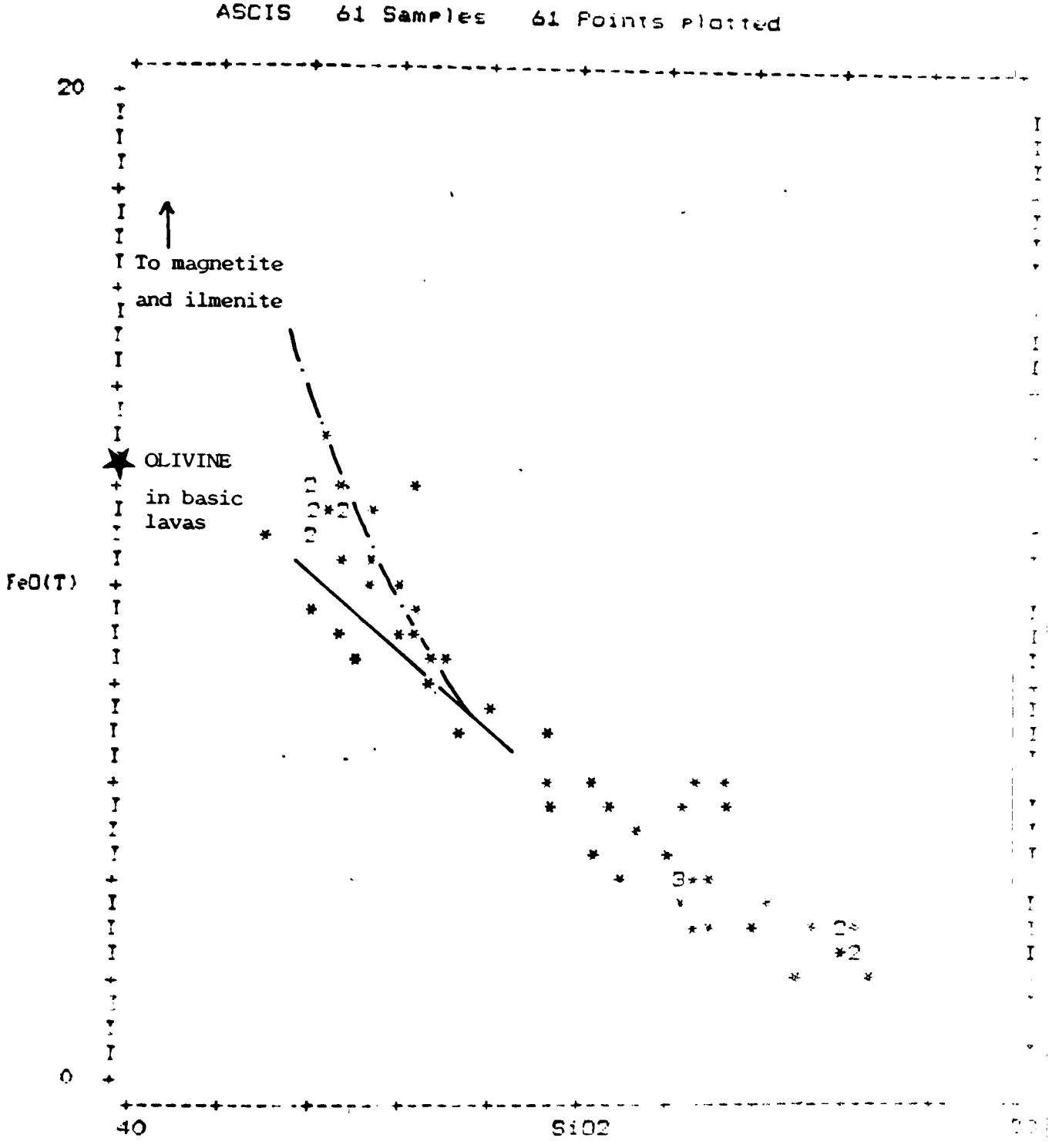


Fig 5.4 Wt% MgO vs SiO_2 in Ascension lavas

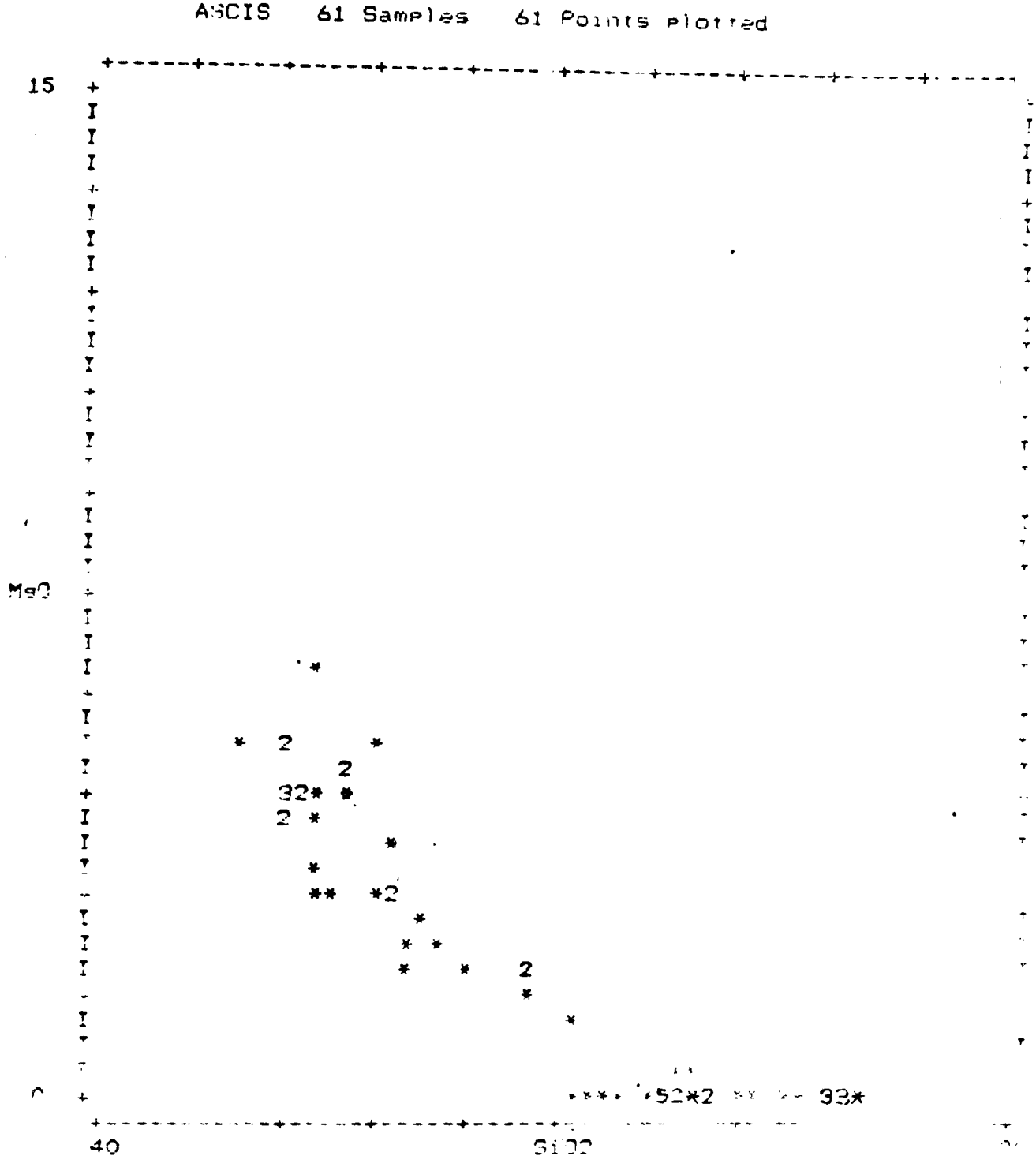


Fig 5.5 Wt% CaO vs SiO_2 in Ascension lavas

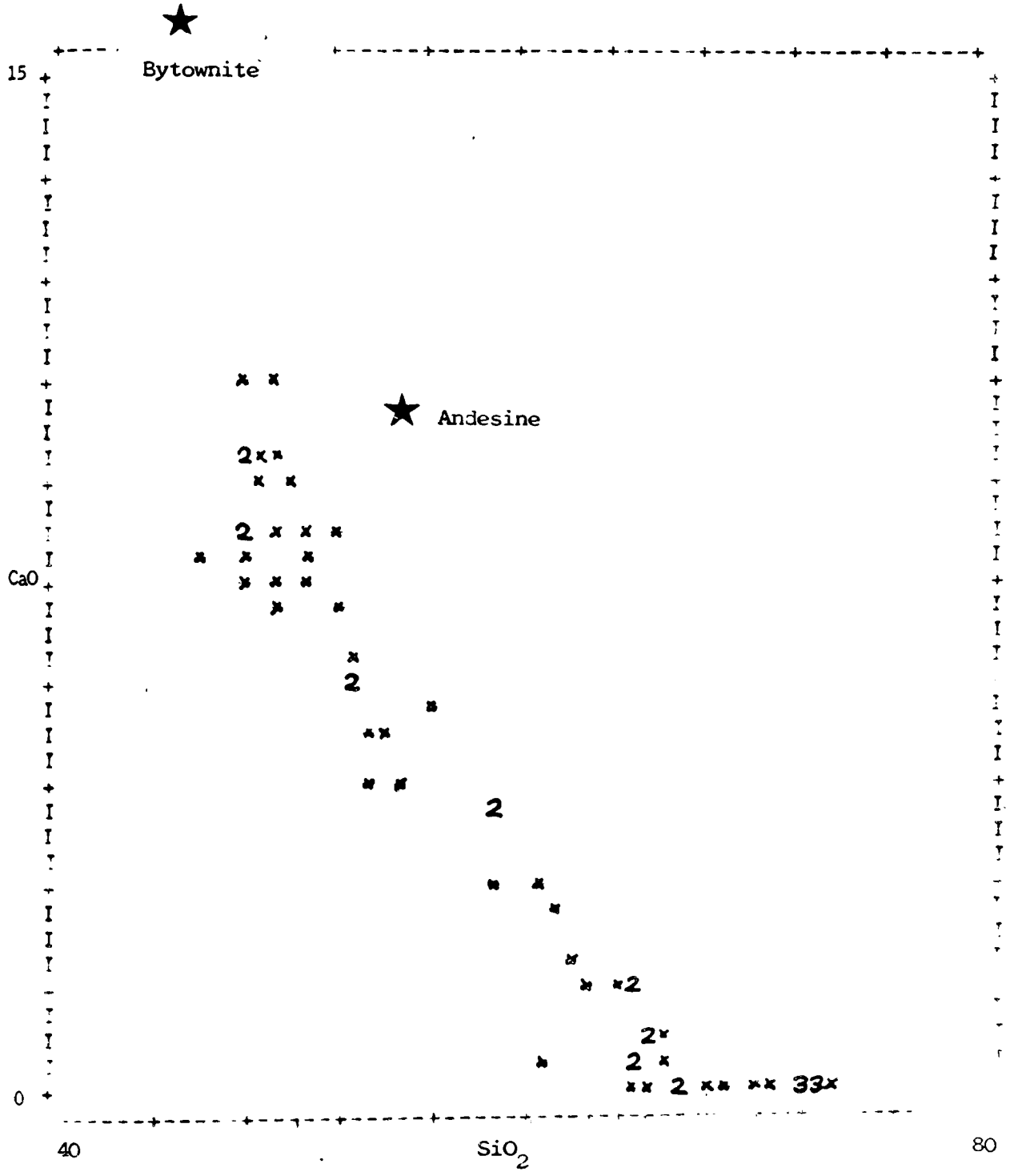


Fig 5.6 Wt% Na_2O vs SiO_2 in analysed lavas

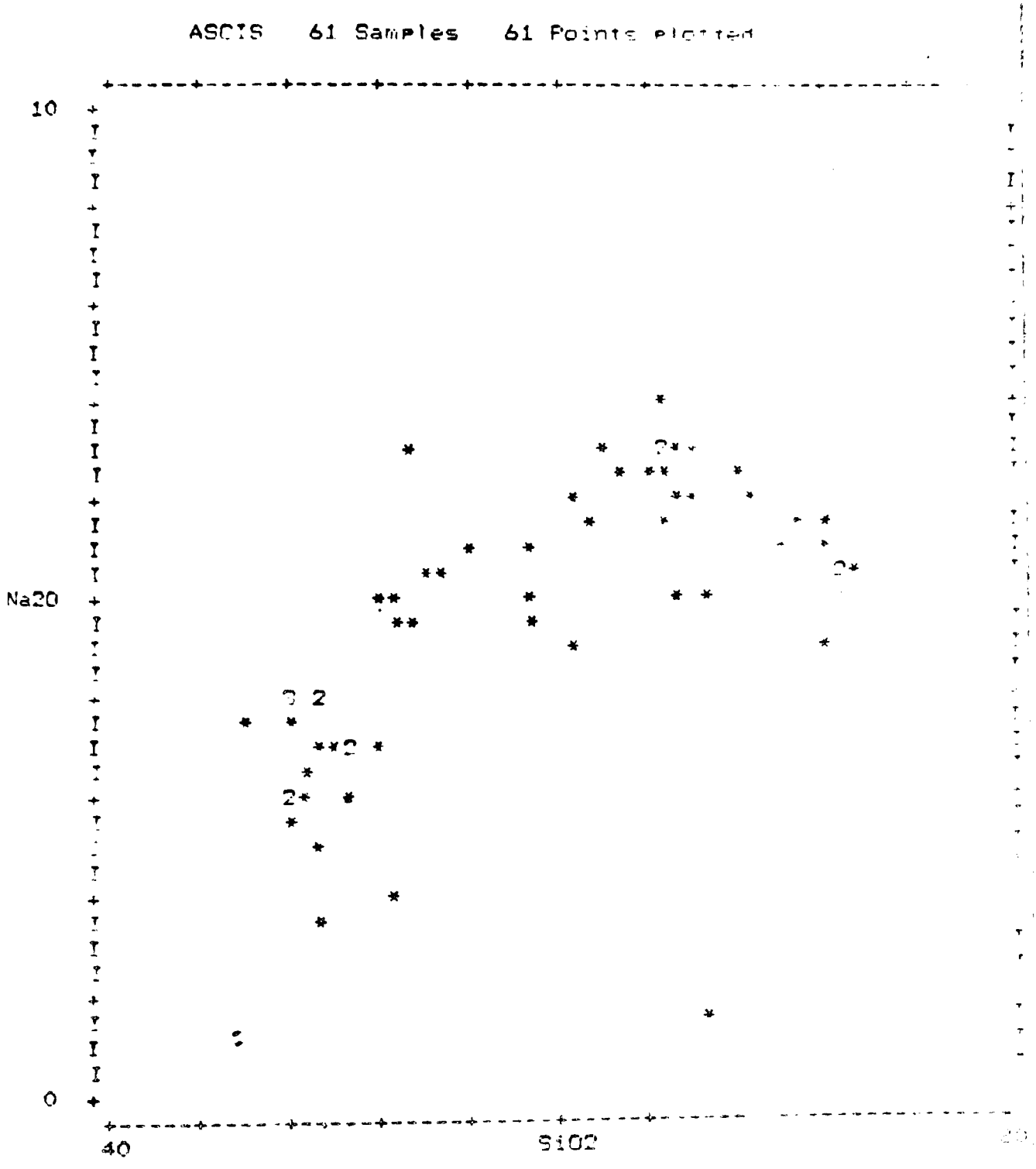


Fig 5.7 Wt% K_2O vs SiO_2 in Ascension lavas

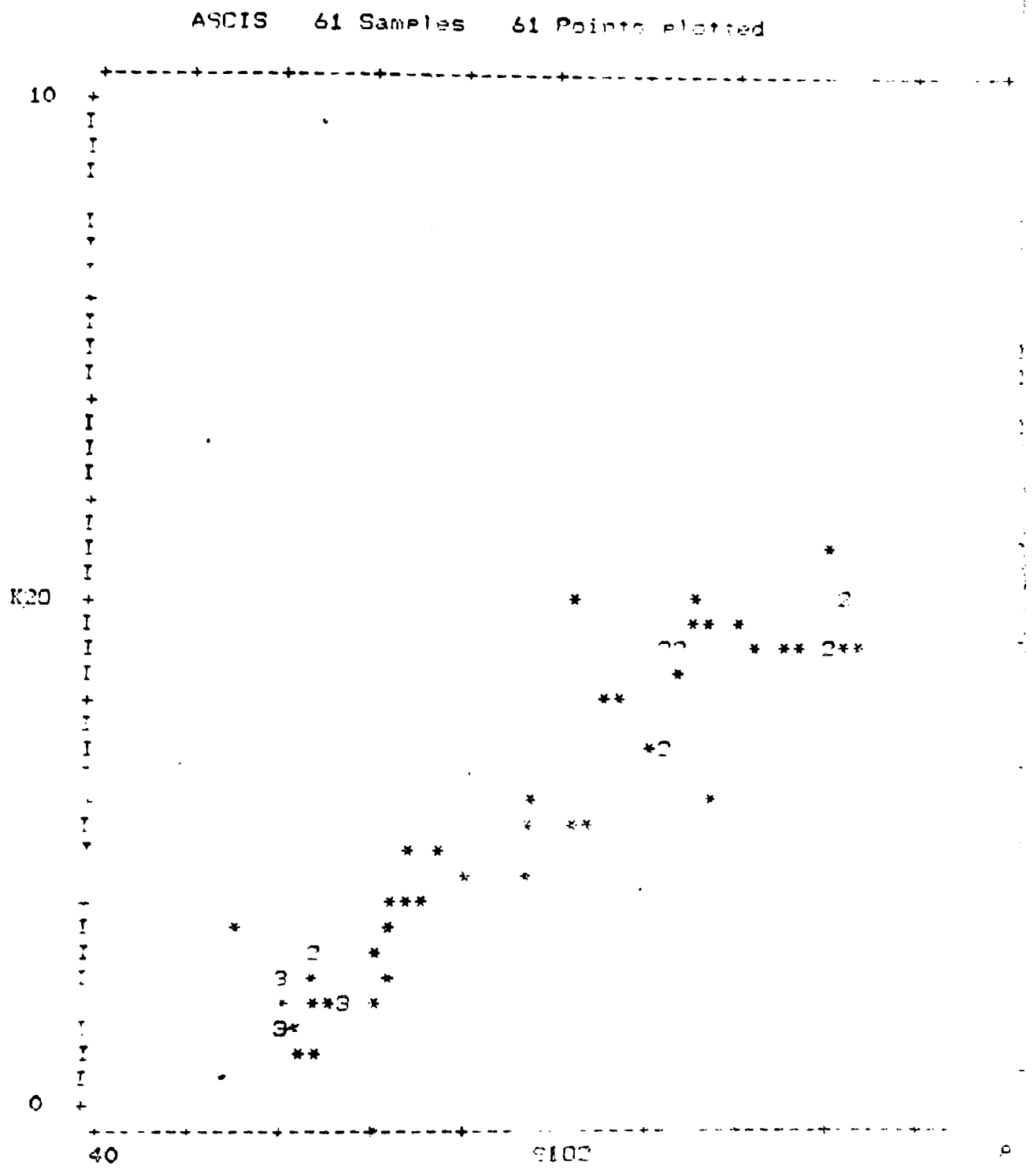


Fig 5.8 Wt% P_2O_5 vs SiO_2 in Ascension lavas

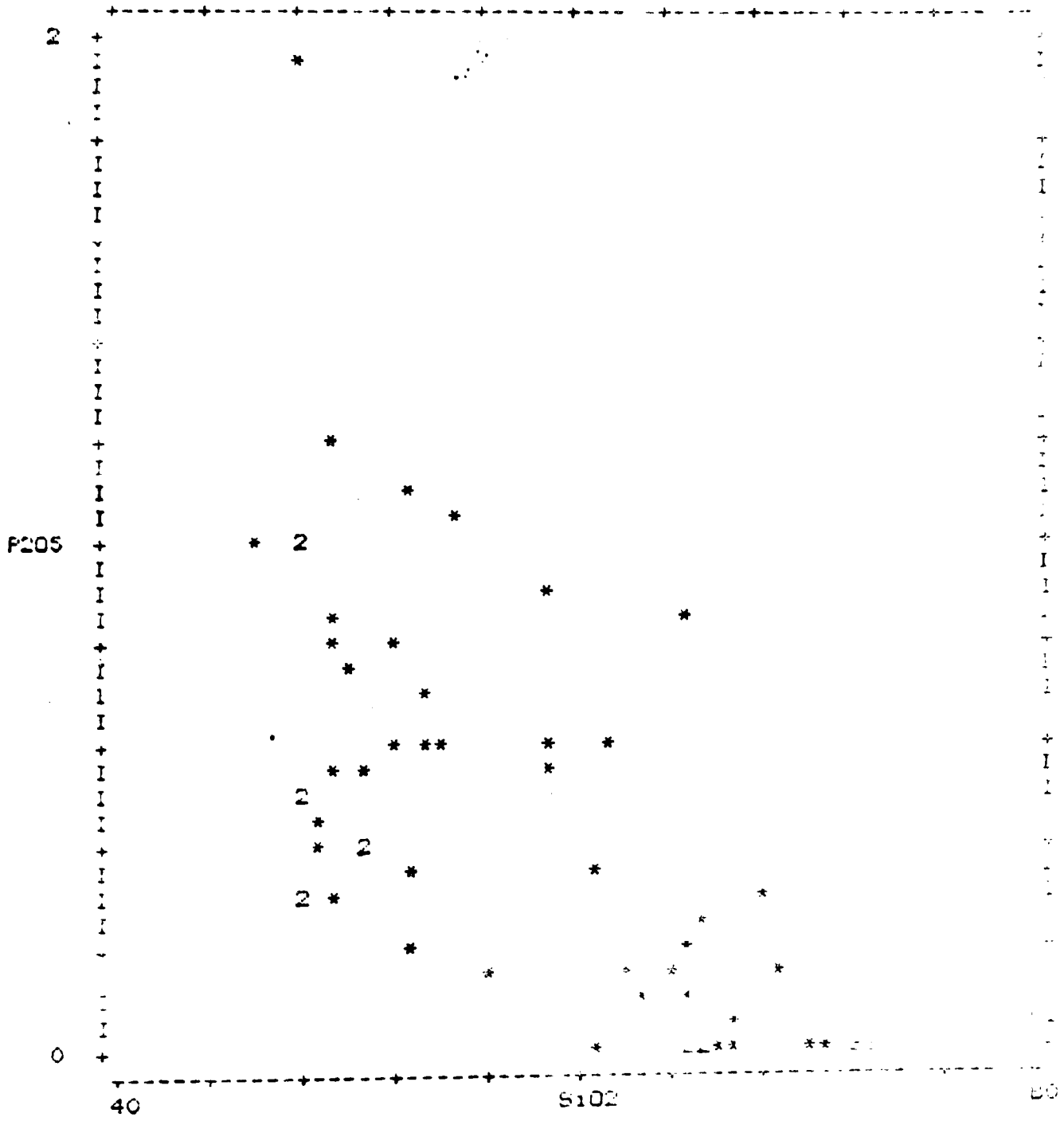


Fig 5.9 Wt% $Na_2O + K_2O$ vs SiO_2 for Ascension lavas . B = basalt, H = hawaiite, T.B. = trachybasalt, T.A. = trachyandesite, Tr = trachyte, C = comendite

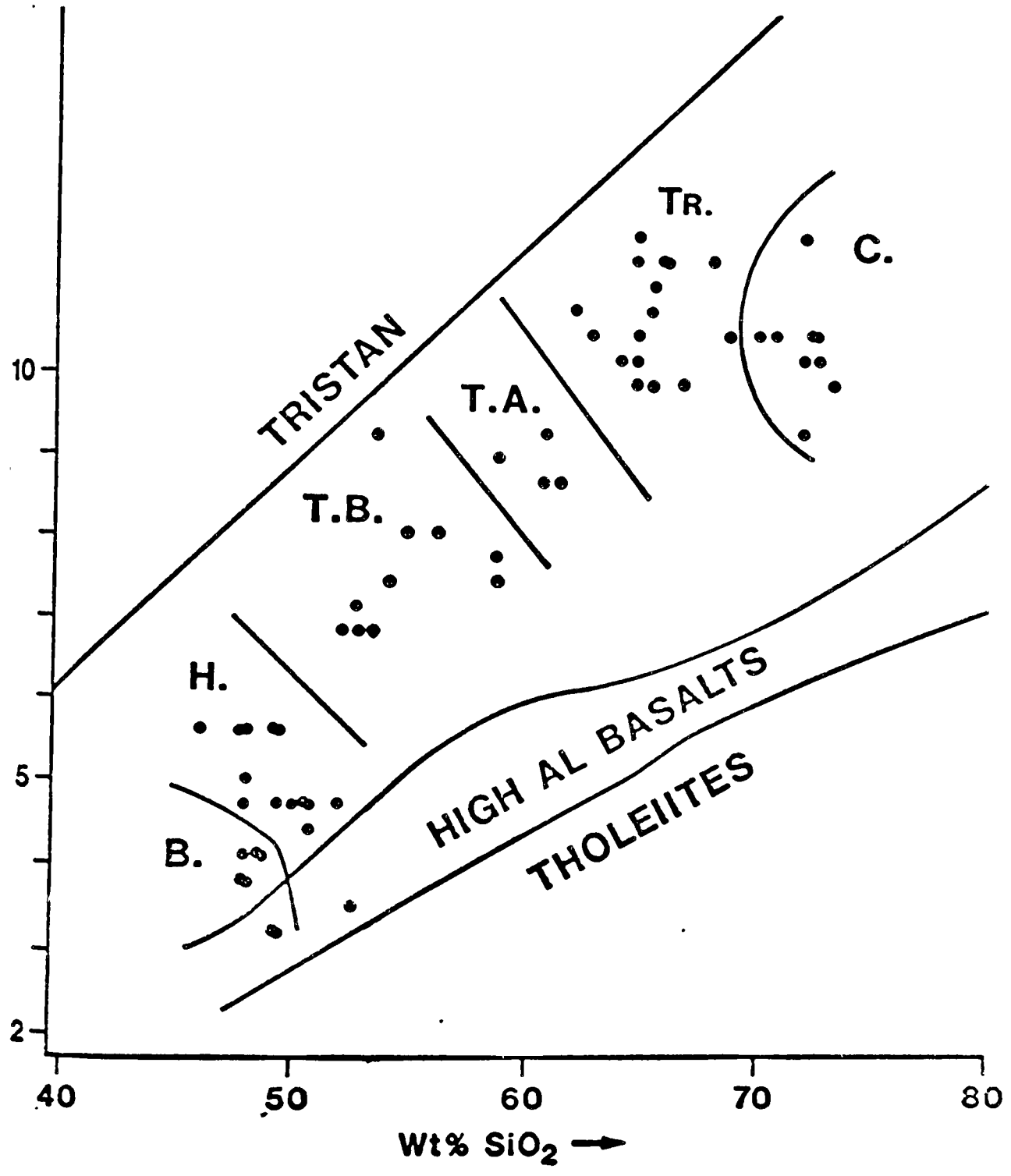


Fig 5.10 Wt% CaO vs MgO in Ascension lavas

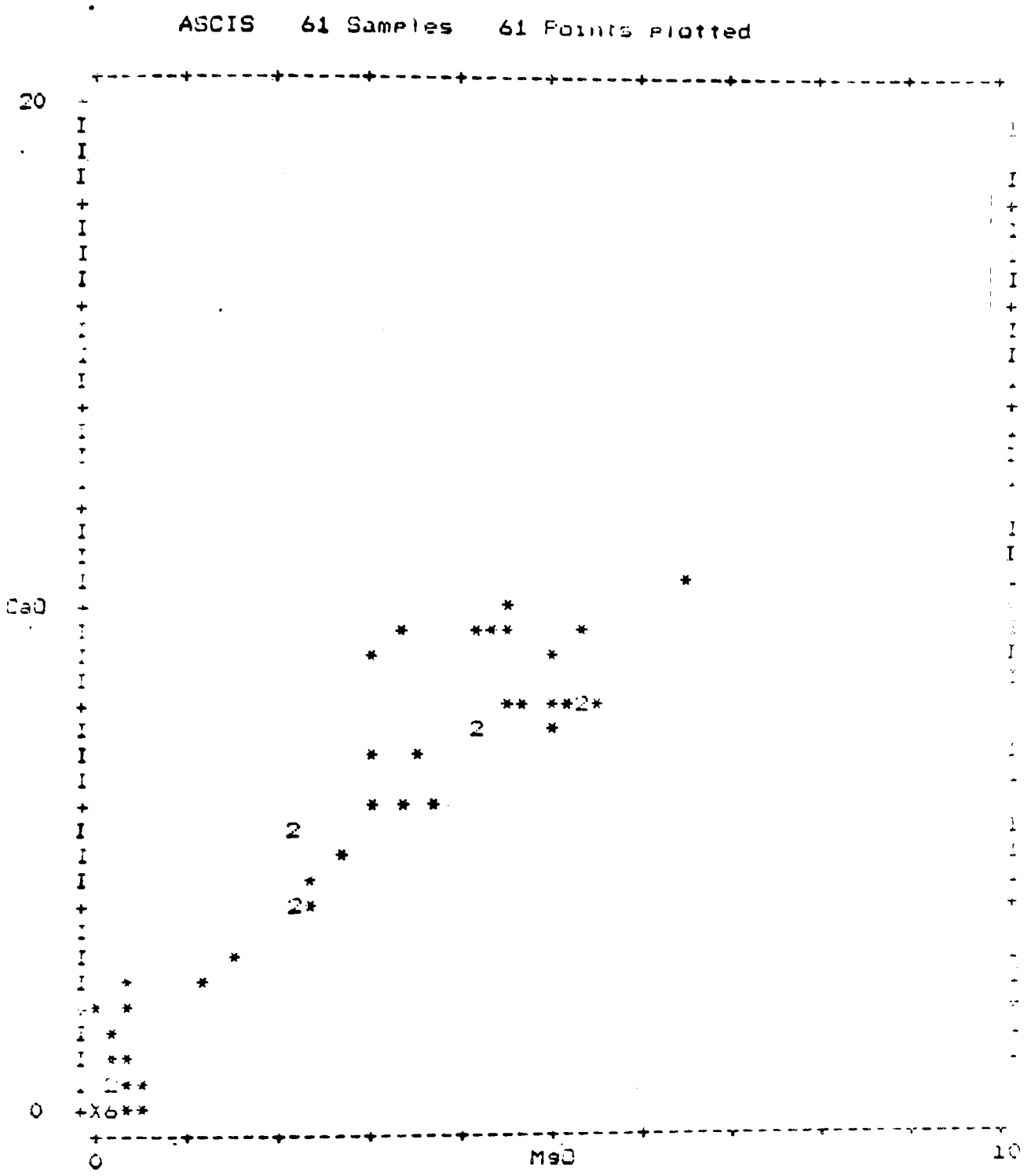


Fig 5.11 Wt% FeO^t vs MgO in Ascension lavas

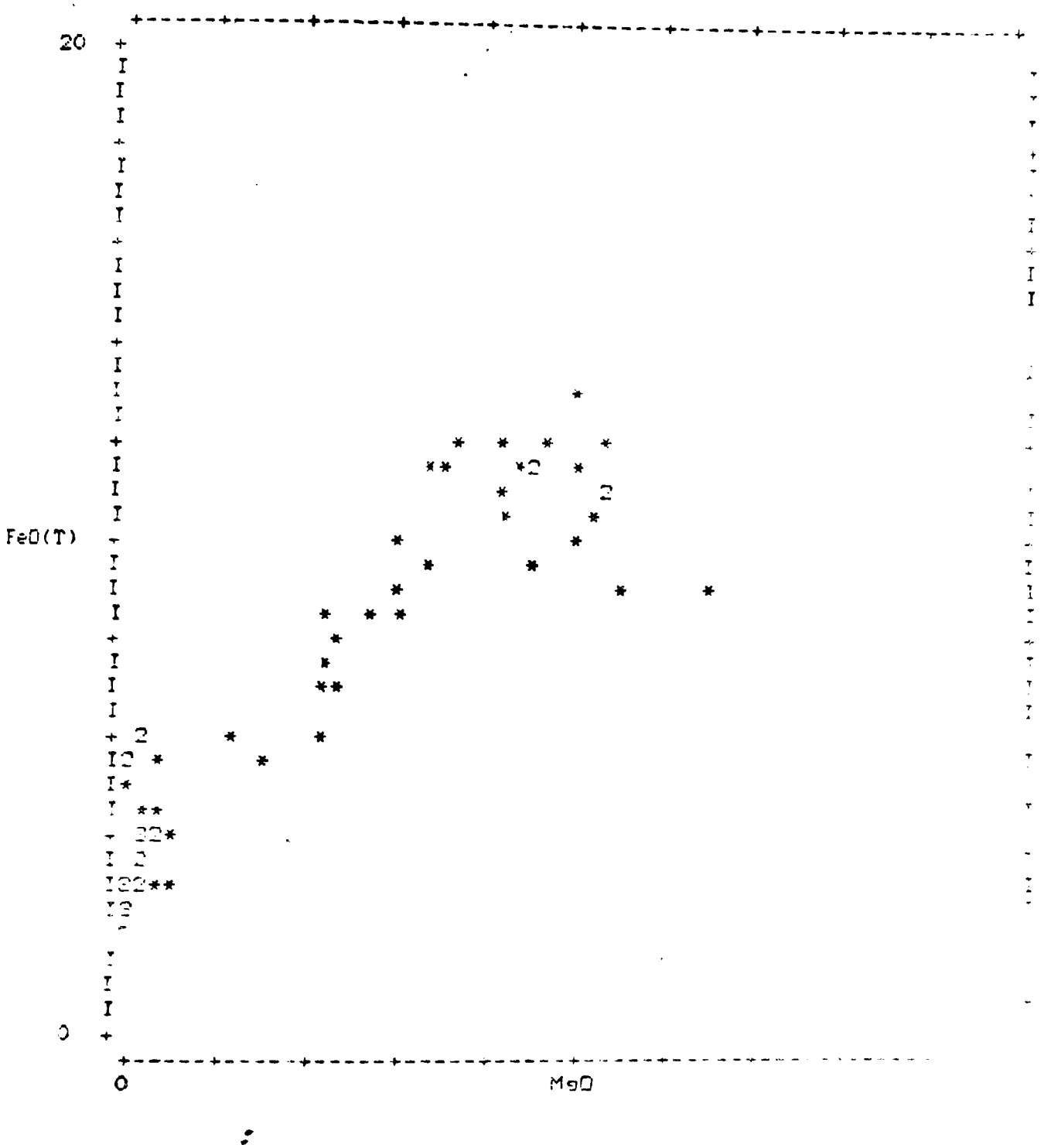


Fig 5.12 PPM Nb vs wt% SiO_2 in Ascension lavas

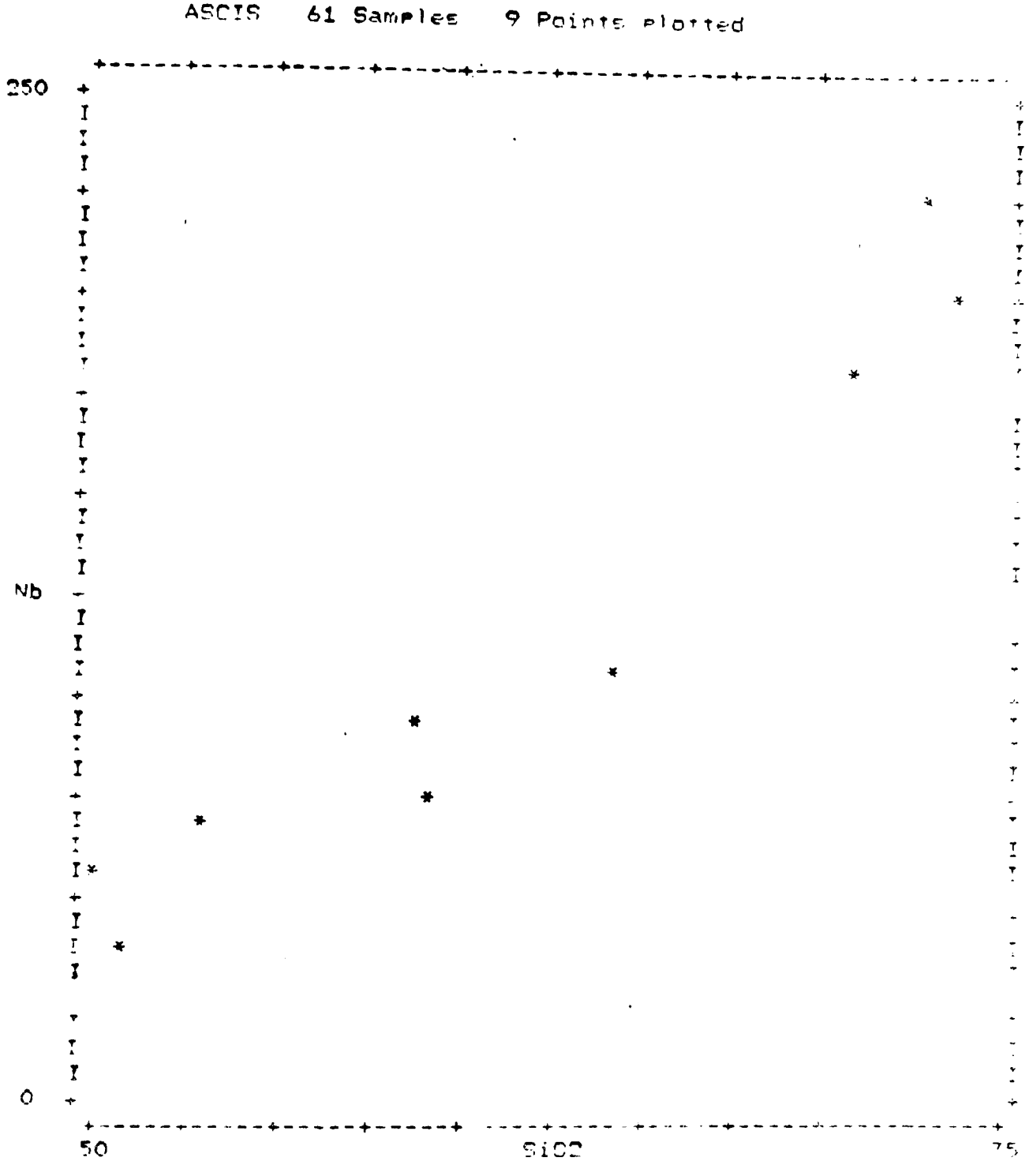


Fig 5.13 PPM Zr vs wt% SiO_2 in Ascension lavas

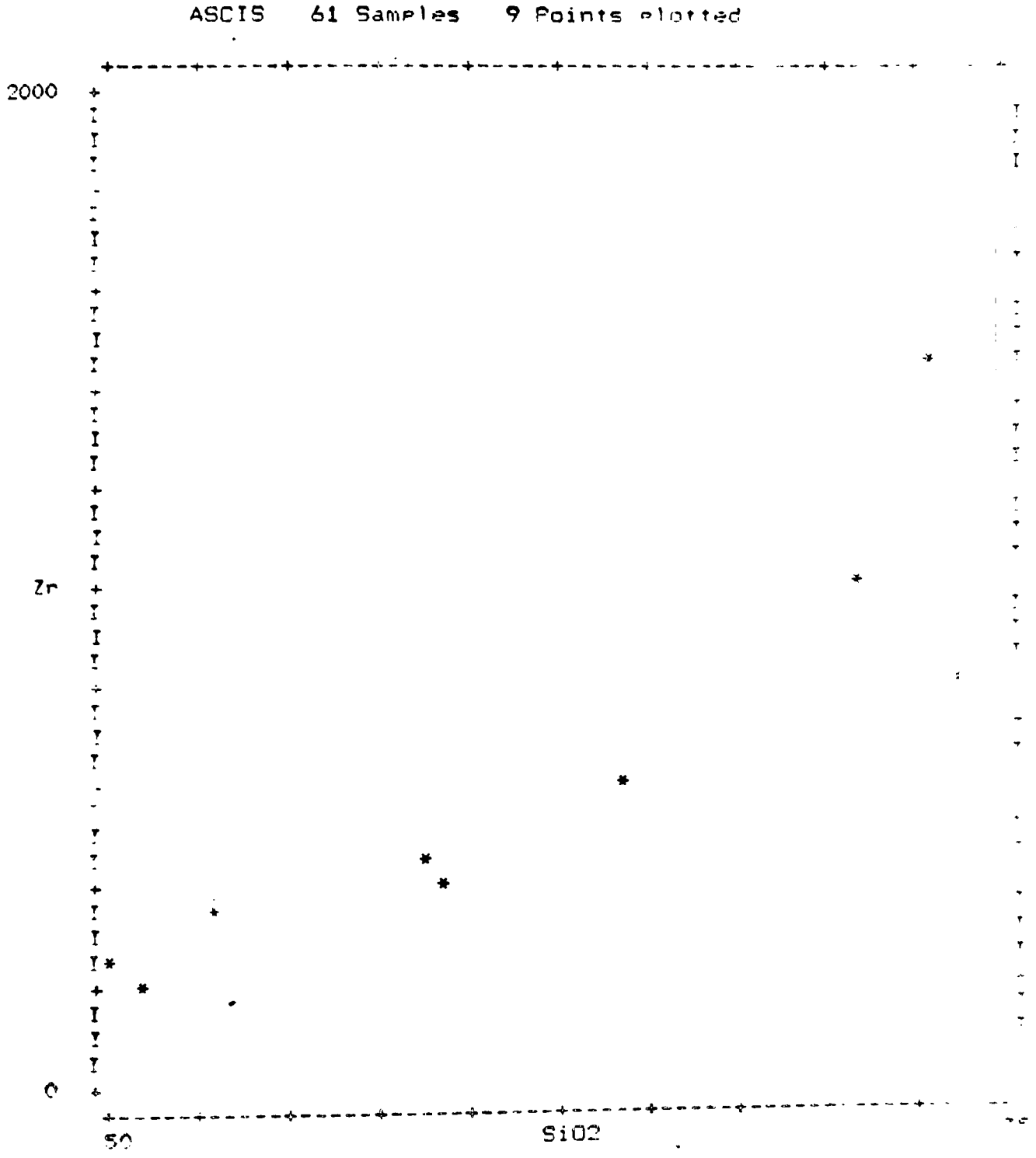


Fig 5.14 PPM Y vs wt% SiO_2 in Ascension lavas

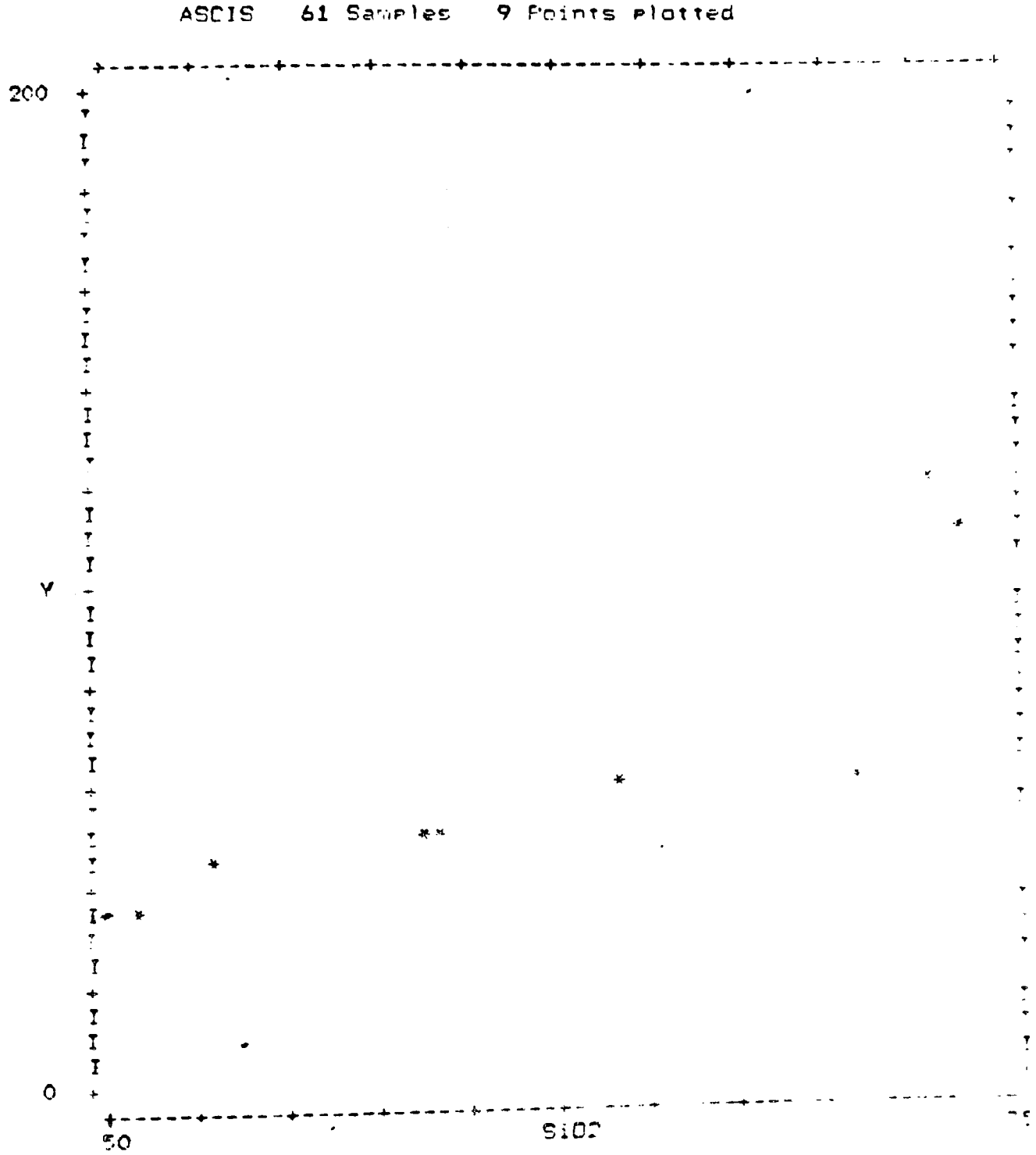


Fig 5.15 PPM Rb vs wt% SiO_2 in Ascension lavas

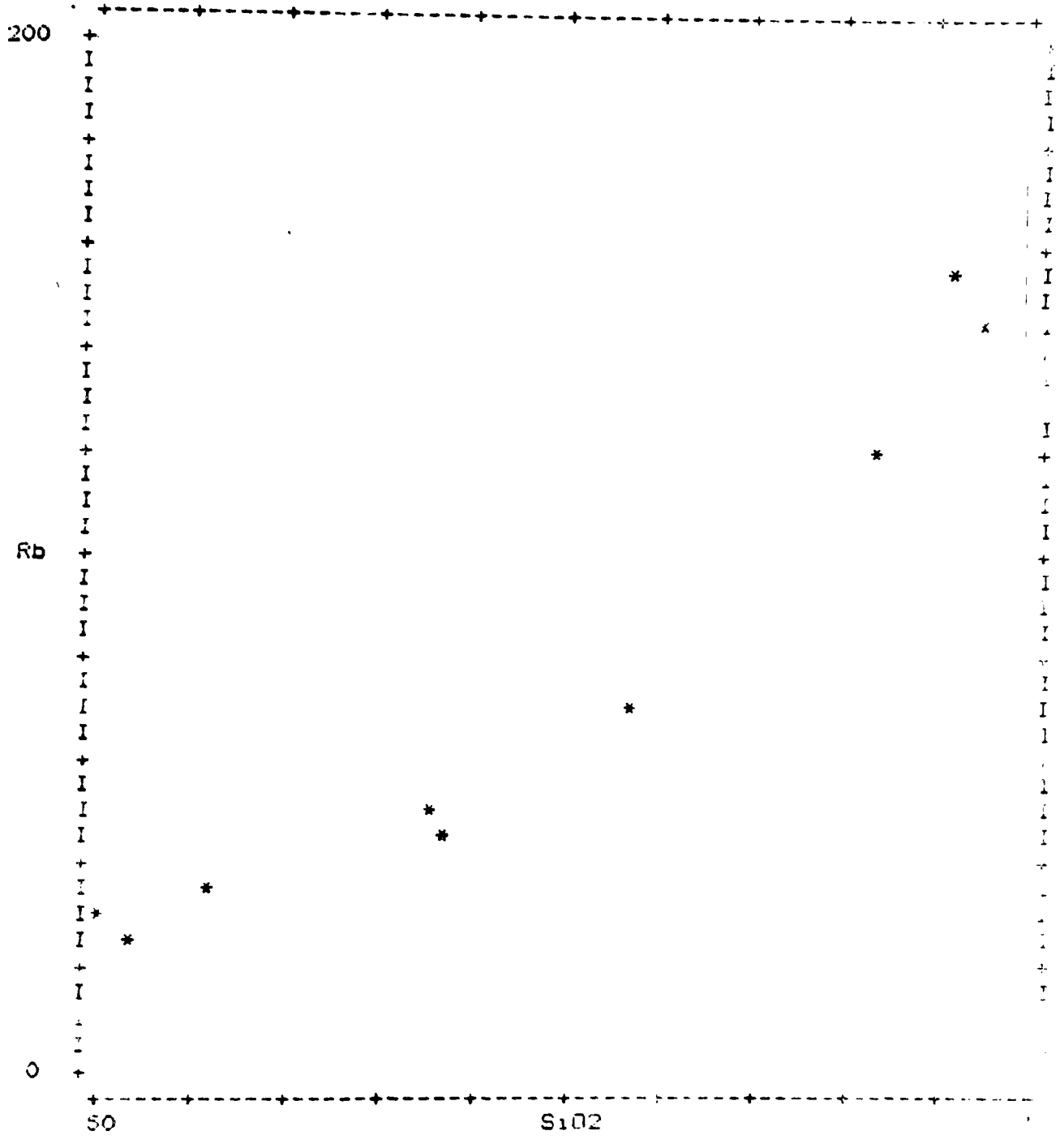


Fig 5.16 PPM Th vs wt% SiO_2 in Ascension lavas

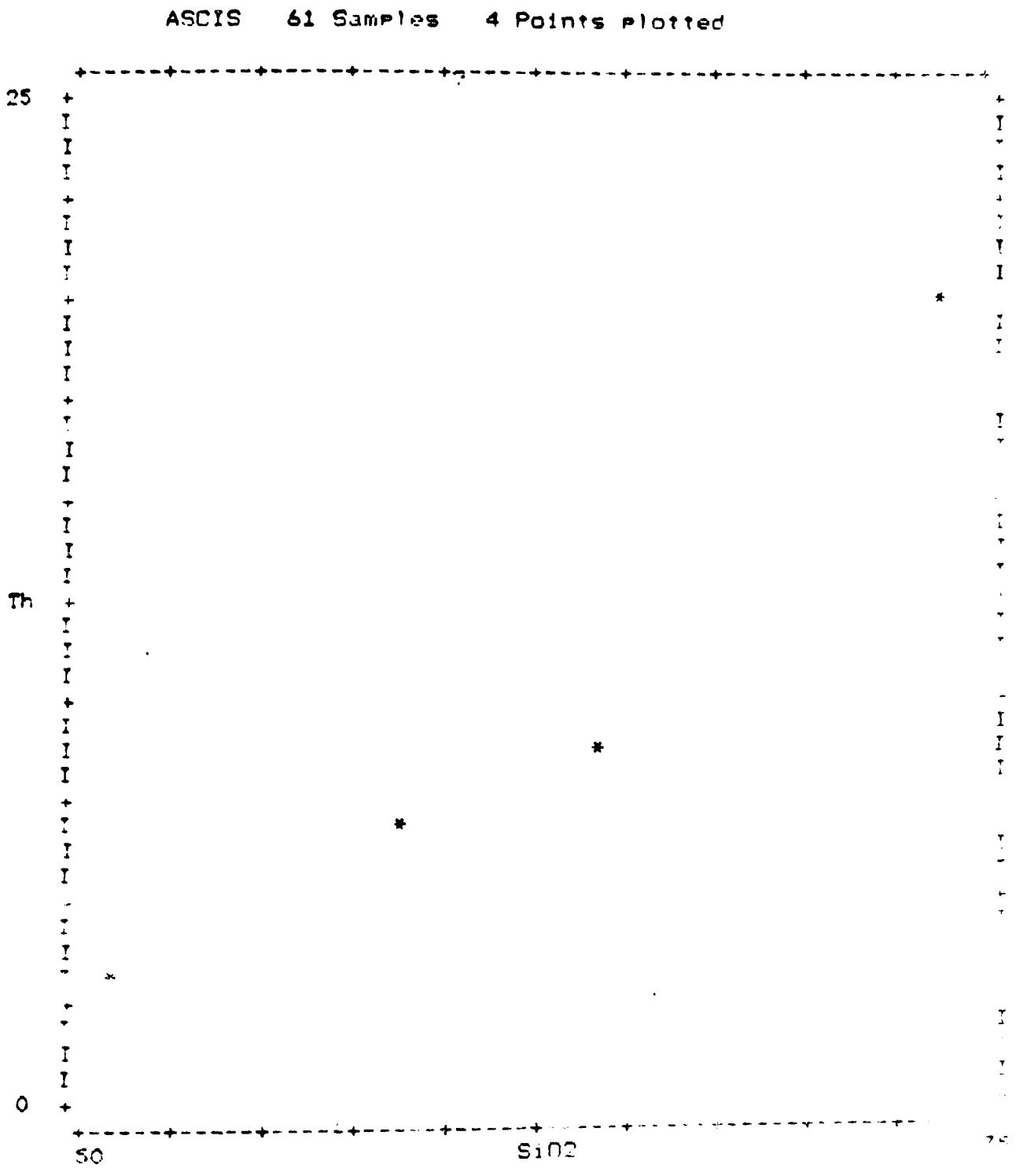


Fig 5.17 PPM Ta vs wt% SiO_2 in Ascension lavas

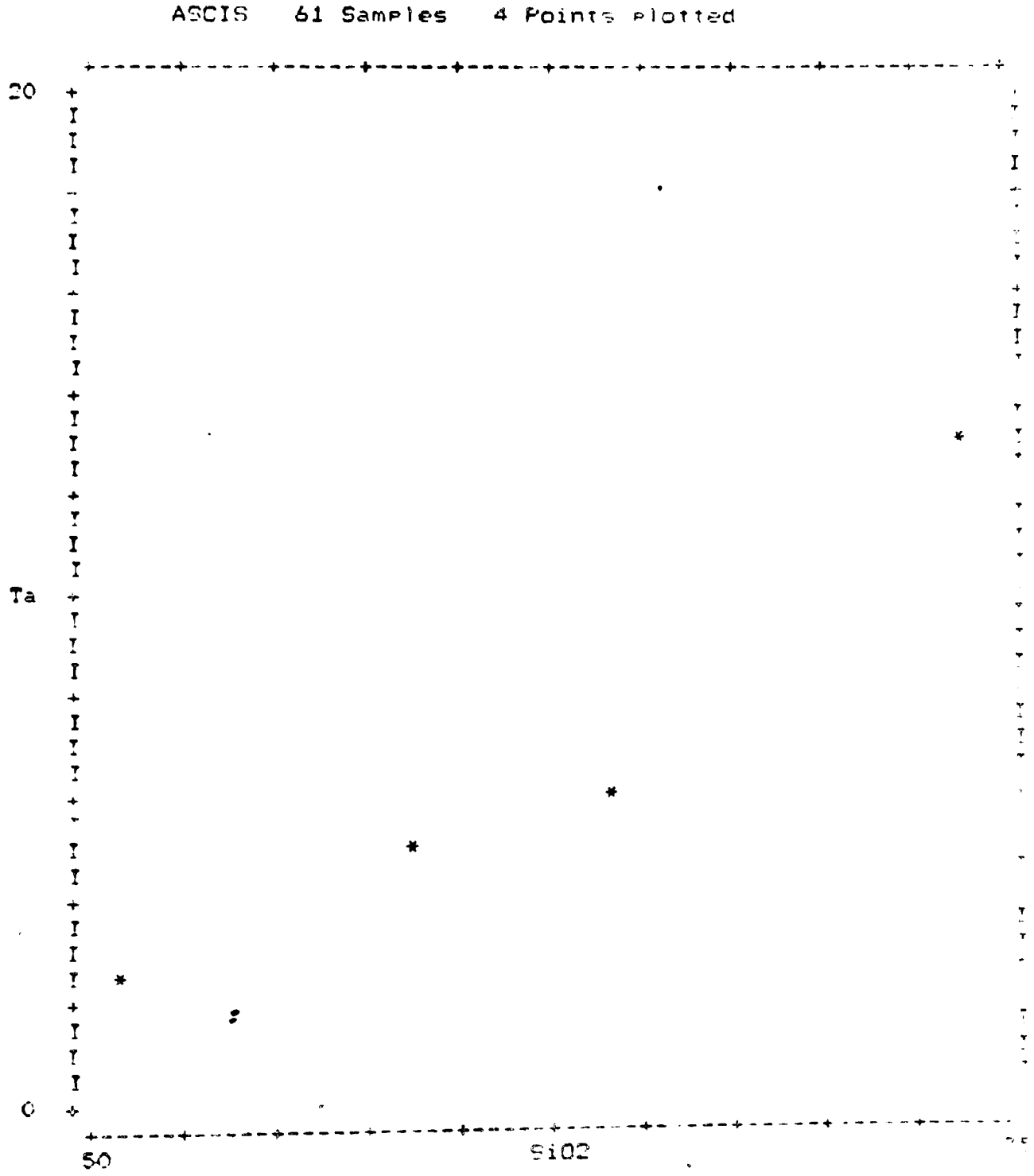


Fig 5.18 PPM Hf vs wt% SiO_2 in Ascension lavas

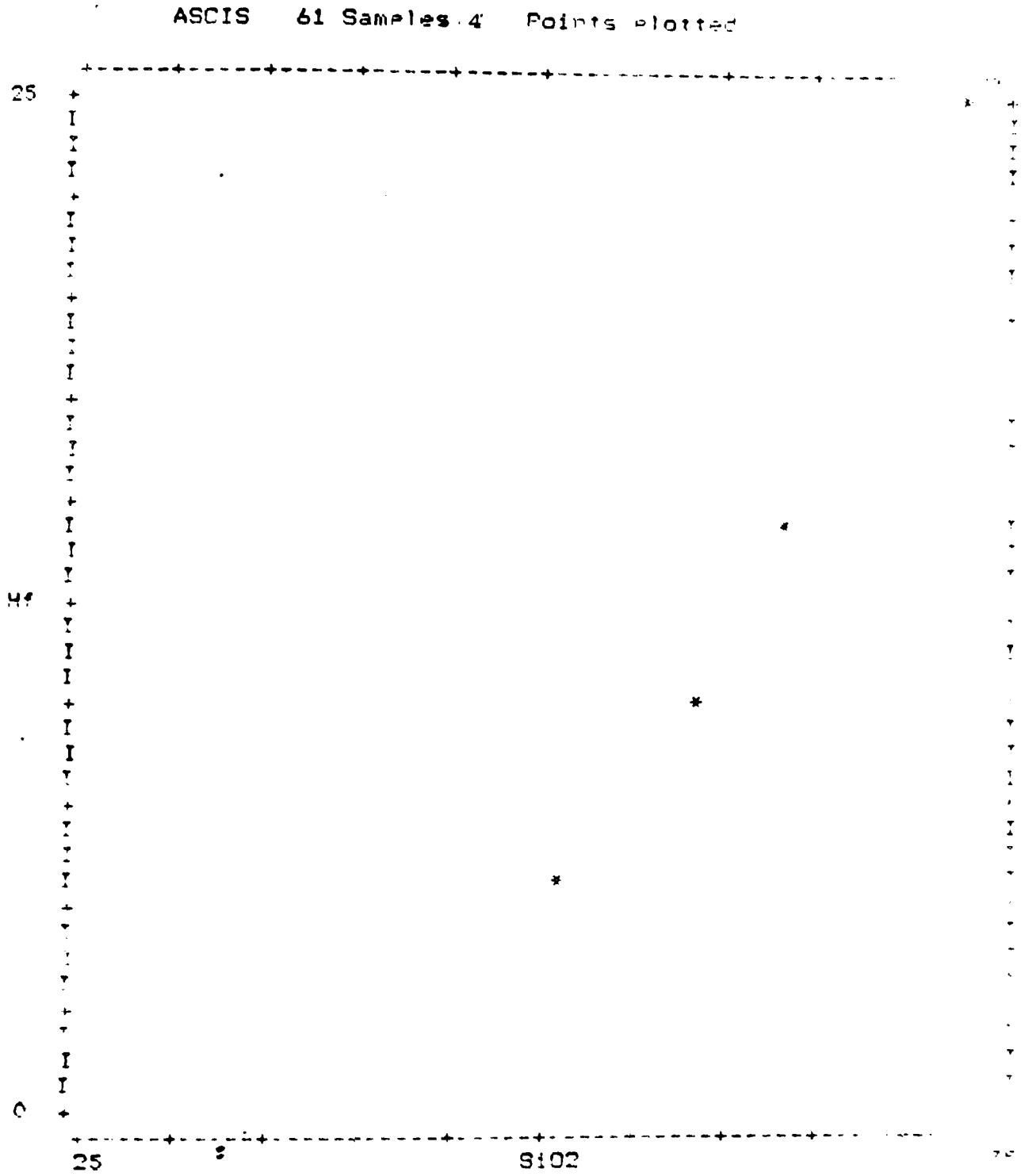


Fig 5.19 PPM Sr vs wt% SiO_2 in Ascension lavas

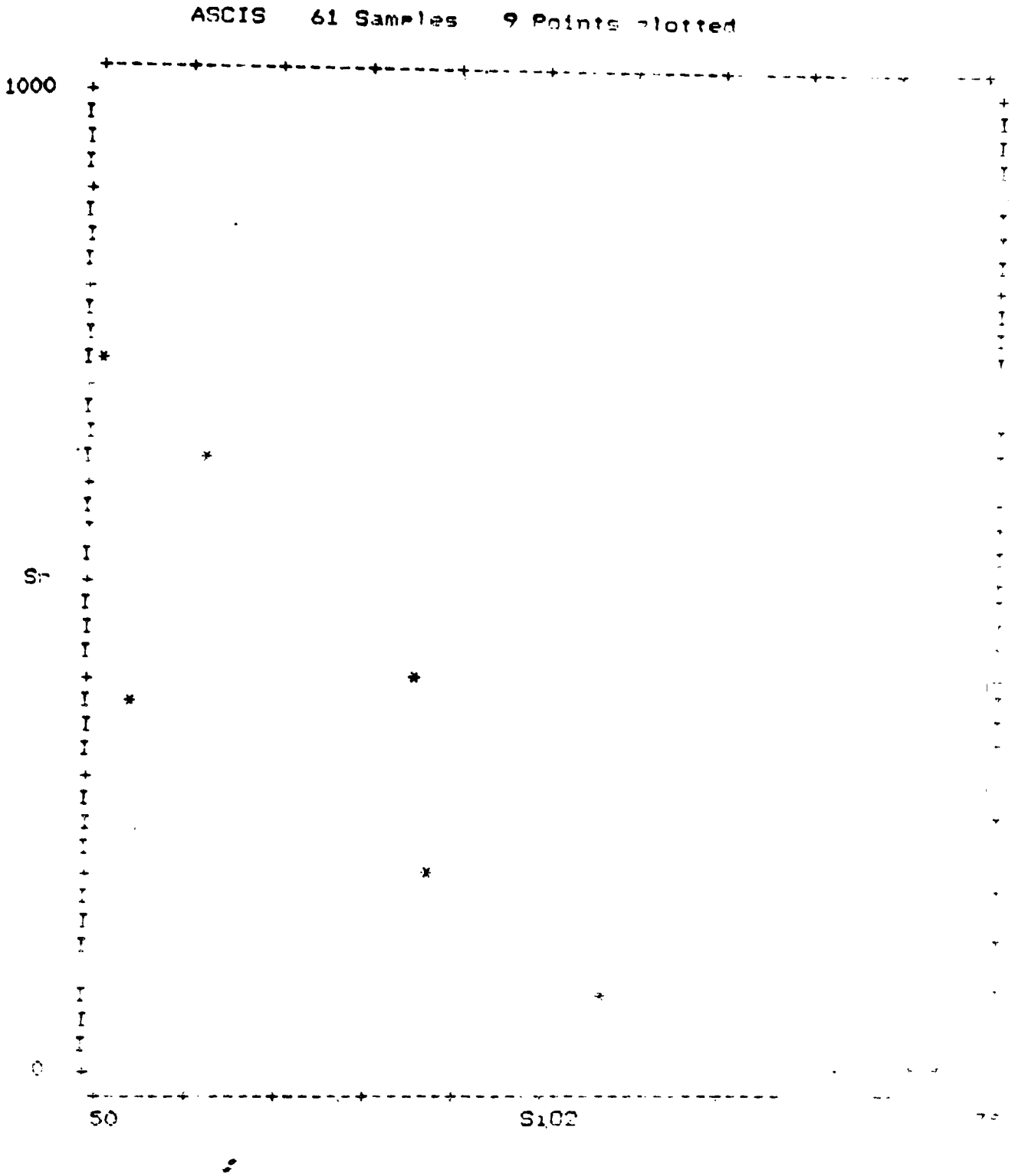


Fig 5.20 A-F-M diagram for Ascension volcanics

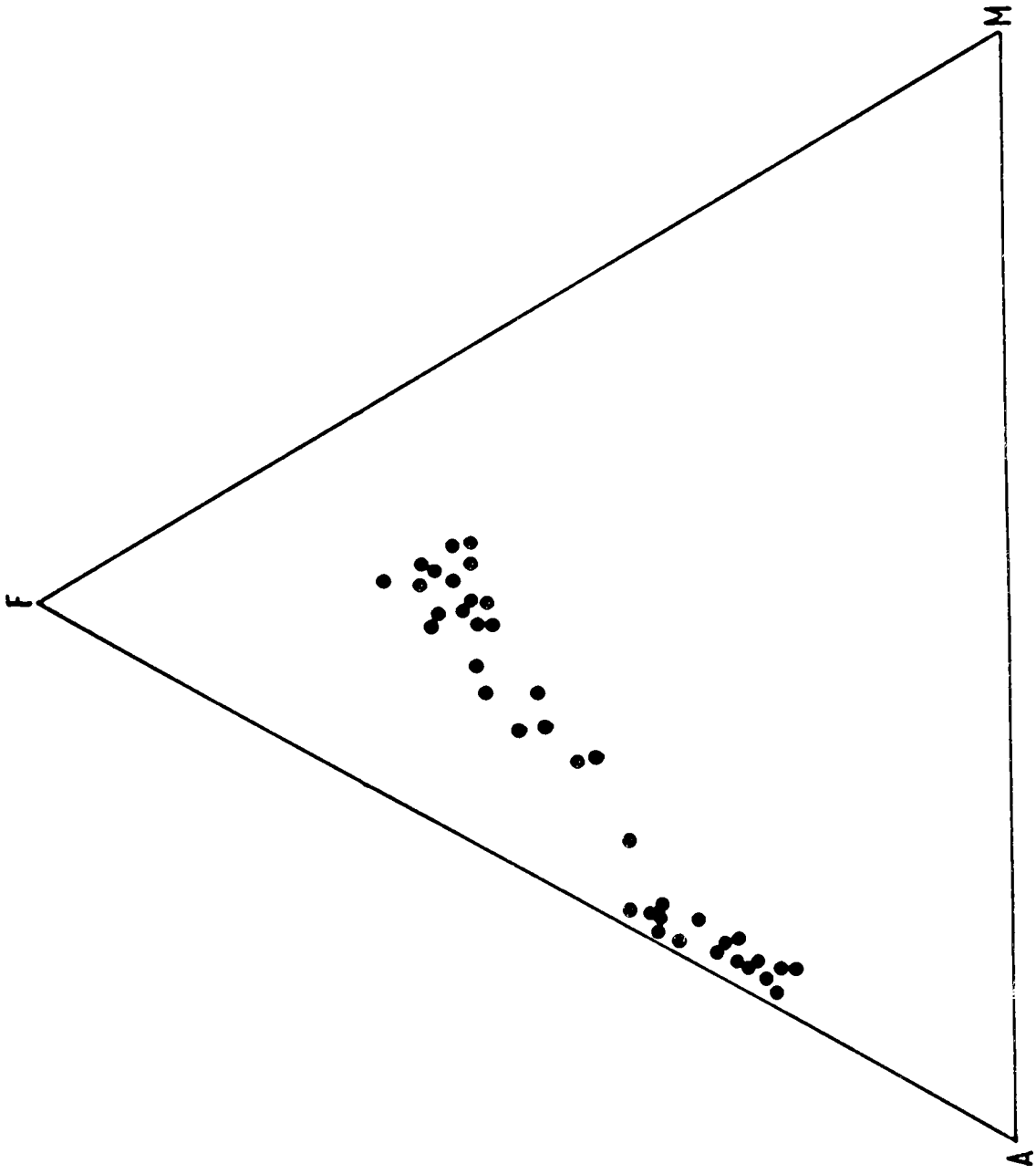


Fig 5.21 Lavas with no normative quartz on Fo-Di-Ne-Hy double triangle (assuming all Fe = FeO).

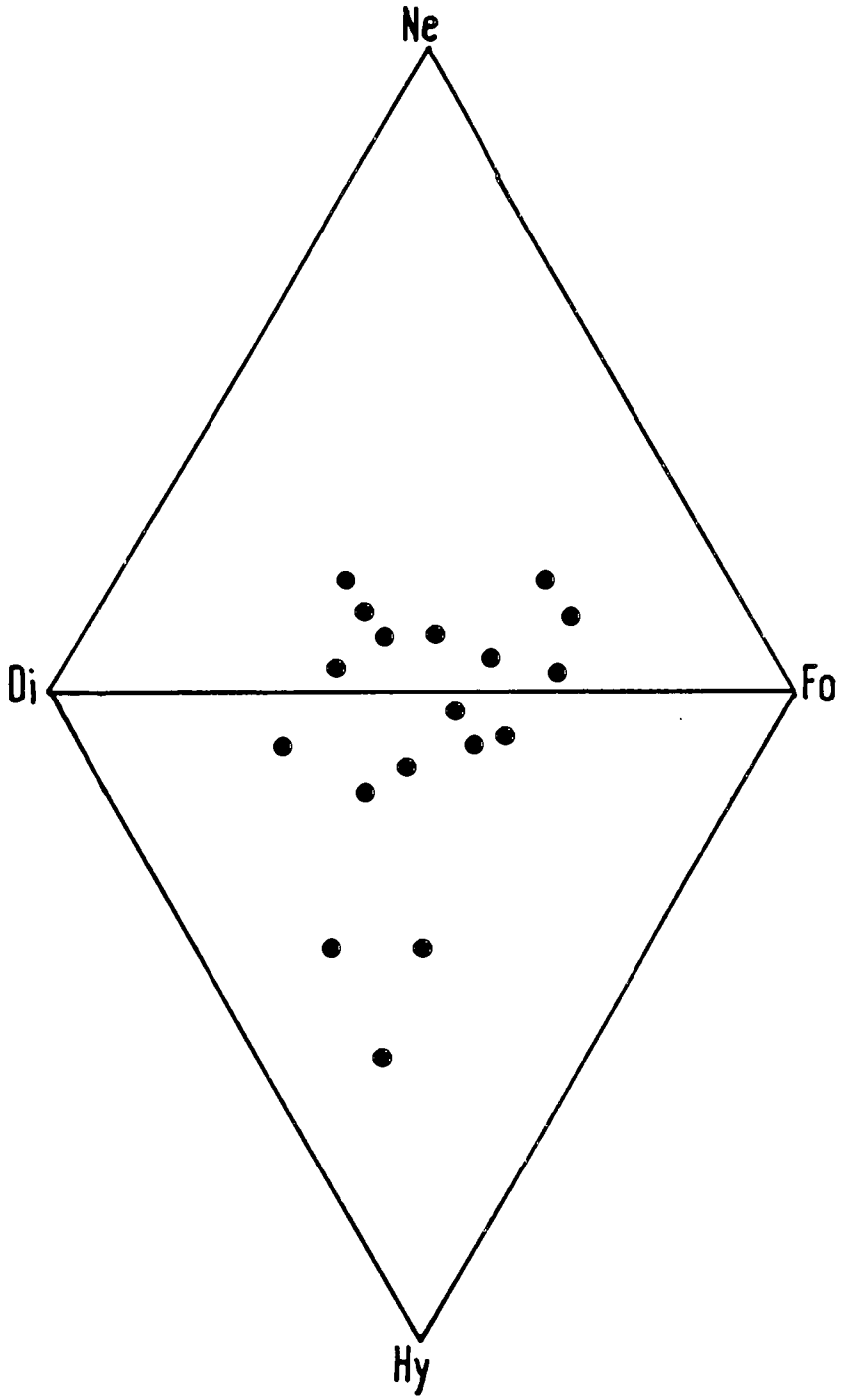


Fig 5.22 Volcanics and blocks with ≤10% normative An on Qz-Ab-Or triangle

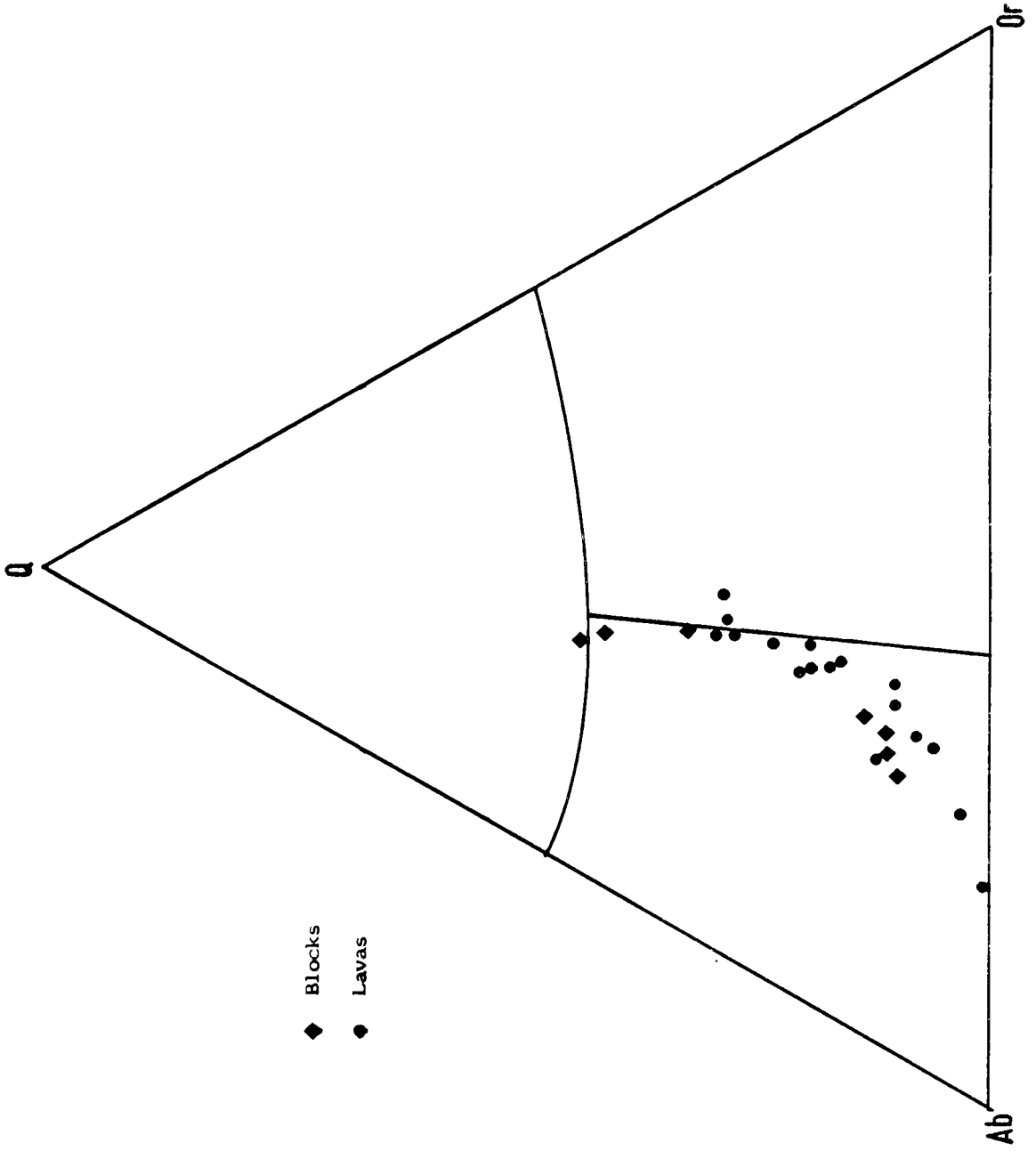


Fig 5.23 Molecular SiO_2-Al_2O_3-K_2O+Na_2O triangle for Ascension lavas with SiO_2 50%

(After Bailey and Macdonald, 1970)

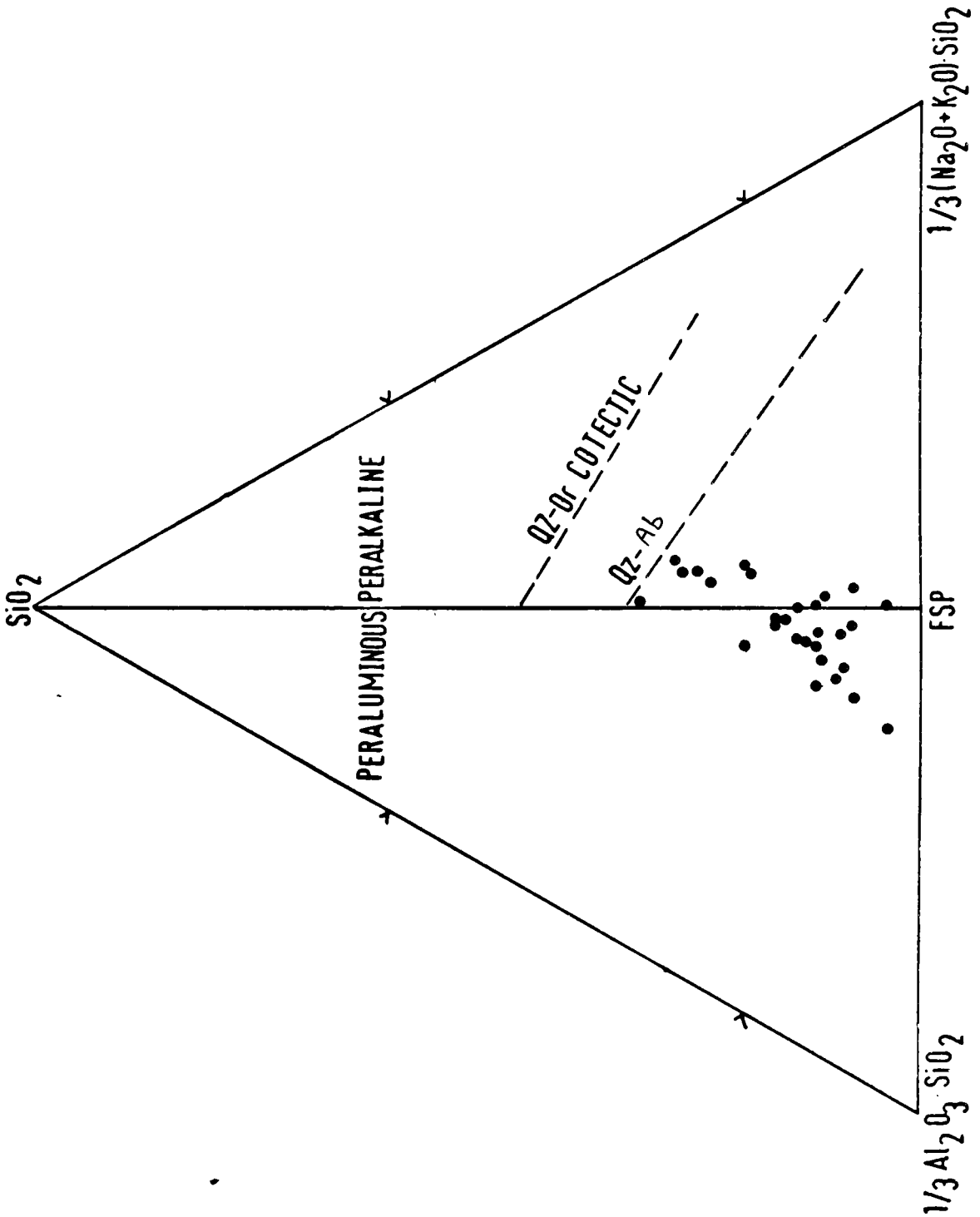


Fig 5.24 Major elements vs SiO_2 for blocks; ⬭ = lavas (61 samples).

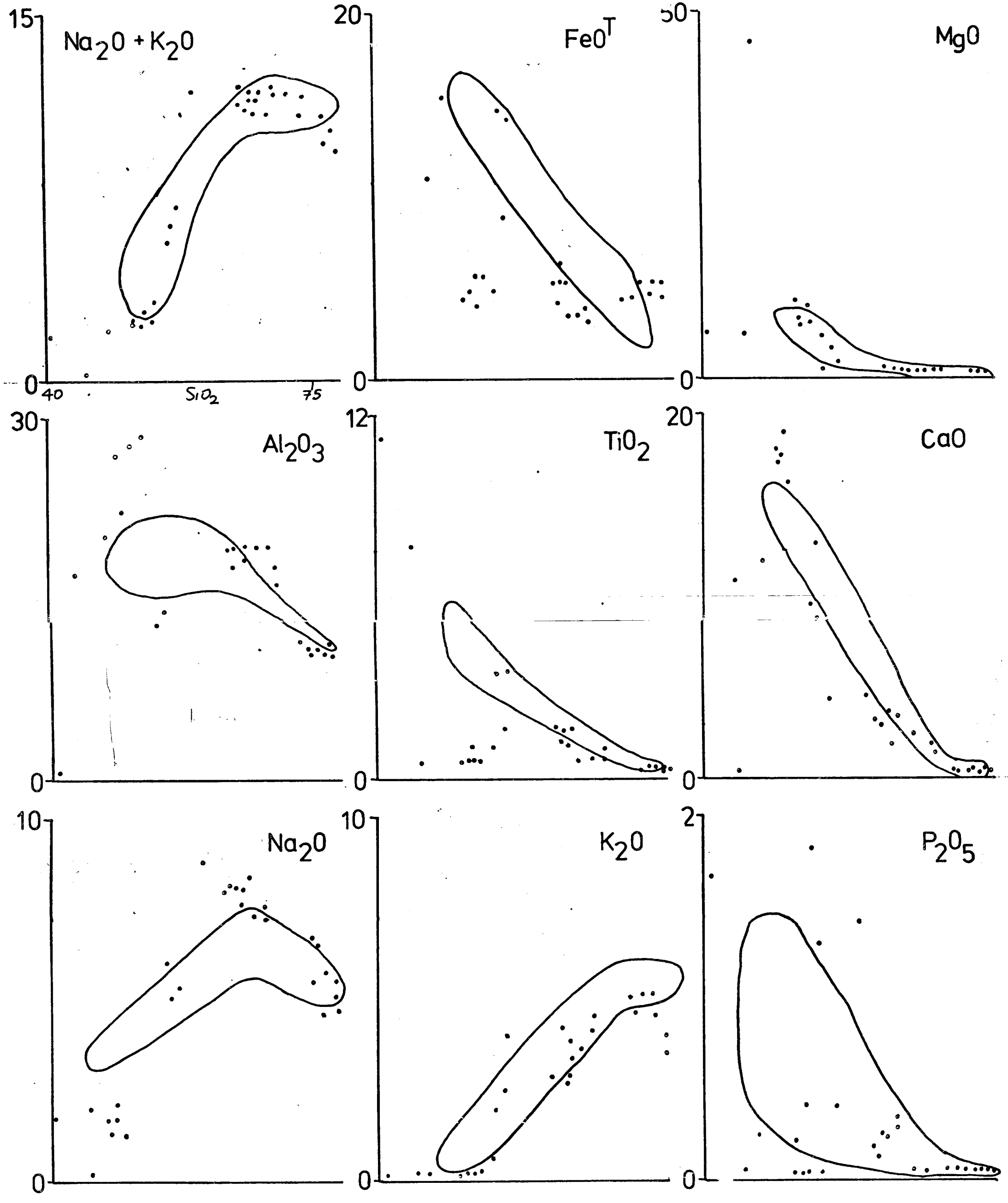
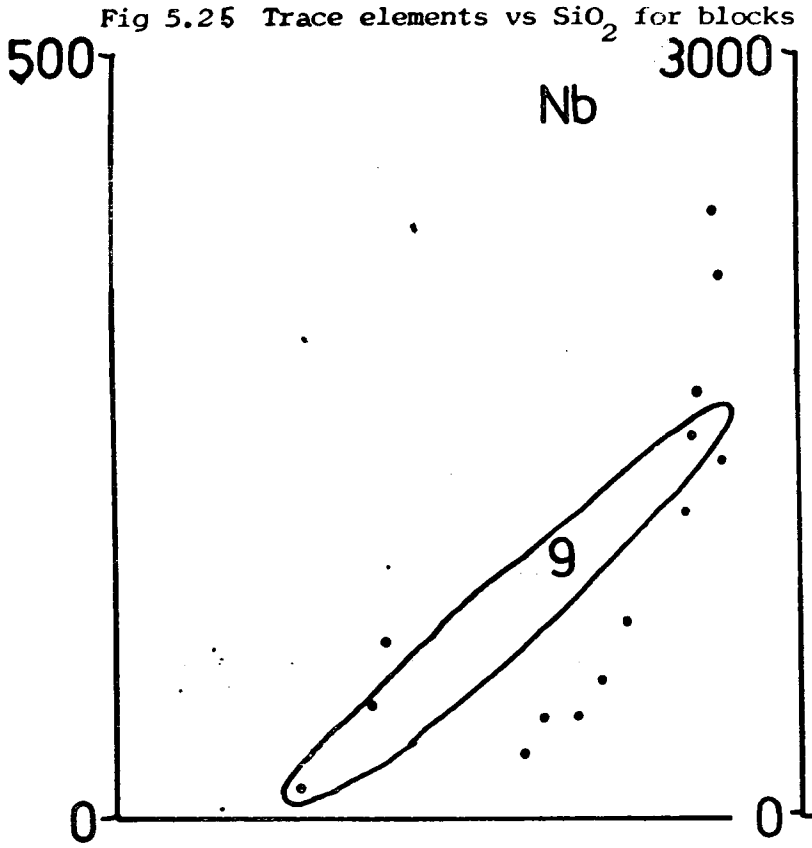
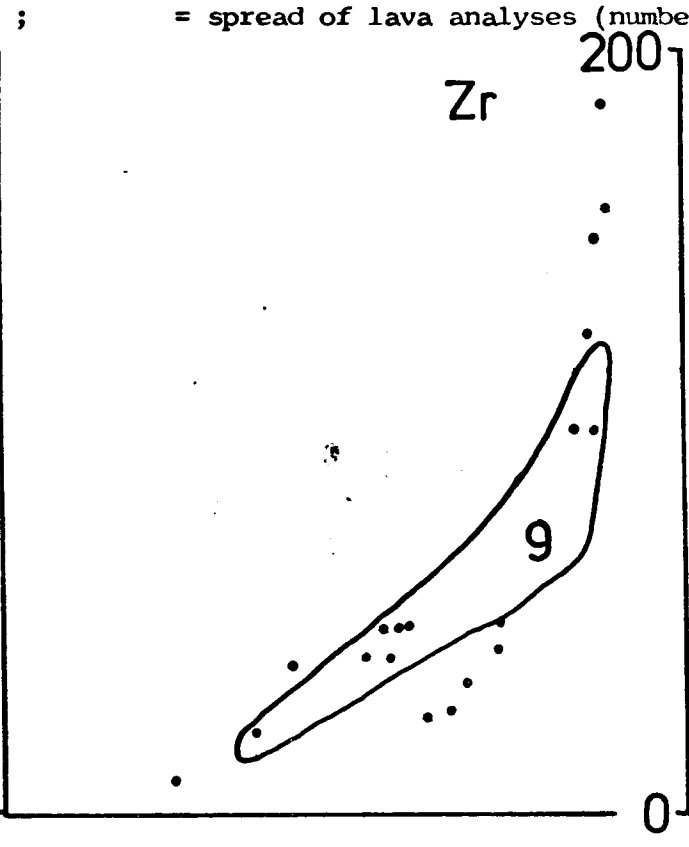
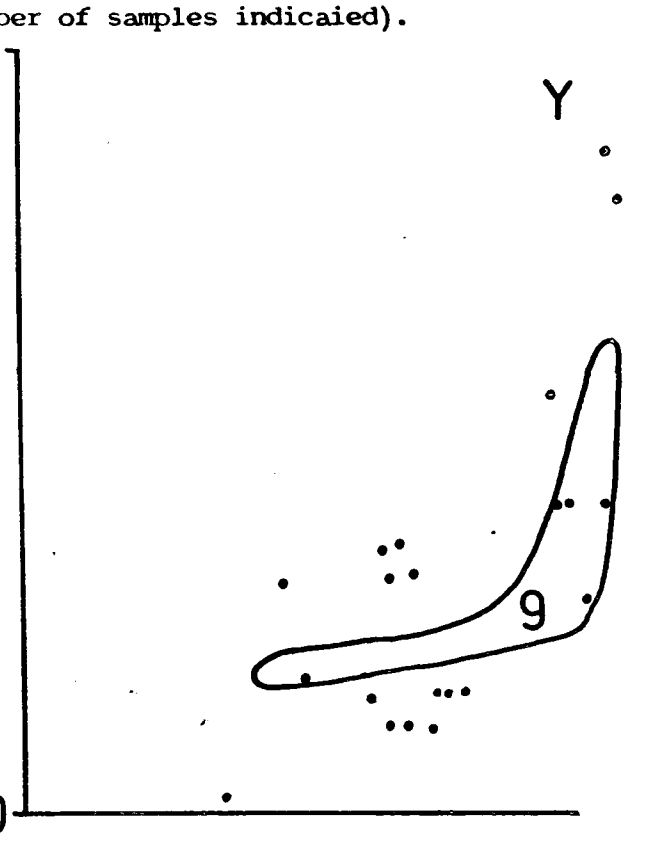
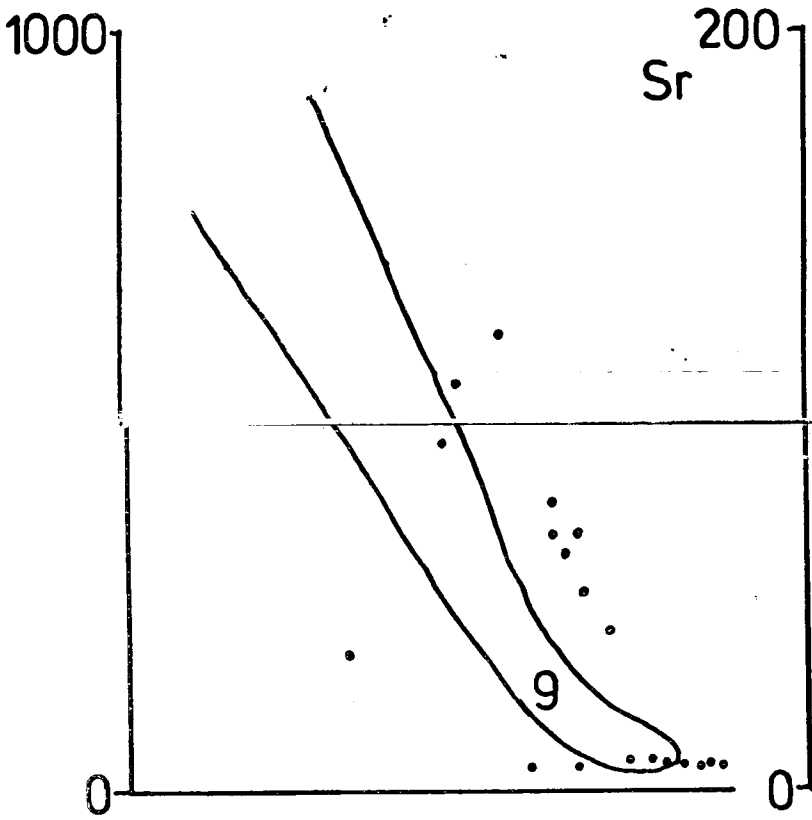


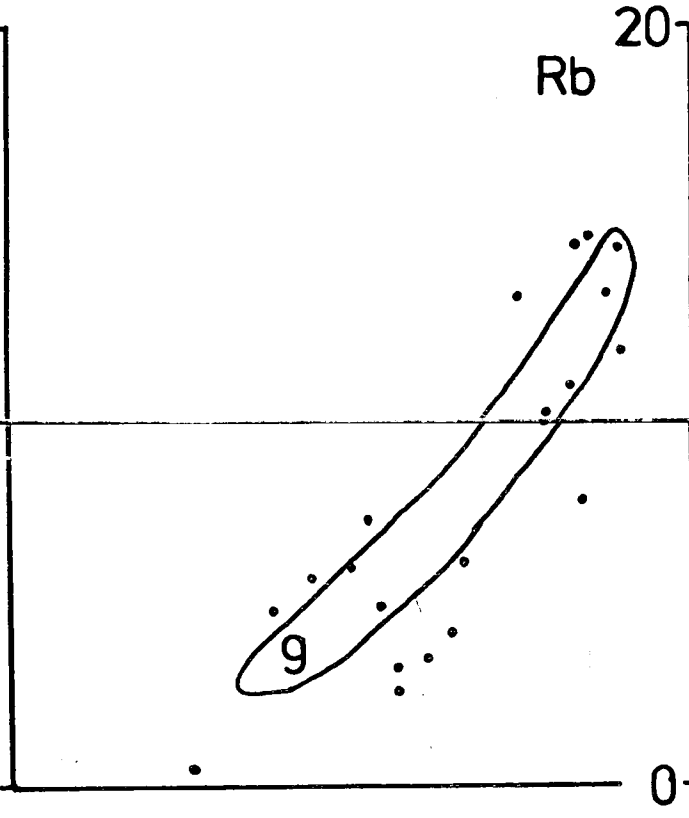
Fig 5.25 Trace elements vs SiO_2 for blocks ; = spread of lava analyses (number of samples indicaied).

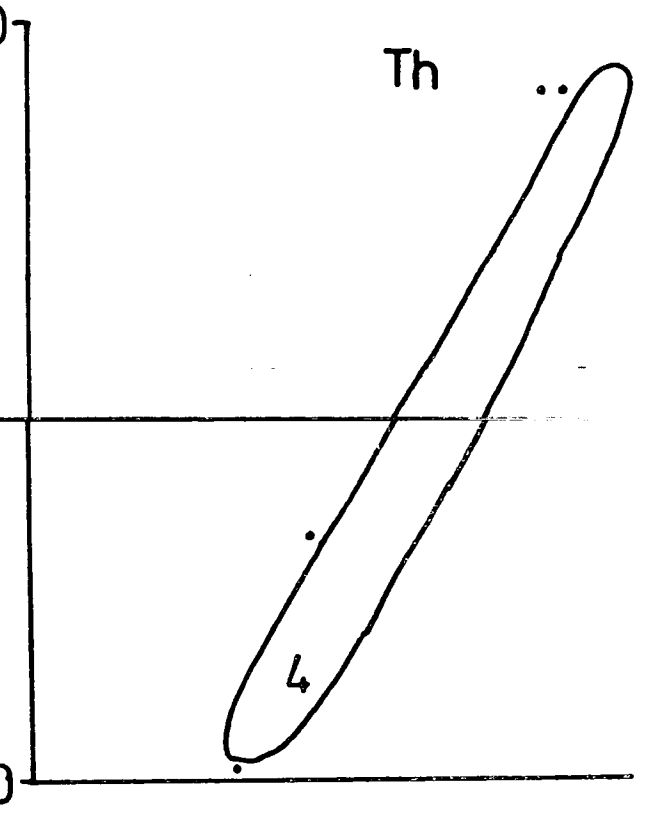


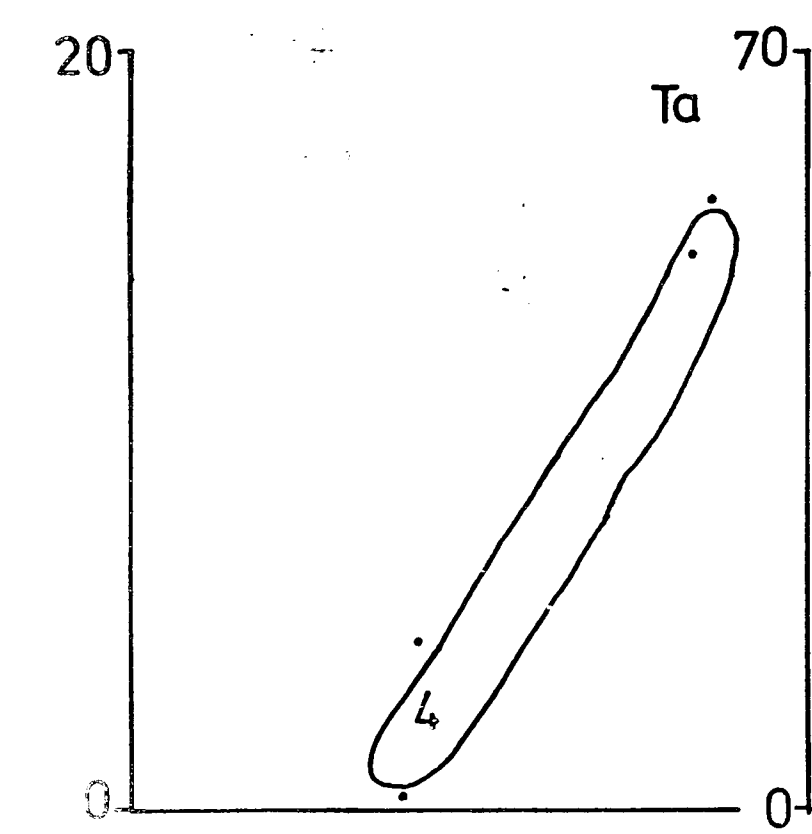












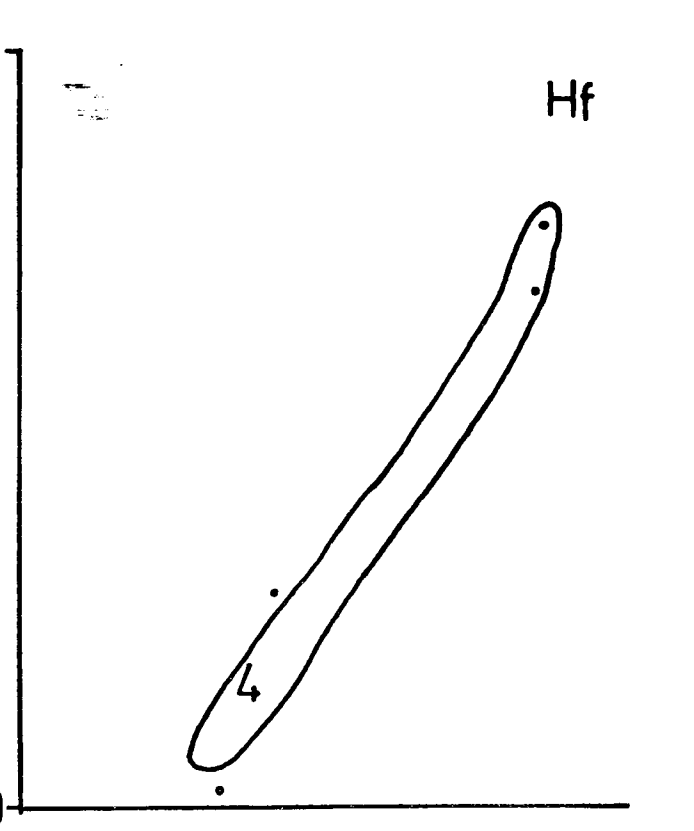


Fig 5.26 Differentiation trend preserved in Middleton's gabbro; solid lines = oxide tie lines for block-residual liquid, dashed lines = trends for lavas (for explaination see text).

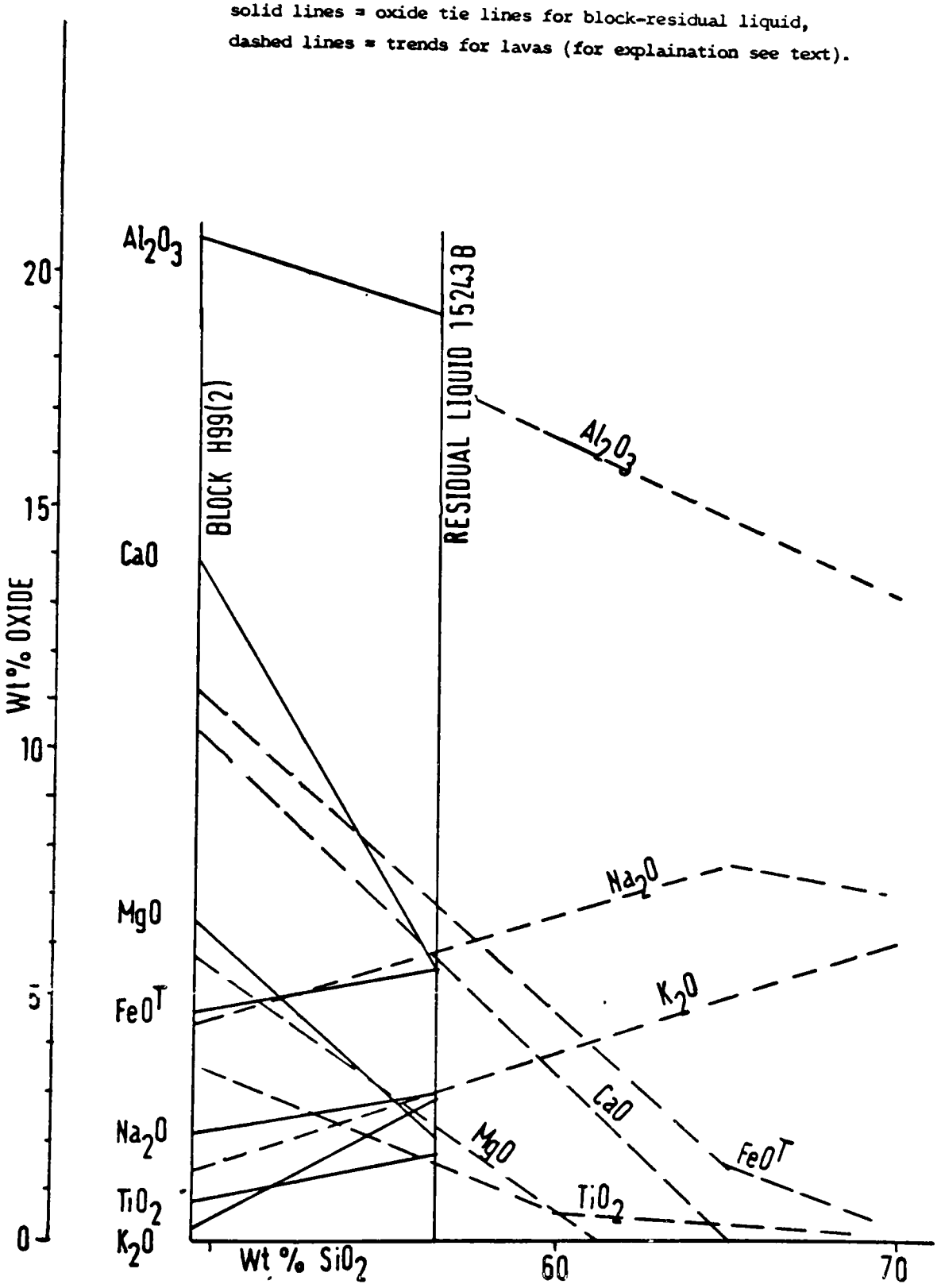


Fig 5.27

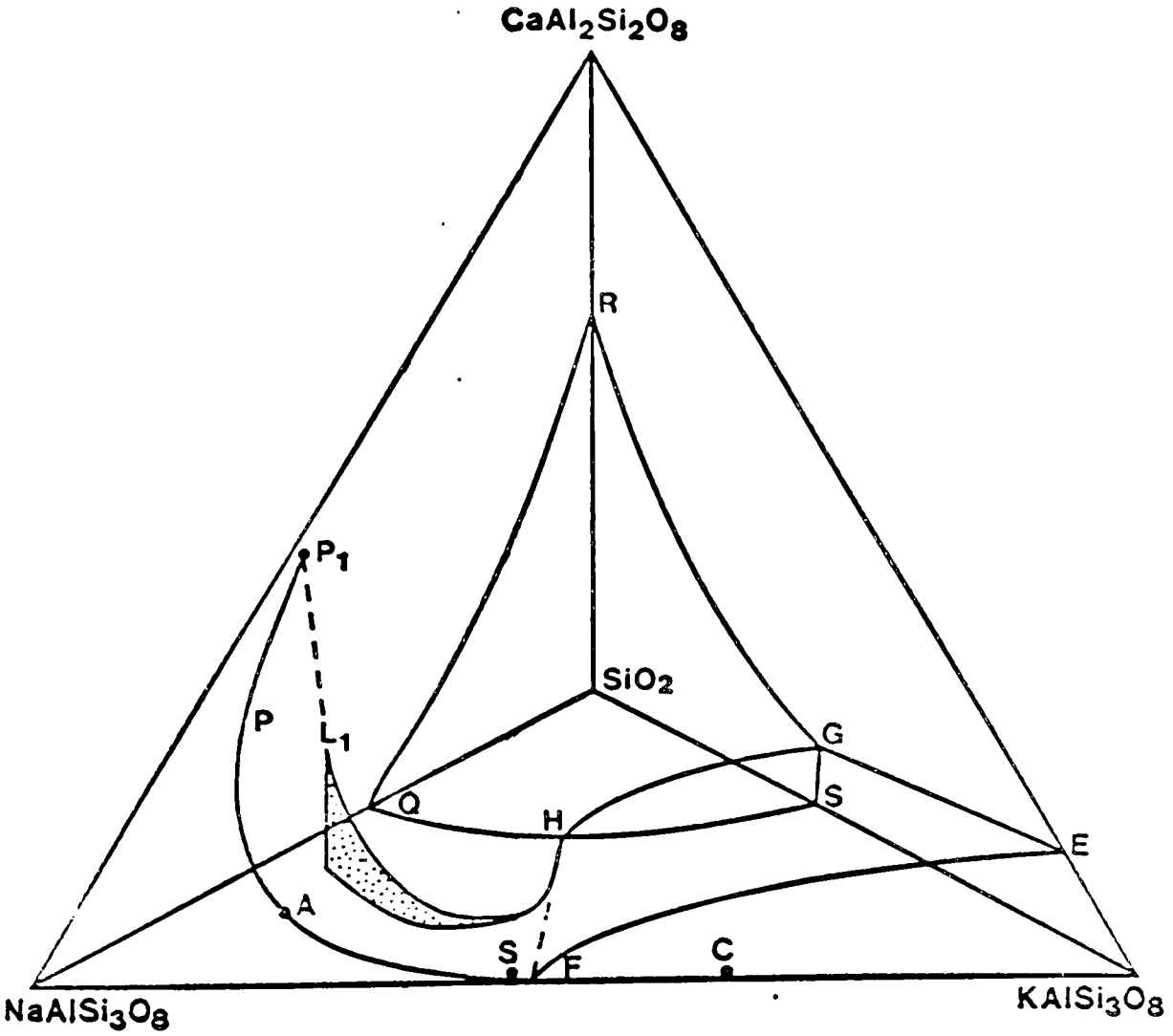
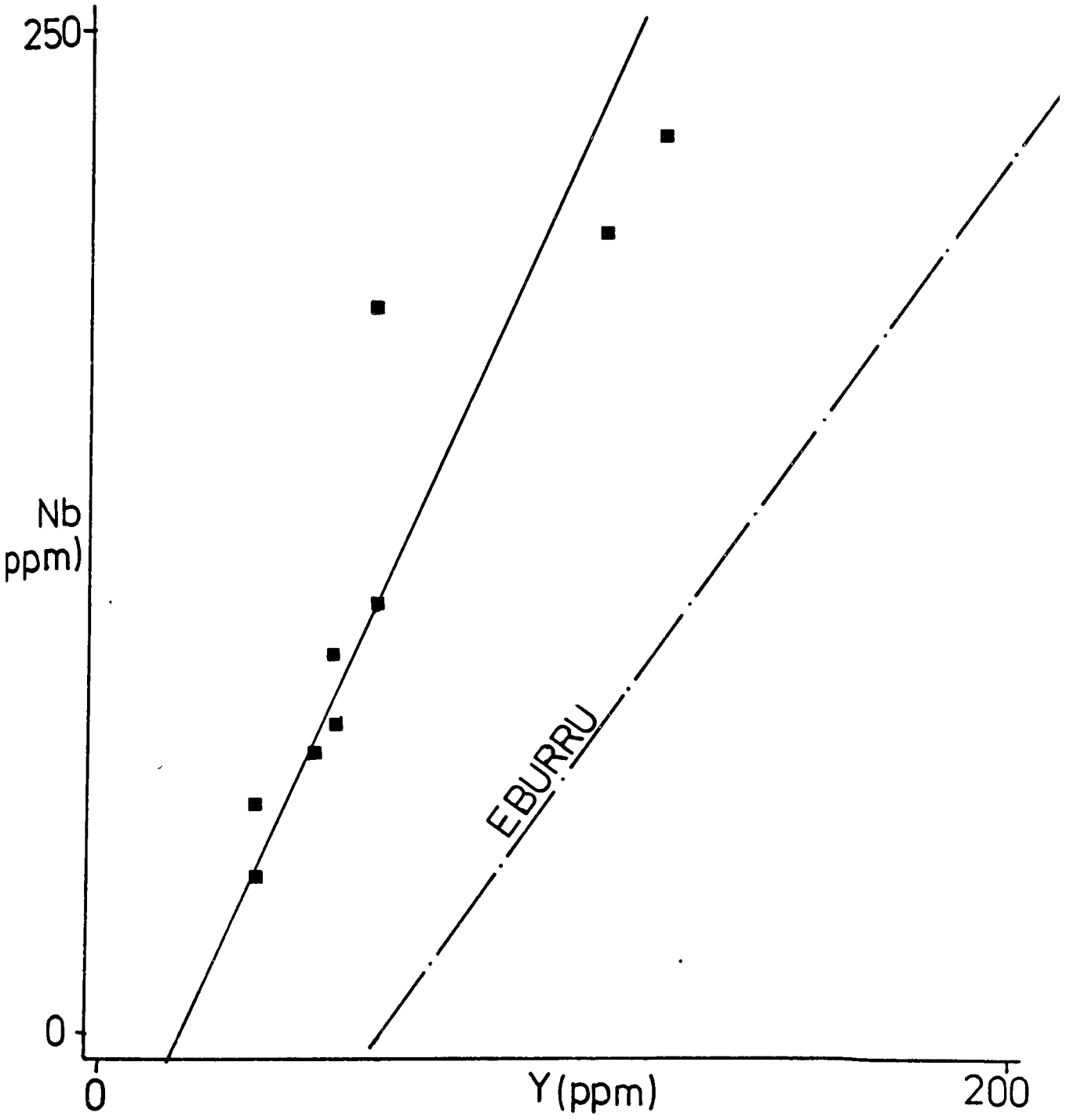


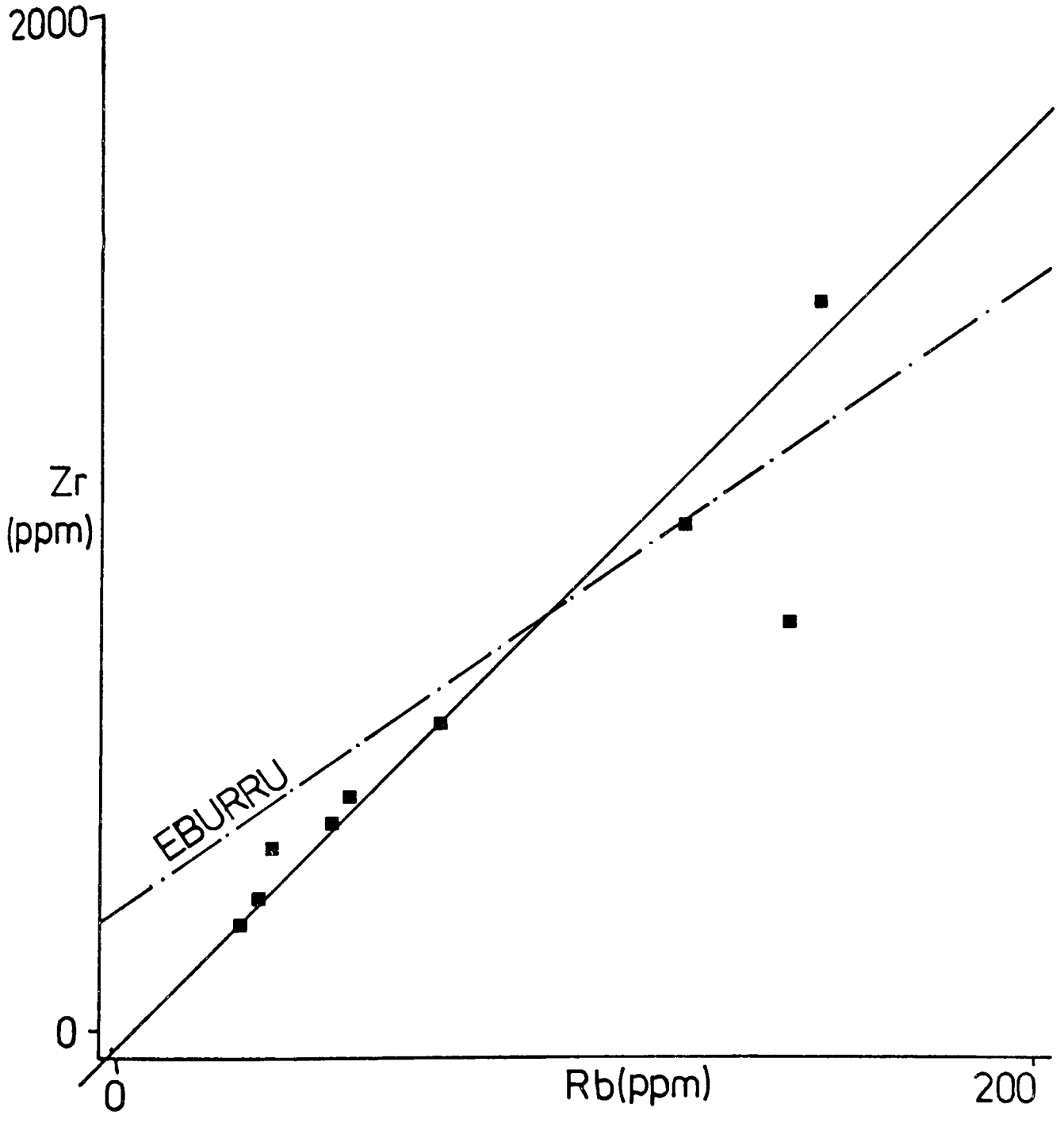
Fig 5.27 Variation in composition of liquid and precipated feldspar plotted onto the quartz-feldspar tetrahedron (after Carmichael et al., 1974). EFGH = two feldspar surface, RQSG = quartz feldspar surface H = isobaric minima. P_1 and L_1 = initial composition of liquid and feldspar. Path of liquid represented by L_1-H, path of feldspar by P_1-C. P = plagioclase, A = anorthoclase, S = sanidine

Fig 5.28 Nb vs Y for analysed lavas. Data for Eburru obsidians from Bailey and Macdonald (1975).



Correlation coefficient for Ascension data = 0.988

Fig 5.29 Zr vs Rb for analysed lavas. Data for Eburru obsidians from Bailey and Macdonald (1975)



Correlation coefficient for Ascension data = 0.933

CHAPTER SIX

TABLES AND FIGURES

Table 6.1 Chemical and petrological details of samples

Sample No.	Locality	Wt% SiO_2	Mineralogy and rock type
DS44	Dark Slope Crater	48.30	Plagioclase gabbro cumulate
H59	Cricket Valley	54.52	Pegmatoid vein in H81L
H81L	Cricket Valley	51.42	Hawaiite lava
A30	N.E. of Cross Hill	53.19	Hawaiite
A29	Cross Hill	64.78	Trachyandesite lava
DS19L	Dark Slope Crater	49.69	Basalt lava
A63	South East Head	59.42	Trachyandesite lava
H30(2)	Five Mile Post	75.42	Granite block
15255	Five Mile Post	73.06	Comendite block
A53	White Hill	71.28	Quartz-trachyte/comendite
DS4	Dark Slope Crater	*40.00	Olivine-plagioclase cumulate
A35	Little White Hill	74.05	Comendite lava (dome)
H30(1)	Five Mile Post	74.00	Granite block

SiO_2 determined by electron probe methods of Dickin & Exley ,1981.

*DS4 by point counting and mineral analysis

Potassium-argon ages for Ascension Island rocks

Number		Age, m.y.	Calculated error, in m.y.
15068	Trachyte, bottom of valley SE of Bear's Back	1.5	± 0.2
14945	Trachyte, capping hill, N of Thistle Hill	1.1	± 0.3
15175	Trachyte, the Crags	1.0	± 0.3
15217	Trachyte, Breakneck Valley	0.87	± 0.06
14944*	Trachyte, Thistle Hill	0.8	± 0.7
15050	Trachyte, Little Ascension flow	0.7	± 0.7
17313*	Hawaiite, Palmer's Flow	0.47	± 0.1
14994	Hawaiite , Cricket Valley	0.35	± 0.03
15001*	Hawaiite, Crater Valley	0.22	± 0.06
15014*	Hawaiite, 1000 yds. SW of Castle Hill	0.2	± 0.07
14999*	Hawaiite, Crystal Bay	0.12	± 0.06
17464	Hawaiite, NW wall, crater of Mountain Red Hill	0.3	± 0.4

Table 6.2

Samples designated * analysed by J. Dymond, Oregon State University.

Other samples analysed by N.H. Gale and J. Symonds, Department of Geology and Mineralogy, University of Oxford.

Table 6.3 Sr data

Sample No.	Rb/ppm)	Sr(ppm)	Rb/Sr	Sr^{87}/Sr^{86}
DS44	n.d.	172	-	0.70296 ± 7
H59	54	332	0.16	0.70290 ± 4
H81L	28	366	0.08	0.70292 ± 4
A30	36	607	0.58	0.70296 ± 5
A29	68	96	0.71	0.70297 ± 3
DS19L	30	690	0.04	0.70323 ± 5
A63	52	398	0.13	0.70281 ± 5
H30(2)	119	2	56	0.70877 ± 8
15255	153	2	97	0.70773 ± 7
A53	125	12	10	0.70345 ± 5
DS4	n.d.	44	-	0.70281 ± 4
A35	147	1	250	0.70898 ± 8
H30(1)	132	2	87	0.71352 ± 7

n.d. = not detected

Rb and Sr to nearest PPM

Rb/Sr to 2 sig. figs.

Table 6.3a

ASCENSION ISLAND - AGE CORRECTED $^{87}Sr/^{86}Sr$ FOR ROCKS WITH LOW Sr AND HIGH $^{87}Sr/^{86}Sr$ ASSUMING AN AGE OF 1.5 Ma.

Rock	Rb (ppm)	Sr (ppm)	Rb/Sr	Age corr.	$^{87}Sr/^{86}Sr$	Corr. $^{87}Sr/^{86}Sr$
H30(1)	117	2.01	58	0.00351	0.7135	0.7100
H30(2)	115	2.72	42	0.00253	0.7087	0.7062
15255	149	2.38	63	0.00380	0.7077	0.7039
A35	147	1.34	109	0.00658	0.7089	0.7023

Table 6.3b

CALCULATED AGE OF THESE ROCKS ASSUMING NO SEDIMENT INCORPORATION AND AN INITIAL $^{87}Sr/^{86}Sr$ RATIO OF 0.7029

	Age (Ma)
H30(1)	4.5
H30(2)	3.4
15255	1.9
A35	1.4

Rb and Sr by isotope dilution

Table 6.4 Pb data

Sample No.	Pb(ppm)	$^{206}/_{204}$	$^{207}/_{204}$	$^{208}/_{204}$
DS44	n.d.	17.924	15.541	37.931
H59	2.0	19.403	15.582	38.914
H81L	0.7	19.335	15.501	38.880
A30	1.9	19.574	15.610	39.122
A29	5.0	19.667	15.610	39.142
DS19L	3.5	19.657	15.657	39.350
A63	4.2	19.533	15.597	39.052
H30(2)	0.7	19.373	15.611	39.025
15255	9.0	19.633	15.622	39.196
A53	7.3	19.629	15.636	39.190
DS4	n.d.	18.112	15.539	38.043
A35	6.1	19.463	15.605	38.975
H30(1)	3.7	19.515	15.619	39.093

n.d. = not detected

Fig 6.1 Sr^{87}/Sr^{86} vs wt% SiO_2 in analysed blocks and lavas

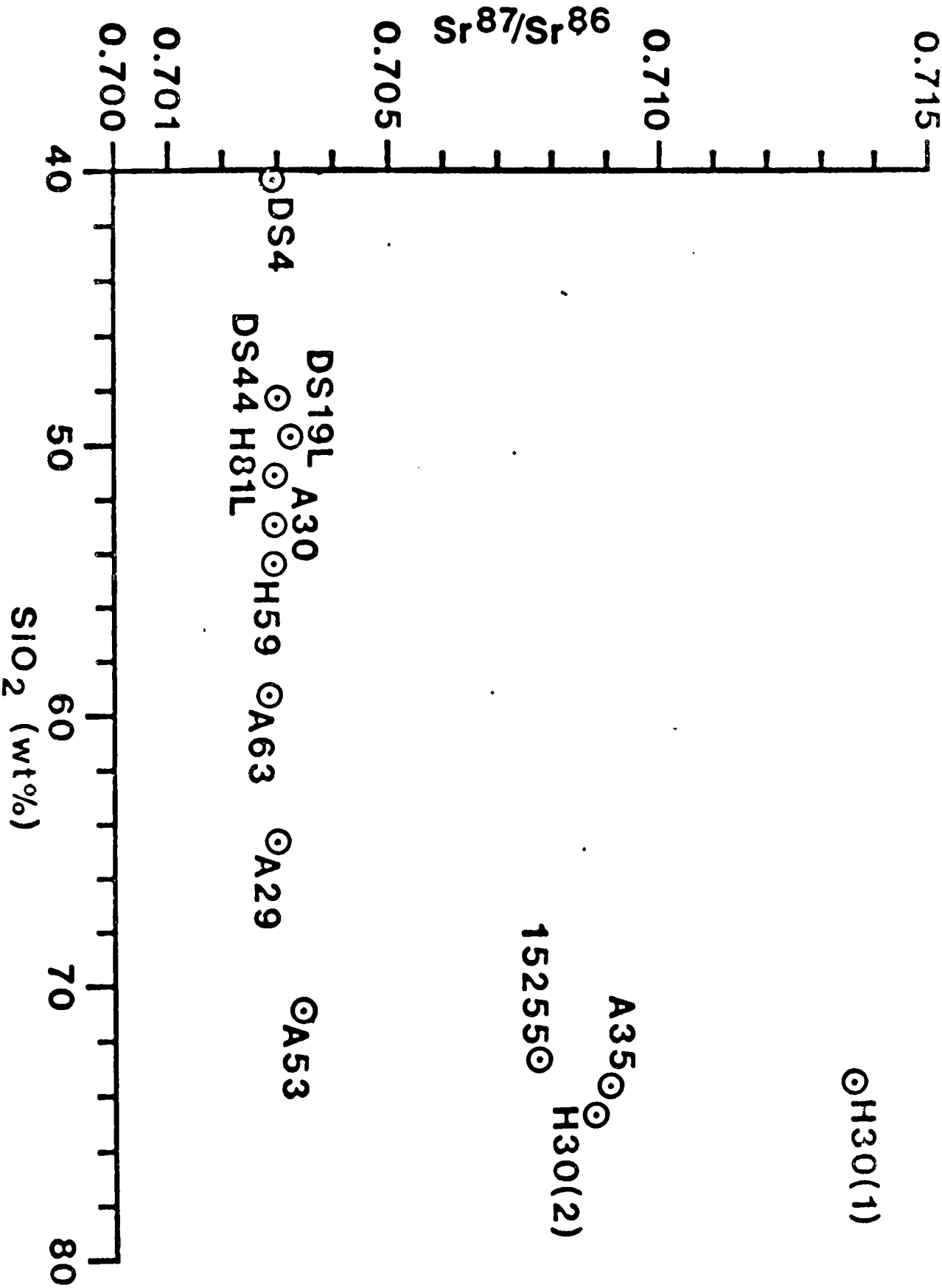


Fig 6.2 Sr^{87}/Sr^{86} vs Sr (ppm) in analysed blocks and lavas

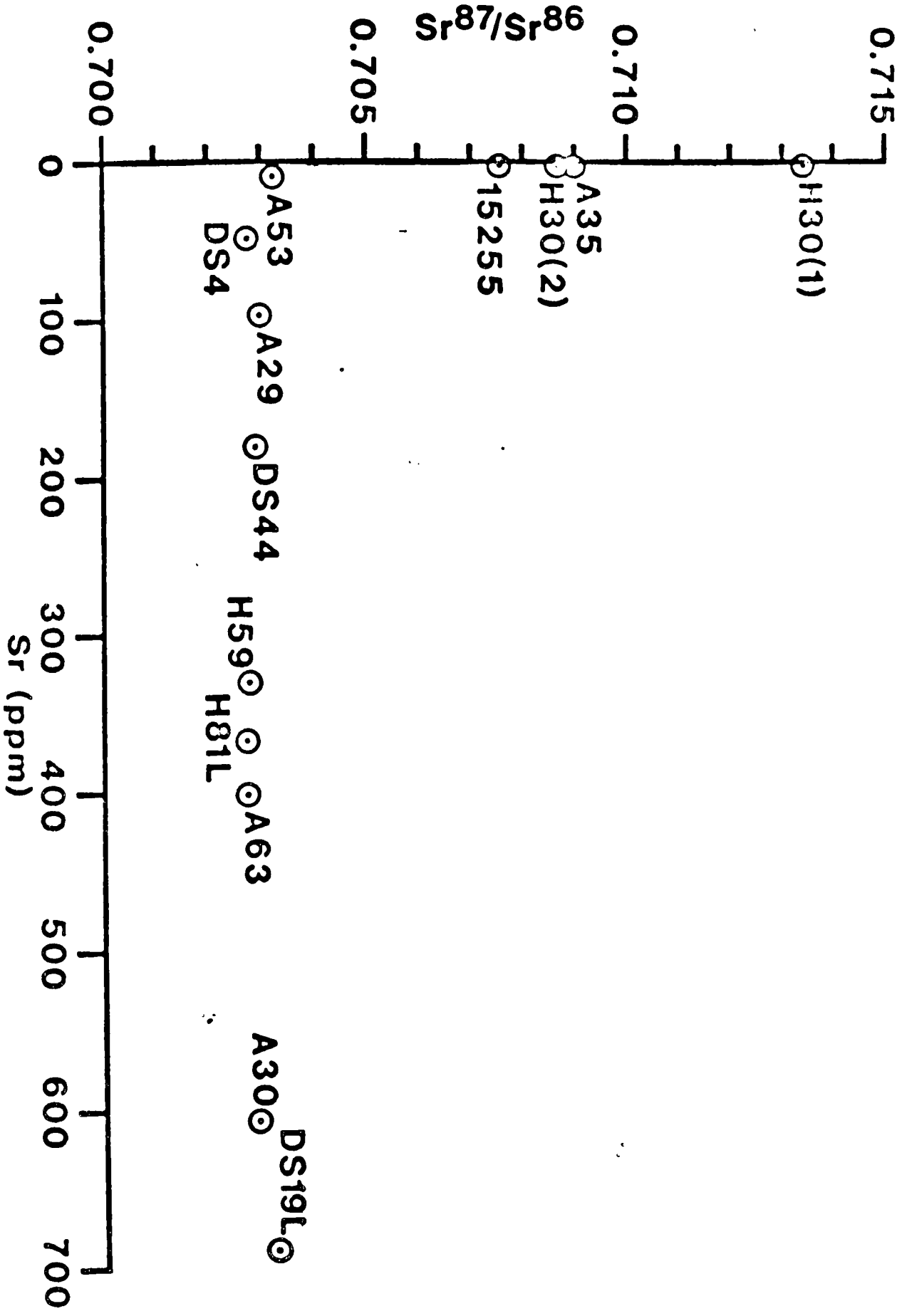


Fig 6.3 Pb^{207}/Pb^{204} vs Pb^{206}/Pb^{204} in analysed blocks and lavas M.O.R.B. field from Cohen et al(1980), oceanic sediments from Stacey and Kremers (1975)

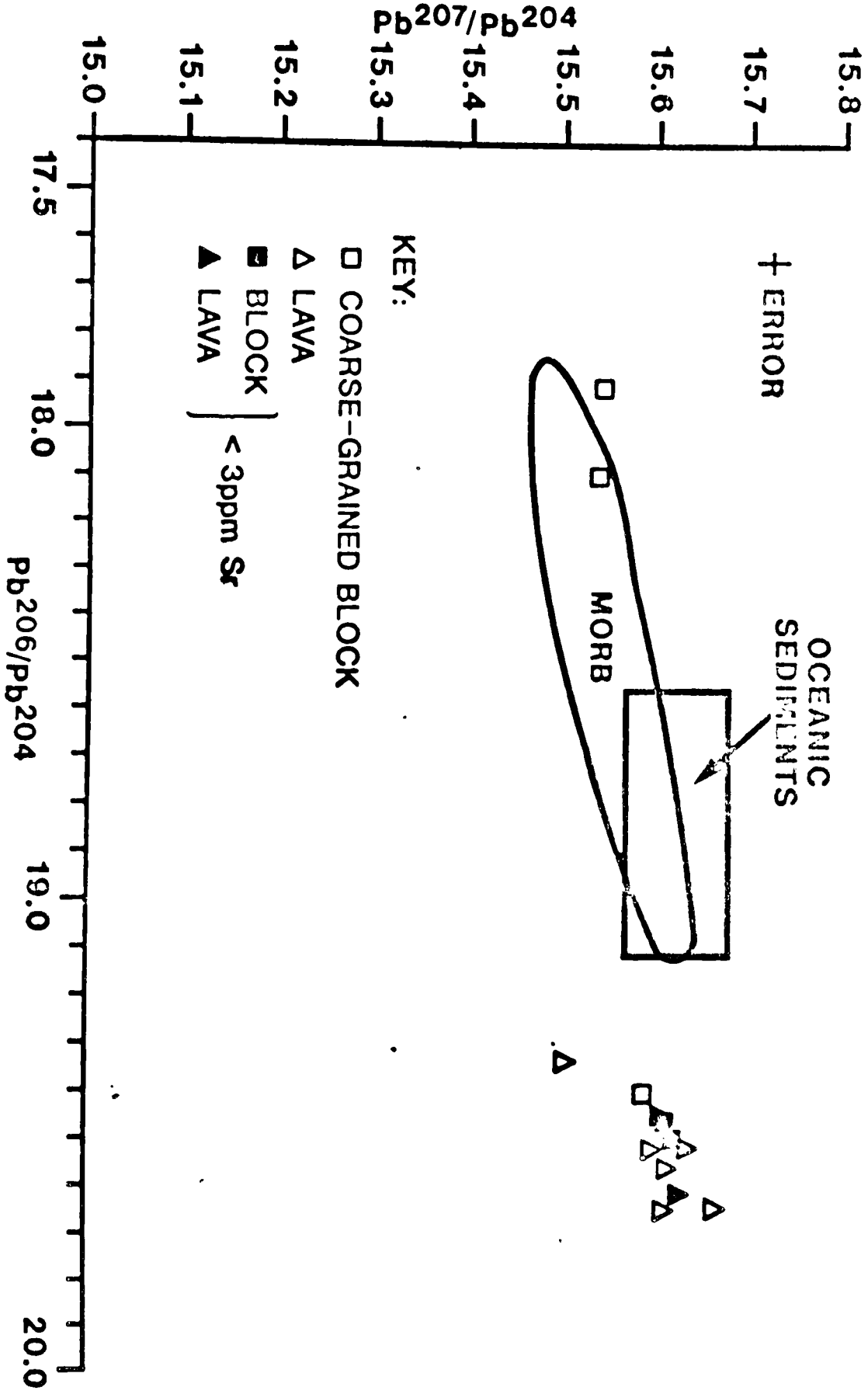


Fig 6.4 Pb^{208}/Pb^{204} vs Pb^{206}/Pb^{204} in analysed blocks and lavas M.O.R.B. field from Cohen et al (1980), oceanic sediments from Stacey and Kremers (1975)

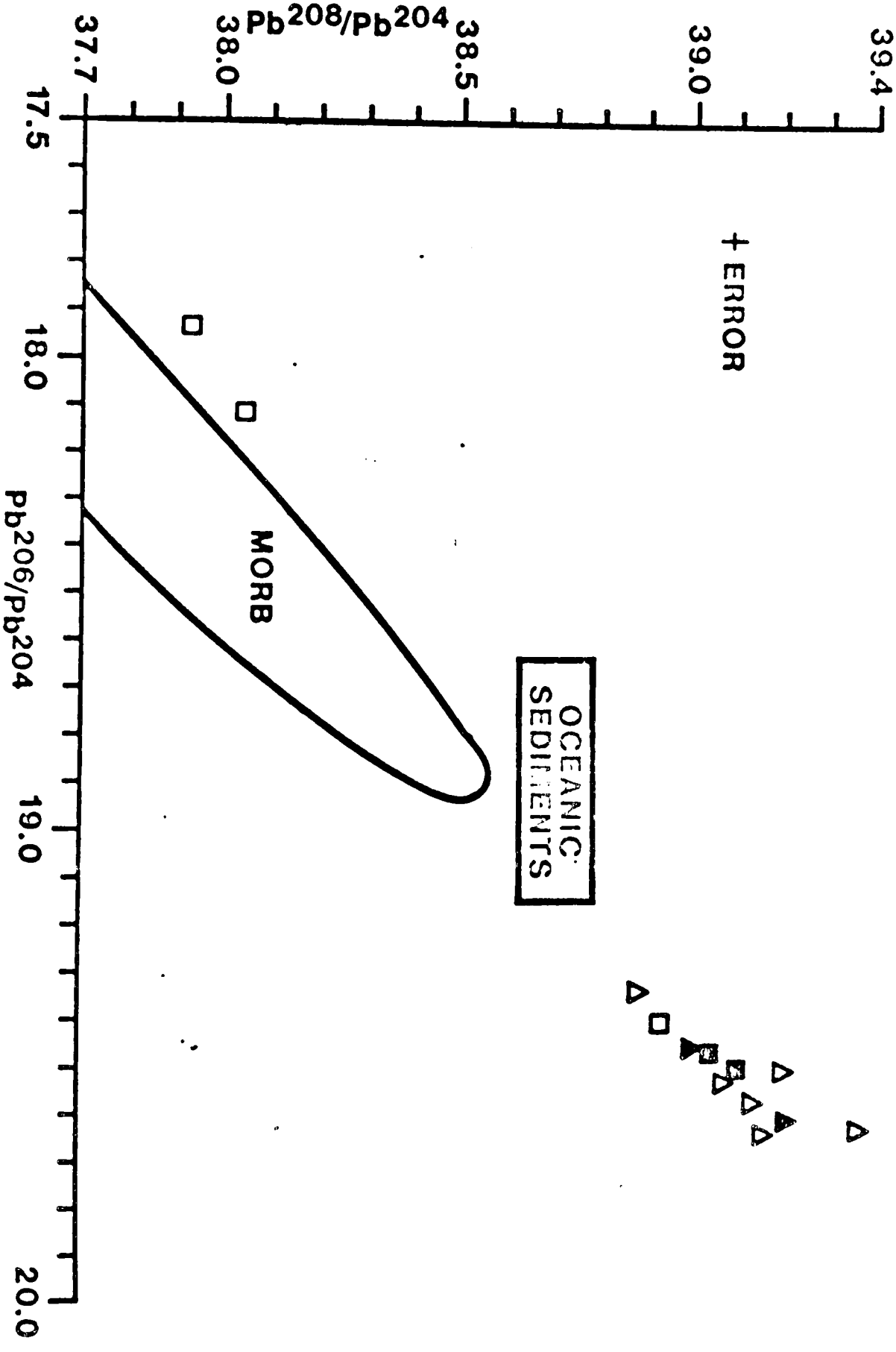
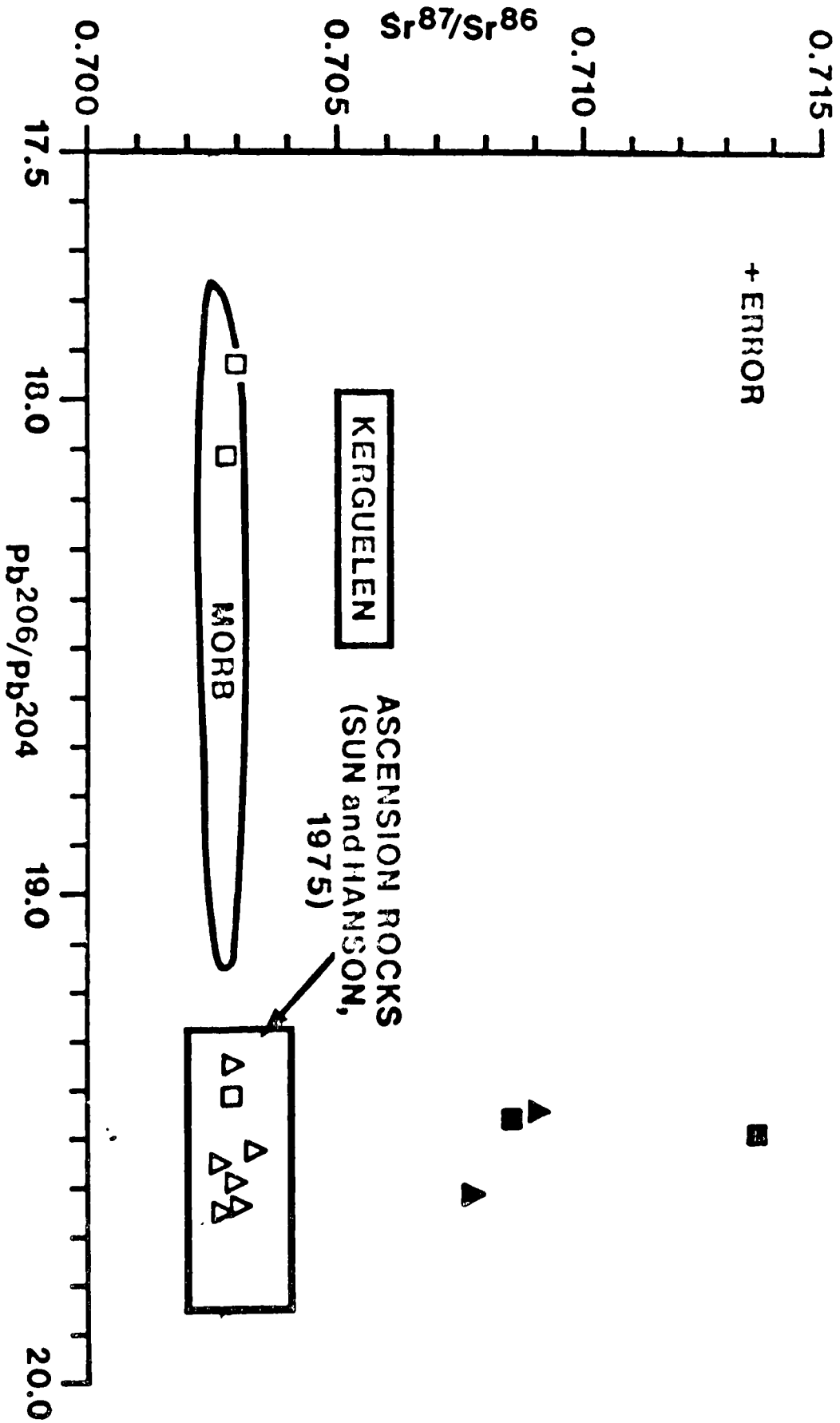


Fig 6.5 Sr^{87}/Sr^{86} vs Pb^{206}/Pb^{204} for analysed blocks and lavas Also shown are the M.O.R.B. field of Cohen et al (1980), the field for previously analysed Ascension rocks (Sun, 1980) and the field for Kerguelen (Vidal and Dosso, 1978). Those blocks and lavas with low Sr are indicated.



CHAPTER SEVEN

TABLES AND FIGURES

Table 7.1 Density of Ascension Lavas at 1250°C

Lava	SiO_2 (wt%)	Density (gcm^{-3})
15209	47.16	2.76
H48L	51.38	2.68
H5L	49.83	2.67
A30L	53.19	2.60
H53L	53.60	2.55
H90L	52.06	2.63
A63L	59.42	2.50
A29L	64.78	2.41
Ob3	70.51	2.34
A35	74.05	2.33
15006	62.67	2.44

Table 7.2a Settling Velocities of 1 cm Diameter Grains in Selected Lavas

Mineral	H5L	A63L	A29L	Ob4	Ob3	A35
	Velocity in cms^{-1}					
Olivine	0.15	6.5×10^{-3}	2.2×10^{-5}	3.2×10^{-6}	1.2×10^{-6}	2.3×10^{-7}
Cpx	0.12	5.8×10^{-3}	2.0×10^{-5}	3×10^{-6}	1.1×10^{-6}	2.1×10^{-7}
Feldspar	0.04	1.3×10^{-3}	2×10^{-6}	3×10^{-7}	1.3×10^{-7}	2.0×10^{-8}
			Velocity in $cm\ yr^{-1}$			
Ol	4.7×10^{6}	2.1×10^{5}	7.0×10^{2}	1.0×10^{2}	3.8×10^{1}	7.3
Cpx	3.8×10^{6}	1.8×10^{5}	6.3×10^{2}	9.5×10^{1}	3.5×10^{1}	6.6
Fsp	1.3×10^{6}	4.1×10^{4}	6.3×10	9.5	4.1	6.3×10^{-1}

Table 7.2b Viscosities of Lavas

Lava	Temp °C	SiO_2	ln n	n (poises)	Type
H5L	1200	49.83	5	148	basalt/hawaiite
A63L	1100	59.42	11	6.0×10^{4}	trachyandesite
A29L	1050	64.78	15	3.3×10^{6}	trachyandesite
Ob4	1030	72.08	17	2.4×10^{7}	obsidian (rhyolitic)
Ob3	1020	70.51	18	6.6×10^{7}	obsidian (rholitic)
A35	1000	74.05	20	4.9×10^{8}	comendite
A35 + 5% H_2O	1000		9	8×10^{3}	

Table 7.3 Two Pyroxene Temperature Determinations (After Wells, 1977)

Rock	Mineralogy	Temp (°C)	Interpretation
H71(1)	Qz syenite	838	Possibly primary Opx
A22(4)	Hbl monzonite	912	"
H83(10)	Gabbro	942	"
H13(1)	Syenite	899	"
H83(14)	Gabbro	971	"
17369(2)	Monzonite	908	Opx formed by reaction (sub-solidus)
174219	Syenite	862	"
15227	Gabbro	961	"
15227(VI)	Gabbro	872	"
15227(5)	Gabbro	1010	"
15227(4)	Gabbro	*1050	Primary Opx
15227(13)	Gabbro	*960	Primary Opx

* High variation due to exsolution, hence high Ca variability.

Table 7.4 Analyses of Average Ilmenites and Magnetites

Rock	HDSA5	H7(5)	DSA3	H95(7)	H60(4)
			MAGNETITE		
TiO_2	15.93	16.62	15.44	13.21	16.17
Al_2O_3	4.78	5.83	4.28	2.87	4.26
Fe_2O_3	32.84	32.43	35.24	40.06	35.06
FeO	39.25	37.79	38.09	38.92	39.08
MnO	0.46	0.36	0.41	0.44	0.43
MgO	4.25	6.02	4.38	2.52	4.53
Total	97.51	99.05	97.92		99.63
			3 Cations		
Ti	0.47	0.44	0.43	0.37	0.44
Al	0.22	0.24	0.18	0.13	0.18
Fe^{3+}	0.95	0.86	0.97	1.13	0.95
Fe^{2+}	1.08	1.12	1.17	1.23	1.17
Mn	0.01	0.01	0.01	0.01	0.01
Mg	0.25	0.32	0.23	0.14	0.24
			ILMENITE		
TiO_2	48.00	46.62	46.98	45.36	47.46
Al_2O_3	0.53	0.77	0.64	0.45	0.77
Fe_2O_3	12.00	15.96	15.26	17.00	15.61
FeO	33.33	29.69	30.84	32.59	29.92
MnO	0.47	0.32	0.37	0.43	0.24
MgO	5.31	6.59	6.12	4.19	6.97
Total	99.64	99.95	100.26	99.91	101.01
			2 Cations		
Ti	0.88	0.85	0.85	0.84	0.85
Al	0.02	0.01	0.02	0.01	0.02
Fe^{3+}	0.22	0.29	0.28	0.31	0.30
Fe^{2+}	0.68	0.60	0.62	0.68	0.60
Mn	0.01	0.01	0.01	0.01	0.01
Mg	0.19	0.24	0.22	0.15	0.25

Table 7.5 Calculated Temperatures using the Method of Fig. 7.4 to Produce Max. Uncertainty in Mgt Ilm Values

	HDSA5	DSA3	H7(5)	H95(7)	H60(4)
T max (°C)	1182	200	1541	1045	1262
T min	874	906	922	936	926
Av T°C	1028	1052	1232	991	1094
T B/L	960	1000	1000	1000	1050
ln aO_2 max	-16.72	-15.64	-6.66	-20.1	-13.8
min	-26.6	-25.31	-23.86	-25.2	-24.2
av	-21.66	-20.48	15.26	-22.7	-19
B/L	-26	-24	-24	-23	-24

B/L = temperature using graphs of Buddington and Lindsley (1964).

Table 7.6

The igneous plagioclase geothermometer of Kudo and Weill (1970).

$$\ln \frac{\lambda}{\sigma} + \frac{12900\,\phi'}{T} = A \cdot T - K$$

λ, σ and ϕ' are composition variables

A and K are P_{H_2O} variables

P_{H_2O} (kb)	A	K
0	0.01034	17.24
0.5	0.01105	17.86
1.0	0.01114	17.67
5.0	0.01218	16.63

$$T = \frac{K + \ln \frac{\lambda}{\sigma} + \sqrt{\left[K + \ln \frac{\lambda}{\sigma}\right]^2 + 51600\,A\,\phi'}}{-2A}$$

Table 7.7 Variables for the Igneous Plagioclase Thermometer of Kudo and Weill, 1970

	σ max	σ min	λ	ϕ'	X An / (X An + X Ab) max	X An / (X An + X Ab) min
15243B		0.334	2.09	.298	.75	
H59(2)		1.22	4.37	0.378	0.45	-
DS19L	0.49	0.45	1.03	0.239	0.69	0.67
H81L	0.49	0.43	2.15	-.287	0.70	0.67
17345	6.69	3.35	25.93	-.528	0.23	0.13
17453	4.56	4.00	18.37	-.498	0.20	0.18
A63L	1.78	1.33	6.58	-.415	0.43	0.36
H90L	0.64	0.35	2.09	-.284	0.74	0.61

Where $\sigma = \frac{X\ Ab}{X\ An}$

$$\lambda = \left(\frac{X\ Na . X\ Si}{X\ Ca . X\ Al}\right)_{melt}$$

$$\phi' = (X\ Ca + X\ Al - X\ Si - X\ Na)_{melt}$$

Table 7.8 Plagioclase-Liquid Equilibrium Temperatures (Kudo and Weill, 1970)

	Max		Min	
Sample	Dry	$pH_2O = 1$	Dry	$pH_2O = 1$
15243B	1341	1251		
H59(2)	1197	1112		
DS19L	1283	1200	1273	1190
H81L	1326	1238	1311	1224
17345	1119	1026	1012	923
17453	1083	995	1065	976
A63L	1197	1108	1158	1073
H90L	1349	1259	1307	1195

Table 7.9 Liquid Norms of Selected Lavas

	Meso-stasis 15243B	DS19L	H81L	17345	17453	A63L	H59(2)	H90L
SiO_2	69.15	59.54	58.08	72.23	71.07	67.89	62.60	59.35
TiO_2	1.66	2.57	2.21	0.35	0.63	1.15	2.81	1.73
$KAlO_2$	4.70	2.38	1.96	5.24	6.39	3.57	3.70	1.98
$NaAlO_2$	7.03	4.46	8.03	14.49	14.22	11.92	10.17	8.09
$CaAl_2O_4$	7.96	8.36	5.43	0.82	1.02	3.73	1.91	6.05
$MgAl_2O_4$	0.77	-	-					
MgO	2.80	8.66	8.92	0.66	0.23	3.78	4.67	9.57
CaO	-	2.44	4.98	1.10	1.49	1.62	6.32	4.33
FeO	5.93	11.97	10.42	4.39	5.28	6.49	12.35	8.95

Table 7.10 Temperatures of Plagioclase-melt Equilibrium (Drake's Thermometer) (°C)

	Max		Min	
Sample	P_{dry}	P_2	P_{dry}	P_2
15243B	1035	880		
H59(2)	860	742		
DS19L	787	679	769	670
H81L	892	768	870	751
17345	973	830	933	801
17453	959	821	931	797
A63L	943	809	915	786
H90L	942	807	852	735

Table 7.11 Plagioclase and Olivine Saturation Temperatures and Equilibrium Compositions

Sample	Plag. Saturation Surface T(°C)	Ol. Saturation Surface T(°C)	Plag.Calc	Plag.obs	Ol.Calc	Ol.obs
15243B	1160	975	An_{68}	An_{75-}	Fo_{68}	Fo_{76-74}
H59(1)	1086	1067	An_{45}	An_{45-0}	Fo_{59}	Fo_{40-30}
H59(2)	1067	1061	An_{42}	An_{45-0}	Fo_{57}	Fo_{30}
DS19L	1238	1139	An_{82}	An_{69-67}	Fo_{71}	Fo_{77-70}
H81L	1189	1139	An_{67}	An_{70-67}	Fo_{74}	Fo_{83-80}
17345	1048	840	An_{19}	An_{23-13}	Fo_{33}	Fo_{20-17}
17453	1057	829	An_{23}	An_{20-18}	Fo_{13}	Fo_{32-27}
A63L	1060	1013	An_{48}	An_{43-36}	Fo_{66}	Fo_{65}
H90L	1206	1141	An_{69}	An_{74-61}	Fo_{78}	Fo_{85-83}
H39L	1123	1002	An_{50}	An_{70-50}	Fo_{64}	Fo_{68-56}

Table 7.12 17364 Liquidus Temperatures Recalculated with Additional FeO

wt %	17364	+1% FeO	+3%	+5%	+7%
SiO_2	48.45	47.97	46.99	46.03	45.07
TiO_2	3.48	3.45	3.38	3.31	3.24
Al_2O_3	14.71	14.56	14.27	13.97	13.67
FeO	11.83	12.71	14.47	16.24	18.00
MnO	.25	.25	.24	.24	.22
MgO	4.52	4.47	4.38	4.29	4.20
CaO	8.4	8.32	8.15	7.98	7.81
Na_2O	4.22	4.18	4.09	4.01	3.93
K_2O	1.48	1.47	1.44	1.41	1.37
P_2O_5	1.99	1.97	1.95	1.89	1.83
Total	99.33	99.35	99.36	99.37	99.34
Ol.surf. temp.	1122	1126.6	1133.9	1141.1	1148.2
Ol.(Fo) comp.	69.41	67.63	64.3	61.09	58.1
Plag.T	1157	1153.1	1146.0	1137.3	1128.9
Plag.(An) comp.	58.68	59.14	60.2	61.4	62.7

Fig 7.1 Density of selected lavas density of phenocrysts in equilibrium with magmas of increasing wt% SiO_2.

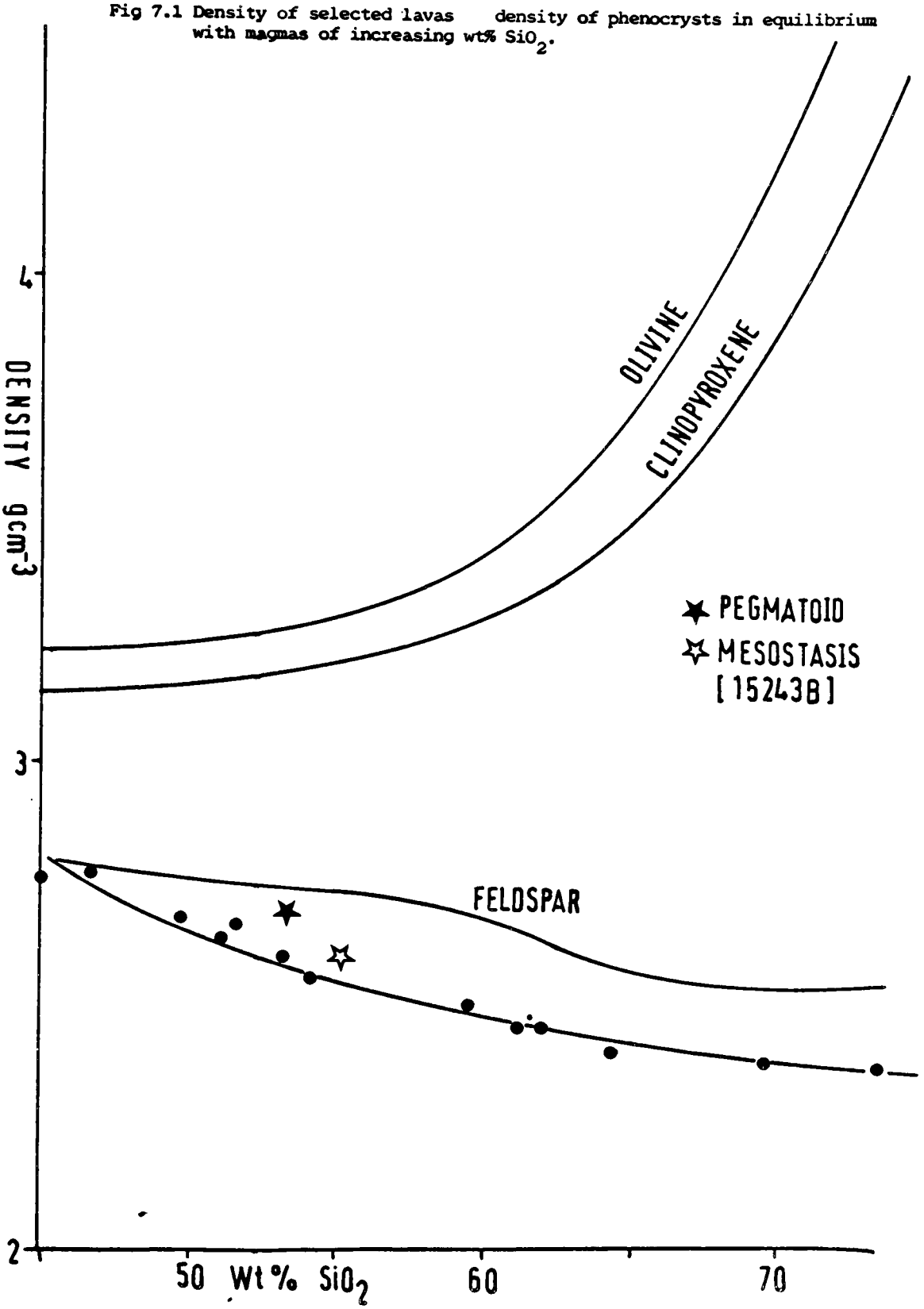


Fig 7.2 $\ln\eta$ vs $10^4/T$ for selected lavas

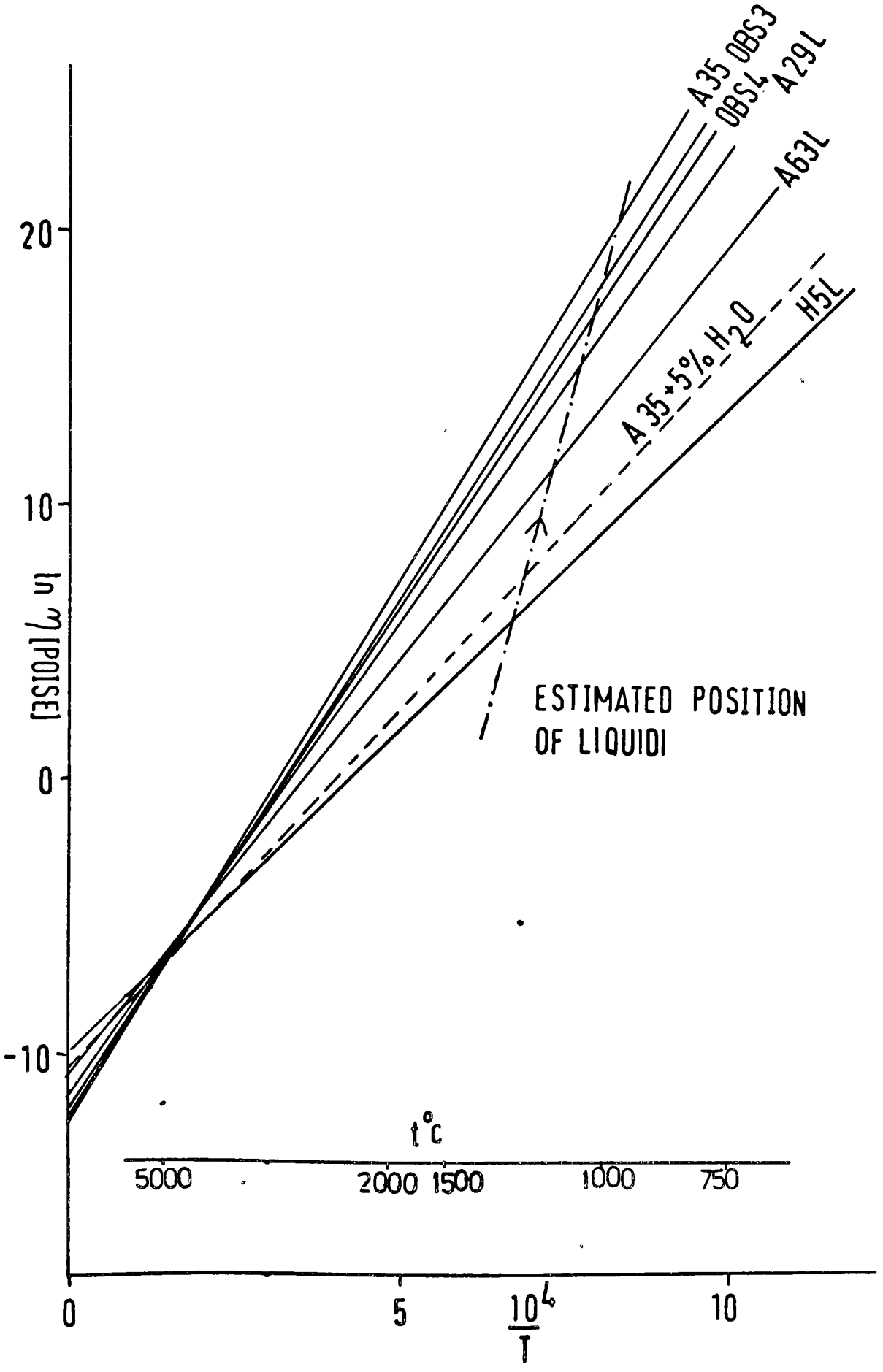


Fig 7.3 X ulvospinel vs X ilmenite in unoxidised blocks.
Solid lines = aO_2 contours, dashed lines = $t^{\circ}c$ contours.

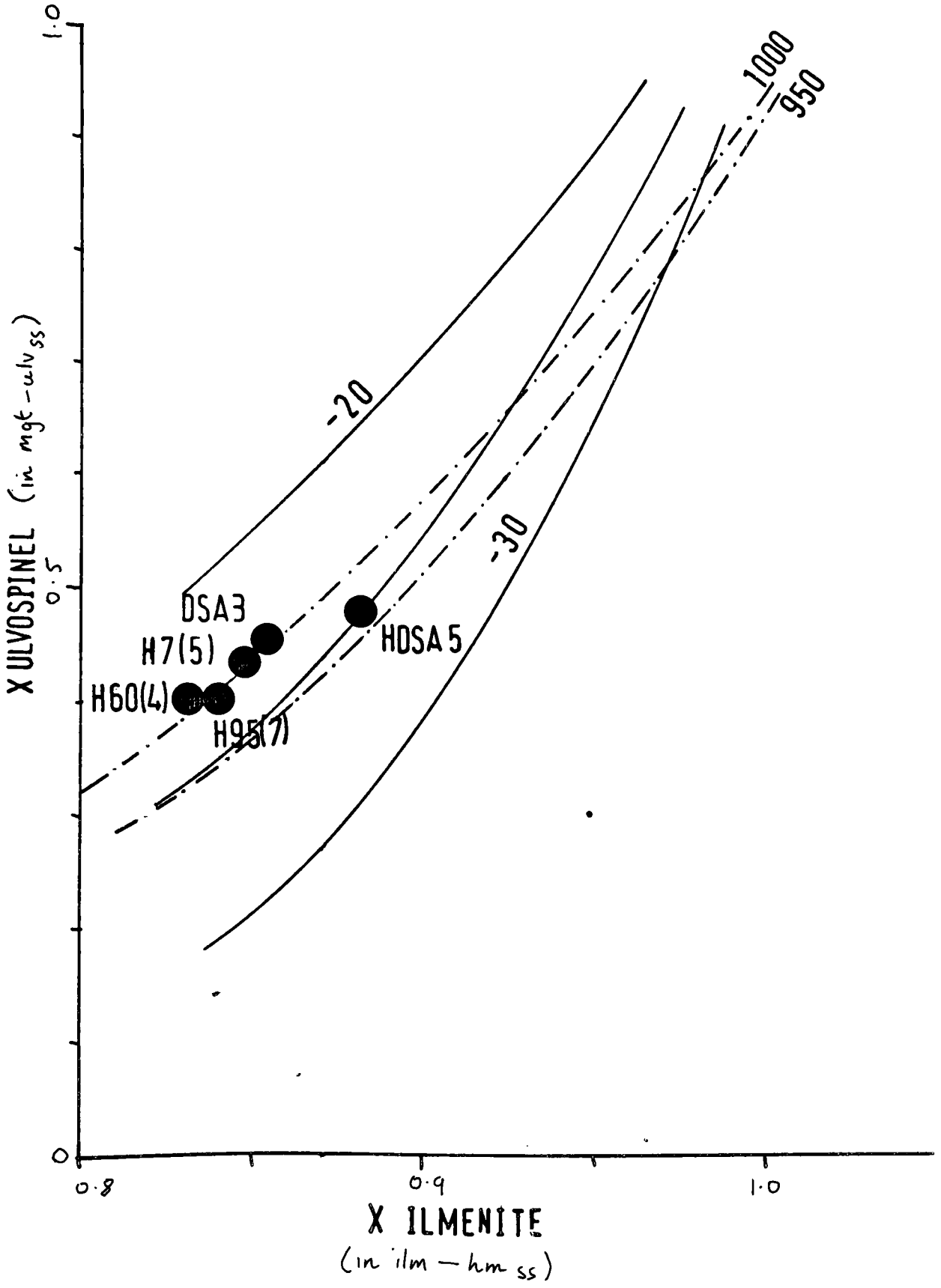
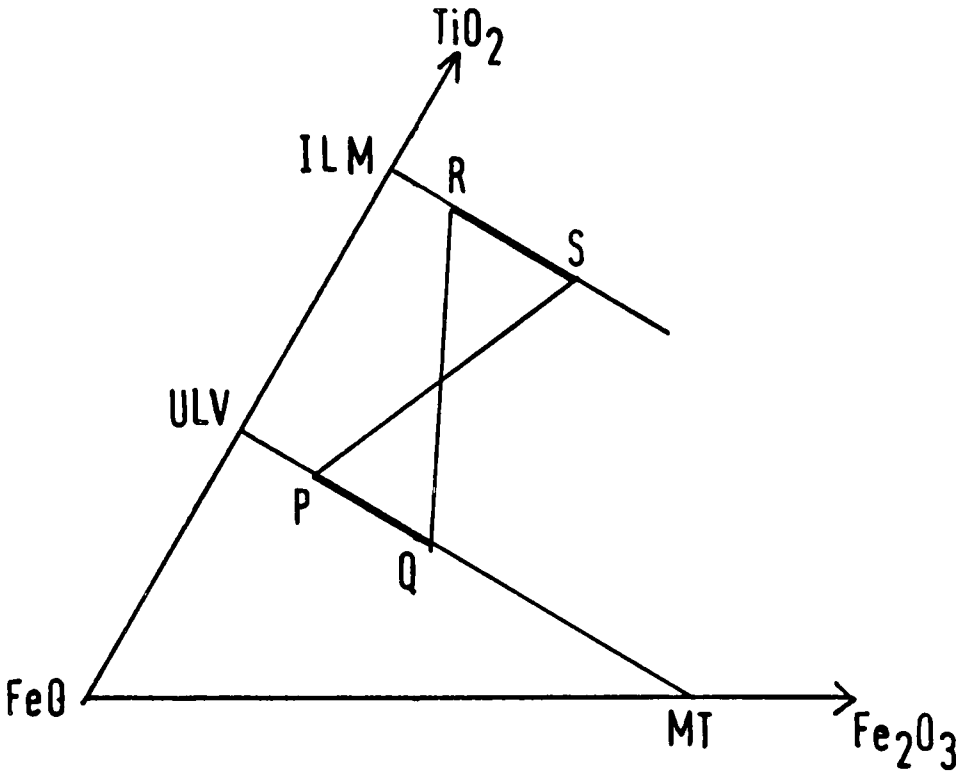


Fig 7.4 The combination of uncertainties in Fe-Ti oxide compositions which produces the maximum variation in T and aO_2.



$$\ln\left(\frac{Xulv \,.\, Xhem}{Xmt \,.\, Xilm}\right) = -\frac{8155}{T} + 4.59$$

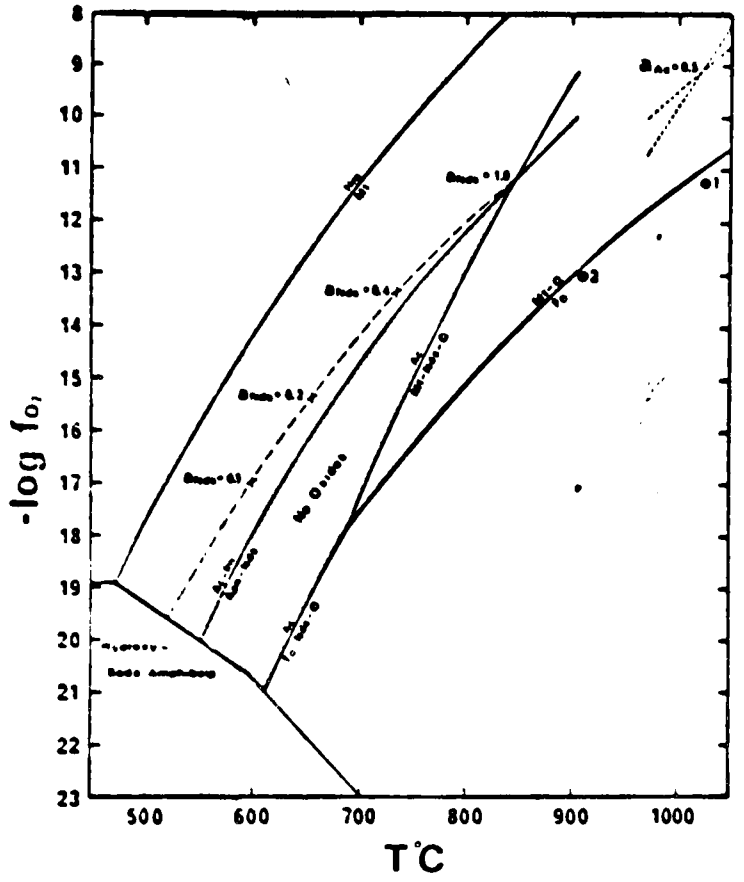
$$T = \frac{8155}{4.59 - \ln\left(\frac{Xulv \,.\, Xhem}{Xmt \,.\, Xilm}\right)}$$

T_{max} is when ln(.....) is max ie (.....) is max

$\frac{Xulv \,.\, Xhem}{Xmt \,.\, Xilm}$ is max for P-S , min for Q-R

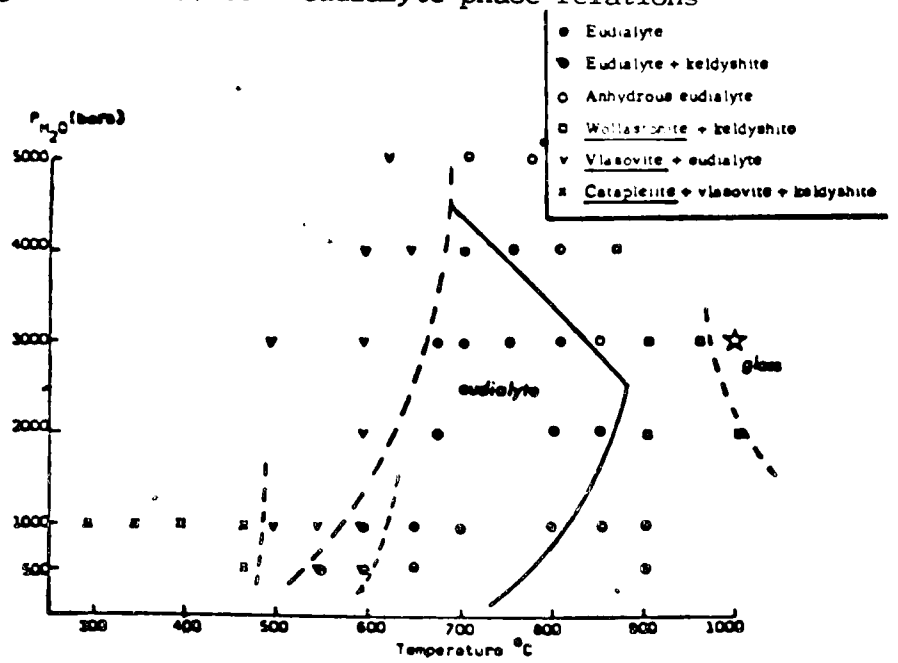
$$\ln aO_2 = \ln (x^2mt.x^6ilm/x^6ulv).(xulv.xhem/xmt.xilm)^{10.702} - 4.94$$

$\ln aO_2$ is max when xulv.xhem/xmt.xilm is P - S



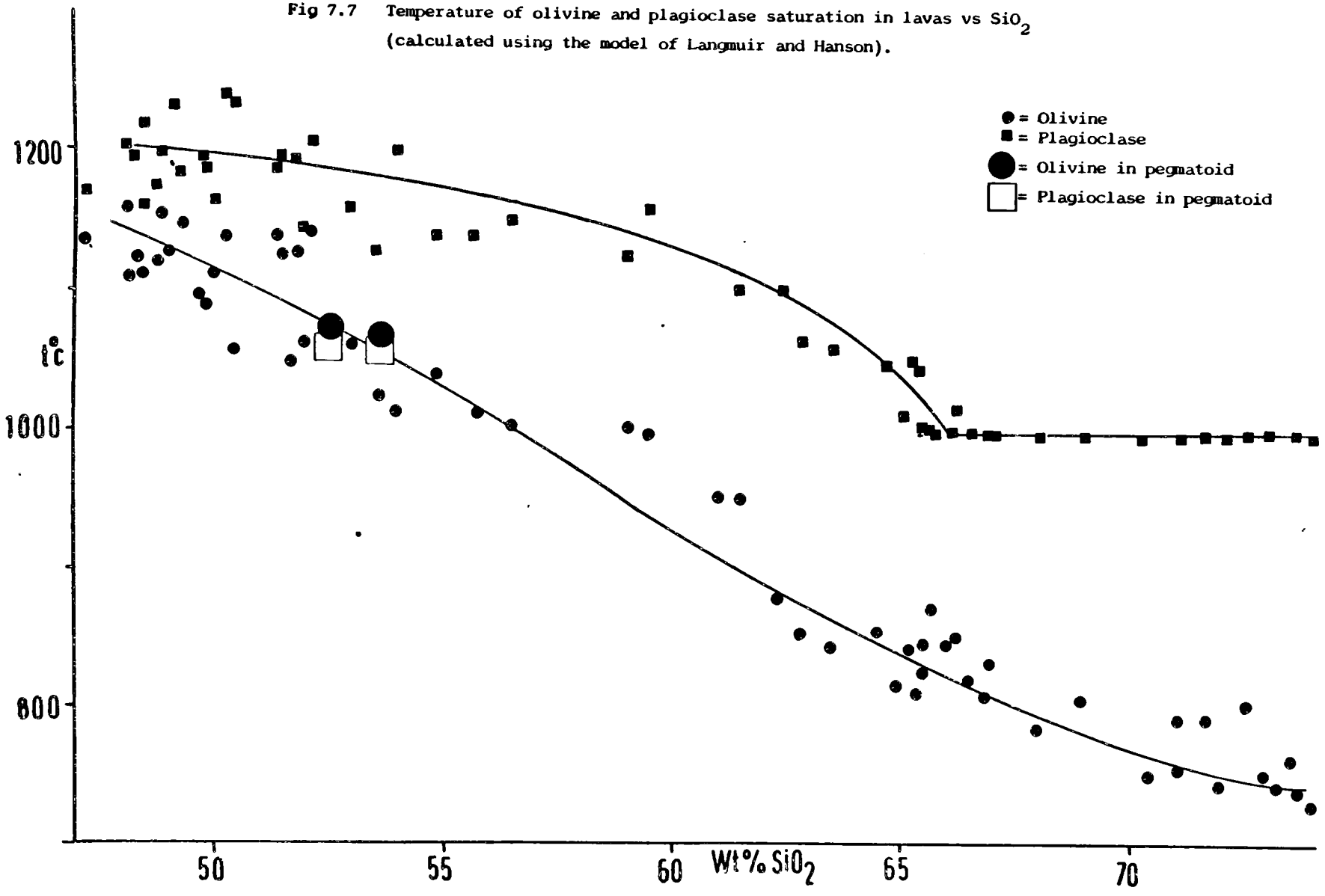
Fugacity of oxygen *vs.* temperature diagram showing the *nocerite* field discussed in text. The upper limit of stability of the hydroxy-richterite-arfvedsonite amphiboles is taken directly from ERNST (1962). The abbreviations are: *Hm* hematite; *Mt* magnetite; *Ac* acmite; *Q* quartz; *Fa* fayalite; *Nds* sodium disilicate; *Aen* aenigmatite; *Im* ilmenite. The magnetite-hematite buffer curve is from EUGSTER and WONES (1962), the quartz fayalite magnetite buffer curve is from WONES and GILBERT (1968). The dashed curve is the locus of intersections of the two curves, *Mt-Nds Q Ac* and *Aen-Nds-Ac Im*, for varying activities of *Nds*, at constant unit activity of acmite, magnetite and ilmenite. The values of the activity (a) of *Nds* are shown at several intersections (x) along this dashed curve. The intersection of the two curves is also shown (small dashed lines) for an activity of acmite = 0.5, with unit activity for the other components. Points 1 and 2 are equilibration data for coexisting Fe-Ti oxide microphenocrysts in pantellerites (CARMICHAEL, 1967.)

Fig 7.6 Vlasovite - eudialyte phase relations



Preliminary diagram showing the field of synthesis of eudialyte. Only the dominant phases are shown for the other fields.

Fig 7.7 Temperature of olivine and plagioclase saturation in lavas vs SiO_2 (calculated using the model of Langmuir and Hanson).



CHAPTER EIGHT

TABLES AND FIGURES

Table 8.1 Chemical and Petrological Details of Samples Analysed for REE

Sample No.	Locality	Wt % SiO_2	Mineralogy and Rock Type
DS44	Dark Slope Crater	48.30	Plagioclase gabbro cumulate
H59	Cricket Valley	54.52	Pegmatoid vein in H81L
H81L	Cricket Valley	51.42	Hawaiite lava
A29	Cross Hill	64.78	Trachyandesite lava
A63	South East Head	59.42	Trachyandesite lava
H30(2)	Five Mile Post	75.42	Granite block
A35	Little White Hill	74.05	Comendite lava (dome)
H30(1)	Five Mile Post	74.00	Granite block

SiO_2 determined by electron probe methods of Dickin and Exley (1981)

Table 8.2 REE and Y Analyses for Eight Lavas and Blocks (ppm)

	A29	A35	A63	DS44	H30(1)	H30(2)	H59	H81L
La	71.1	83.7	57.3	ND	108.5	88.9	53.1	28.0
Ce	153.3	189.3	123.4	(3.2)	222.0	178.8	131.7	64.5
Nd	72.8	85.8	62.6	ND	108.7	88.9	76.7	37.3
Sm	14.3	18.8	12.8	ND	21.8	18.8	15.3	7.8
Eu	6.10	1.17	4.21	0.23	1.89	1.63	4.72	2.48
Gd	(13.8)	16.8	11.8	ND	(20.4)	ND	14.5	(7.9)
Tb	2.06	3.32	2.01	ND	3.22	2.59	2.65	1.32
Tm	0.94	1.94	(0.86)	ND	1.75	(1.68)	(0.99)	(0.52)
Yb	5.95	12.46	5.22	(0.24)	11.05	12.20	6.30	3.37
Lu	(0.87)	(1.45)	(0.70)	ND	1.72	2.34	(1.05)	ND
Y	60.1	113.9	55.9	2.6	85.7	68.5	71.7	36.2
Th	9.40	20.80	7.10	ND	18.90	18.90	6.40	3.91
Ta	6.75	13.55	5.50	ND	16.20	17.30	5.40	2.98
Hf	14.50	25.00	10.90	ND	41.20	54.50	10.8	6.00
Sc	11.5	1.3	12.0	14.6	1.1	1.1	24.8	25.0
Co	ND	16.7	6.1	24.1	0.2	ND	38.2	43.3

ND = not detected

Data in brackets have Gamma fit errors of 10-20% (1σ)

Y by XRF, others by INAA (Open University

Table 8.3 Effect of Eudialyte on REE Content of H30(1) (ppm)

	A35	H30(2)	H30(1)	H30(1) - Eudialyte
La	83.7	88.9	108.5	95.4
Ce	189.4	178.8	222.0	197.2
Nd	85.8	88.9	108.7	98.2
Sm	18.8	18.8	21.8	19.0
Eu	1.17	1.63	1.89	
Gd	16.8	-	(20.4)	13.2
Tb	3.32	2.59	3.22	-
Tm	1.94	(1.68)	1.75	-
Yb	12.46	12.20	11.05	9.45
Lu	(1.45)	2.34	1.72	-
Y	113.9	68.5	85.7	43.9

Table 8.4 Max. and Min. Y_N and Ce_N, and Ce_N/Y_N for the Same Analyses of Zircons

Rock	Ce_N	Y_N	Ce_N/Y_N
17360(111)	3.5×10^2	2.7×10^3	0.13
	-	1.0×10^3	
15231A	2.3×10^2	3.1×10^3	0.07
	-	1.9×10^3	
H49(16)	2.3×10^2	2.4×10^3	0.10
	-	5.6×10^2	
15231 b	5.2×10^3	7.4×10^4	0.07
	4.6×10^2	1.6×10^4	0.03
17318P	1.1×10^4	1.4×10^3	0.08
	2.3×10^2	1.2×10^3	0.19
K17318	4.6×10^2	1.6×10^4	0.03
	1.9×10^3	3.1×10^2	0.06
15226(17)	2.3×10^2	1.2×10^3	0.19
	1.2×10^2	2.0×10^2	0.06
H15231(6)	8.9×10^3	5.9×10^3	1.5
	2.3×10^2	3.1×10^2	0.7
H21(12)	1.8×10^3	2.2×10^4	0.08
	8.1×10^2	1.5×10^4	0.05
H21(9)	1.2×10^2	2.2×10^3	0.06
	-	8.7×10^2	-
H39(2)	1.2×10^2	2.1×10^3	0.06
	3.6×10^2	1.6×10^3	0.23
15226(4)	-	1.6×10^3	-
	1.2×10^2	4.6×10^2	0.26

Table 8.5 Max. and Min. Ce_N and Y_N, and Ce_N/Y_N for the Same Analyses of Apatites from Ascension Blocks

Rock	Ce_N	Y_N	Ce_N/Y_N	Av Feldspar
H49(2)	6.1×10^3	3.6×10^2	16.9	An_{50}
"	2.5×10^3	3.1×10^2	8.1	An
H59	3.7×10^3	6.1×10^2	6.1	An_{40} (initial)
"	1.3×10^3	5.6×10^2	2.3	
H13(1)	9.5×10^3	1.0×10^3	8.6	Or_{20}
	8.6×10^3	1.3×10^3	7.3	
15226(17)	4.0×10^3	1.1×10^3	3.6	An_0 (highly zoned)
	3.6×10^3	8.2×10^2	4.4	
H32(1)	3.2×10^3	4.1×10^2	7.8	An_{40}
	2.4×10^3	2.04×10^2	11.8	
H61(2)	5.3×10^3	3.6×10^2	14.7	An_{40}
	4.4×10^3	4.6×10^2	9.6	
DSA(3)	1.7×10^3	2.0×10^2	8.5	An_{52}
	1.2×10^3	2.0×10^2	6.0	
17360(iii)	1.1×10^4	1.5×10^3	7.3	An_0 (Anorthoclase)
	8.4×10^3	1.5×10^3	5.6	
H49(1)	5.5×10^3	4.6×10^2	12.0	An_{60}
	2.3×10^3	2.6×10^4	8.8	
H83(6)	3.2×10^3	3.1×10^2	10.3	An_{60}
	3.2×10^3	2.0×10^2	16.0	
H49(10)	1.13×10^4	9.7×10^2	11.6	An_0 (Anorthoclase)
	8.9×10^3	6.1×10^2	14.6	

Fig 8.1 REE profiles for lavas and blocks analysed by INAA.
N.B. in DS44 only Ce and Eu above detection limit and Gd estimated for H30(2).

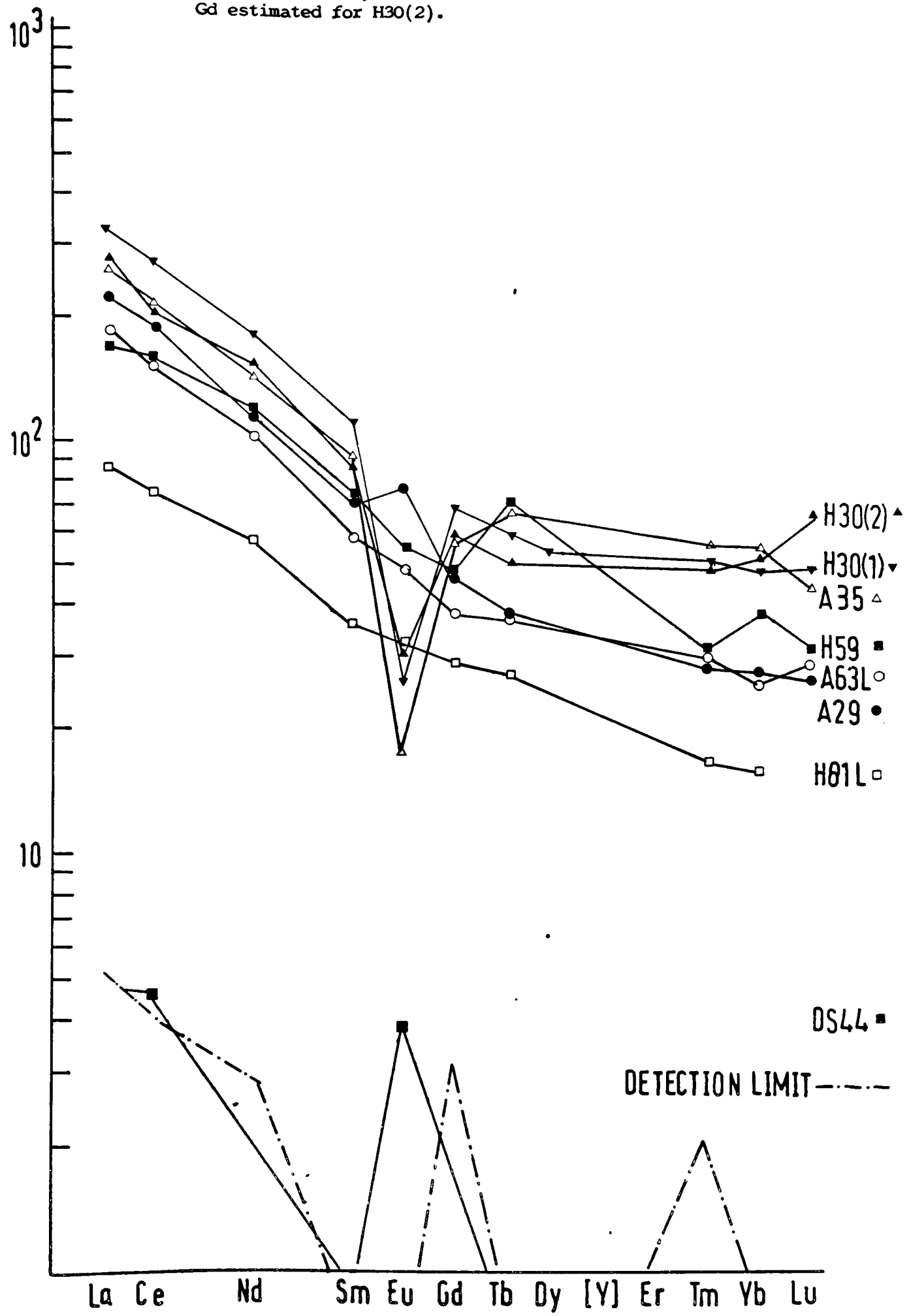


Fig 8.2 REE profile of average Ascension granite and estimated profile for coexisting zircon (using KD s of Nagasawa, 1970). Also plotted are max and min Y_N values for analysed granite blocks.

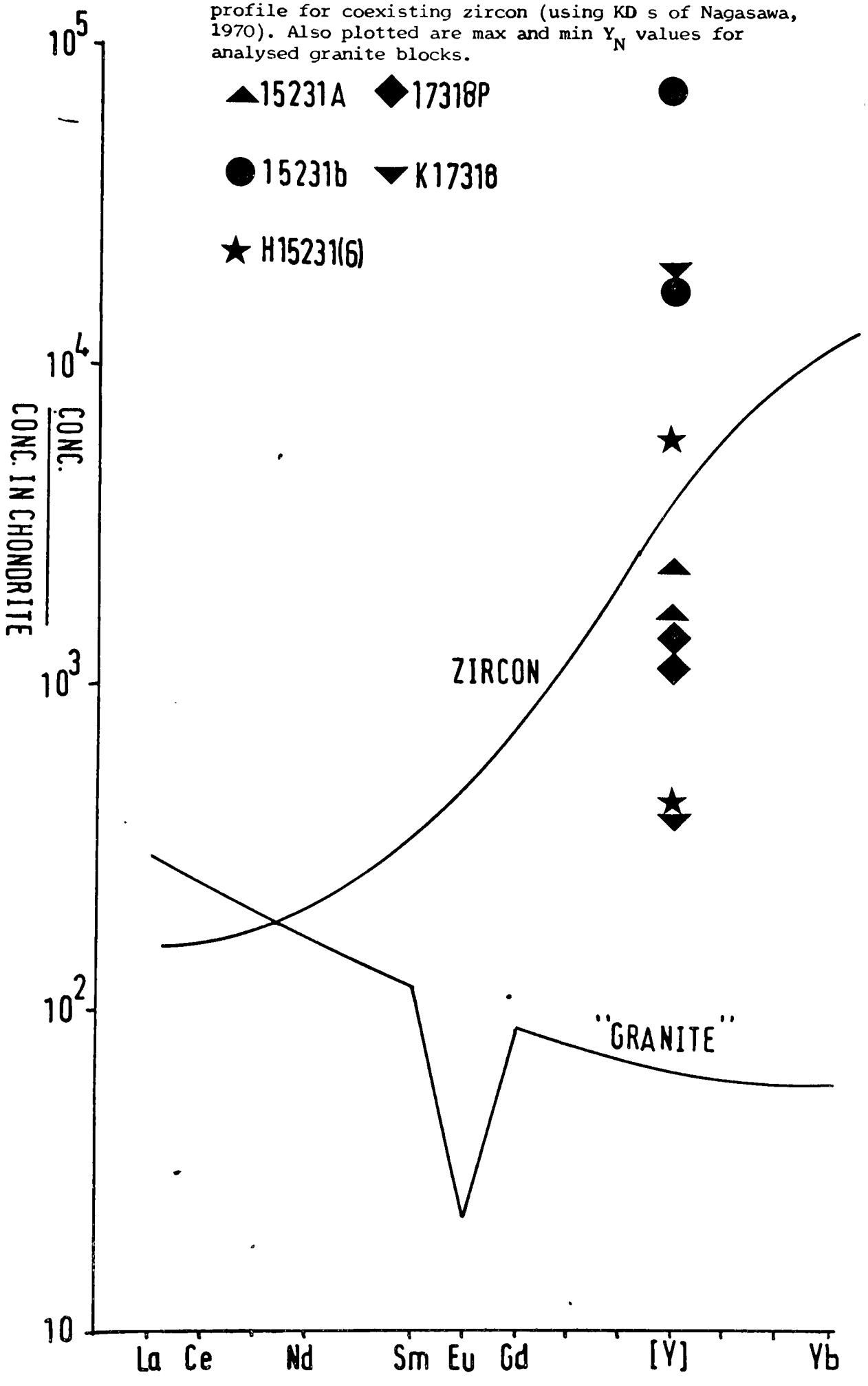


Fig 8.3 Range in Ce_N/Y_N vs feldspar composition in analysed apatites.

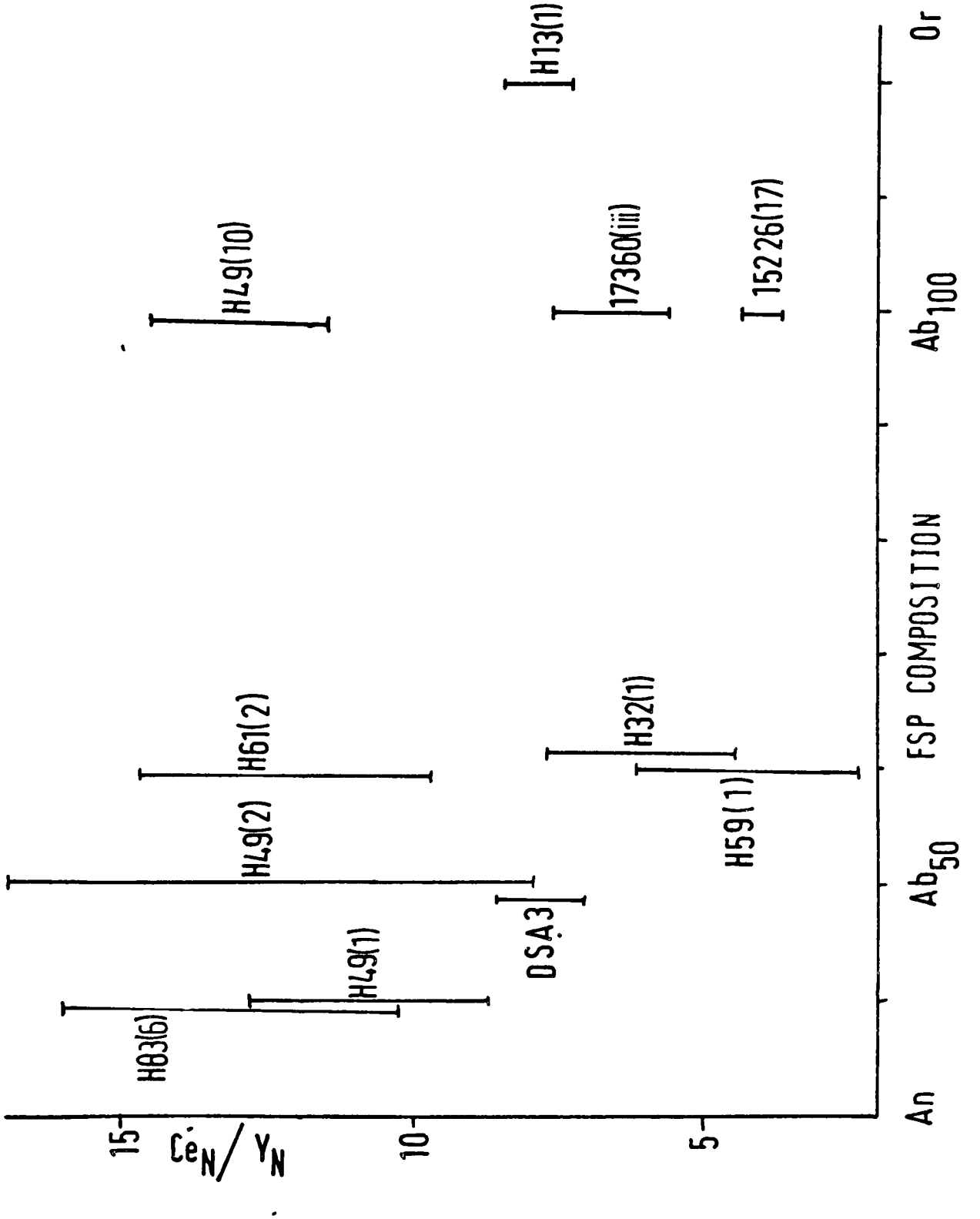


Fig 8.4 Ce_N and Y_N in apatite vs composition of coexisting feldspar.

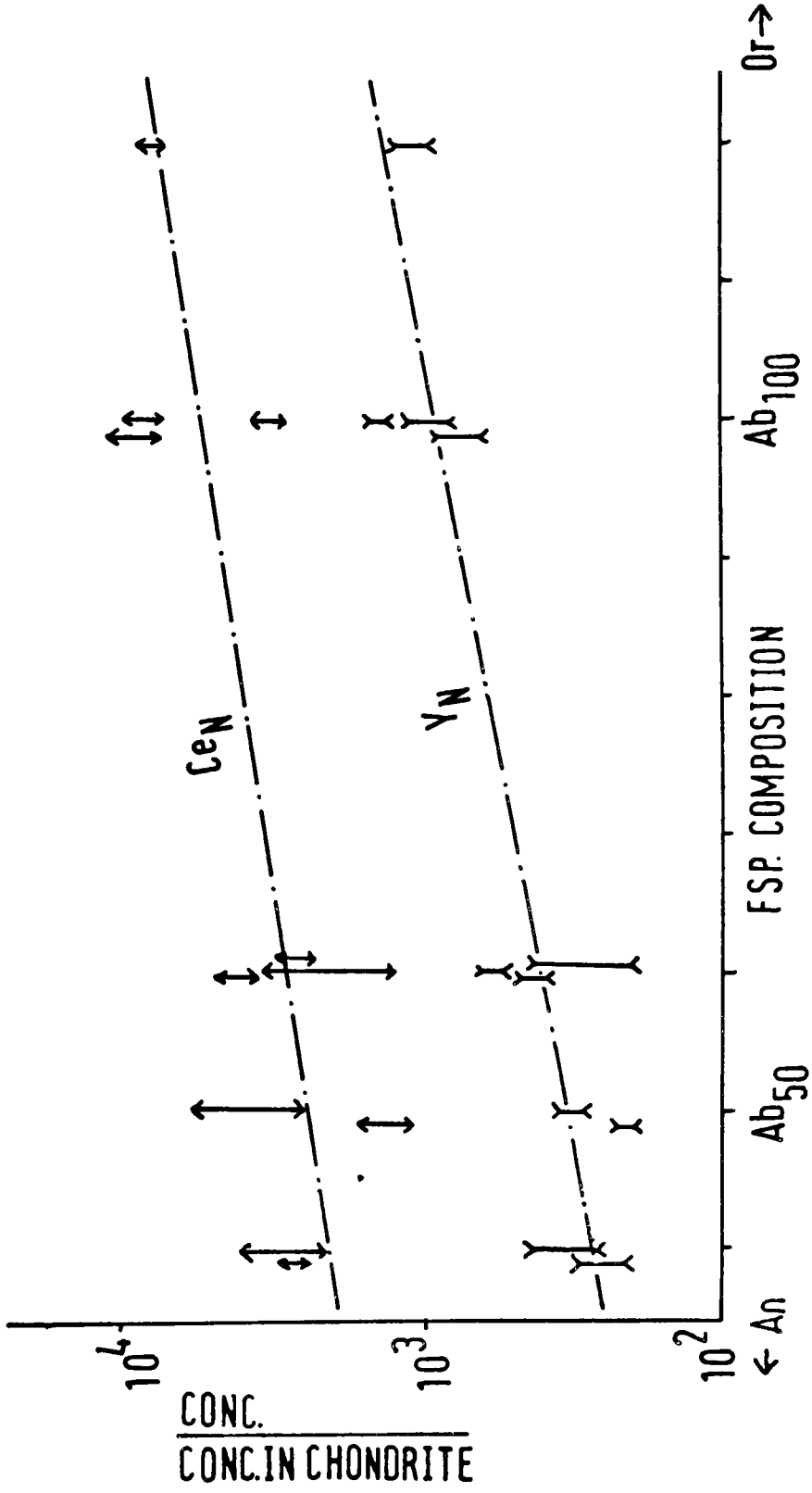
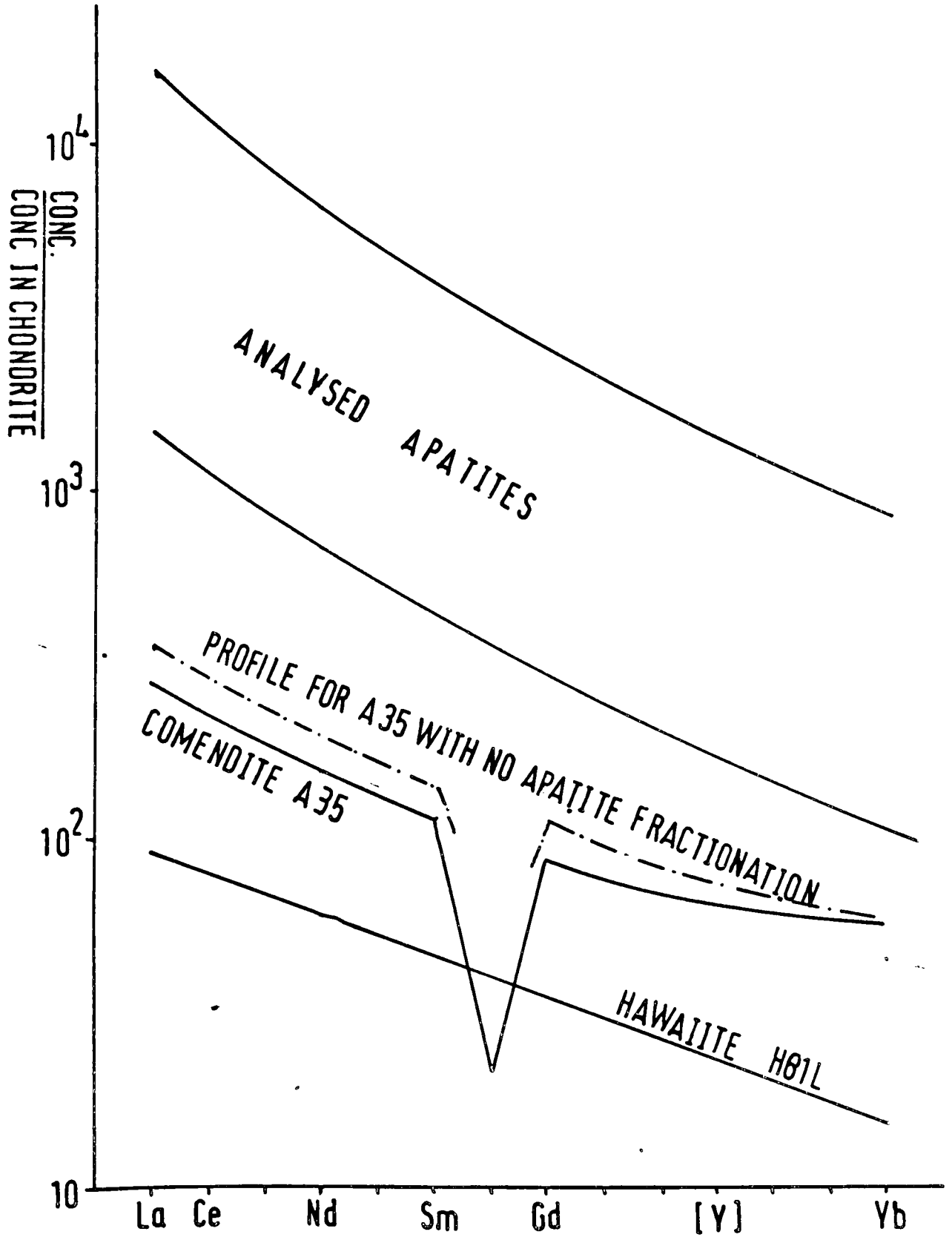


Fig 8.5 Apatite REE content and the effect of apatite fractionation on the REE profile of the comendite (A35).



CHAPTER NINE

FIGURES

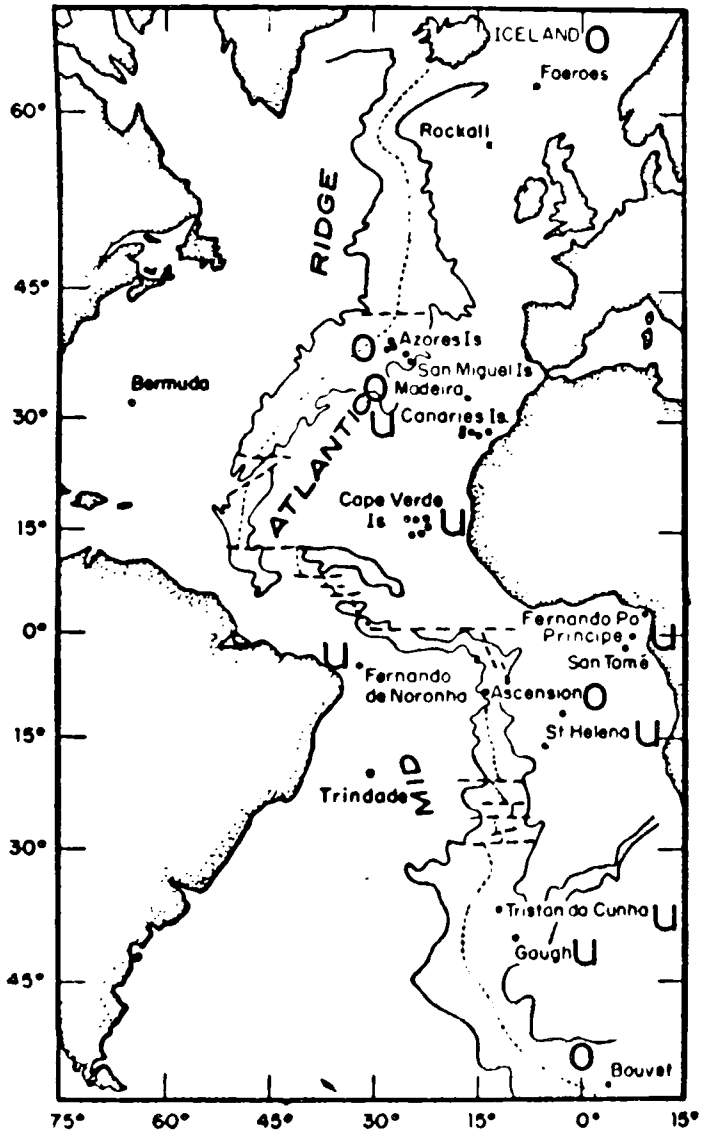


Fig 9.1 Volcanic islands of the Atlantic from McBirney and Gass (1967)

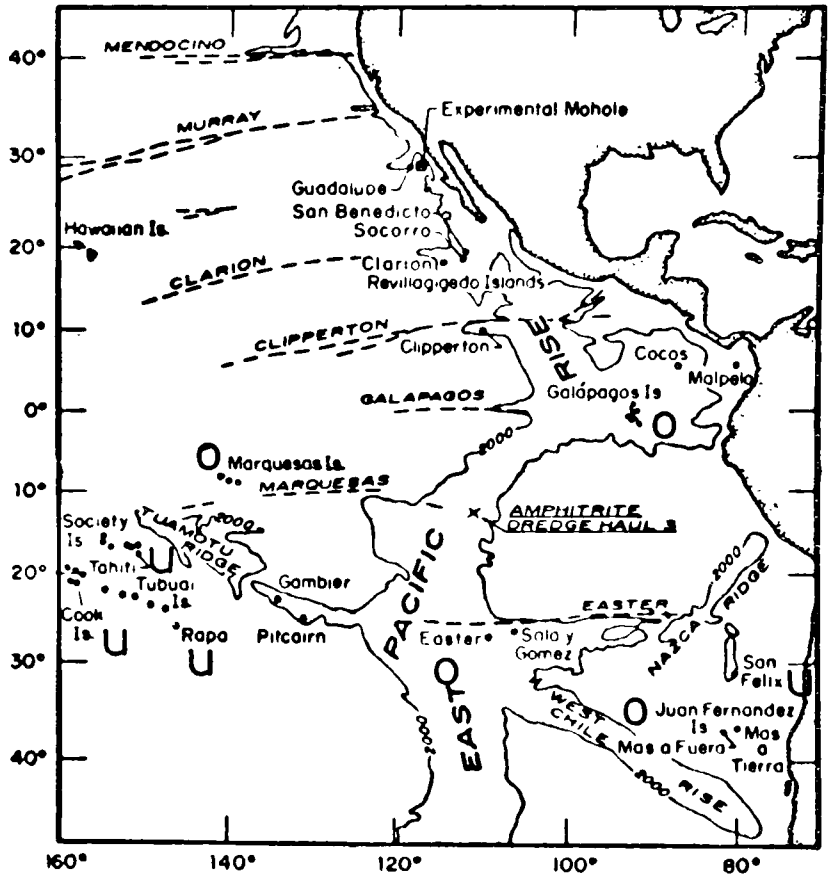
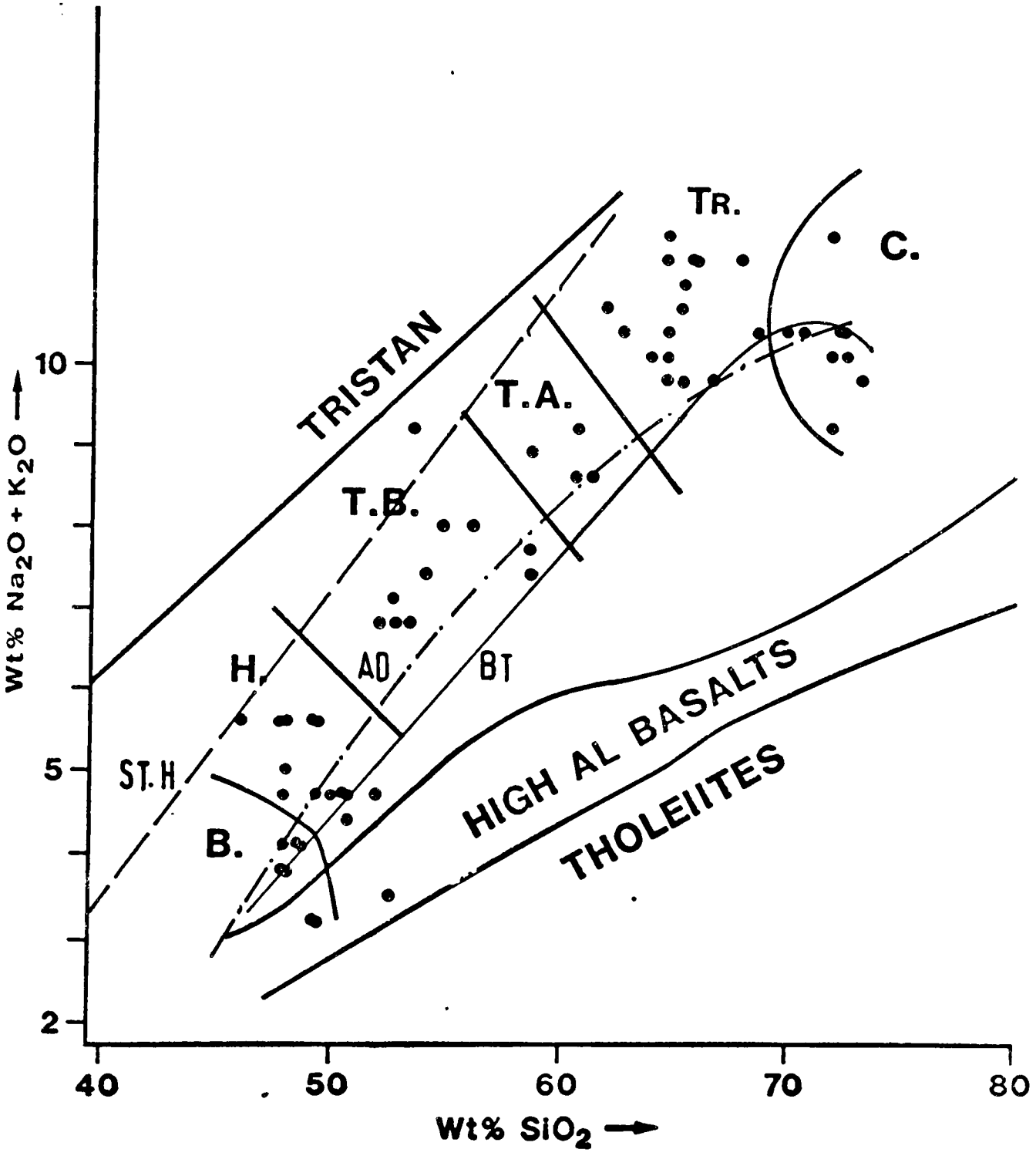


Fig 9.2 Generalised map of volcanic islands of the East Pacific, from McBirney and Gass (1967)

O = oversaturated U = undersaturated

Fig 9.3 Alkali - silica diagram for Ascension lavas + other oceanic islands. Tristan =Tristan da Cunha(Baker et al,1963), St H =St Helena (Baker,I,1969),Ad = Aden (Hill,1974) and Bt = Bouvet (Baker,1967).



Specimen Localities 1979/80

Number	Rock Type	Location
H1L	lava	Cross Hill
H2L	"	"
H3	gabbro	"
H4	lava	"
H5	"	"
H6	"	"
H7	gabbro	Middleton's
H8	"	"
H9	lava	Mt. Road
H10	"	"
H11	"	Cricket Valley
H12	gabbro	"
H13	various	"
H14	"	"
H15	gabbro	Dark Slope Crater
H16	"	"
H17	"	"
H18	"	"
H19	"	"
H20	"	"
H21	granite	Devil's Riding School
H22	"	"
H23	syenite	"
H24	"	"
H25	various	NASA Road
H26	"	"

Number	Rock Type	Location
H27	various	NASA Road
H28	"	"
H29	syenite	Dampiers
H30	granite	Five Mile Post
H31	lava	East Crater
H32	syenite	"
H33	"	"
H34	"	"
H35	various	U. Valley Crater
H36	"	N. East Bay
H37	"	NASA Road
H38	"	Green Mt.
H39	syenite	Porpoise Pt.
H40	lava	U. Valley Crater
H41	syenite	Dampiers
H42	"	NASA Road
H43	lava	Crags
H44	various	Green Mt.
H45	various	Crystal Bay
H46	"	"
H47	"	"
H48	"	"
H49	"	"
H50	lava	Little White Hill
H51	"	Letterbox
H52	gabbro	"
H53	syenite	Powers Peak
H54	gabbro	Dark Slope Crater

Number	Rock Type	Location
H55	gabbro	Dark Slope Crater
H56	"	"
H57	various	Cricket Valley
H58	"	"
H59	pegmatoid	"
H60	various	NASA Road
H61	"	"
H62	"	"
H63	"	"
H64	syenite	Cocoanut Bay
H65	"	"
H66	"	"
H67	"	"
H68	lava	"
H69	"	"
H70	syenite	"
H71	"	"
H72	gabbro	Pillar Bay
H73	"	"
H74	"	"
H75	gabbro	Summerhouse Ridge
H76	"	"
H77	"	Green Mt.
H78	"	"
H79	"	"
H80	"vesicular feldspar"	L. Valley Crater
H81	lava	Cricket Valley
H82	granite	Palmers

Number	Rock Type	Location
H83	gabbro	Mt. Red Hill
H84	various	Middleton's
H85	gabbro	Dark Slope Crater
H86	syenite	Devil's Riding School
H87	granite	Middleton's
H88	gabbro	Middleton's
H89	"	Hummock Pt.
H90	lava	"
H91	syenite	Devil's Cauldron
H92	vesicular feldspar	NE Bay Road
H93	bombs	Lady Hill
H94	gabbro	"
H95	"	"
H96	various	Grazing Valley
H97	"	"
H98	granite	Middleton's
H99	gabbro	"
H100	syenite	Mt. Road
A1	lava	Weather Post
A2	cinders	Devil's Riding School
A3	concretions	"
A4	lava	"
A5	"	East Crater
A6	"	"
A7	various	Bear's Back
A8	"	"
A9	"	Turtle Back
A10	"	"

Number	Rock Type	Location
A11	cinders	Turtle Back
A12	"	"
A13	"	"
A14	"	"
A15	lava	"
A16	"	Bear's Back
A17	"	"
A18	"	"
A19	"	"
A20	"	"
A21	"	"
A22	various	U. Valley Crater
A23	lava	"
A24	"	S. Gannet Flow
A25	"	"
A26	"	"
A27	guano	Crags
A28	lava	"
A29	"	Cross Hill
A30	"	"
A31	"	Crystal Bay
A32	olivine sand	"
A33	gabbro	Wig Hill
A34	lava	L. White Hill
A35	"	"
A36	gabbro	"
A37	obsidian	Middleton's
A38	lava	Palmers

Number	Rock Type	Location
A39	?	?
A40	lava	Breakneck Valley
A41	cinders	"
A42	various	Green Mt.
A43	"	"
A44	"	"
A45	lava	NE Cottage
A46	gabbro	"
A47	"	"
A48	sand	Green Mt.
A49	"	"
A50	gabbro	"
A51	granite	Green Mt. Rd.
A52	lava	White Hill
A53	"	"
A54	"	"
A55	"	"
A56	"	Devil's Riding School
A57	obsidian	Middleton's
A58	guano	S. Gannet Flow
A59	halite	Shelly Beach
A60	lava	Middleton's
A61	"	"
A62	obsidian	"
A63	lava	Devil's Ink Stain

H1 - H100 collected by C. Harris

A1 - A63 collected by F.B. Atkins

There are often many samples grouped under the same member (e.g. H30(1) - H30(37)).

For convenience all Dark Slope specimens are prefixed DS, e.g. DS30. Lavas are suffixed L, e.g. A63L (=A63).